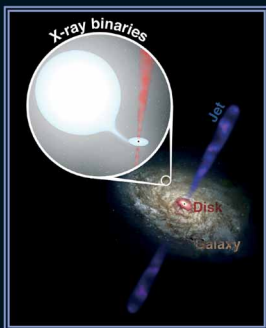


From X-ray Binaries to Quasars: Black Holes on All Mass Scales

Edited by

Thomas J. Maccarone, Robert P. Fender and Luis C. Ho



ASTROPHYSICS AND SPACE SCIENCE

From X-Ray Binaries to Quasars: Black Holes on all Mass Scales

**FROM X-RAY BINARIES TO QUASARS:
BLACK HOLES ON ALL MASS SCALES**

Edited by:

T.J. MACCARONE, R.P. FENDER and L.C. HO

Reprinted from *Astrophysics and Space Science*
Volume 300, Nos. 1–3, 2005

 Springer

Library of Congress Cataloging-in-Publication Data is available

ISBN 1-4020-4084-9

2003055495

Published by Springer,
P.O. Box 17, 3300 AA Dordrecht, The Netherlands.

Printed on acid-free paper

All Rights Reserved
© Springer 2005

No part of the material protected by this copyright notice may be reproduced or utilized in any form or by any means, electronic or mechanical, including photocopying, recording or by any information storage and retrieval system, without written permission from the copyright owner.

Printed in the Netherlands

TABLE OF CONTENTS

R. FENDER, T. BELLONI and E. GALLO / A Unified Model for Black Hole X-Ray Binary Jets?	1–13
S. HEINZ, A. MERLONI, T. DI MATTEO and R. SUNYAEV / On the Relationship Between the Jets from X-Ray Binaries and AGN	15–21
A. CELOTTI / A Transition in the Accretion Properties of AGN	23–30
J. MALZAC, A. MERLONI and A.C. FABIAN / Jet-Disc Coupling in the Accreting Black Hole XTE J1118+480	31–38
A.P. MARSCHER / Are 3C 120 and Other Active Galactic Nuclei Overweight Microquasars?	39–44
A. MERLONI, S. HEINZ and T. DI MATTEO / A Fundamental Plane of Black Hole Activity: Pushing Forward the Unification Scheme	45–53
D.L. MEIER / Magnetically Dominated Accretion Flows (MDAFS) and Jet Production in the Lowhard State	55–65
J.C. LEE / Black Hole Systems Seen at High Spectral Resolution: Inflow and Outflow	67–70
C.S. REYNOLDS, L.W. BRENNEMAN and D. GAROFALO / Black Hole Spin in AGN and GBHCs	71–79
R.L.C. STARLING, M.J. PAGE, G. BRANDUARDI-RAYMONT, A.A. BREEVELD, R. SORIA and K. WU / The Seyfert-Liner Galaxy NGC 7213: An <i>XMM-Newton</i> Observation	81–86
K. BECKWITH and C. DONE / Observational Effects of Strong Gravity	87–96
A.C. FABIAN / Broad Iron Lines in AGN and X-Ray Binaries	97–105
J. HOMAN and T. BELLONI / The Evolution of Black Hole States	107–117
S. VAUGHAN, A.C. FABIAN and K. IWASAWA / Rapid X-Ray Variability of Seyfert 1 Galaxies	119–125
M.A. ABRAMOWICZ and W. KLUŻNIAK / Epicyclic Frequencies Derived from the Effective Potential: Simple and Practical Formulae	127–136
K.M. LEIGHLY / X-Ray Periodicity in AGN	137–142
W. KLUŻNIAK and M.A. ABRAMOWICZ / Resonant Oscillations of Accretion Flow and kHz QPOs	143–148
M. VAN DER KLIS / Comparing Black Hole and Neutron Star Variability	149–157
M. NOWAK / X-Ray and Radio Monitoring of GX 339-4 and CYG X-1	159–166
C. DONE and M. GIERLIŃSKI / Accretion in Strong Gravity: From Galactic to Supermassive Black Holes	167–175

R. NARAYAN / Low-Luminosity Accretion in Black Hole X-Ray Binaries and Active Galactic Nuclei	177–188
S. MARKOFF / Exploring the Jet/Accretion Flow Relationship in Low Disk Luminosity Sources	189–195
S. MIGLIARI and R. FENDER / What Can We Learn from Neutron Star X-Ray Binaries’ Jets?	197–209
E. KÖRDING and H. FALCKE / A Unifying Scheme for Low-Luminosity XRBs and AGN	211–217
L.C. HO / “Low-State” Black Hole Accretion in Nearby Galaxies	219–225
J.M. MILLER / Present Evidence for Intermediate Mass Black Holes in ULXs and Future Prospects	227–238
T.J. MACCARONE, R.P. FENDER and A.K. TZIOUMIS / Finding Faint Intermediate-Mass Black Holes in the Radio Band	239–245
S.F. PORTEGIES ZWART, J. DEWI and T. MACCARONE / Formation and Evolution of Intermediate Mass Black Hole X-Ray Binaries	247–253
F. AHARONIAN and A. NERONOV / TeV Gamma Rays from the Galactic Center Direct and Indirect Links to the Massive Black Hole in Sgr A	255–265
J.M. PAREDES / AGNs and Microquasars as High-Energy γ -Ray Sources	267–274
S. CORBEL / Large Scale Jets in Microquasars	275–281
C.R. KAISER, J.L. SOKOLOSKI, K.F. GUNN and C. BROCKSOPP / Is GRS 1915+105 a Microquasar?	283–288

A UNIFIED MODEL FOR BLACK HOLE X-RAY BINARY JETS?

ROB FENDER¹, TOMASO BELLONI² and ELENA GALLO³

¹*School of Physics & Astronomy, University of Southampton, SO17 1BJ, UK;*

E-mail: rpf@phys.soton.ac.uk

²*INAF—Osservatorio Astronomico di Brera, Via E. Bianchi 46, I-23807 Merate, Italy*

³*Astronomical Institute 'Anton Pannekoek', University of Amsterdam, Kruislaan 403,
1098 SJ Amsterdam, The Netherlands*

(Received 8 April 2005; accepted 1 June 2005)

Abstract. We have recently put forward a 'unified' semi-empirical model for the coupling between accretion and jet production in galactic black hole X-ray binaries. In this paper, we summarise this model and briefly discuss relevant considerations that have arisen since its publication.

Keywords: accretion, black hole physics, ISM: jets and outflows

1. Introduction

Relativistic jets are a fundamental aspect of accretion onto black holes on all scales. They can carry away a large fraction of the available accretion power in collimated flows which later energise particles in the ambient medium. The removal of this accretion power and angular momentum must have a dramatic effect on the overall process of accretion. In their most spectacular form they are associated with supermassive black holes in active galactic nuclei (AGN), and with gamma-ray bursts (GRBs), the most powerful and explosive engines in the Universe, respectively. However, parallel processes, observable on humanly accessible timescales, are occurring in the accretion onto black holes and neutron stars in binary systems within our own galaxy.

We (Fender et al., 2004; hereafter FBG04) have recently published a 'unified' model for the 'disc-jet' coupling in galactic black hole binaries. In the next few pages we shall quickly summarise this model.

2. The Model

In our model, we attempt to pin down as accurately as possible the moment at which the major radio outburst occurred and relate this to the X-ray state at the time. We subsequently compare this with the X-ray state corresponding to the lower-luminosity steady jets, to the evolution of transient outbursts, and to the velocity

and power associated with each ‘type’ of jet, in order to draw up a framework for a unified model of black hole X-ray binary jet production.

Several black hole systems are investigated in this paper, and in addition we compare these with the neutron star systems Cir X-1 and Sco X-1. The data relating to the radio flares, jet Lorentz factors (if measured), corresponding X-ray luminosities, estimated distances and masses, are summarised in Table I of FBG04. In FBG04, we focus in particular on the spectral evolution of four black hole binaries, GRS 1915+105, GX 339-4, XTE J1859+226 and XTE J1550-564. Precise details of the X-ray data analysis are presented in FBG04. Figure 1 presents the X-ray (flux and hardness) and radio flux of these four systems around periods of state transitions. Several key features are apparent from careful inspection of this figure, in particular, the optically thin radio outbursts occur around the transition from ‘hard VHS (very high state)/IS (intermediate state)’ to ‘soft VHS/IS’ states, and not at the transitions to or from the canonical low/hard or high/soft states.

3. Jets as a Function of X-Ray State: New Perspectives

Based upon the investigation we have performed, we are better able to associate the characteristics of the radio emission as a function of X-ray state, and therefore to probe the details of the jet–disc coupling. While the previously established pattern of

- LS (low state): steady jet
- HS (high state): no jet

remains valid, additional information has clearly come to light about the details of jet formation in the VHS/IS during transient outbursts.

3.1. BEHAVIOUR OF THE JET IN THE ‘HARD VHS/IS’

It was previously established that the canonical low/hard state was associated with a steady jet, the emission from which followed a ‘universal’ correlation in the $L_X:L_{\text{radio}}$ plane (e.g. Fender, 2001; Corbel et al., 2003; Gallo et al., 2003). Furthermore the canonical ‘high/soft’ state was associated with a dramatic reduction in the radio emission (Tanabaum et al., 1972; Fender et al., 1999; Gallo et al., 2003). The study presented in FBG04 has further revealed that almost until the point of the major ejection, after the spectrum has started softening (in the ‘hard VHS/IS’ state) the steady radio jet stays ‘on’.

However, following the persistence of the steady LS-like radio emission into the hard VHS/IS, the data do indicate that a *change* in the radio emission does occur prior to the radio flare. In brief, it appears that the radio emission starts to become more variable, with a peaked or (more) optically thin spectrum shortly before the radio flare. At present we do not have a clear picture of what is going on during this

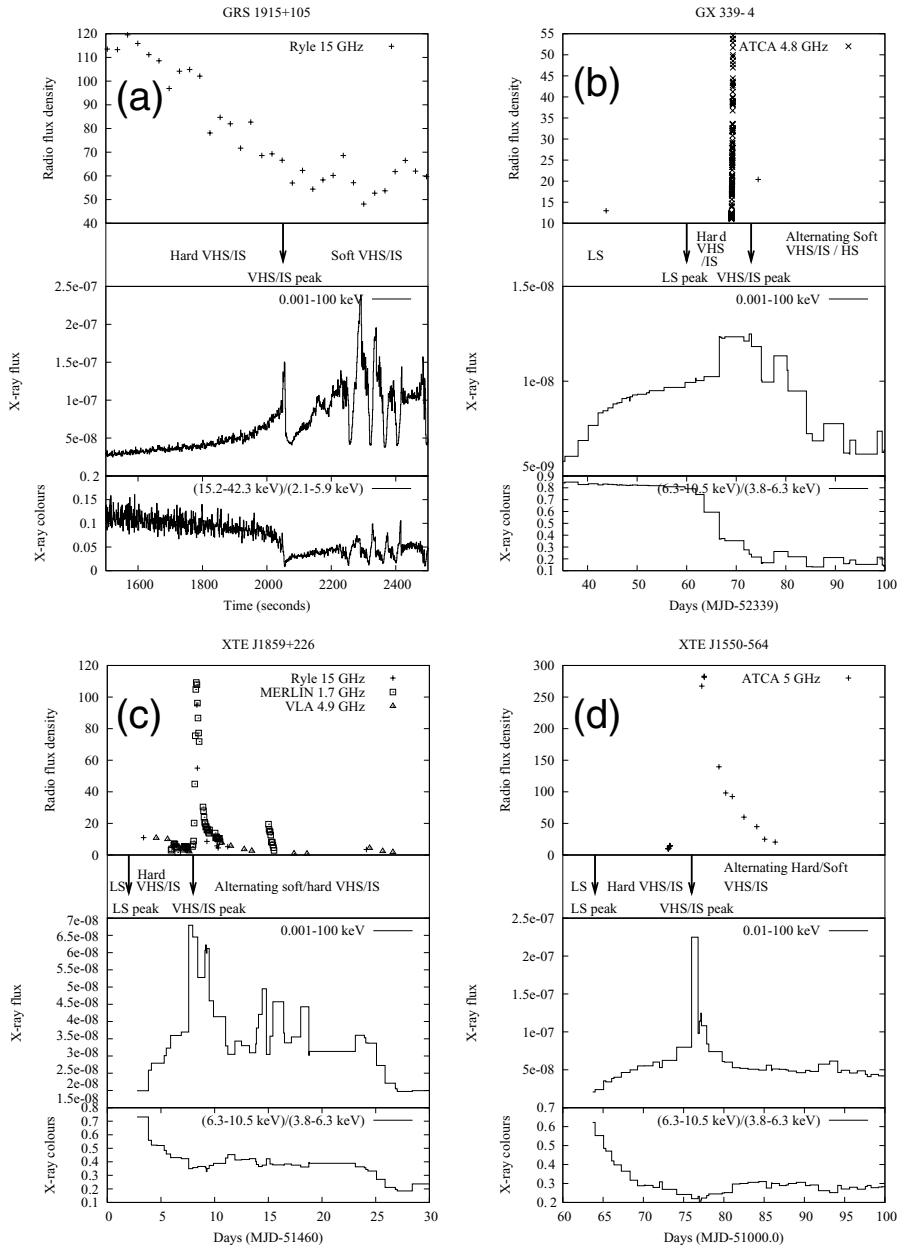


Figure 1. Radio and X-ray light curves, X-ray colours and X-ray state classifications during periods around transient jet formation, for four black hole (candidate) X-ray binaries. In GRS 1915+105 the canonical LS or HS are never reached; in GX 339-4, XTE J1859+226 and XTE J1550-564 the delay between the canonical LS peak and subsequent VHS/IS peak ranges from a few days to 2 weeks. Nevertheless, in all four cases the radio flare occurs at the time of the VHS peak, indicating a clear association between this, and not the previous LS, and the major ejection. The units of the X-ray flux are $\text{erg s}^{-1} \text{cm}^{-2}$.

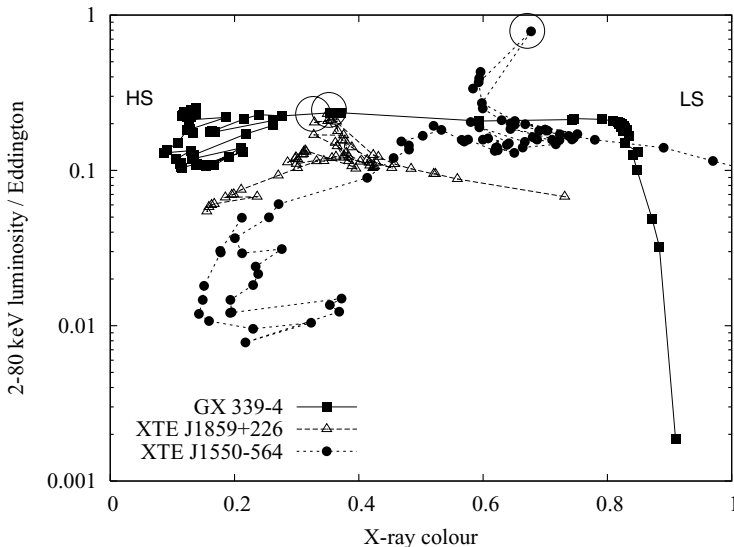


Figure 2. Combined X-ray hardness–luminosity diagram for GX 339-4, XTE J1859+226 and XTE J1550-564. The X-ray fluxes plotted in Figure 1b–1d have been scaled to Eddington-ratioed luminosities; all the sources move approximately anti-clockwise in the diagram. Note that ejections in GX 339-4 and XTE J1859+226 occur at almost exactly the same colour and X-ray luminosity. Most of the data points correspond to varying degrees of the VHS/IS, and not the canonical LS (to the right) or HS (to the left).

phase, but it hints that the major ejection episode is already inevitable some days in advance of its observational signature. See FBG04 for more details.

3.2. ASSOCIATION OF THE OUTBURST WITH THE SOFT VHS/IS PEAK

The clearest observational fact to be gleaned from Figure 1 is that the major optically thin radio outbursts occur in a transition from the ‘soft VHS/IS’ to the ‘hard VHS/IS’. Figure 2 indicates the point of radio outburst in hardness–luminosity plane. This aspect is discussed in considerably more detail in FBG04 but it suffices to note here that to our knowledge there are no exceptions to this pattern of behaviour in any black hole X-ray binary. It is important to note that very similar conclusions about the behaviour of the radio emission in the VHS/IS were drawn by Corbel et al. (2004).

4. Increasing Jet Velocity in Outburst?

In Figure 3, we plot estimated limits on the Lorentz factors of jets from a handful of X-ray binary systems as a function of X-ray luminosity at the point of the jet launch. It is important to realise that the lower-left point is an upper limit on the mean Lorentz factor of jets in the low/hard state (Gallo et al., 2003; but see also Heinz

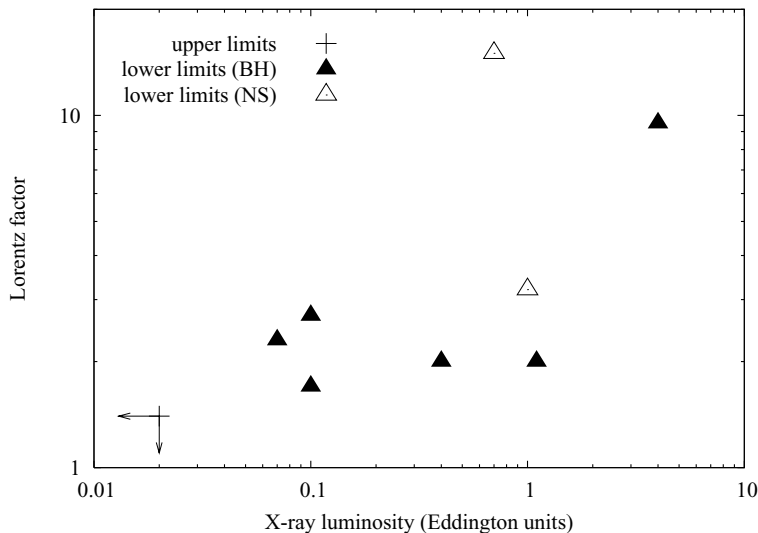


Figure 3. Limits on jet Lorentz factors as a function of the estimated bolometric X-ray luminosity at the time of jet launch. The arrows in the lower left of the figure indicate the condition that jets in the general LS state have $v \leq 0.8c$. The rest of the symbols are lower limits only to the Lorentz factors from individual black hole (filled symbols) and neutron star (open symbols) X-ray binaries; the data are listed in Table I.

and Merloni, 2004), and that all the other points are lower limits. The key point is that we have seen highly relativistic motions from the transient jets associated with outbursts, but not with the steady low/hard state jets. Thus, the data seem to support the idea that the powerful jets produced at the transition from the ‘hard VHS/IS’ to the ‘soft VHS/IS’ are at a higher velocity than those which preceded them. This leads naturally to the likelihood of internal shocks in the jet, as we shall discuss below.

5. Radio Emission and Jet Power

It is also crucial to estimate the jet power as a function of X-ray luminosity/state. In the following we present simplified expressions for the power in both optically thick and optically thin jets, in Eddington units, as a function of observable radio and X-ray emission.

5.1. THE LOW/HARD STATE OPTICALLY THICK JET

In Fender et al. (2003), it was argued that the total jet power L_J , in the absence of significant advection, was related to the accretion luminosity L_X as follows:

$$L_J = A_{\text{steady}} L_X^{0.5}$$

where $A_{\text{steady}} \geq 6 \times 10^{-3}$ (the normalisation is referred to simply as A in Fender et al., 2003).

Studies of the rapid variability from the ‘hard’ transient XTE J1118+480, which remained in the LS throughout its outburst, have supported the idea that the optical emission may originate in an outflow and not reprocessed emission from the disc (Merloni et al., 2000; Kanbach et al., 2001; Spruit and Kanbach, 2002; Malzac et al., 2003). Detailed modelling of the correlated variability by Malzac et al. (2004) has resulted in a normalisation of the jet/outflow power which corresponds to $A_{\text{steady}} \sim 0.3$ in the above formalisation, which would imply that all LS sources are jet-dominated. For now we shall take this as the largest likely value of A_{steady} (see also Yuan et al., 2005 who estimate a value for the radiative efficiency for the jet in XTE J1118+480 which lies between the lower limit of Fender et al., 2003 and the estimate of Malzac et al., 2004).

5.2. THE OPTICALLY THIN JETS

The power associated with the production of optically thin jets can be calculated from the peak luminosity and rise time of the event, adapting the minimum energy arguments of Burbidge (1959). We furthermore argue that an additional correction factor of 50 is applicable to compensate for bulk relativistic motion (see FBG04 for details).

A best-fit power-law to the data for the transient events is of the form

$$L_{\text{jet}} = A_{\text{trans}} L_X^{0.5 \pm 0.2}$$

where the fitted value is $A_{\text{trans}} = (0.4 \pm 0.1)$, within uncertainties the same index as inferred for the steady jets. Note that since for the transient jets $L_X \sim 1$ (in Eddington units) this indicates near equipartition of L_X and L_J around the time of such events.

6. Internal Shocks

The arguments given above clearly indicate that as the X-ray luminosity of the accreting source increases, then so does the velocity of the outflow (although whether this is in the form of a step, or other functional form, is as yet unclear). Since most, probably all, outbursting sources have followed a path in which they have become monotonically brighter in a hard state before making a transition to a soft state, this tells us that a shock should form in the previously generated ‘steady’ jet as the faster-moving VHS/IS jet catches up and interacts with it. This internal shock is therefore a natural origin for the optically thin events observed at the beginning of X-ray transient outbursts. Internal shocks have previously been proposed for AGN (e.g. Rees, 1978; Marscher and Gear, 1985; Ghisellini, 1999; Spada et al., 2001)

and gamma-ray bursts (e.g. Rees and Meszaros, 1994; van Paradijs et al., 2000 and references therein). Indeed in the context of X-ray binaries an internal-shock scenario has already been discussed previously for GRS 1915+105 by Kaiser et al. (2000), Vadawale et al. (2003) and Turler et al. (2004), and their ideas have significantly inspired this work. In the context of the changes in Lorentz factor estimated here, internal-shock efficiencies as high as 30% may be possible, although lower efficiencies seem more likely.

Internal shocks at relatively large distances from the base of the jet are a natural explanation for why the emission in such outburst is optically thin, unlike the steady self-absorbed jet which preceded it. Also, as discussed in Vadawale et al. (2003) the strength of the shock is likely to be related to the amount of material lying in the path of the faster ‘VHS/IS’ jet. They discussed this in the context of GRS 1915+105, where the strength of ‘post-plateau jets’ (Klein-Wolt et al., 2002) is shown to be correlated with the total X-ray fluence of the preceding ‘plateau’ (which was presumably a phase of slower jet production). Generalising this phenomenon to other X-ray transients, it provides a natural explanation for why, although there are often multiple radio-flaring events, the first is invariably the strongest.

7. Towards a Unified Model

Based upon the key generic observational details assembled above, we have attempted to construct a unified, semi-quantitative, model for the disc–jet coupling in black hole X-ray binaries. A simplified version of the model specific to GRS 1915+105 has been presented in Fender and Belloni (2004). The model is summarised in Figure 4, which we describe in detail below. The diagram consists of a schematic X-ray hardness–intensity diagram above a schematic indicating the bulk Lorentz factor of the jet and inner accretion disc radius as a function of X-ray hardness. The four sketches around the outside of the schematics indicate our suggestions as to the state of the source at the various phases **i–iv**. The path of a typical X-ray transient is as indicated by the solid arrows.

- **Phase i:** Sources are in the low-luminosity LS, producing a steady jet whose power correlates as $L_{\text{jet}} \propto L_{\text{X}}^{0.5}$ (ignoring any mass term). This phase probably extends down to very low luminosities (‘quiescence’).
- **Phase ii:** The motion in the HID, for a typical outburst, has been nearly vertical. There is a peak in the LS after which the motion in the HID becomes more horizontal (to the left) and the source moves into the ‘hard’ VHS/IS. Despite this softening of the X-ray spectrum the steady jet persists, with a very similar coupling, quantitatively, to that seen in the LS.
- **Phase iii:** The source approaches the ‘jet line’ (the solid vertical line in the schematic HID) in the HID between jet-producing and jet-free states. As the boundary is approached the jet properties change, most notably its velocity. The

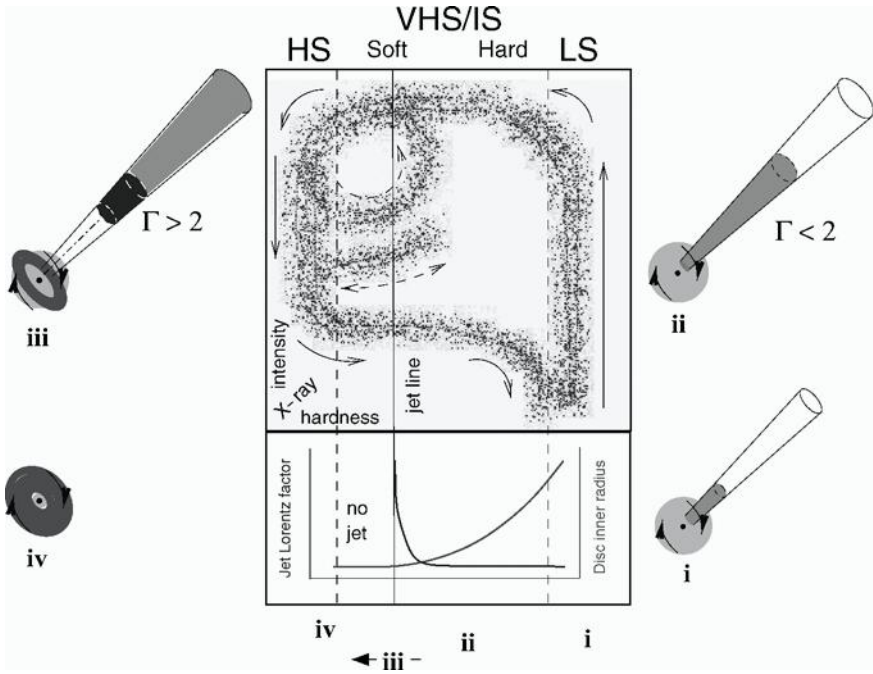


Figure 4. A schematic of our simplified model for the jet–disc coupling in black hole binaries. The central box panel represents an X-ray hardness–intensity diagram (HID); ‘HS’ indicates the ‘high/soft state’, ‘VHS/IS’ indicates the ‘very high/intermediate state’ and ‘LS’ the ‘low/hard state’. In this diagram, X-ray hardness increases to the right and intensity upwards. The lower panel indicates the variation of the bulk Lorentz factor of the outflow with hardness—in the LS and hard-VHS/IS the jet is steady with an almost constant bulk Lorentz factor $\Gamma < 2$, progressing from state **i** to state **ii** as the luminosity increases. At some point—usually corresponding to the peak of the VHS/IS— Γ increases rapidly producing an internal shock in the outflow (**iii**) followed in general by cessation of jet production in a disc-dominated HS (**iv**). At this stage fading optically thin radio emission is only associated with a jet/shock which is now physically decoupled from the central engine. As a result the solid arrows indicate the track of a simple X-ray transient outburst with a single optically thin jet production episode. The dashed loop and dotted track indicate the paths that GR 1915+105 and some other transients take in repeatedly hardening and then crossing zone **iii**—the ‘jet line’—from left to right, producing further optically thin radio outbursts. Sketches around the outside illustrate our concept of the relative contributions of jet (blue), ‘corona’ (yellow) and accretion disc (red) at these different stages.

final, most powerful, jet, has the highest Lorentz factor, causing the propagation of an internal shock through the slower-moving outflow in front of it.

- Phase **iv**: The source is in the ‘soft’ VHS/IS or the canonical HS, and no jet is produced. For a while following the peak of phase **iii** fading optically thin emission is observed from the optically thin shock.

Following phase **iv**, most sources drop in intensity in the canonical HS until a (horizontal) transition back, via the VHS/IS, to the LS. Some sources will

make repeated excursions, such as the loops and branches indicated with dashed lines in Figure 4, back across the jet line. However, with the exception of GRS 1915+105, the number of such excursions is generally ≤ 10 . When crossing the jet line from right to left, the jet is re-activated but there is (generally) no slower-moving jet in front of it for a shock to be formed; only motion from left to right produces an optically thin flare (this is a prediction). Subsequently, the motion back towards quiescence is almost vertically downwards in the HID.

The model as outlined above has many similarities with the scenarios described by Meier (1999, 2001, 2003) who has approached the problem from a more theoretical point of view. Meier (2001) has suggested that in low-luminosity states the jet is powered by a modification of the Blandford and Payne ('BP') (1982) mechanism taking into account frame-dragging near a rotating black hole (Punsly and Coroniti, 1990). This 'BP/PC mechanism' can extract black hole spin by the coupling of magnetic field lines extending from within the ergosphere to outside of it. Meier (2001) further suggests that during phases of very high accretion the Blandford and Znajek ('BZ') (1977) mechanism may work briefly. This may be associated with a 'spine jet' which is considerably more relativistic than the 'sheath jet' produced by the BP/PC mechanism. Note that the power of the jets as given in Meier (2001, 2003) is about linearly proportional to the accretion rate; in the formulation of Fender et al. (2003) this corresponds to the 'jet-dominated state' (see also Falcke et al., 2004).

We can revisit the scenarios of Meier in the light of our compilation of observational results and steps toward a unified model. In the faint LS (phase **i** in Figure 4) is the jet formed by the BP or BP/PC mechanisms? Given that the jet may be formed at relatively large distances from the black hole in such states, there may not be any significant influence of the black hole spin on the jet-formation process. However, it is also likely that in such states the jet-formation process is not occurring within thin discs, as is the basis of the BP mechanism, but rather in a geometrically thick flow (see also e.g. Blandford and Begelman, 1999; Meier, 2001; Merloni and Fabian, 2002).

As the accretion rate increases the power of this disc-jet will increase and the geometrically thin accretion disc will propagate inwards. During this phase the jet-formation process may migrate from BP \rightarrow BP/PC. However, the suggestion that the most relativistic jets are formed by the BZ process seems at odds with the observation of significantly relativistic outflows from two neutron stars systems (Fomalont et al., 2001a,b; Fender et al., 2004). In a related work, the results of Yu et al. (2004) indicate that the subsequent evolution of X-ray transient outbursts is approximately determined *before* the soft VHS/IS peak, in both neutron star and black hole systems. This suggests that already by the time of the LS peak we can estimate the size of the ejection even which is to follow, and is a further indication that the study of neutron stars will shed important light on the physics of jet formation in black hole systems.

8. Summary of the Model

We have examined the observational properties of the jets associated with black hole X-ray binary systems. The key observations can be summarised as

1. *The radio:X-ray coupling:* We have established that the steady radio emission associated with the canonical LS persists beyond the softening of the X-ray spectrum in the ‘hard’ VHS/IS. At the end of the transition from ‘hard’ to ‘soft’ VHS/IS, usually associated with a local maximum in the X-ray light curve, a transient radio outburst occurs. The radio emission is subsequently suppressed until the source X-ray spectrum hardens once more. Some source may repeatedly make the transition from ‘hard’ to ‘soft’ VHS/IS and back again, undergoing repeated episodes of steady and transient jet formation.
2. *Jet velocities:* We have argued that the measured velocities for the transient jets, being relativistic with $\Gamma \geq 2$ are significantly larger than those of the steady jets in the LS, which probably have $\Gamma \leq 1.4$.
3. *Jet power:* We have furthermore established that our best estimates of the power associated with the transient jets are compatible with extrapolations of the functions used to estimate the power in the LS (albeit with a relatively large normalisation).

Essentially equivalent conclusions about the radio:X-ray coupling have been drawn by Corbel et al. (2004). Putting these observational aspects together we have arrived at a semi-quantitative model for jet production in black hole XRBs. We argue that for X-ray spectra harder than some value (which may be universal or vary slightly from source to source) a steady jet is produced. The power of this jet correlates in a non-linear way (approximately given as $L_J \propto L_X^{0.5}$) with the X-ray luminosity. As the X-ray luminosity increases above $\sim 1\%$ of the Eddington rate the X-ray spectrum begins to soften. Physically this probably corresponds to the heating of the inner edge of the accretion disc as it propagates inwards with increasing accretion rate. Initially the jet production is not affected. As the disc progresses inwards the jet velocity increases. As it moves through the last few gravitational radii before the ISCO, the Lorentz factor of the jet rises sharply, before the jet is suppressed in a soft disc-dominated state. The rapid increase in jet velocity in the final moments of its existence results in a powerful, optically thin, internal shock in the previously existing slower-moving outflow.

The inner disc may subsequently recede, in which case a steady jet is reformed, but with decreasing velocity and therefore no internal shocks. If the disc once more moves inwards and reaches the ‘fast jet’ zone, then once more an internal shock is formed. In fact while jets are generally considered as ‘symptoms’ of the underlying accretion flow, we consider it possible that the reverse may be true. For example, it may be the ‘growth’ of the steady jet (via e.g. build up of magnetic field near the ISCO/black hole) which results in the hardening of the X-ray spectrum, perhaps via pressure it exerts on the disc to push it back, or simply via Comptonisation of the

inner disc as it spreads (for further discussions see e.g. Nandi et al., 2001; Tagger et al., 2004).

In the context of the nature and classification of black hole ‘states’, these states, whether ‘classical’ or as redefined by McClintock and Remillard (2004) do not have a one-to-one relation with the radio properties of the source. It seems that as far as the jet is concerned, it is ‘on’—albeit with a varying velocity—if the disc does not reach ‘all the way in’, which probably means as far as the ISCO. The dividing ‘jet line’ (Figure 4) HID, may also correspond, at least approximately, to a singular switch in X-ray timing properties (Belloni, 2004; Belloni et al., 2005; Homan and Belloni, 2004; see also the discussion in McClintock and Remillard, 2004) and may be the single most important transition in the accretion process. Further study of the uniqueness of the spectral and variability properties of sources at this transition point should be undertaken to test and refine our model.

Finally, given that Merloni et al. (2003) and Falcke et al. (2004) (see also Heinz and Sunyaev, 2003; Maccarone et al., 2003) have recently demonstrated quantitatively the scaling of radio:X-ray coupling across a range of $\geq 10^7$ in black hole mass, it is obviously of great interest to see if the model we are working towards for the coupling of accretion and jet formation in black hole binaries may also be applied to AGN. In addition, detailed modelling of the internal-shock scenario is required to see if the coupling, as outlined above, really could allow us to predict radio light curves from X-ray, and vice versa. These two areas should be the next steps forward.

9. And Afterwards . . .

The model outlined above was published in December 2004, 5 months ago at the time of writing. Since this time we have not discovered, or been made aware of, any major flaws. There is of course still plenty of time, and exceptions to the patterns discussed will certainly be found (and we encourage people to be critical!).

In particular Homan and Belloni (2005, these proceedings) have demonstrated very clearly that the neat shape sketched out for the evolution of black hole outbursts in the HID varies from source to source, and indeed between outbursts for the same source. Clearly the sketch should be considered as an idealisation; nevertheless the overall properties of the pattern in the HID are consistent with our simple sketch.

Furthermore, both Homan and Belloni and Remillard (2005) have noted that the X-ray variability behaviour of the black holes, in particular of different types of QPOs, may fit empirically into the model. This is clearly an exciting next step.

Both of these points indicate ways in which the model can be significantly refined, especially in the context of adding the timing properties.

Finally, several people have discussed with us possible applications of the model to AGN. In particular we would like to note the implication, first spotted by Chris

Simpson, that if AGN follow the same patterns of outburst there should be some sources with radio-quiet cores and yet ‘relic’ radio lobes.

Acknowledgements

RPF would like to thank many people for useful discussions related to the ideas presented here, including Catherine Brocksopp, Annalisa Celotti, Stephane Corbel, Peter Jonker, Marc Klein-Wolt, Tom Maccarone, Dave Meier, Simone Migliari, Jon Miller, Felix Mirabel, Chris Simpson and *especially* Jeroen Homan.

References

- Belloni, T.: 2004, in: E.P.J. van den Heuvel, J.J.M. in’t Zand and R.A.M.J. Wijers (eds.), *Nuclear Physics B – Proceedings Supplements*, **132**, 337–345, *Proceedings of the 2nd BeppoSAX Conference: The Restless High-Energy Universe*.
- Belloni, T., Mendez, M., van der Klis, M., Hasinger, G., Lewin, W.H.G. and van Paradijs, J.: 1996, *ApJ* **472**, L107.
- Belloni, T., Mendez, M., King, A.R., van der Klis, M. and van Paradijs, J.: 1997, *ApJ* **488**, L109.
- Belloni, T., Klein-Wolt, M., Mendez, M., van der Klis, M. and van Paradijs, J.: 2000, *A&A* **355**, 271.
- Belloni, T., Homan, J., Casella, P., van der Klis, M., Nespoli, E., Lewin, W.H.G., Miller, J.M. and Méndez, M.: 2005, *A&A* **440**, 207.
- Blandford, R.D. and Znajek, R.L.: 1977, *MNRAS* **179**, 433.
- Blandford, R.D. and Payne, D.G.: 1982, *MNRAS* **199**, 883.
- Blandford, R.D. and Begelman, M.C.: 1999, *MNRAS* **303**, L1.
- Burbidge, G.R.: 1959, *ApJ* **129**, 849.
- Corbel, S., Nowak, M.A., Fender, R.P., Tzioumis, A.K. and Markoff, S.: 2003, *A&A* **400**, 1007.
- Corbel, S., Fender, R., Tomsick, J.A., Tzioumis, A.K. and Tingay, S.: 2004, *ApJ* **617**, 1272.
- Falcke, H., Körding, E. and Markoff, S., 2004, *A&A* **414**, 895.
- Fender, R.P.: 2001, *MNRAS* **322**, 31.
- Fender, R.P.: 2003, *MNRAS* **340**, 1353.
- Fender, R.P.: 2005, in: W.H.G. Lewin and M. van der Klis (eds.), *Compact Stellar X-Ray Sources* (astro-ph/0303339) (in press).
- Fender, R.P. and Belloni, T.: 2004, *ARA&A* **42**, 317.
- Fender, R.P., Belloni, T. and Gallo, E.: 2004, *MNRAS* **355**, 1105.
- Fender, R.P., Gallo, E. and Jonker, P.: 2003, *MNRAS* **343**, L99.
- Fomalont, E.B., Geldzahler, B.J. and Bradshaw, C.F.: 2001a, *ApJ* **553**, L27.
- Fomalont, E.B., Geldzahler, B.J. and Bradshaw, C.F.: 2001b, *ApJ* **558**, 283.
- Gallo, E., Fender, R.P. and Pooley, G.G.: 2003, *MNRAS* **344**, 60.
- Ghisellini, G.: 1999, *AN* **320**, 232.
- Heinz, S. and Sunyaev, R.A.: 2003, *MNRAS* **343**, L59.
- Heinz, S. and Merloni, A.: 2004, *MNRAS* **355**, L1.
- Homan, J. and Belloni, T., 2004, in: T.J. Maccarone, R.P. Fender and L.C. Ho (eds.), *From X-Ray Binaries to Quasars: Black Hole Accretion on All Mass Scales*, Kluwer, Dordrecht, (astro-ph/0412597).
- Homan, J., Wijnands, R., van der Klis, M., Belloni, T., van Paradijs, J., Klein-Wolt, M., Fender, R. and Méndez M.: 2001, *ApJS* **132**, 377.
- Kaiser, C.R., Sunyaev, R. and Spruit, H.C.: 2000, *A&A* **356**, 975.

- Kanbach, G., Straubmeier, C., Spruit, H.C. and Belloni, T.: 2001, *Nature* **414**, 180.
- Klein-Wolt, M., Fender, R.P., Pooley, G.G., Belloni, T., Migliari, S., Morgan, E.H. and van der Klis, M.: 2002, *MNRAS* **331**, 745.
- McClintock, J.E. and Remillard, R.A.: 2004, in: W.H.G. Lewin and M. van der Klis (eds.), *Compact Stellar X-Ray Sources (astro-ph/0306213)* (in press).
- Maccarone, T., Gallo, E. and Fender, R.P.: 2003, **345**, L19.
- Malzac, J., Merloni, A. and Fabian, A.C.: 2004, *MNRAS* **351**, 253.
- Malzac, J., Belloni, T., Spruit, H.C. and Kanbach, G.: 2003, *A&A* **407**, 335.
- Marscher, A.P. and Gear, W.K.: 1985, *ApJ* **298**, 114.
- Meier, D.L.: 1999, *ApJ* **522**, 753.
- Meier, D.L.: 2001, *ApJ* **548**, L9.
- Meier, D.L.: 2003, *New Astronomy Rev.* **47**, 667.
- Merloni, A. and Fabian, A.C.: 2002, *MNRAS* **332**, 165.
- Merloni, A., Fabian, A.C. and Ross, R.R.: 2000, *MNRAS* **313**, 193.
- Merloni, A., Di Matteo, T. and Fabian, A.C.: 2000, *MNRAS* **318**, L15.
- Merloni, A., Heinz, S. and di Matteo, T., 2003: *MNRAS* **345**, 1057.
- Nandi, A., Chakrabarti, S.K., Vadawale, S.V. and Rao, A.R.: 2001, *A&A* **380**, 245.
- Punsly, B. and Coroniti, F.V.: 1990, *ApJ* **354**, 583.
- Rees, M.J.: 1978, *MNRAS* **184**, 61.
- Rees, M.J. and Meszaros, P.: 1994, *ApJ* **430**, L93.
- Remillard, R.A.: 2005, in: P. Chen (ed.), *SLAC Electronic Conference Proceedings Archive* (CD Rom) (astro-ph/0504129).
- Spada, M., Ghisellini, G., Lazzati, D. and Celotti, A.: 2001, *MNRAS* **325**, 1559.
- Spruit, H.C. and Kanbach, G.: 2002, *A&A* **391**, 225.
- Tagger, M., Varniere, P., Rodriguez, J. and Pellat, R.: 2004, *ApJ* **607**, 410.
- Turler, M., Courvoisier, T.J.-L., Chaty, S. and Fuchs, Y.: 2004, *A&A* **415**, L35.
- Vadawale, S.V., Rao, A.R., Naik, S., Yadav, J.S., Ishwara-Chandra, C.H., Pramesh Rao, A. and Pooley, G.G.: 2003, *ApJ* **597**, 1023.
- Van Paradijs, J., Kouveliotou, C. and Wijers, R.A.M.J.: 2000, *ARA&A* **38**, 379.
- Yu, W., van der Klis, M. and Fender, R.: 2004, *ApJ* **611**, L121.
- Yuan, F., Cui, W. and Narayan, R.: 2005, *ApJ* **620**, 905.

ON THE RELATIONSHIP BETWEEN THE JETS FROM X-RAY BINARIES AND AGN

SEBASTIAN HEINZ,¹ ANDREA MERLONI,² TIZIANA DI MATTEO²
and RASHID SUNYAEV²

¹*Kavli Institute for Astrophysics and Space Research, MIT, USA; Chandra Fellow;*
E-mail: heinzs@space.mit.edu

²*Max-Planck-Institute for Astrophysics, Garching, Germany*

(Received 1 October 2004; accepted 1 December 2004)

Abstract. The scale invariance model (Heinz, S. and Sunyaev, R.A.: 2003, *MNRAS* **343**, L59) can be used to derive robust scaling relations between the radio luminosity from accreting black holes and the black hole mass and accretion rate. These relations agree well with the recently found “fundamental plane” of black hole activity (Merloni, A., Heinz, S. and Di Matteo, T.: 2003, *MNRAS* **345**, 1057). This relation provides a new, powerful tool for the comparison of jets from black holes of different masses and accretion rates. The regression coefficients of this relation contain information about the nature of the X-ray emission mechanism driving the correlation. We argue that X-ray synchrotron emission from the base of the jets is unlikely to be the dominant contribution to the X-ray spectrum in most of the sources.

Keywords: radiation mechanisms, non-thermal: galaxies, active: galaxies, jets: x-rays, binaries: radio continuum, general

1. Introduction

Jets are a tell-tale sign of accretion onto a central, massive object. They occur on different mass scales (from stellar mass central objects to supermassive black holes, spanning 8 orders of magnitude in mass), different accretion rates (e.g., for very low accretion rates in objects like Sgr A* and low-luminosity X-ray binaries and active galactic nuclei (AGNs), to far super-Eddington accretion rates in gamma-ray bursts), and for different classes of central objects (young stars, white dwarfs, neutron stars, and black holes).

Jets play an important role in regulating and facilitating black hole growth. Firstly, they energize and transform the surrounding medium and are one of the primary candidates for large-scale feedback in structure formation. Some modes of accretion onto black holes seem to not only facilitate jet formation, but actually require it (Blandford and Begelman, 1999) and there is mounting evidence from the X-ray binary community that steady jets are universally present in objects that are in the so-called low/hard state. This necessity might arise from the fact that jets can carry away mass, energy, and angular momentum from the accretion flow.



Furthermore, jets offer a direct probe of the innermost regions around black holes where they are formed, and are thus important probes of strong gravity.

Despite the seeming importance of jets for the study of black hole growth, feedback in structure formation, and as test beds of relativity, we still lack some of the most fundamental information about the nature of jets. Their particle and magnetic field content is still not known definitively, as are the processes that collimate and accelerate them and the actual bulk velocities of the jet plasma.

Based on morphological and spectral similarities between X-ray binary jets and AGN jets, and starting from the assumption that gravity, which governs the dynamics of the inner accretion disk, is scale invariant, we will argue that jets from black holes of different masses should be fundamentally similar in their properties in the sense that their dynamical properties are invariant under changes in black hole mass. Building on this premise, we will show that one can understand the radiative properties of jets in terms of very robust, general relations and we will present evidence that these relations can be observed in the form of a correlation between black hole mass, radio luminosity, and X-ray luminosity in AGNs and XRBs (Section 2). We will argue further that we can use this relation to constraint the emission process that is responsible for the X-rays from these black holes (Section 3).

2. A New Diagnostic Tool for Accreting Black Holes

The recent discovery of a fundamental relation between the radio emission from jets in X-ray binaries (XRBs) and the X-ray luminosity in these objects (Corbel et al., 2003; Gallo et al., 2003) has inspired a new approach to study the nature of jets, which tries to determine important jet properties without the necessity to understand every complex detail of jet structure and evolution in detail. We will lay out later how this method can be used to study jets and accretion flows.

In Heinz and Sunyaev (2003), we presented the scale invariance model, which builds the basis of the following arguments. The main idea of the model is that only very few parameters govern the physics of the inner accretion disk, namely the black hole mass M , the accretion rate \dot{m} , and possibly black hole spin (which we will neglect in the following).

The only relevant scale imposed by these parameters is assumed to be the gravitational radius r_g and we will assume that all relevant jet physics is invariant under changes of this scale. In other words, a jet from a black hole of mass M_1 will have the same proportions and spatial evolution of dynamical variables as a jet from a black hole of mass M_2 , but its spatial scales will be different by a factor of M_1/M_2 . Mathematically, this means that any quantity f relevant to jet dynamics can be expressed in the form

$$f(\mathbf{r}, M, \dot{m}, a) = \Phi_f(M, \dot{m}, a)\Psi_f(\mathbf{r}/r_g, a) \quad (1)$$

(Heinz and Sunyaev, 2003). Φ_f are functions describing the normalization of variable f at the base of the jet, and they are typically provided by accretion disk theory. We will take $\Phi_B = \sqrt{\dot{m}/M}$ as our fiducial expression for how the magnetic field strength at the base of the jet varies with M and \dot{m} . The functions Ψ_f are structure functions that describe the spatial variation of f , i.e., collimation, acceleration, etc. They are currently not well known. We will further assume that the electrons responsible for the synchrotron emission to follow a powerlaw distribution in energy: $f(\gamma) = C\gamma^{-p}$, with $\Phi_C = \Phi_B^2$, with a fiducial value of $p = 2$. Finally, by dimensional analysis we will assume that the kinetic jet power follows the proportionality $L_{\text{kin}} \propto B^2 M^2 \propto M\dot{m}$.

By inserting Eq. (1) into the expressions for the synchrotron radio luminosity of the jet, it is straightforward to show that the radio luminosity from the jet follows the relation (for $p = 2$, see (Heinz and Sunyaev, 2003) for the general expression)

$$L_r \propto M^{17/12 - \alpha_r/3} \dot{m}^{17/12 + 2\alpha_r/3} \propto L_{\text{kin}}^{1.42 + 2\alpha_r/3} M^{-\alpha_r} \quad (2)$$

(Heinz and Sunyaev, 2003; see also Falcke and Biermann, 1995) where α_r is the radio spectral index. The functions Φ_f determine the powerlaw index, while the unknown functions Ψ_f are subsumed into α_r , which is an observable. Typically, $\alpha_r \sim 0$ for the optically thick, flat spectrum cores of jets we are interested in here, so $L_r \propto M^{1.42} \dot{m}^{1.42} \propto L_{\text{kin}}^{1.42}$.

This relation is robust and model independent, since the functions Ψ_f drop out. It is valid both for optically thick radiation with $\alpha_r \sim 0$ and optically thin radiation at higher frequencies with $\alpha = (p - 1)/2 \sim 0.5$. As recently shown by Heinz (2004), it is possible to extend this analysis to include synchrotron losses of the radiating electrons. This allows us to treat synchrotron X-rays from the jet and derive the scaling relations governing them. In this case (again for $p = 2$),

$$L_x \propto M^{(3\alpha_x)/2} \dot{m}^{(5-3\alpha_x)/2} \propto L_{\text{kin}}^{(5-3\alpha_x)/2} M^{\alpha_x - 1} \quad (3)$$

To test these relations observationally, we must make a connection between the accretion rate \dot{m} and an observable. Since we are particularly interested in low-luminosity objects, we will consider the hard (2–10 keV) X-ray luminosity as a proxy of the accretion activity, because it is not affected significantly by absorption, and because it is known to correlate with the radio emission in XRBs.

In order to look for evidence of any relation between L_r , M , and \dot{m} , we collected a large sample of black holes with measured masses and radio and X-ray luminosities. The sample contains 99 AGNs and 8 XRBs at 50 different epochs for a total of 149 data points. The details of this sample can be found in Merloni et al. (2003). We do want to point out, though, that the sample was selected with the goal to avoid selection effects induced by relativistic beaming (Blazars and BL Lac objects were excluded, and the only powerful quasar included is 3C273; most objects are at low luminosities).

Partial correlation tests show that there is strong evidence that L_r correlates with both M and L_x . Thus, a multivariate correlation analysis is necessary to find the dependence of L_r on M and L_x . Looking for a correlation between, say, L_r and M is not sufficient and will not yield meaningful results. We have performed such an analysis (Merloni et al., 2003), and found the following relation:

$$\log L_r = 0.78 \log M + 0.6 \log L_x + 7.33 \quad (4)$$

with a scatter of $\sigma \sim 1$. In the following we will refer to this relation as the “fundamental plane” of black hole activity (FP for short).

It is worth noting that the dependence of L_r on M is well constrained to be $L_r \propto M^{1.4}$ (note that L_x depends on M , presumably through $L_x \propto M$, thus Eq. (4) is consistent with this statement), which confirms the predictions from Eq. (2) very nicely.

Finally, we can attempt to make a connection between L_x and the accretion rate. For different emission mechanisms and accretion disk scenarios, the dependence of L_x on \dot{m} will differ. For example, inefficient accretion flows tend to have steep dependences of the form $L_x \sim \dot{m}^2$, X-ray synchrotron emission from the jet follows Eq. (3), while for efficient accretion disks, $L_x \sim \dot{m}$. Fitting the predicted scaling relations from Eqs. (2) and (3) leads to the following results: inefficient flows with steep L_x - \dot{m} dependences (such as ADAFs) can reproduce the FP relation from Eq. (4) very well. X-ray synchrotron radiation is marginally consistent with this relation (see Section 3). Finally, efficient accretion is ruled out completely.

3. Constraints on the X-Ray Emission Mechanism

We can go further in testing the origin of the X-rays in the sources that contribute to the correlation in Eq. (4). For a synchrotron origin in the jet, we expect spectral signatures of radiative losses to appear at high enough frequencies, simply because the cooling time is proportional to $\nu^{-1/2}$. Given Eq. (3), we can test the consistency of the FP correlation with a synchrotron origin of the X-rays.

For a number of AGNs in our sample, spectral index information is available in the literature. Figure 1 shows the measured spectral indices for these sources. The canonical range of synchrotron spectra produced in strong shocks by Fermi acceleration ranges from $\alpha_x \sim 0.5$ to ~ 0.65 , which is in line with observed optically thin radio synchrotron spectra from AGN jets. For spectra steeper than this, one can say with some confidence that, if produced by synchrotron radiation, they are probably affected by radiative losses.

As can be seen from the figure, a large number of sources satisfy this criterion, and we can assume that, if synchrotron radiation is the source of the X-rays in these sources, they will have been affected by cooling. Thus, Eq. 3 is necessary and sufficient to derive the scaling relations between the radio luminosity, the

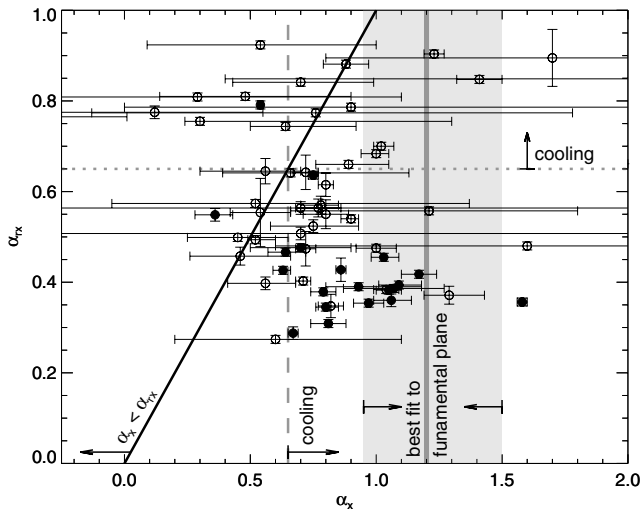


Figure 1. Plot of the measured radio–X-ray spectral index α_{rx} against the measured X-ray spectral index α_x for the AGNs in the “fundamental plane” sample where this information is available. *Left of black line*: X-ray spectrum flatter than radio-to-X-ray spectrum, $\alpha_x < \alpha_{rx}$, difficult to reconcile with global synchrotron spectrum. *Light grey area*: X-ray spectral indices from best fit to “fundamental plane” correlation (see Figure 2). *Dashed and dotted grey lines*: cooling or steep injection spectrum necessary to the right of and above these lines. *Filled dots*: sources with X-ray luminosity $L_x > 10^{-3} L_{\text{Edd}}$. *Empty dots*: sources with $L_x < 10^{-3} L_{\text{Edd}}$.

synchrotron X-ray luminosity, and the black hole mass. While the RXTE-ASM data products for the XRBs used in the FP sample are not sufficient to measure the X-ray spectral index, it is well known that the sources display X-ray spectral indices of $\alpha_x \sim 0.7$ in the low–hard state. Again, this is on the steep side for standard shock acceleration models, so we feel confident that radiative cooling is probably involved in shaping the observed X-ray spectra, if they are indeed of synchrotron origin.

Furthermore, the global, radio–X-ray spectral index of a large fraction of the source in the sample is steeper than the canonical range produced in strong shocks, which again argues for the presence of radiative cooling if the X-rays are synchrotron radiation.

Similar to the procedure used in Merloni et al. (2003), we can fit the FP data set with the predicted scaling relations from Eqs. (2) and (3) for different parameters p and α_x . Taking the fiducial value of $\alpha_r \approx 0$, combining these two equations gives the radio–X-ray–mass relation for synchrotron X-rays (Heinz, 2004):

$$L_r \propto L_x^{\frac{2p+13}{(p+4)(2p+1-3\alpha_x)}} M^{\frac{(2p+13)(p-1-\alpha_x)}{(p+4)(2p+1-3\alpha_x)}} \quad (5)$$

The scatter in the FP relation is much larger than the typical measurement error, so we isotropize the uncertainty estimate and use the same orthogonal bisector error

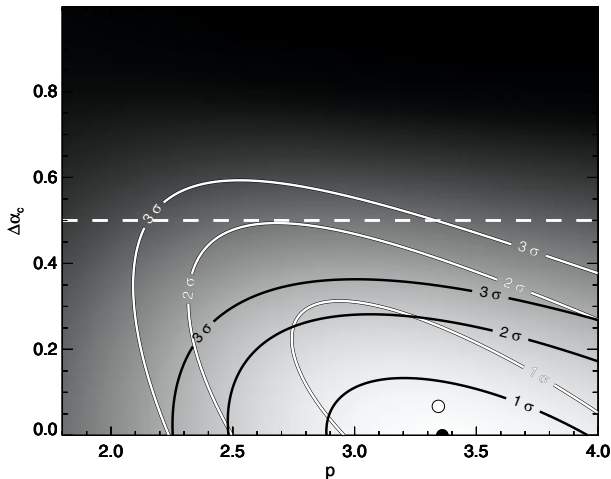


Figure 2. Chi-square map of the particle spectral index p and synchrotron cooling break $\Delta\alpha_c$, derived by fitting the “fundamental plane” radio–X-ray–mass correlation with cooled synchrotron emission as the source of the X-rays and a flat, optically thick radio synchrotron spectrum with index $\alpha_r = 0$. Overplotted are the 1-, 2-, and 3-sigma contours (thick black lines), the best fit (black dot), and the canonical cooling break of $\Delta\alpha_c = 1/2$ (white dashed line). A reasonable fit requires an unbroken, i.e. *uncooled* global spectrum that is steeper than ~ 3 . Also shown are the same 1-, 2-, and 3-sigma contours and the best fit obtained by fitting only low X-ray luminosity sources with $L_x \leq 10^{-3} L_{\text{Edd}}$ (white contours and white dot).

estimate used in Merloni et al. (2003). The result of this fit is shown in Figure 2 in the form of confidence contours on the parameters p and $\Delta\alpha_x \equiv \alpha_x - (p - 1)/2$, where $(p - 1)/2$ is the optically thin synchrotron spectral index for a population of electrons with powerlaw index p (thus, $\Delta\alpha_x$ measures the spectral break introduced by cooling, and for the simplest model of continuous injection of fresh particles, we expect $\Delta\alpha_x = 1/2$).

As can be seen from this plot, the FP relation requires very steep electron spectra: $p \sim 3.4_{-0.3}^{+0.3}$ that are *unbroken*: $\Delta\alpha_x \sim 0$. In other words, the FP relation is best fit by a very steep, uncooled global electron spectrum. Both of these requirements are at odds with what we know about the nature of particle acceleration and the typical amount of cooling expected in highly magnetized environment such as the base of jets. Furthermore, the actually observed X-ray spectral indices shown in Figure 1 are not nearly this steep: most points in Figure 2 fall to the left of the range in α_x allowed by Figure 1 (shown as the grey vertical bar between $0.95 < \alpha_x < 1.5$). Thus, we have conflicting information from the spectral information and the FP correlation.

There are two ways to resolve this conflict: Either (1) some aspect of the scale invariance model presented earlier that works so well in predicting the mass dependence of the core radio luminosity fails, in which case the bulk of the X-ray

emission could well be synchrotron. Or (2), the bulk of the emission from most of the sources is not of synchrotron origin. Instead, the X-rays might originate in a radiatively inefficient accretion flow or wind, or as inverse Compton emission in the jet. However, while synchrotron emission is probably not the dominant source of the X-rays, there is little doubt that it does contribute to the spectrum at some level and might be responsible for most of the X-rays in a smaller sub-sample of the sources considered in the FP sample.

4. Conclusions

We argued that the assumption of scale invariance of jets from black holes can be used to derive robust, model independent scaling relations between the jet radio luminosity and the black hole mass and accretion rate. The recently found “fundamental plane” relation between radio luminosity, black hole mass, and X-ray luminosity confirms the predictions from the scale invariance hypothesis.

Including spectral information into the analysis of the radio–X-ray–mass correlation provides further evidence that synchrotron X-rays are likely not the dominant source of the X-rays that drive the correlation.

Support for this work was provided by NASA Chandra Fellowship grant, Award Number PF3-40026, under NASA contract NAS8-39073. Any opinions, findings, and conclusions or recommendations expressed in this material are those of the authors and do not necessarily reflect the views of the Smithsonian Astrophysical Observatory or the National Aeronautics and Space Administration.

References

- Blandford, R.D. and Begelman, M.C.: 1999, *MNRAS* **303**, L1.
Corbel, S., Nowak, M.A., Fender, R.P., Tzioumis, A.K. and Markoff, S.: 2003, *A&A* **400**, 1007.
Falcke, H. and Biermann, P.L.: 1995, *A&A* **293**, 665.
Gallo, E., Fender, R.P. and Pooley, G.G.: 2003, *MNRAS* **344**, 60.
Heinz, S.: 2004, *MNRAS*, in press.
Heinz, S. and Sunyaev, R.A.: 2003, *MNRAS* **343**, L59.
Merloni, A., Heinz, S. and Di Matteo, T.: 2003, *MNRAS* **345**, 1057.

A TRANSITION IN THE ACCRETION PROPERTIES OF AGN

ANNALISA CELOTTI

S.I.S.S.A., via Beirut 2-4, Trieste, Italy;

E-mail: celotti@sissa.it

(Received 11 December 2004; accepted 1 June 2005)

Abstract. This contribution focuses on the evidence for a bimodality in the luminosity believed to be associated with the accretion process in AGN. In particular, it will be stressed that this behavior does seem to be present in an analogous way both in radio-loud and radio-quiet AGN, as inferred from samples selected in an independent way. The found bimodality can be naturally – although not uniquely – interpreted in the frame of the ADIOS solution for radiative inefficient accretion flows. The (so far) qualitative analogy with the behavior of XRB provides an interesting perspective to find a unique framework for the accretion and jet production in accreting black hole systems.

Keywords: active galactic nuclei, accretion

1. Introduction

The issue of the presence of supermassive black holes radiating well below the limits predicted within the standard solutions for gas accretion – for the inferred accretion rate – has been present for about 20 years (Rees et al., 1982). The last 10 years have seen a renewed focus on the problem due to more robust observational constraints, the evidence of the presence of supermassive black holes in basically all nearby spheroidal galaxies and the theoretical development of the early models (Fabian and Rees, 1995; Kormendy and Richstone, 1995; Narayan and Yi, 1995).

Within this frame, the aspect discussed here concerns the transition between AGN with relatively high accretion levels, with evidence of radiatively efficient flows, and the so-called low-luminosity AGN-inactive galaxies, in terms of the modality of the underlying transition. Clearly, several physical parameters are involved in determining such transition: the mass of the black hole (BH), the accretion rate and its time history, the angular momentum of the material accreting onto it – tied to the physical processes and structure of the accretion disc and possibly to the existence and nature of jets, the magnetic field configuration etc. Here we summarize the results of a phenomenological study of such aspect, which considers both the radio-loud and radio-quiet AGN populations: the analysis of both classes provides the opportunity of adopting different selection criteria and understanding whether/how the transition might be associated to the presence of collimated outflows, the BH mass, the host morphology.



2. Radio-Loud AGN

Several observational indicators point to extremely low accretion luminosities in low power radio galaxies (RG) and BL Lac objects compared to powerful RG and radio-loud quasars (e.g. Urry and Padovani, 1995 for a review, Celotti et al., 1998; O’Dowd et al., 2002). The radiated output in some RG is orders of magnitude lower than that corresponding to the (Bondi) accretion rate of the detected hot gas at the accretion radius, for a 10% radiative efficiency (Fabian and Rees, 1995; Pellegrini et al., 2003): in M87, the limit from X-rays corresponds to $\sim 10^{-7} L_{\text{Edd}}$, and $\sim 10^{-4}$ of the Bondi luminosity (Di Matteo et al., 2003).

In order to explore the transition to these levels of activity, Marchesini et al. (2004) considered a sample unbiased with respect to the nuclear emission. The extended, low frequency radio emission is considered to be an isotropic parameter. We thus selected a sample of sources selected on its basis, comprising low-power (FRI, Fanaroff and Riley, 1974) and high-power (FR II) RG and radio-loud quasars, where the former ones constitute a complete subsample (3C RG at $z < 0.3$).

The BH masses of these objects – estimated from the found correlation with the host bulge B-magnitude (Merritt and Ferrarese, 2001; Gebhardt et al., 2003; Häring and Rix, 2004) – span a relatively large range, but clustered around 10^8 – $10^9 M_{\odot}$. No systematic differences in their values are found between FRI, FR II RG and quasars. However, in terms of nuclear optical (HST) and bolometric luminosity Marchesini et al. (2004) not only find full agreement with the indications of low accretion levels in the low-power systems (see also Chiaberge et al., 2002), but its distribution appear to be bimodal. Even more so the distribution in the corresponding mass accretion rate in Eddington units $\dot{m} \equiv L/\epsilon L_{\text{Edd}}$ (where $\epsilon = L/\dot{M}c^2$ is the radiative efficiency) which shows two peaks around $\dot{m} \sim 10^{-3}$ and ~ 1 (for $\epsilon = 0.1$). Such bimodality is present also within the complete subsample of RG.

While the two peaks broadly comprise the FRI and FR II+quasar populations, respectively, the behavior of FR II narrow line RG reflects their spectroscopic (nuclear line) properties, in the sense that low excitation line RG behave as FRI, while high excitation FR II galaxies likely have obscured nuclei (as already proposed, e.g., by Laing et al., 1994; Jackson and Wall, 1999; Chiaberge et al., 2002, see also Marchesini et al., 2005). If the obscuration of the high excitation RG is taken into account, the distribution in \dot{m} reveals a region between the two peaks, extending for about two orders of magnitude, $\text{few } 10^{-5} \leq \dot{m} \leq \text{few } 10^{-1}$, which is characterized by a marked deficiency of sources (see Figure 1).

We refer to Marchesini et al. (2004) for a complete description of the assumptions and tests against significant biases and calibration uncertainties. In particular, the robustness of the results has been examined in relation to the adopted bolometric correction via the use of different theoretical spectral energy distributions and the comparison with the photoionizing luminosity required by the detected narrow emission lines. Here we stress that these checks turned out to be satisfactory (and

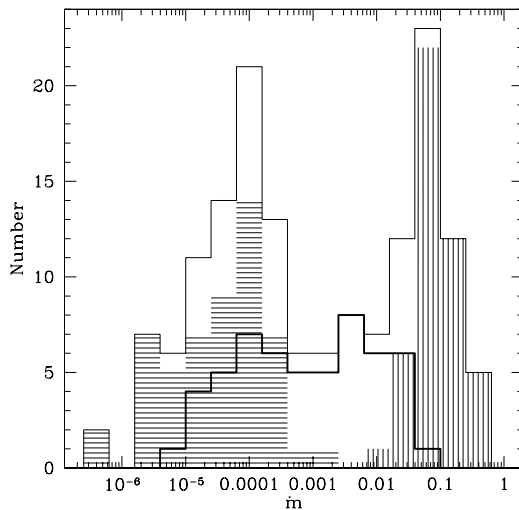


Figure 1. Distribution of m (for $\epsilon = 1$) for the radio-loud population (Marchesini et al., 2004). The objects are divided according to their nuclear line classification: horizontal shaded and vertical shaded areas represent FRI and radio-loud quasars, respectively and the thick line the FRII RG. Among the latter ones, absorbed sources (HEG) populate the region between the two peaks.

consistent with the adopted values) and possible observational biases turned out not be responsible for the deduced bimodality.

3. Radio-Quiet AGN

In the light of the earlier results and in order to further explore this issue it has been mandatory to examine what happens in other classes of AGN, to understand whether the shape of the distribution and the values at which a transition might occur depend on, e.g. the presence of powerful jets, the black hole mass, the morphology of the host, the adopted selection criteria.

Ballo and Celotti (2005) have thus considered the nuclear emission properties of a sample of radio-quiet sources,¹ with the main requirement of having some information on and covering the widest possible range of nuclear luminosity.

As a nuclear luminosity estimator we used narrow emission lines, as relatively unaffected by obscuration, and in particular lines of high ionization, which are believed to be tied to the nuclear radiative output and thus unbiased with respect to the contrast with the host galaxy emission.

¹The most striking case of low luminosity galactic nucleus in a radio-quiet system is that of Sgr A*, for which the observational limits indicate nuclear levels corresponding to a few $10^{-9} L_{\text{Edd}}$ of the associated black hole (e.g. Yuan et al., 2003).

The two main suitable samples with large enough statistics are the LINERs and Seyfert galaxies in the CfA Redshift Survey (Huchra and Burg, 1992), and the emission-line nuclei in the Palomar Survey (Ho et al., 1997). As individually these samples do not span a wide enough range in luminosity we combined the two catalogs, despite of the consequent loss in completeness (see e.g. Ho and Peng, 2001). Indeed, the (lack of) completeness of the sample has been a major issue in interpreting the robustness of the results. In order to assess its role on our findings we:

- (a) considered the effect of the selection criteria of the two samples on the nuclear properties – in particular, the host galaxy magnitude ranges of the two samples largely overlap and do not correlate with the observed $L_{[\text{O III}]}$;
- (b) examined and compared the results for these two samples with the properties of other smaller, uncomplete samples, but selected on the basis of completely different criteria and in different spectral bands (Maiolino and Rieke, 1995; Maiolino et al., 1997; Risaliti et al., 1999; Whittle, 1992; Mulchaey et al., 1996; Grupe et al., 2004; Rush et al., 1993). The properties of these various sources do follow the same behavior found for the CfA + Palomar sample.

As mentioned, in order to minimize the effect of absorption (and also adopt a nuclear indicator different from that used for the radio population) the nuclear luminosity has been estimated – via rather conventional assumptions – as that responsible for photoionizing the narrow line emitting gas, typically the $[\text{O III}]$ emission.²

From the optical bulge luminosity we inferred the BH masses, which clearly span a range lower than that of the radio-loud population, with a distribution peaking around 10^8 solar masses (the masses for the CfA and Palomar samples span a similar interval). A caveat worth reminding is that the correlations found between BH mass and properties of the bulge of the host galaxy (Merritt and Ferrarese, 2001; Gebhardt et al., 2000; Kormendy and Richstone, 1995) are mostly calibrated on spheroidal galaxies, while comparatively less is known about (lower mass) spiral bulges. For this reason and in order to look for a possible dependence on morphology, we examined the results also separately for late and early type hosts: the obtained distributions of $L_{[\text{O III}]}$ and \dot{m} are similar for the two morphological classes (within the low statistics).

In Figure 2 we show the $L_{[\text{O III}]}$ distribution for the sample, with sources divided according to their spectral type (type 1, 2, intermediate nuclei). This is bimodal, with LINERs and Seyfert located in different regions. Notably, the distribution of Seyfert 2 extends to values of $L_{[\text{O III}]}$ lower than that of Seyfert 1, and odds with

²Although the relation adopted to estimate the bolometric luminosity from $L_{[\text{O III}]}$ has been assessed only for Seyfert galaxies, the luminosities we find for LINERs well overlap with the values obtained from direct HST observations of nuclear emission of a few LINERs (Chiaberge et al., 2004).

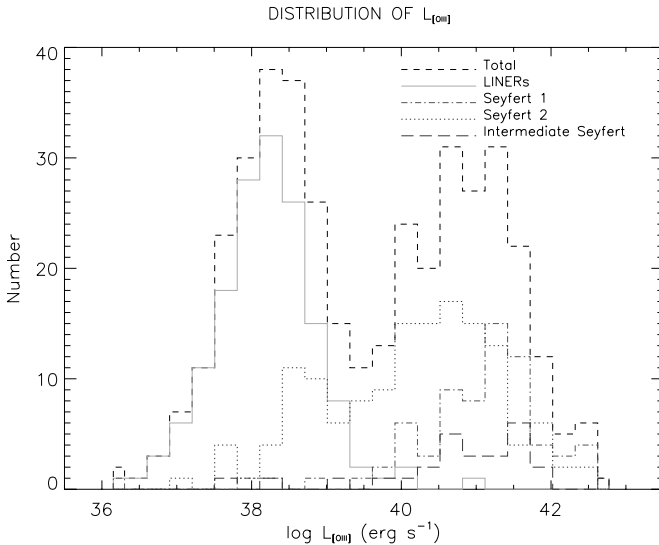


Figure 2. Distribution of $L_{[\text{OIII}]}$ for the sample of radio-quiet AGN (Ballo and Celotti, 2005). The objects are divided according to their nuclear spectral classification.

the zero-order unification scenario (as $L_{[\text{OIII}]}$ should be an isotropic indicator). The extension of such distribution (and the corresponding one in \dot{m}) for Seyfert 2 is confirmed by the type 2 sources in the Sloan Digital Sky Survey,³ although with a smaller fraction of sources at low values. The presence of type 2 Seyfert with typical luminosities lower than the type 1 population has been widely discussed in the literature. Among the proposed interpretations, a fraction of classified Seyfert 2 could be affected by absorption due to large scale, galactic dust (i.e. not nuclear) or orientation effects with respect to the nuclear dusty structure could play a role (e.g. Gu et al., 2001). We also note that six of the low luminosity Seyfert 2 in our sample have been studied by Panessa et al. (2004) in the X-ray band: on the basis of the low X-ray luminosity observed and using typical diagnostic diagrams, these authors suggest that they are misclassified LINERs.

Finally, in order to compare the results for radio-quiet and radio-loud objects, we estimated the values of \dot{m} . The corresponding distribution, clearly (statistically) bimodal (see Figure 3) presents a ‘minimum’ at an accretion rate fully consistent to that found for the radio-loud sources, even though not so sharp. If the Seyfert 2 sample were indeed contaminated by sources affected by large-scale dust and/or orientation effects, the minimum would be however expected to deepen.

³<http://www.mpa-garching.mpg.de/SDSS/>.

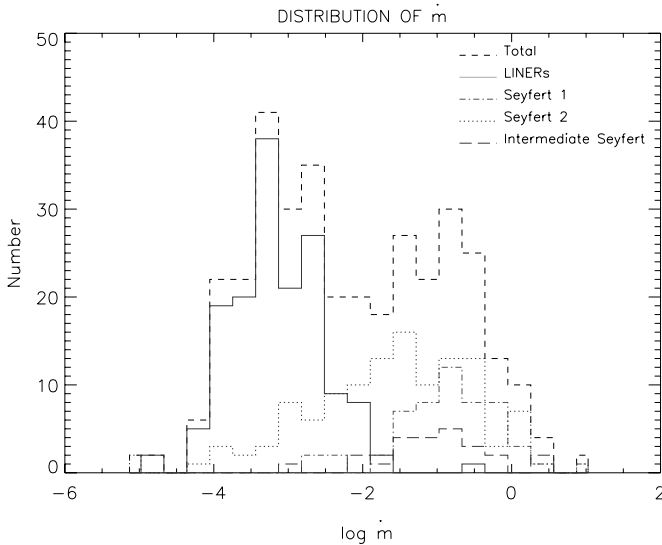


Figure 3. Distribution of \dot{m} ($\epsilon = 0.1$) for the sample of radio-quiet AGN (Ballo and Celotti, 2005). The objects are divided according to the nuclear line classification.

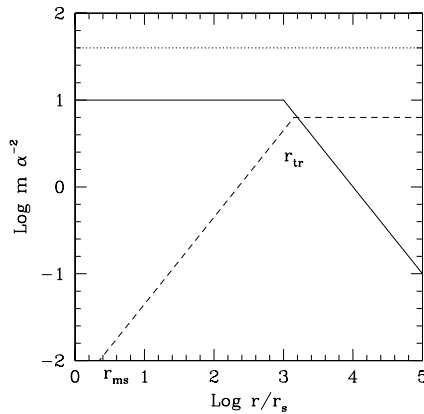


Figure 4. Schematic diagram (from Begelman and Celotti, 2004), showing the accretion rate as a function of radius, according to the ADIOS scenario. The solid curve shows the maximum accretion rate, \dot{m}_{crit} , for which a two-temperature hot flow is possible. A flow with $\dot{m} > \dot{m}_{\text{crit,max}}$ (dotted line) exhibits a thin, radiative disk at all radii, and conserves mass. It is conjectured that flows with $\dot{m} < \dot{m}_{\text{crit,max}}$ (dashed line) become hot within $r \sim 10^3$ and lose most of their mass before reaching the black hole.

4. Conclusions

There is evidence for a bimodal behavior in the nuclear emission in radio-loud and radio-quiet nearby sources, for samples selected on independent criteria.

The bimodality in the \dot{m} distributions appear intriguingly similar, with a minimum/transition at $\dot{m} \sim 10^{-2}$ (for $\epsilon = 0.1$). The low \dot{m} ‘peak’ comprises low excitation narrow line RG, LINERs and some low ionization Seyfert 2. The similarity found between the behavior of radio-loud and radio-quiet sources, spanning a different range of BH masses and having different host galaxies, thus suggests that such bimodal transition might indeed occur in all accreting systems.

As briefly discussed in Marchesini et al. (2004) and Ballo and Celotti (2005), one can envisage different processes leading to such a distribution and in particular to a transition and a gap in the luminosity/inferred accretion rate. A relatively rapid transition in the accretion rate between the high and low \dot{m} regimes or the presence of an unstable disc configuration at intermediate \dot{m} are possibilities. An inefficient jet formation process at intermediate \dot{m} (e.g. Meier, 2001) appears disfavored by the presence of a dichotomy also in radio-quiet systems. Clearly, a further physical reason for such results can be the transition of the flow to a radiatively inefficient regime at accretion rates similar to what estimated. Indeed, Begelman and Celotti (2004) argued that a bimodal luminosity distribution with a significant gap of sources at intermediate regimes – as clear in the case of radio-loud sources – is a natural consequence of the adiabatic inflow–outflow (ADIOS) scenario (Blandford and Begelman, 1999, 2004). The uncertainties on the determination of \dot{m} and the incompleteness of the radio-quiet sample do not allow (so far) to set more robust/quantitative constraints on the physics of such flows or their accretion history.

Within the spirit and aims of the conference, such results qualitatively invoke the analogy with XRB systems, and their corresponding state transitions. An even deeper similarity might be possible, including not only the accretion disc regime but also its link with the presence and nature of jets.

Acknowledgements

I would like to thank Danilo Marchesini and Lucia Ballo for their collaboration and the Organizers for setting up this interesting meeting, and acknowledge the Italian MIUR and INAF for financial support.

References

- Ballo, L. and Celotti, A.: 2004, *MNRAS*, submitted for publication.
 Begelman, M. and Celotti, A.: 2004, *MNRAS* **352**, L45.
 Blandford, R.D. and Begelman, M.C.: 1999, *MNRAS* **303**, L1 (BB99).
 Blandford, R.D. and Begelman, M.C.: 2004, *MNRAS* **349**, 68.
 Celotti, A., Fabian, A.C. and Rees, M.J.: 1998, *MNRAS* **293**, 239.
 Chiaberge, M., Capetti, A. and Celotti, A.: 2002, *A&A* **394**, 791.
 Chiaberge, M., Capetti, A. and Macchetto, F.: 2004, submitted for publication.
 Di Matteo, T., Allen, S.W., Fabian, A.C., Wilson, A.S. and Young, A.J.: 2003, *ApJ* **582**, 133.

- Fabian, A.C. and Rees, M.J.: 1995, *MNRAS* **277**, L55.
- Fanaroff, B.L. and Riley, J.M.: 1974, *MNRAS* **167**, 31.
- Gebhardt, K., et al.: 2000, *ApJ* **539**, L13.
- Gebhardt, K., et al.: 2003, *ApJ* **583**, 92.
- Grupe, D., Wills, B.J., Leighly, K.M. and Meusinger, H.: 2004, *AJ* **127**, 156.
- Gu, Q., Maiolino, R. and Dultzin-Hacyan, D.: 2001, *A&A* **366**, 765.
- Häring, N. and Rix, H.W.: 2004, *ApJ* **604**, L89.
- Ho, L.C., Filippenko, A.V. and Sargent, W.L.W.: 1997, *ApJS* **112**, 315.
- Ho, L.C. and Peng, C.Y.: 2001, *ApJ* **555**, 650.
- Huchra, J. and Burg, R.: 1992, *ApJ* **393**, 90.
- Jackson, C.A. and Wall, J.V.: 1999, *MNRAS* **304**, 160.
- Kormendy, J. and Richstone, D.: 1995, *ARA&A* **33**, 581.
- Laing, R.A., Jenkins, C.R., Wall, J.V. and Unger, S.W.: 1994, in: G.V. Bicknell, M.A. Dopita and P.J. Quinn (eds.), *The First Stromlo Symposium: The Physics of Active Galaxies, ASP Conference Series*, Vol. 54, p. 201.
- Maiolino, R. and Rieke, G.H.: 1995, *ApJ* **454**, 95.
- Maiolino, R., Ruiz, M., Rieke, G.H. and Papadopoulos, P.: 1997, *ApJ* **485**, 552.
- Marchesini, D., Celotti, A. and Ferrarese, L.: 2004, *MNRAS* **351**, 733.
- Marchesini, D., Capetti, A. and Celotti, A.: 2005, *A&A*, in press.
- Meier, D.L.: 2001, *ApJ* **548**, L9.
- Merritt, D. and Ferrarese, L.: 2001, in: J.H. Knapen, J.E. Beckman, I. Shlosman and T.J. Mahoney (eds.), *The Central Kiloparsec of Starbursts and AGN: The La Palma Connection, ASP Conference Series*, Vol. 249, p. 335.
- Mulchaey, J.S., Wilson, A.S. and Tsvetanov, Z.: 1996, *ApJS* **102**, 309.
- Narayan, R. and Yi, I.: 1995, *ApJ* **444**, 231.
- O'Dowd, M., Urry, C.M. and Scarpa, R.: 2002, *ApJ* **580**, 960.
- Panessa, F., et al.: 2004, *American Astronomical Society, HEAD meeting*, Vol. 8, p. 26.10.
- Pellegrini, S., Venturi, T. Comastri, A., Fabbiano, G., Fiore, F., Vignali, C., Morganti, R. and Trinchieri, G.: 2003, *ApJ* **585**, 677.
- Rees, M.J., Begelman, M.C., Blandford, R.D. and Phinney, E.S.: 1982, *Nature* **295**, 17.
- Risaliti, G., Maiolino, R. and Salvati, M.: 1999, *ApJ* **522**, 157.
- Rush, B., Malkan, M.A. and Spinoglio, L.: 1993, *ApJS* **89**, 1.
- Urry, C.M. and Padovani, P.: 1995, *PASP* **107**, 803.
- Whittle, M.: 1992, *ApJS* **79**, 49.
- Yuan, F., Quataert, E. and Narayan, R.: 2003, *ApJ* **598**, 301.

JET-DISC COUPLING IN THE ACCRETING BLACK HOLE XTE J1118+480*

JULIEN MALZAC¹, ANDREA MERLONI² and ANDREW C. FABIAN³

¹*Centre d'Etude Spatiale des Rayonnements, (CNRS/UPS/OMP), 9, Avenue du Colonel Roche, BP4346, 31028 Toulouse Cedex 4 France*

²*Max-Planck-Institut für Astrophysik, Garching, Germany*

³*Institute of Astronomy, Cambridge, United Kingdom; E-mail: malzac@cesr.fr*

(Received 22 October 2004; accepted 1 June 2005)

Abstract. We interpret the rapid correlated UV/optical/X-ray variability of XTE J1118+480 as a signature of the coupling between the X-ray corona and a jet emitting synchrotron radiation in the optical band. We propose a scenario in which the jet and the X-ray corona are fed by the same energy reservoir where large amounts of accretion power are stored before being channelled into either the jet or the high energy radiation. This time-dependent model reproduces the main features of the rapid multi-wavelength variability of XTE J1118+480. A strong requirement of the model is that the total jet power should be at least a few times larger than the observed X-ray luminosity, implying a radiative efficiency for the jet $\epsilon_j \sim 3 \times 10^{-3}$. This would be consistent with the overall low radiative efficiency of the source. We present independent arguments showing that the jet probably dominates the energetic output of all accreting black holes in the low-hard state.

Keywords: accretion, black-hole physics, star: XTE J1118+480, X-rays: binaries

1. Introduction

The X-ray nova XTE J1118+480, was discovered by the Rossi X-Ray Timing Explorer (*RXTE*) All-Sky Monitor (*ASM*) on 2000 March 29 (Remillard et al., 2000). The optical spectrophotometry proved a low-mass X-ray binary system containing a black hole of at least six solar masses (McClintock et al., 2001a; Wagner et al., 2001). The interstellar extinction towards the source is exceptionally low (Garcia et al., 2000). This fact allowed an unprecedented wavelength coverage (Mauche et al., 2000; Hynes et al., 2000; McClintock et al., 2001b; Hynes et al., 2003; Chaty et al., 2003 and references therein). In the radio to optical bands, a strong non-thermal component was associated with synchrotron emission from a powerful jet or outflow (Fender et al., 2001). In the optical to EUV bands the spectral energy distribution is dominated by a thermal component from the accretion disc. The X-ray emission consists of a typical powerlaw spectrum with photon index $\Gamma \sim 1.8$. Such a spectrum is generally associated with Comptonisation in the hot inner part of the disc or corona. During the whole outburst duration, the X-ray

*Partially supported by PPARC.



properties of the source, as well as the presence of strong radio emission, were typical of black-hole binaries in the hard state.

2. Optical X-ray Correlations

Interestingly, fast optical and UV photometry allowed by the weak extinction, revealed a rapid optical/UV flickering presenting complex correlations with the X-ray variability (Kanbach et al., 2001; Hynes et al., 2003, hereafter K01 and H03, respectively). This correlated variability cannot be caused by reprocessing of the X-rays in the external parts of the disc. Indeed, the optical flickering occurs on average on shorter time-scales than the X-ray one (K01), and reprocessing models fail to fit the complicated shape of the X-ray/optical cross correlation function (H03). Spectrally, the jet emission seems to extend at least up to the optical band (McClintock et al., 2001b; Chaty et al., 2003, hereafter C03), although the external parts of the disc may provide an important contribution to the observed flux at such wavelengths. The jet activity is thus the most likely explanation for the rapid observed optical flickering. For this reason, the properties of the optical/X-ray correlation in XTE J1118+480 might be of primary importance for the understanding of the jet-corona coupling and the ejection process.

The simultaneous optical/X-ray observations are described at length in a number of papers (K01; Spruit and Kanbach, 2001; H03; Malzac et al., 2003, hereafter M03). As discussed in these works, the observations are very challenging for any accretion model. The most puzzling pieces of evidence are the following: (a) the optical/X-ray Cross-Correlation Function (CCF) shows the optical band lagging the X-ray by 0.5 s, but with a dip 2–5 s in advance of the X-rays (K01); (b) the correlation between X-ray and optical light curves appears to have time scale-invariant properties: the X-ray/optical CCF maintains a similar, but rescaled, shape on time scales ranging at least from 0.1 s to few tens of seconds (M03); (c) the correlation does not appear to be triggered by a single type of event (dip or flare) in the light curves; instead, as was shown by M03, optical and X-ray fluctuations of very different shapes, amplitudes and time scales are correlated in a similar way, such that the optical light curve is related to the time derivative of the X-ray one. Indeed, in the range of time scales where the coherence is maximum, the optical/X-ray phase lag are close to $\pi/2$, indicating that the two lightcurves are related through a differential relation. Namely, if the optical variability is representative of fluctuations in the jet power output P_j , the data suggest that the jet power scales roughly like $P_j \propto -\frac{dP_x}{dt}$, where P_x is the X-ray power.

3. The Energy Reservoir Model

Malzac et al. (2004, hereafter MMF04) have shown that the complex X-ray/optical correlations could be understood in terms of an energy reservoir model. In this

picture, it is assumed that large amounts of accretion power are stored in the accretion flow before being channelled either into the jet (responsible for the variable optical emission) or into particle acceleration/heating in the Comptonising region responsible for the X-rays. MMF04 have developed a time-dependent model which is complicated in operation and behaviour. However, its essence can be understood using a simple analogue: Consider a tall water tank with an input pipe and two output pipes, one of which is much smaller than the other. The larger output pipe has a tap on it. The flow in the input pipe represents the power injected in the reservoir P_i , that in the small output pipe the X-ray power P_x and in the large output pipe the jet power P_j . If the system is left alone the water level rises until the pressure causes $P_i = P_j + P_x$. Now consider what happens when the tap is opened more, causing P_j to rise. The water level and pressure (proportional to E) drop causing P_x to reduce. If the tap is then partly closed, the water level rises, P_j decreases and P_x increases. The rate P_x depends upon the past history, or integral of P_j . Identifying the optical flux as a marker of P_j and the X-ray flux as a marker of P_x we obtain the basic behaviour seen in XTE J1118+480. In the real situation, we envisage that the variations in the tap are stochastically controlled by a shot noise process. There are also stochastically controlled taps on the input and other output pipes as well. The overall behaviour is therefore complex. The model shows however that the observed complex behaviour of XTE J1118+480 can be explained by a relatively simple basic model involving several energy flows and an energy reservoir. This simple model is largely independent of the physical nature of the energy reservoir. In a real accretion flow, the reservoir could take the form of either electromagnetic energy stored in the X-ray emitting region, or thermal (hot protons) or turbulent motions. The material in the disc could also constitute a reservoir of gravitational or rotational energy behaving as described above. In a stationary flow, the extracted power $P_j + P_x$ would be perfectly balanced by the power injected, which is, in the most general case, given by the difference between the accretion power and the power advected into the hole and/or stored in convective motions: $P_i \simeq \dot{M}c^2 - P_{\text{adv,conv}}$. However, observations of strong variability on short time scale clearly indicate that the heating and cooling of the X-ray (and optical) emitting plasma are highly transient phenomena, and the corona is unlikely to be in complete energy balance on short time scales. We therefore introduce a time-dependent equation governing the evolution of its total energy E :

$$\dot{E} = P_i - P_j - P_x, \quad (1)$$

and we assume that all the three terms on the right-hand side are time-dependent. The optical variability is produced mainly from synchrotron emission in the inner part of the jet at distances of a few thousands gravitational radii from the hole. We assume that at any time the optical flux O_{pt} (resp. X-ray flux) scales like the jet power P_j (plasma heating power P_x). We introduce the instantaneous dissipation

rates K_j and K_x :

$$P_j(t) = K_j(t)E(t), \quad P_x(t) = K_x(t)E(t), \quad (2)$$

For a specific set of parameters we generate random independent fluctuations (time series) for K_x , K_j and P_i , solve the time evolution of the energy reservoir E and then use the solution to derive the the resulting optical and X-ray light curves (see MMF04 for details).

Combining Eqs. (1) and (2) we obtain the following relation for the total instantaneous jet power:

$$P_j = P_i - \left(1 + \frac{\dot{K}_x}{K_x^2}\right)P_x - \dot{P}_x/K_x. \quad (3)$$

We can see from this equation that the differential scaling $P_j \propto -\dot{P}_x$, observed in XTE J1118+480, will be rigorously reproduced provided that: (1) K_x is a constant; (2) $P_i - P_x$ is a constant. It is physically unlikely that those conditions will be exactly verified. In particular, P_x is observed to have a large RMS amplitude of variability of about 30%. However, the observed differential relation holds only roughly and only for fluctuations within a relatively narrow range of time-scales 1 – 10 s. Therefore, the above conditions need only to be fulfilled approximatively and for low frequency fluctuations (> 1 s). In practice, the following requirements will be enough to make sure that the low frequency fluctuations of the right-hand side of Eq. (3) are dominated by \dot{P}_x :

- $P_x \ll P_i$, implying that the jet power, on average, dominates over the X-ray luminosity;
- the amplitude of variability of K_x and P_i in the 1–10 s range is low compared to that of P_j . In other words the 1–10 s fluctuations of the system are mainly driven by the jet activity, implying that the mechanisms for dissipation in the jet and the corona occur on quite different time scales.

Figure 1 shows the results of a simulation matching the main timing properties of XTE J1118+480. In this simulation jet power was set to be 10 times larger than the X-ray power. The model produces an X-ray power spectrum with a plateau up to ~ 0.1 Hz and a power-law component with slope ~ 1.4 above that frequency, with most of the X-ray variability occurring around 0.1 Hz. The optical PDS power-law has a flatter slope (~ 1) up to 1 Hz and then softens to a slope similar to that of the X-ray PDS. The resulting optical ACF is significantly narrower than the X-ray one. The full-width-at-half-maximum (FWHM) of the two ACFs differs by a factor > 2 . The overall coherence is low (< 0.4): reaching a maximum in the 0.1–1 Hz range and decreasing rapidly both at lower and higher frequency. The phase-lags are close to $\pi/2$ in the 0.1–1 Hz range and increase from 0 at low frequencies up to

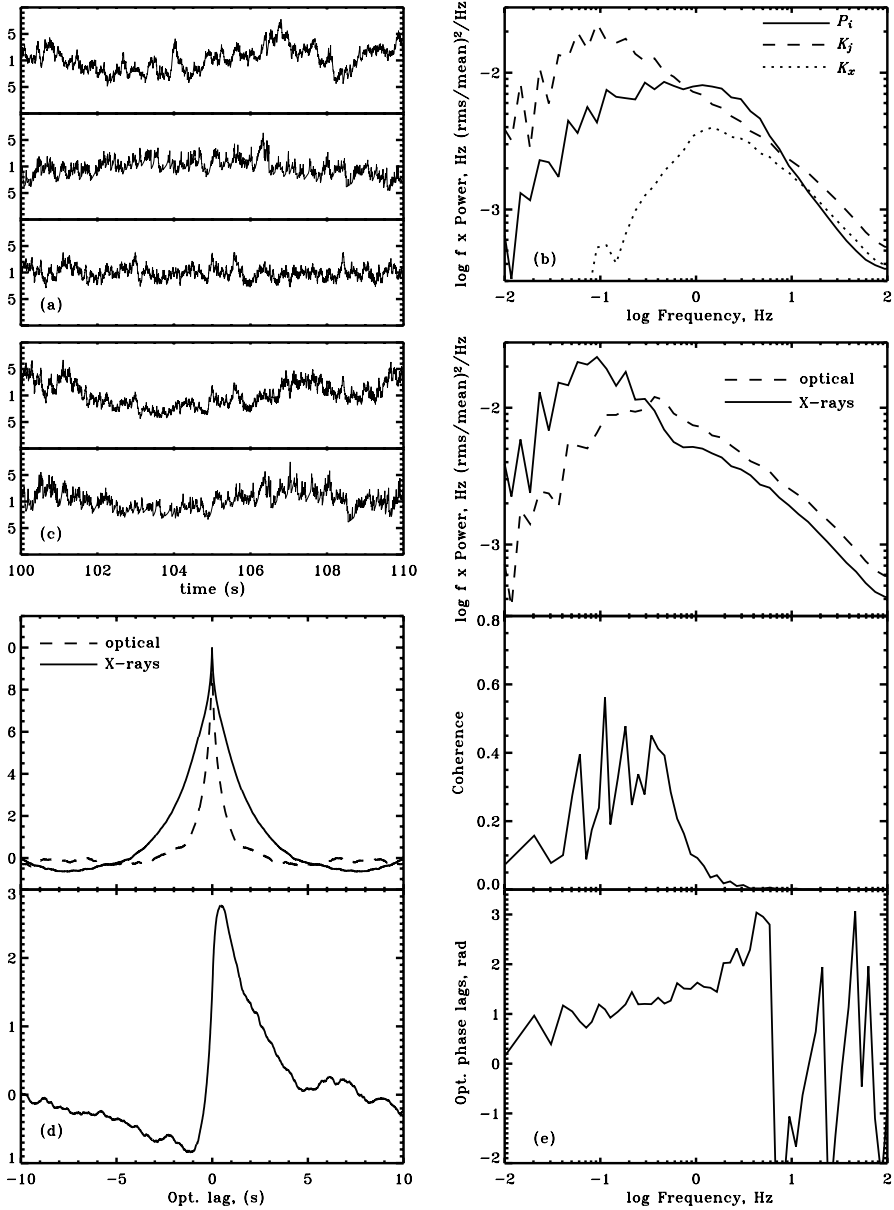


Figure 1. Sample input time series (panel a) and power spectra (panel b) of P_i , K_j , K_x , resulting X-ray and optical fluxes light curves (panel c), X-ray/optical autocorrelation and cross-correlation functions (panel d), power spectra, coherence and phase-lags (panel e).

π at around 6 Hz. At higher frequencies the phase lags spectrum is characterized by large oscillations. Finally the resulting CCF rises very quickly at positive optical lags, peaks around 0.5 s (this is the post-peak) and then declines slowly at larger lags. The two bands appear to be anti-correlated at negative optical lags indicating

a systematic optical dip 1–2 s before the X-rays reach their maximum (pre-dip). All these characteristics are observed in XTE J1118+480.

4. Jet Dominance in XTE J1118+480 and Other Low-Luminosity Sources

The total mass accretion rate onto the black hole can be estimated from the observed luminosity of the cold disc component which in the case of XTE J1118+480 can be estimated from fits to the optical, UV and EUV spectra (see e.g. Chaty et al., 2003). The result depends on several assumptions regarding the geometry and the physical mechanisms for energy dissipation in the disc and the hot comptonising medium. However, for reasonable parameters, the estimated accretion rate is much larger than the observed bolometric luminosity (by at least a factor of 10). The important issue, however, would be to determine whether the missing accretion power escapes the system in the (low radiative efficiency) jet or in other forms of non-radiative losses, such as a slow wind, or large-scale convective motions, or advection into the black hole. The answer to this question resides in the exact determination of the jet kinetic power. Unfortunately, there are major uncertainties in this determination, mainly because the jet radiative efficiency is not known. The jet is expected to be a poor radiator because most of the energy is lost in adiabatic expansion. Thus, although the radiation from the jet represents a small fraction of the bolometric luminosity the jet could dominate the energetics. For the case of XTE J1118+480, typical efficiency $\epsilon_j \sim 0.01$ would already imply that the total jet power dominates over the X-ray luminosity. As discussed above, the analysis of our time-dependent modeling strongly requires $f_x \lesssim 0.1$, corresponding to a jet efficiency $\epsilon_j \lesssim 3 \times 10^{-3}$.

There are additional independent arguments in favour of jet dominance in low/hard state sources and in XTE J1118+480 in particular. Based on the observed radio flux (L_R) and X-ray correlation observed in hard states sources (Falcke and Biermann, 1996; Gallo et al., 2003), as well as on standard synchrotron formulae (Heinz and Sunyaev, 2003), Fender et al. (2003, hereafter FGP03) have shown that, provided that advection into the black-hole horizon and/or convective motions do not store a large fraction of the accretion power, there should exist a critical accretion rate, \dot{m}_{cr} , below which an accreting black hole is jet-dominated. The exact value for the critical accretion rate could be inferred from the observations, if we knew the total jet power at a certain X-ray luminosity, and is given by $\dot{m}_{\text{cr}} = 2P_j^2/L_x$, corresponding to a critical X-ray luminosity $L_{x,\text{cr}} = \dot{m}_{\text{cr}}/2$. Fender et al. (2001) derived a lower limit for the jet to X-ray power ratio in XTE J1118+480: $P_j/L_x = 0.2$, and FGJ03 used this conservative estimates to determine the value of the critical rate $\dot{m}_{\text{cr}} \simeq 7 \times 10^{-5}$. However, such a low value of the critical luminosity leads to several problems.

First, as shown in FGJ03, during the transition from a disc to a jet-dominated state, the dependence of the X-ray luminosity on the accretion rate changes from being $L_x \propto \dot{m}^2$, the right scaling for *radiatively inefficient flows*, to $L_x \propto \dot{m}$, the

scaling for *radiatively efficient flows* (see Figure 1 of FGJ03). This would imply that with $L_x \sim 10^{-3}$, XTE J1118+480 should be a *radiatively efficient* system. As discussed above, there is however strong observational evidence of the contrary.

Furthermore, black holes in the hard state should show some kind of spectral transition in the X-ray band at the critical luminosity $L_{x,cr} \sim 3 \times 10^{-5}$, due to the drastic changes in emission mechanisms that are needed to account for the different scalings of L_x with the accretion rate. The observations of low/hard-state sources at such low luminosities are few and hard to perform, however no indication of any dramatic spectral change in any hard state source down to quiescent level has ever been reported (Kong et al., 2002; Hameury et al., 2003). In fact, the only physical transition that we do actually observe is the transition between the hard and the soft state that occurs at luminosities of at least a few percent of Eddington luminosity (Maccarone 2003). We believe that, if the above-mentioned difficulties are to be solved, then \dot{m}_{cr} has to correspond to luminosities that are comparable to, or larger than, hard-to-soft state transition luminosities. For the case of XTE J1118+480, instead of using the lower limit for the jet to X-ray power ($P_j/L_x = 0.2$), we can adopt the much larger value $P_j/L_x \sim 10$ required by our variability model. Then we find $\dot{m}_{cr} \sim 0.2$, involving a transition at $L_{x,cr} = \dot{m}_{cr}/2 \sim 0.1$. This is in agreement with the idea that the transition from jet dominated to X-ray dominated states occurs at luminosities similar or slightly higher than the hard to soft state transition. Thus, if the arguments of FGJ03 are correct, an important consequence of the jet dominance in XTE J1118+480 is that *all hard state sources are jet-dominated* (in the sense that the jet power dominates over the X-ray power). This jet dominance also implies that *all hard state sources should be radiatively inefficient*. The reason for this inefficiency could be advection into the jet as well as advection into the black hole.

5. Conclusions

The puzzling optical/X-ray correlations of XTE J1118+480, can be understood in terms of a common energy reservoir for both the jet and the Comptonizing electrons. Any energy reservoir model for XTE J1118+480 requires that the total jet power dominates over the X-ray luminosity. Following the same line of arguments as FGJ03, we showed that this situation is likely and probably represents a common feature of all black holes in the low-hard state.

References

- Celotti, A. and Fabian, A.C.: 1993, *MNRAS* **264**, 228.
 Chaty, S., Haswell, C.A., Malzac, J., Hynes, R.I., Schrader, C.R. and Cui, W.: 2003, *MNRAS* **346**, 689.
 Falcke, H. and Biermann, P.L.: 1996, *A&A* **308**, 321.

- Fender, R.P., Gallo, E. and Jonker, P.G.: 2003, *MNRAS* **343**, L99.
- Gallo, E., Fender, R.P. and Pooley, G.G.: 2003, *MNRAS* **344**, 60.
- Hameury, J.-M., Barret, D., Lasota, J.-P. et al.: 2003, *A&A* **399**, 631.
- Hynes, R.I. et al.: 2003, *MNRAS* **345**, 292.
- Kanbach, G., Straubmeier, C., Spruit, H.C. and Belloni, T.: 2001, *Nature* **414**, 180.
- Kong, A.K.H., McClintock, J.E., Garcia, M.R., Murray, S.S. and Barret, D.: 2002, *ApJ* **570**, 277.
- Maccarone, T.J.: 2003, *A&A* **409**, 697.
- Malzac, J., Belloni, T., Spruit, H.C. and Kanbach, G.: 2003, *A&A* **407**, 335.
- Malzac, J., Merloni, A. and Fabian, A.C.: 2004, *MNRAS* **351**, 253.
- McClintock, J.E., Haswell, C.A., Garcia, M.R. et al.: 2001b, *ApJ* **555**, 477.
- Remillard, R., Morgan, E., Smith, D. and Smith, E.: 2000, *IAU Circ.* **7389**, 2.
- Spruit, H.C. and Kanbach, G.: 2002, *A&A* **391**, 225.

ARE 3C 120 AND OTHER ACTIVE GALACTIC NUCLEI OVERWEIGHT MICROQUASARS?

ALAN P. MARSCHER

*Institute for Astrophysical Research, Boston University, 725 Commonwealth Avenue, Boston,
MA 02215, USA; E-mail: marscher@bu.edu*

(Accepted 1 June 2005)

Abstract. The appearance of superluminal radio knots follows drops in the X-ray flux in the FR1 radio galaxy 3C 120 and possibly the FR2 source 3C 111. This corresponds in a very general way to the behavior of the X-ray binary GRS 1915 + 105, but the light curves of the microquasar are much richer in detail. Starting in 2003.7, the character of the radio and X-ray light curves of 3C 120 changed, perhaps signaling a new stage of activity. I discuss here what one might expect when a microquasar is scaled up to AGN dimensions, and compare this with what we see in 3C 120. There is a mismatch between expectations and observations.

Keywords: active galactic nuclei, jets, accretion disks, black holes

1. Introduction

The discovery that some black-hole binary systems have relativistic jets has led to their nickname “microquasars” as well as to the hope that we might test our models for radio-loud active galactic nuclei (AGNs) by observing these nearby cousins (Mirabel and Rodríguez, 1994). Comparisons are hampered, though, by the utter dominance of the jet emission in blazars and the wimpiness of the jets in Seyfert galaxies, the AGNs that most resemble black-hole binaries at X-ray energies. Fortunately, there are a few broad-line radio galaxies whose jets lie at somewhat wider angles to our line-of-sight than is the case for blazars. These have optical and X-ray properties similar to Seyfert galaxies and microquasars, as well as prominent radio jets that display strong variability and superluminal apparent motions.

Along with a team of collaborators, I have been studying the FR1 radio galaxy 3C 120 extensively since 1997 in order to determine whether its behavior bears any resemblance to that of microquasars. Since March 2004 we have been observing the FR2 radio galaxy 3C 111 as well. The availability of two superb instruments—the *Rossi* X-ray Timing Explorer (RXTE) and the Very Long Baseline Array (VLBA)—makes it possible to engage in long-term monitoring programs with outstanding time coverage. The resulting X-ray light curves are exquisitely detailed, as are the ever-changing images at high radio frequencies.



As I describe below, there is an association of short-term low-hard X-ray states with injections of energy into the jet in 3C 120—and possibly in 3C 111 as well—that is reminiscent of the X-ray binary GRS 1915 + 105. The scaling of time scales with black-hole mass is not linear, however, and the rich detail of the X-ray light curves of the microquasar is either masked or absent in the radio galaxies. In other words, we still have a lot to learn before we can relate the phenomena at opposite ends of the luminosity, mass, and size scale.

2. The Long-Term Behavior of 3C 120

Early results (Marscher et al., 2002) demonstrated that each appearance of a superluminal knot in the radio jet of 3C 120 is preceded by a significant dip in the 2–20 keV X-ray flux. Under the premise that the X-rays are predominantly from the accretion disk or its immediate environs (e.g., a corona, a hot wind, or the base of the jet), some disturbance in the central engine seems literally to send a shock wave down the jet. This is the same scenario as that imagined to explain similar connections between transitions to low-hard X-ray states and energization of the jet in the microquasar GRS 1915 + 105 (Mirabel and Rodríguez, 1998, and papers by Fender and others in these proceedings).

Figure 1 displays the X-ray light curve we have accumulated since resuming our monitoring program in 2002. The date of each superluminal “ejection”—the time of coincidence of the centroid of a moving knot with the position of the core as determined from a linear fit to a plot of core-knot separation versus time—is marked. There were two periods of low X-ray flux between 2002.15 and 2003.7: a long dip in early 2002 and a double-dip in summer 2003. The X-ray spectrum was flatter during the dips than during most high-flux states. The onset of the first dip preceded the appearance of a bright superluminal radio knot with a delay of 0.1 ± 0.03 yr. The pair of dips in 2003 were followed by the ejection in rapid succession (1.5-month interval) of two bright superluminal knots. The apparent velocities of the knots are $4.7c$ (for a Hubble constant of $70 \text{ km s}^{-1} \text{ Mpc}^{-1}$), similar to those measured during the period 1997–1999 (Gómez et al., 2001; Marscher et al., 2002). The 37-GHz flux rose dramatically from 2003.65 to 2003.7 (Ogle et al., 2004) to herald the ejection of the first knot after the double dip, and then maintained a high level well into 2004. The delay of 0.04 year between the start of the 37-GHz flare and the coincidence of the knot with the core probably corresponds to either (1) half the light-travel time across the knot, (2) the time it takes for the knot to become energized (or optically thin) as it enters the core region, or (3) the bulk acceleration time of the knot. For any of these, the time interval measured in the observer’s frame must be corrected for the Doppler effect.

I associate the start of the 37-GHz flare at 2003.65 with the edge of the highly energized jet flow created by an event in or near the accretion disk that caused the X-ray dip starting at 2003.50. We can then infer a travel time of 0.15 year between

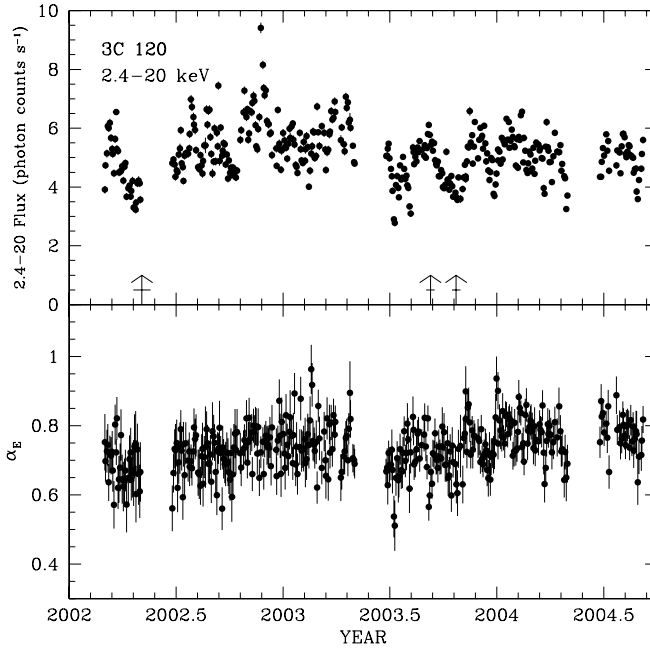


Figure 1. X-ray light curve and energy spectral index versus time of 3C 120. Note the tendency for the spectrum to be flatter during periods of lower flux. The extrapolated times when the positions of superluminal radio knots coincided with the core are marked by vertical arrows, with horizontal bars giving the uncertainty in the time of coincidence.

the disk and the position of the 43-GHz compact radio core as measured in our frame. This is 1.5 times longer than the value derived in Marscher et al. (2002) from the minima of the X-ray dips. The new determination should be more appropriate. We therefore raise the estimate of the displacement between the central engine and the ~ 40 -GHz core to >0.6 pc. This corresponds to the distance traveled down the jet in 0.15 year: $4.7 \times 0.15 \times (\sin \theta)^{-1}$ lt-year, where the angle between the velocity vector and the line-of-sight $\theta \leq 20^\circ$ (Gómez et al., 2001; Jorstad et al., 2005). If the jet accelerates or if the viewing angle $< 20^\circ$, the core must be farther downstream from the black hole. Ogle et al. (2005) report that the flux density at 250 GHz was very high before the onset of the 37-GHz flare, hence the “true” core—where the jet plasma is energetically excited or where it reaches its asymptotic flow velocity (Marscher, 1995), as opposed to the boundary where the optical depth ~ 1 at the frequency of observation—is probably closer to the black hole.

From the appearance of the first superluminal knot in 2003.7 until 2004.3, the X-ray flux varied more smoothly than seen previously. This conclusion is supported by a change in the break in the structure function, which occurs at 13 days during most of the observations but lengthens to 37 days during the above interval. Furthermore, the X-ray flux is moderately correlated (with a coefficient ~ 0.5) with the 37-GHz radio flux (Ogle et al., 2005) over the same time range, with zero lag. This

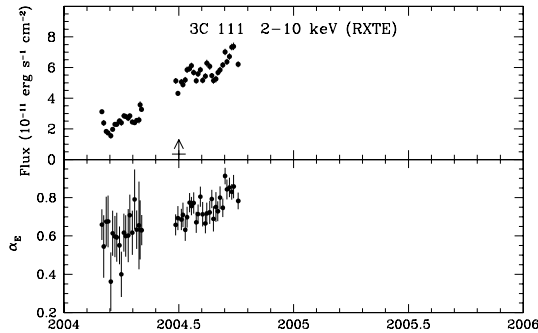


Figure 2. X-ray light curve and energy spectral index versus time of 3C 111. The extrapolated time when the positions of a superluminal radio knot coincided with the core is marked by a vertical arrow, with horizontal bars giving the uncertainty in the time of coincidence.

implies that a substantial fraction of the X-rays observed during this period may have been emitted by the jet near the radio core region, perhaps via inverse Compton scattering. In this case, the iron line equivalent width should have been lower, a possibility that we are currently checking by re-examining our RXTE database. The X-ray continuum has been flatter since early 2002 (α mostly in the range of 0.6–0.8) than in 1997 and 1999 (energy spectral index α_E from 0.8 to 1.0; Marscher et al., 2002) despite similar flux levels. This could be a sign of either a stronger jet-to-disk emission ratio or a physical change in the primary X-ray emission region.

3. The FR2 Radio Galaxy 3C 111

Figure 2 presents the X-ray light curve we have obtained thus far for 3C 111. After an initial decline by a factor ~ 2 , the flux has risen almost linearly by a factor ~ 4 over 6 months up to the time of writing. A bright superluminal knot with flux density at 43 GHz comparable to that of the core emerged in July 2004, with a “birth” date 0.3 year after the minimum in the X-ray light curve. The continuation of our monitoring program will determine whether this is an X-ray dip/superluminal ejection episode similar to those in 3C 120 but on a larger size scale, or an outburst of X-rays associated with the new knot. In support of the dip interpretation is the essentially linear relation between X-ray spectral index and flux. This is similar to, but even more pronounced than, the spectral flattening observed during the X-ray dips in 3C 120 (see earlier section).

4. Discussion and Conclusions

Our observations have established an association between low X-ray states and enhanced flow of energy into the relativistic jet in at least one radio galaxy, 3C 120.

Although this is to zeroth order what is seen in the microquasar GRS 1915 + 105 (e.g., Mirabel and Rodríguez, 1998), the details are quite different. The intensity of the jet in 3C 120 fluctuates with position but never drops to zero, while the microquasar jet flows seem to be more episodic. The X-ray light curves of microquasars involve more pronounced, distinct phases than seen in 3C 120: prolonged low-hard states rather than ragged dips, quasi-periodic oscillations, high-soft states, etc. It therefore appears that the systems do not scale completely as one goes from a 10–20 M_{\odot} to a $(5.5 \pm 3) \times 10^7 M_{\odot}$ black hole (mass estimates by Peterson et al. (2004), and Marshall et al. (2004)).

Although the Marscher et al. (2002) paper appeals to chunks of disk material plunging into the black hole as a possible mechanism for the X-ray dips, there is little evidence in the X-ray spectrum for this interpretation. No low-energy wing has ever been observed in the spectrum of 3C 120, a point emphasized by A. Fabian (these proceedings). Another scenario that seems more appealing is a change in the magnetic field structure in and above the disk. As discussed by Livio et al. (2003 and these proceedings), a turbulent magnetic field, which presumably provides the main source of viscosity in the disk, can spontaneously align in the poloidal direction. This would reduce the viscosity at the same time as it directs flow of energy into the jet. The lower viscosity would decrease the dissipation of energy and therefore suppress the optical, ultraviolet, and X-ray flux. We hope to obtain more optical observations in the future to test this.

Since our original goal was to apply what we can learn from microquasars to AGNs, we need to consider how one might expect black-hole accretion systems to scale as the mass is increased from $M_{\text{BH}} = 10 - 20 M_{\odot}$ to $M_{\text{BH}} \geq 10^7 M_{\odot}$. Unfortunately, this involves too much guesswork to be accurate, but we can at least do some crude approximations. The size of the inner accretion disk should scale directly as M_{BH} , and we imagine that the dimensions of other structures near the black hole (e.g., the base of the jet) should scale in the same manner. The cooling time of electrons owing to thermal bremsstrahlung, on the other hand, is approximately proportional to the square-root of the temperature divided by the square of the density. If we imagine the latter to be roughly independent of M_{BH} , then the ratio of the cooling to the dynamical time scale decreases with mass, leading to cooler disks around more massive black holes, a well-known result. If the magnetic field plays an important role in controlling outflow from the disk, then we should note that the Alfvén speed varies as the field strength divided by the square-root of the density, and probably does not depend strongly on black-hole mass. This means that the system should be slower to respond to re-configurations of the magnetic field in the AGNs. One might then expect transition times to be roughly proportional to M_{BH} .

In 3C 120, the recovery from X-ray dips occurs over 10^5 – 10^6 s, while in GRS 1915 + 105 the duration of transitions between states ranges from about 10 s to several minutes. The ratio of black-hole masses, on the other hand, is 2 – 4×10^6 . This means that 3C 120 actually varies faster than one would anticipate

by scaling up a microquasar. So, the duration of a long dip in 3C 120, 3×10^6 s, would correspond to a drop in flux lasting only ~ 1 s in GRS 1915 + 105. That is, the dip/ejection events observed in 3C 120 might be seen as some relatively unimportant, rapid “blip” in a microquasar, while the counterparts to the 5–10 minute low-hard states of X-ray binaries would last for decades in an FR1 source like 3C 120 and even longer in higher luminosity AGNs.

However, at this point we should admit to ourselves that our knowledge of accretion-disk/jet systems is not yet sophisticated enough to bridge the gap between systems containing stellar-mass and supermassive black holes. Rather, we need to continue to develop our understanding of both microquasars and AGNs separately while keeping in mind the observed similarities and differences between the two classes.

Acknowledgements

This ongoing work is supported in part by NASA grants NAG5-13074 and NNG04GD81G, and by National Science Foundation grant AST-0406865. The VLBA is a facility of the National Radio Astronomy Observatory, operated by Associated Universities Inc. under cooperative agreement with the National Science Foundation.

References

- Gómez, J.L., Marscher, A.P., Alberdi, A., Jorstad, S.G. and García-Miró, C.: 2001, *Science* **289**, 2317.
Jorstad, S.G., Marscher, A.P., Lister, M.L. et al.: 2005, *ApJ*, submitted.
Livio, M., Pringle, J.E. and King, A.R.: 2003, *ApJ* **593**, 184.
Marscher, A.P.: 1995, *Proc. Natl. Acad. Sci. USA* **92**, 11439.
Marscher, A.P. et al.: 2002, *Nature* **417**, 625.
Marshall, K., Ferrara, E.C., Miller, H.R., Marscher, A.P. and Madejski, G.: 2004, in: P. Kaaret, F.K. Lamb and J.H. Swank (eds.), AIP Conference Proceedings No. 714, X-Ray Timing 2003: Rossi and Beyond, p. 182.
Mirabel, I.F. and Rodríguez, L.F.: 1998, *Nature* **371**, 46.
Mirabel, I.F. and Rodríguez, L.F.: 1998, *Nature* **392**, 673.
Ogle, P.M., Davis, S.W., Antonucci, R.R.J. et al.: 2004, *ApJ*, submitted (preprint astro-ph/0408007).
Peterson, B.M., Ferrarese, L., Gilbert, K.M. et al.: 2004, *ApJ* **613**, 682.

A FUNDAMENTAL PLANE OF BLACK HOLE ACTIVITY: PUSHING FORWARD THE UNIFICATION SCHEME

ANDREA MERLONI¹, SEBASTIAN HEINZ² and TIZIANA DI MATTEO³

¹Max-Planck-Institut für Astrophysik, Garching, Germany; E-mail: am@mpa-garching.mpg.de

²Center for Space Research, MIT; Chandra Fellow

³Max-Planck-Institut für Astrophysik, Garching, Germany

(Received 11 October 2004; accepted 1 June 2005)

Abstract. We examine the disc-jet connection in stellar mass and supermassive black holes by investigating the properties of their compact emission in the hard X-ray and radio bands. We compile a sample of ~ 100 active galactic nuclei with measured mass, 5 GHz core emission, and 2–10 keV luminosity, together with eight galactic black holes with a total of ~ 50 simultaneous observations in the radio and X-ray bands. Using this sample, we study the correlations between the radio (L_R) and the X-ray (L_X) luminosity and the black hole mass (M). We find that the radio luminosity is correlated with *both* M and L_X , at a highly significant level. We show how this result can be used to extend the standard unification by orientation scheme to encompass unification by mass and accretion rate.

Keywords: black holes, accretion disks, jets, active galactic nuclei, X-ray binaries

1. Introduction: Unified Pictures

Some galaxies are known to emit radiation with extremely high luminosities in the γ -ray, X-ray, UV and radio continuum from a very concentrated volume in the nuclear region. Such active cores are the so-called active galactic nuclei (AGN) and their radiation is believed to be produced by accretion onto a supermassive black hole.

The intrinsically complex nature of such systems and the differences in the terminology among different scientific communities (radio, optical, and X-ray astronomers) has led to an extremely complicated nomenclature for the AGN zoo. As the wealth of observations piled up, and with them the number of different AGN types, the opposite enterprise of finding unification schemes has progressively gained support. The basic idea behind the standard unification scheme is that AGN are asymmetric and anisotropic systems. This is natural, as all rotating systems necessarily single out a preferential axis in space and break the full spherical symmetry of non-rotating bodies. Therefore, the orientation of the AGN rotation axis with respect to our line of sight becomes another important parameter that can cause apparent observational differences in two sources that are intrinsically identical (*unification by orientation*).



According to the current widely accepted paradigm (Urry and Padovani, 1995), there are two principal causes of anisotropic radiation: obscuration and relativistic beaming. The former is usually associated with a torus of gas and dust obscuring the optical, UV and (sometimes) soft X-ray radiation along some line of sights, the latter with outflows of energetic particles (jets) along the symmetry axis: the high velocity plasma in the jet beams radiation relativistically in the forward direction. The powerful source of radiation and the launching site of the collimated jet lies in the center of the system.

Observationally, jet morphologies and spectral properties of both radio and X-ray cores are remarkably similar in the case of black holes of stellar mass (Galactic black holes, hereafter GBH) and of their supermassive counterparts in the nuclei of galaxies (hereafter SMBH). If jets are launched in the innermost parts of the accretion flows, as commonly assumed, then these similarities suggest that it should be possible to extend the unification scheme further and to understand the physics of both black hole accretion and jet production by studying all those systems as a single class (*unification by mass*). Furthermore, the recent discovery that SMBH lie at the center of the majority (possibly all) galactic nuclei, even in apparently inactive ones (Kormendy and Richstone, 1995; Magorrian et al., 1998), naturally leads to the idea that a grand unification is possible by taking into account the differences in fueling rates among different objects (*unification by accretion rate*).

In the following, we will show how to proceed quantitatively towards a grand unification of active black holes by studying the multivariate correlation among masses, radio luminosities and hard X-ray luminosities of objects traditionally classified in the more diverse ways. The underlying theoretical assumption is that both accretion and jet production are fundamental manifestation of black hole activity, and are somehow physically connected (Begelman et al., 1984; Rawlings and Saunders, 1991; Falcke and Biermann, 1995; Heinz and Sunyaev, 2003).

2. Unification by Mass and Accretion Rate

Here we briefly describe the main results of the correlation analysis carried on in Merloni, Heinz and Di Matteo (2003, hereafter MHD03). A more detailed description of the sample used, of the selection effects and of the statistical analysis can be found there, together with a comprehensive list of references to the observational data. For future reference, we define the dimensionless black hole mass $M = M_{\text{BH}}/M_{\odot}$ and accretion rate $\dot{m} \equiv (L_{\text{bol}}/\epsilon)/L_{\text{Edd}} = \dot{M}c^2/L_{\text{Edd}} \propto \dot{M}/M$, where ϵ is the accretion efficiency.

We have selected from the existing literature a sample of black hole-powered systems with measured masses, the nuclei of which have been observed both at

5 GHz (mostly with arcsecond resolution with the VLA) and in the 2–10 keV band. The main obvious advantage of this choice lies in the fact that obscuration is unimportant, or easily accounted for, in these spectral bands.

We first considered the full sample of ~ 40 nearby inactive, or weakly active galaxies with existing nuclear black hole mass measurements from observations of spatially resolved kinematics. To these we have added a comparable number of bright AGNs (and QSOs) with nuclear black hole mass measured from reverberation mapping of their broad line region. From this sample we selected all objects which have been observed in both the radio and X-ray bands. In order to obtain a more statistically representative sample, we also searched the existing literature for both nearby low-luminosity galactic nuclei and for relatively bright Seyfert nuclei (either type 1, type 2 or Narrow Line Seyfert 1) and radio galaxies with available radio and X-ray flux measurements. We assign black hole masses to these systems using the observed correlation between black hole masses and stellar velocity dispersion (Gebhardt et al., 2000; Ferrarese and Merritt, 2000).

Relativistically beamed sources (i.e. those whose jet axis points towards our line of sight) are dominated by the boosted jet emission, and cannot be used to test the disc-jet coupling. We therefore excluded from our sample BL Lac objects. Among the Quasars in our sample, only 3C 273, which has an extremely high radio loudness and a blazar-like spectrum, is likely to suffer from strong Doppler boosting of the radio jet. On the other hand, according to the unification scheme, Seyfert 2 nuclei should not be preferentially viewed pole on, while for all the other sources (mainly low-luminosity AGN and Seyfert 1), for which the nature of the (relatively faint) radio emission is not well established, we have assumed that the orientation of their jets with respect to line of sight is randomly distributed.

The Galactic X-ray binaries included in our sample have been selected to have (a) simultaneous X-ray and radio observations, or *RXTE* All-Sky-Monitor (ASM) X-ray data in conjunction with radio fluxes available from the literature, and (b) publicly available *RXTE*-ASM X-ray and Green-Bank Interferometer (GBI) radio lightcurves (from which we estimated the 5 GHz fluxes by interpolating between the 2.25 GHz and the 8.3 GHz channels).

The final sample consists of ~ 100 active galactic nuclei with measured mass, 5 GHz core emission, and 2–10 keV luminosity, together with eight galactic black holes with a total of ~ 50 simultaneous observations in the radio and X-ray bands (see MHD03 for a full list of the sample sources).

In Figure 1, we show the radio core luminosity versus the black hole mass for objects of different spectral classes. We concentrate on the SMBH only in order to show how, at a fixed black hole mass, sources which are classically regarded as powerful accretors (QSOs, Narrow Line Seyfert 1, Seyfert 1) tend to lie above the so-called Low-Luminosity AGN (here represented by LINERs), with Seyfert 2 galaxies spanning a large area in the vertical direction. Figure 2 shows instead the core radio luminosity versus the ratio of the X-ray nuclear luminosity to the Eddington luminosity (probably a good estimator of \dot{m} , see below). We represent

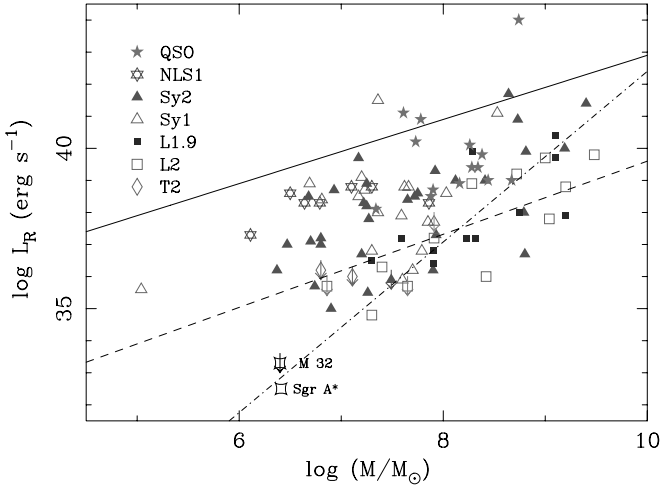


Figure 1. Radio core luminosity at 5 GHz versus black hole mass of SMBH only. Upper limits are marked with *arrows*, different symbols indicate objects belonging to different spectral classes. The *dot-dashed line* gives the regression fit proposed by Franceschini et al. (1998), the *dashed line* that proposed by Nagar et al. (2002), both obtained using different samples of SMBH only. The *thick solid upper line* gives the maximum core radio power as calculated by Ho (2002) for sources accreting at the Eddington rate.

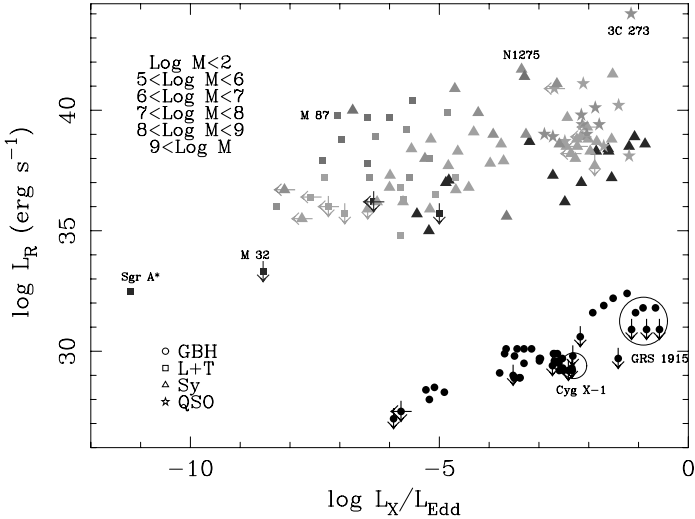


Figure 2. Radio core luminosity at 5 GHz vs. the ratio L_X/L_{Edd} of X-ray to Eddington luminosity. Upper limits are marked with *arrows*, different symbols indicate objects belonging to different spectral classes and different colors objects in different mass bins. The color-coding of the different mass bins makes the mass segregation more evident.

objects in different mass bins with different colors. It is clear that, when the data points are grouped into mass bins, objects in different bins tend to lie on parallel tracks. The presence of a mass segregation suggests that the radio luminosity of an object likely depends both on its accretion rate and on its mass.

We can proceed to quantify the degree of correlation between our three observables (radio luminosity at 5 GHz, L_R , X-ray luminosity in the 2–10 keV band, L_X and black hole mass). We fit the data with the function $\log L_R = \xi_{RX} \log L_X + \xi_{RM} \log M + b_R$, and obtain well constrained values for the correlation coefficients, meaning that, if we define the instantaneous state of activity of a black hole of mass M , by the radio and hard X-ray luminosity of its compact core, and represent such an object as a point in the three-dimensional space ($\log L_R$, $\log L_X$, and $\log M$), all black holes (either of stellar mass or supermassive) will lie preferentially on a plane (the ‘fundamental plane’ of black hole activity, see Figure 3), described by the following equation:

$$\log L_R = (0.60^{+0.11}_{-0.11}) \log L_X + (0.78^{+0.11}_{-0.09}) \log M + 7.33^{+4.05}_{-4.07}. \quad (1)$$

with a dispersion $\sigma_R = 0.88$ (see Figure 3).

The value we obtain for the ξ_{RX} correlation coefficient is consistent, within the errors, with that found in low/hard state GBH ($\xi_{RX} \approx 0.7$) by Gallo et al. (2003). This also means that individual GBH sources for which the correlation between radio and X-ray luminosities is well established (GX 339-4 and V404 Cyg) do indeed follow the same global trend defined by black holes of all masses included in our sample.

3. Scale Invariance and Jet Dominance in Black Hole Accretors

In a recent paper, Heinz and Sunyaev (2003) have demonstrated that, under the general assumption that the jet formation process is not qualitatively different among SMBH of different mass or between SMBH and GBH, it is in fact possible to derive a universal scaling between the jet (radio) luminosity at a given frequency and both mass and accretion rate. The derived relation is independent of the jet model and has scaling indices that depend only on the (observable) spectral slope of the synchrotron emission in the radio band (α_r), and on the accretion model. In particular, it was shown that, if the magnetic field B_0 at the base of the jet is in equipartition with the particles pressure and the total jet power scales as $W_{\text{jet}} \propto B_0^2 M^2 \propto \dot{M}$ (see also Falcke and Biermann, 1995; Heinz et al., this proceedings), and under the standard assumption that the electrons responsible for the jet synchrotron emission follow a power-law distribution in energy, with index $p = 2$, then $L_R \propto M^{17/12 - \alpha_r/3} \dot{m}^{17/12 + 2\alpha_r/3}$. For the optically thick, flat spectrum

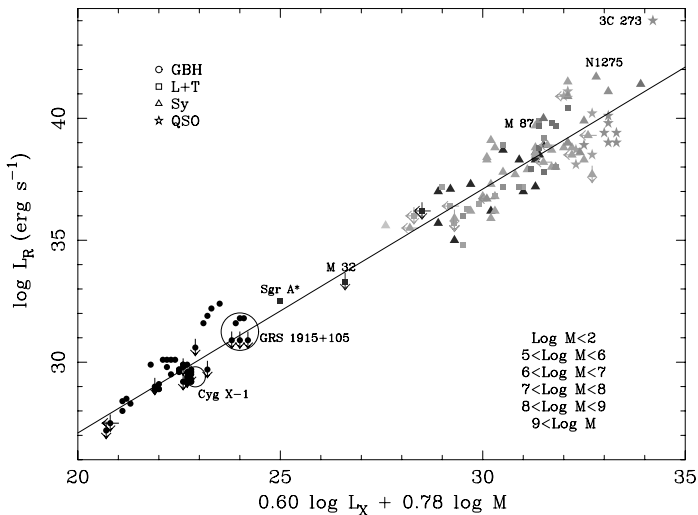


Figure 3. The edge-on view of the ‘fundamental plane of black hole activity’. The *solid line* shows the best fitting function (1).

cores we are mostly interested in ($\alpha_r \simeq 0$), then:

$$L_R \propto (M\dot{m})^{1.42}. \quad (2)$$

To compare this prediction with the observed fundamental plane correlation, one needs to explicate the dependence of the hard X-ray luminosity on the accretion rate, $L_X \propto \dot{m}^q$. In MHD03 it was shown how indeed the prediction of standard synchrotron theory for the radio-X-ray-mass correlation of Heinz and Sunyaev (2003) are verified if, and only if, $q \approx 2$, i.e. if the accretion process is radiatively inefficient. Detailed models for the X-ray emission from such flows do indeed show that $q = 2.3$ (MHD03), and in this case $L_{R,q=2.3} \propto \dot{m}^{1.38} M^{1.38} = \dot{M}^{1.38}$, i.e. L_R scales with the physical accretion rate only. This is tantalizingly close to the predicted dependence of Eq. (2), and such a result can be interpreted in the following way: (1) the scale invariance hypothesis at the heart of the Heinz and Sunyaev (2003) calculations is correct, and black holes can indeed be further unified by considering their masses and accretion rates, and (2) the largest area of the fundamental plane is covered by radiatively inefficient sources.

The total power released by the accretion/jet system may be written as $W_{\text{tot}} \simeq \dot{M}c^2 = L_{\text{bol}} + W_{\text{jet}} + W_{\text{adv,conv}}$, where the first term on the right hand side is the total radiated luminosity and the last one include contributions from the energy advected and/or stored in the convective motions. Our results suggest that the flow must be radiatively inefficient, therefore, for small enough accretion rates we have $L_{\text{bol}} \simeq \dot{M}mc^2 \ll \dot{M}c^2 \sim W_{\text{jet}} + W_{\text{adv,conv}}$. On the other hand, $W_{\text{jet}} \propto W_{\text{adv,conv}} \propto Mc^2$. Therefore, the issue of what the relative fraction of the total accretion energy

dissipated into the jet is (or, alternatively, of when a source is ‘jet dominated’; Fender et al., 2003; Falcke et al., 2004) reduces to the determination of the value of the constant $W_{\text{jet}}/W_{\text{adv,conv}}$. This requires the specification of a jet model or the direct measure of the total kinetic power carried by the jet (see, e.g. Heinz et al. 2004), together with a dynamical model for the disc-jet coupling.

4. Accretion Mode Changes

It is well accepted, both from theory and observations, that accretion can proceed in different modes (or states), with different radiative efficiencies and spectral properties. By fitting the whole dataset at our disposal with a single linear relationship (1), we have implicitly neglected the possibility of a global accretion mode change. This is clearly implausible, as the QSOs and the bright Seyferts in our sample, which occupy the region of high accretion rates, are independently known to have spectral characteristics inconsistent with models of low radiative efficiency. They should therefore depart from the observed correlations. For GBHs, it has indeed been shown that the correlation between radio and X-ray luminosity breaks down as the sources switch to their high states (Maccarone, 2003; Gallo et al., 2003). However, because both such modes of accretion are expected to occur only above accretion rates about a few percent of Eddington, and because another advective accretion mode is expected to ensue at around the Eddington limit (due to efficient radiation trapping, see e.g. Abramowicz et al., 1995), we would expect the $\log M - \log L_{\text{R}} - \log L_{\text{X}}$ correlation to break down only in a limited range of \dot{m} . In other words, independently on the actual number of radiatively efficient sources, the area of the fundamental plane covered by them will always be limited, and the overall orientation of the plane will always be dominated by the radiatively inefficient ones. This also means that any (statistically significant) departure from the fundamental plane relation could be used to identify different modes of accretion. In fact, Maccarone et al. (2003) have already shown how is possible to use the fundamental plane relation as a baseline against which identify AGN in a high/soft state (HSS) analogous to that of X-ray binaries.

The analogy with GBH can indeed be very useful to classify and understand the properties of bright AGN. Let us consider, for example, a recent paper by Fender et al. (2004), where it was shown that the intermittent, powerful radio flares from the so-called microquasars, associated with the rapid variability in the very high state (VHS), seem to follow a similar radio-X-ray correlation as the low/hard state sources, albeit with a much larger scatter. Can we extend this result to the larger family of radio loud AGN?

In Figure 4 we plot, as a function of the ratio $L_{\text{X}}/L_{\text{Edd}}$, the radio luminosity divided by $M^{1.38}$ of all the sources in our sample. As expected, by rescaling the radio luminosity in such a way all the different tracks corresponding to different

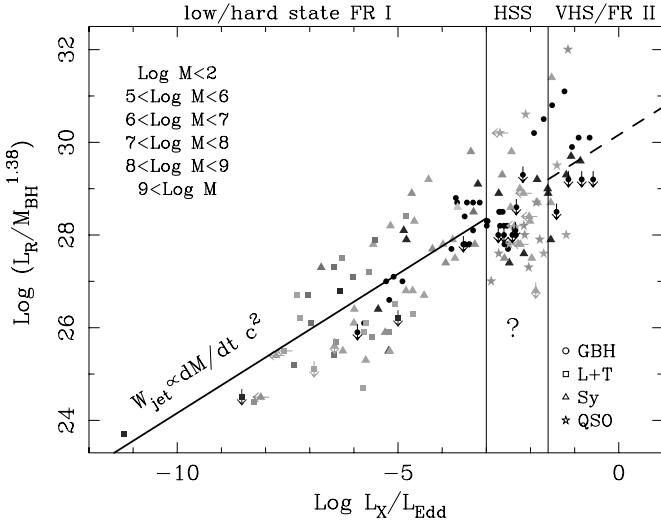


Figure 4. The radio luminosity $\log L_R$, divided by $M^{1.38}$ as a function of the ratio L_X/L_{Edd} . Upper limits are marked with *arrows*, different symbols indicate objects belonging to different spectral classes and different colors objects in different mass bins. Two vertical lines mark the boundary of the region where we expect the critical luminosity for the mode change between radiatively inefficient and efficient accretion. To the left of these lines, GBH are in the low/hard state and SMBH are mostly FR I. To the right, GBH are in the very high state (VHS) and SMBH are mostly FR II. In between, possibly the restricted region of the parameter space where pure discs accretion is allowed (high/soft state, HSS).

mass bins in Fig. 2 collapse into a single one, with some residual scatter. The region between the two vertical lines corresponds to the theoretically expected values of L_X/L_{Edd} above which a change of accretion mode, from radiatively inefficient to standard radiatively efficient is expected to occur. To the left of these lines, GBH are in the low/hard state and SMBH are mostly FR I, or low-luminosity, radio loud AGN. To the right, GBH are in the very high state (VHS) and SMBH are mostly FR II. In between, possibly lies the restricted region of the parameter space where pure discs accretion is allowed (HSS). Interestingly, it appears as if both low and high luminosity sources at the two sides of the HSS region obey a similar scaling $W_{\text{jet}} \propto \dot{M} c^2$.

We may thus speculate that the famous (and still much debated) radio loud/radio quiet dichotomy of quasars will appear only at the highest values of \dot{m} , and be caused mainly by a switch of accretion mode analogous to the high/very high transition in GBH. At low accretion rates, black holes seem to follow the more regular behavior circumscribed by the fundamental plane of Eq. (1). Such sources not only tend to be radio loud (Ho and Peng, 2001; Ho, 2002), but also their radio loudness parameter, R_X (here defined as the ratio of radio to X-ray luminosity), obeys the following scaling: $R_X \equiv L_R/L_X \propto L_X^{-2/5} M^{4/5}$. Therefore, the smaller the X-ray

luminosity, the more radio loud these sources are. In this regime, no dichotomy need be expected, as already suggested by Nagar et al. (2002).

5. Conclusions

We have argued that the fundamental plane analysis presented here is a powerful tool to extend the unified scheme of accreting black holes. Such a relation between mass, radio and hard X-ray luminosity is affected very little by obscuration and beaming, provided that sources whose relativistic jets are in our line of sight can be effectively identified and excluded. Thus, the fundamental plane relation does not depend on orientation, and as such is complementary to the standard unification scheme. Moreover, the relation itself is perfectly consistent with the scaling relations predicted by standard synchrotron theory under a scale invariance assumption. The main scaling parameters are the mass of the black hole and its accretion rate. Finally, we have shown how the observed correlation can be effectively used to classify objects on the basis of their mode of accretion (and/or accretion/ejection coupling) rather than just on specific observational characteristics, as in the true spirit of unification models.

References

- Abramowicz, M.A., Chen, X., Kato, S., Lasota, J.-P. and Regev, O.: 1995, *ApJ* **438**, L37.
 Begelman, M.C., Blandford, R.D. and Rees, M.J.: 1984, *Rev. Mod. Phys.* **56**, 255.
 Falcke, H. and Biermann, P.L.: 1995, *A&A* **293**, 665.
 Falcke, H., Körding, E. and Markoff, S.: 2004, *A&A* **414**, 895.
 Fender, R.P., Gallo, E. and Jonker, P.: 2003, *MNRAS* **343**, L99.
 Fender, R.P., Belloni, T. and Gallo, E.: 2004, *MNRAS* in press, astro-ph/0409360.
 Franceschini, A., Vercellone, S., Fabian, A.C.: 1998, *MNRAS* **297**, 817.
 Gallo, E., Fender, R.P. and Pooley, G.G.: 2003, *MNRAS* **344**, 60.
 Heinz, S. and Sunyaev, R.A.: 2003, *MNRAS* **343**, L59.
 Heinz, S., Sunyaev, R.A., Merloni, A., and Di Matteo, T.: 2004, to appear in the Proceedings of ‘Growing Black Holes’, Garching, Germany, June 21–25, 2004. A. Merloni, S. Nayakshin and R. Sunyaev (eds.), Springer-Verlag series of ‘ESO Astrophysics Symposia’.
 Ho, L.C.: 2002, *ApJ* **564**, 120.
 Ho, L.C. and Peng, C.Y.: 2001, *ApJ* **555**, 650.
 Kormendy, J. and Richstone, D.: 1995, *ARA&A* **33**, 581.
 Maccarone, T.: 2003, *A&A* **409**, 697.
 Maccarone, T., Gallo, E. and Fender, R.P.: 2003, *MNRAS* **345**, L19.
 Magorrian, J. et al.: 1998, *AJ* **115**, 2285.
 Merloni, A., Heinz, S. and Di Matteo, T.: 2003, *MNRAS* **345**, 1057 (MHD03).
 Nagar N.M., Wilson, A.S., Falcke, H. and Ulvestad, J.S.: 2002, *A&A* **392**, 53.
 Rawlings, S. and Saunders, R.: 1991, *Nature* **349**, 138.
 Urry, C.M. and Padovani, P.: 1995, *PASP* **107**, 803.

MAGNETICALLY DOMINATED ACCRETION FLOWS (MDAFS) AND JET PRODUCTION IN THE LOWHARD STATE

DAVID L. MEIER

*Jet Propulsion Laboratory, California Institute of Technology, Pasadena, CA, USA;
E-mail: dlm@sgra.jpl.nasa.gov*

(Received 23 October 2004; accepted 3 February 2005)

Abstract. In this paper I propose that the inner part of a black hole accretion inflow ($<100 r_g$) may enter a magnetically dominated, magnetosphere-like phase in which the strong, well-ordered fields play a more important role than weak, turbulent fields. In the low/hard state this flow is interior to the standard ADAF usually invoked to explain the observed hot, optically thin emission. Preliminary solutions for these new MDAFs are presented.

Time-dependent X-ray and radio observations give considerable insight into these processes, and a new interpretation of the X-ray power spectrum (as arising from many disk radii) may be in order. While an evaporative ADAF model explains the noise power above 0.01 Hz, an inner MDAF is needed to explain the high-frequency cutoff near 1 Hz, the presence of a QPO, and the production of a jet. The MDAF scenario also is consistent with the phenomenological models presented at this meeting by several authors.

Keywords: black holes, accretion, magnetic fields, jets

1. Introduction: The ‘Black Hole Problem’

A generic, robust electrodynamic model for producing most astrophysical jets is now well understood. It has two basic requirements:

- A strong magnetic field ($V_A \equiv B/(4\pi\rho)^{1/2} \gg C_S \equiv (\Gamma p/\rho)^{1/2}$, where V_A is the Alfvén speed and C_S is the sound speed) that rotates fairly rapidly ($\Omega \lesssim \Omega_K$, where Ω_K is the Keplerian angular velocity).
- Some means of loading this rotating magnetic field with plasma at fairly high elevations ($Z \sim R$ in a cylindrical $[R, Z, \theta]$ coordinate system). Early models accomplished this loading by centrifugal action from a thin disk, but more recent studies suggest that the primary means is thermal, (heating the plasma to roughly the virial temperature; Meier, 2001).

The means by which this configuration produces a jet was first proposed by Blandford (1976) and Lovelace (1976) and has been reviewed recently by the author (Meier et al., 2001; Meier, 2004). The rotation of the magnetic field lines is retarded by the inertia of the plasma load, creating a rotating helical field configuration. Lorentz forces simultaneously push plasma up and out of the system along the rotation axis and collimate the flow with magnetic hoop stress by squeezing it toward the rotation axis, converting rotational energy of the central engine into



directed kinetic outflow energy along the rotation axis. The jet is accelerated to the local Alfvén speed by the rotational Alfvén wave and beyond that to the local magnetosonic speed by the toroidal magnetic pressure gradient. The terminal velocity of the jet is approximately equal to the escape speed at the footpoint of the magnetic field in the rotating central engine.

1.1. SPECIFIC MODELS FOR STELLAR JETS

While this model gives a general description of how astrophysical jets form, it does not answer the question of how each source produces the above two main ingredients—the global rotating magnetic field and the plasma loading. For stellar sources the first requirement is straightforward: the global magnetic field is that produced by the star’s magnetosphere itself. The discovery of strong magnetic fields in pulsars and protostar systems is considered confirmation of the MHD jet production model.

The plasma loading is more problematical. In pulsars it has been shown that pair production can occur in ‘spark gaps’ in the very strong magnetic field (10^{11-13} G), producing the needed plasma inside the magnetosphere itself (Goldreich and Julian, 1969; Ruderman and Sutherland, 1975). In protostar systems, however, the field is not nearly as strong, so pair production cannot operate. Instead, the protoplanetary accretion disk is used to pinch the field near the equator, creating an “X-point” (Shu et al., 1994), where plasma is allowed to flow freely from the disk onto the rotating stellar field.

Finally, for jets produced in collapsing supernova cores (Wheeler et al, 2002), the plasma comes pre-loaded, since the magnetic field of the collapsing core has become threaded into the progenitor mantle during the late stages of stellar evolution. It is the rapid rotation of the core that is suddenly and rapidly generated, by the collapse of that iron core to proton-neutron star densities.

1.2. THE BLACK HOLE PROBLEM

While it is clear that black hole systems often produce fast and powerful jets, they present a serious challenge to the electromagnetic theory of jet production. The plasma loading itself is a relatively easy problem to solve. The fact that black hole systems that produce jets are associated with hot accretion flows (Fender et al., 1999) indicates that the plasma must be loaded onto the field lines from the accretion flow by some thermal means.

However, by themselves, black holes cannot support a magnetic field.¹ They can have such a field only if there is an external supply of plasma in which cur-

¹It is true that a charged, rotating black hole has a dipole magnetic moment (Misner et al., 1973). However, a strongly charged black hole will induce charge separation in any surrounding plasma, accreting charges opposite in sign to that on the hole and expelling those of like sign. This will effectively discharge the hole in a few light-crossing times.

rents generate magnetic flux that can then thread the black hole. In the absence of a significant amount of external plasma, a black hole loses its field in a few light-crossing times (Thorne et al., 1986). The field, therefore, must be supported by currents in the black hole accretion flow. This conclusion itself presents a problem, however. Accretion disks are believed to be weakly magnetized plasmas in highly turbulent, orbital flow about the black hole (Balbus and Hawley, 1998). How does a global, well-ordered rotating magnetosphere develop naturally from a turbulent accretion disk?

In addition, even if a global magnetosphere can be constructed, there is a question as to how that magnetosphere can couple to black hole rotation to produce a strong jet. While the accretion disk itself can produce rotation of the magnetic field, it cannot be the main source of jet power in many jet-producing supermassive black hole systems. Radio galaxies and quasars that have similar optical properties, and therefore similar accretion disks, can differ in their radio jet luminosities by factors of 10^{5-6} . This is most easily explained by tying jet production to rotation of the central object, just as it is done in stellar jet-producing systems. In addition, black hole systems are known to produce jets ~ 30 times stronger than those from neutron stars with similar accretion rates (Migliari et al., 2003). While this comparison may be complicated by effects of the neutron stars' magnetic field, a strong coupling of jet production to the black hole spin also may be at work.

To solve this problem we will assume here that the “magnetic Penrose” mechanism of extracting rotational energy is at work (Koide et al., 2002): if plasma threaded with a magnetic field enters the ergosphere, then that plasma can be accelerated in a direction *opposite* to the black hole's spin, acquiring *negative* energy and angular momentum in the process. Positive energy and angular momentum then is transferred to the rotating magnetic field, which uses that to accelerate and collimate the jet.

The purpose of this paper is to explore answers to the two remaining questions: (1) how does a turbulent, magnetized disk create a global, well-ordered magnetic field that can couple to the black hole rotation and (2) how does the accretion disk load the field lines with plasma?

2. Basics of Magnetically Dominated Accretion Flows

2.1. WHAT IS AN MDAF?

An MDAF is an accretion flow in which the magnetic forces dominate over the thermal and radiation forces. In a normal accretion disk model, the weak magnetic field creates a “magnetorotational instability” (MRI) (Balbus and Hawley, 1998) in which turbulence dominates the angular momentum transport and the eddy turnover time τ_{turb} is shorter than the inflow time $\tau_{\text{inflow}} \equiv R/V_R$. A steady disk structure develops in which magnetic field components $B_R \sim B_\phi \propto R^{-5/4}$ and pressure

scales as $p \propto R^{-3/2}$. The ratio of magnetic to thermal forces $\alpha \propto B_R B_\phi / p$ remains constant at ~ 0.01 – 1.0 .

We recognize two types of magnetically dominated accretion flows. The first is still turbulent, but now the ratio of the time scales is reversed: $\tau_{\text{inflow}} < \tau_{\text{turb}}$. Small eddies continue to transport angular momentum, but the larger ones are stretched out in the R direction before they have a chance to turn over. In this case, $B_R \propto R^{-5/2}$ and $B_\phi \propto R^{-1/2}$ decouple and $p \propto R^{-3/2}$, so that magnetic stresses increase as R decreases: $\alpha \propto R^{-3/2}$. We call this type of flow “transitional”, because it connects a turbulent flow with $\alpha < 1$ to one with $\alpha > 1$ and the MRI turned off. If α_0 is the value at R_0 , and R_1 is the radius where α attains unit value, then

$$R_1/R_0 = \alpha_0^{-2/3} \quad (1)$$

If $\alpha_0 \sim 0.3$, as is expected in advection-dominated accretion flows (Narayan et al., 1998), then $R_1/R_0 \sim 0.5$. So, if the interior of an ADAF becomes magnetically dominated, the transition region will be rather narrow in radius.

In the second type of MDAF, which is a solution to “Gammie flow” (Gammie, 1999), MRI turbulence has ceased and the inflow is laminar along strong magnetic field lines. $B_R \propto R^{-3/2}$ and $B_\phi \propto R^{-1}$ are still decoupled. The thermal pressure scaling depends critically on the energy balance in the gas now, but simple models indicate $p \propto R^{-1/2}$. So $\alpha \propto R^{-2}$ continues to increase inward, and the flow continues to become *more* magnetically dominated as it approaches the black hole. Figure 1 shows a schematic of our low-state model and will be discussed more fully below.

MDAF-type solutions are seen in MRI simulations only in the plunging region very near the black hole, not out to distances as large as $\sim 100r_g$. Why? The reason may be the assumption implicit in the simulations that the flow is radiatively inefficient. This may be the case for $R \gtrsim 100 r_g$ (where $r_g \equiv GM/c^2$); in this case the temperature remains $T \lesssim 5 \times 10^9$ K. However, inside this radius electrons radiate copiously by synchrotron, pair production, and other relativistic processes. While ADAF models assume that the ion temperature can remain hot ($T_i \sim 10^{12} \text{K} (R/r_g)^{-1}$), if there is strong coupling between ions and electrons, the ions will cool to the $\gtrsim 10^9$ K temperature as well. It is often assumed that such cooling would lead once again to a geometrically thin, optically thick disk. However, these models show that there is another solution: cool, but still optically thin flow along strong magnetic field lines. It, therefore, is extremely important to begin performing MRI simulations with a *real* energy equation, including separate evolution of the ions and electrons.

2.2. WHAT ARE THE PROPERTIES OF MDAFS?

The inner MDAF is an extraordinarily *inefficient* flow. It is a nearly radial in-spiral, geometrically thick because of *magnetic* pressure support (Meier, 2004). Virtually

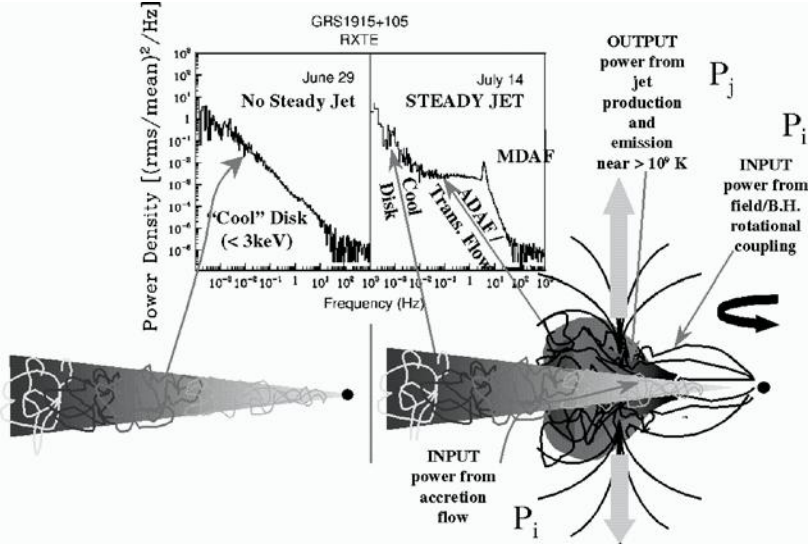


Figure 1. Schematic diagram of the MDAF model for GRS 1915+105. Power spectrum data are taken from Morgan et al. (1997). A cool disk fits the power spectrum in the high state (left) when no jet is produced. In the hard state (right) we not only need an ADAF (extended corona) but also an MDAF (inward-facing magnetosphere) to produce the few Hz cutoff and QPO, and an outward-facing magnetosphere to produce the jet. The jet will be launched from the transition radius near $\sim 100 r_g$. The input and output powers $P_{i,j}$ correspond to those in the Malzac et al. model. An MDAF is also expected in some intermediate accretion states when the cool disk is still truncated at a radius $> r_g$.

all orbital angular momentum is transferred out to R_1 along the strong field lines. The plasma experiences only compressional heating and radiative cooling by electrons and could remain quite cool; the majority of the gravitational energy released is converted into radial infall kinetic energy, not heat.

Because the magnetic radial channels are potentially distinct, the flow may break up into inhomogeneous “spokes”. A signature of an MDAF may be a quasi-periodic oscillation at one or more of two transition radius frequencies: (1) the orbital/Alfvén frequency

$$\nu_A = V_A / 2\pi R_1 = 1.1 \text{ Hz} (M_\bullet / 10 M_\odot)^{-1} \quad (2)$$

and (2) the MHD slow mode (“organ pipe”) frequency

$$\nu_S = V_S / 2\pi R_1 \approx C_S / 2\pi R_1 = 0.02 - 0.13 \nu_A \quad (3)$$

or ~ 20 – 140 mHz for a $10 M_\odot$ black hole, depending on the azimuthal length of the resonating magnetic tubes. Because ν_S is excited acoustically near R_1 along the length of these tubes, it may be characterized by multiple harmonics, whereas the orbital/Alfvén mode should be rather pure.

The magnetic field lines extending inward toward the black hole may tap the hole's rotational energy if they penetrate the ergosphere. However, in general the hole rotation rate will not match the, usually slower, v_A . One therefore might expect an episodic interaction, where the field enters the ergosphere, is wound up rapidly, reconnects in a series of rapid flares separated by the ergosphere rotation time, and finally pulls back from the hole for a secular time. The behavior of SgrA at the Galactic center (Genzel et al., 2003) is very similar to what might be expected from a rotating black hole/MDAF interaction.

In addition to an inner magnetosphere of closed field lines reaching toward the black hole, there also may be open field lines extending from R_1 to infinity (see Fig. 1 and Meier, 2004). The transition radius, therefore, has all the properties necessary to launch a jet: the base of large-scale, open, rotating magnetic field lines being loaded with hot ADAF material. Excess angular momentum is deposited at R_1 by the radial field lines that connect periodically to the black hole ergosphere. An outflowing MHD wind/jet would be a good candidate for carrying off this excess angular momentum.

3. Discussion

3.1. MDAFS AND THE LOW/HARD (PLATEAU) STATE OF XRBs

When the transient X-ray binary (XRB) source GRS 1915+105 is in the soft state and not producing a jet, its photon spectrum is dominated by a cool thermal spectrum, and its *power* spectrum is a rather featureless power law of $dP/d\nu \propto \nu^{-4/3}$. When the source begins to produce a steady jet, it enters a low/hard state in which the photon emission is dominated by a *non*-thermal spectrum. And the power spectrum develops bandwidth-limited noise (a flat ($dP/d\nu \propto \nu^0$) shoulder with a steep cutoff above ~ 3 Hz) and a QPO at 1–3 Hz. It is natural to associate the non-thermal photon spectrum and bandwidth-limited noise with the optically thin, turbulent ADAF that has formed in the center of the disk. But what produces the QPO, and why would the ADAF be bandwidth-limited? Why does its turbulence not extend all the way to the natural frequencies near the black hole (~ 100 Hz)?

The inner MDAF model provides natural answers to these questions. While the thin accretion disk is truncated by the ADAF at, perhaps, $\sim 1000 r_g$, the ADAF itself is truncated at $R_1 \sim 100 r_g$ by the MDAF, cutting off the ADAF turbulence above a few Hz. The slope of this cutoff may represent the high frequency tail of the turbulence spectrum near R_1 . The QPO is produced by the magnetic flux tubes that stretch toward the black hole and rotate at roughly the orbital R_1 frequency—again a few Hz.

The power spectrum at each disk radius should be dominated by a rather narrowly peaked *local* spectrum (Maron and Blackman, 2002). We therefore can approximate the *total* disk power spectrum by assuming the local spectrum to be a delta function

and simply plotting the variation of the turbulence *strength* with radius against the variation of the principal local (orbital) frequency with radius:

$$P[r(v)] = (2\pi \Delta R \delta H) \rho V_{\text{turb}}(R)^2 \quad (4)$$

where $\Delta R \sim R$ is the annulus over which ρ and V_{turb} remain roughly constant, and δH is the skin depth over which the turbulent eddies can be seen by the observer (roughly the optical depth). For an α -disk (Shakura and Sunyaev, 1973), we find $P(r) \propto R^{1/2} \propto v^{-1/3}$, or $dP/dv \propto v^{-4/3}$, in agreement with GRS 1915+105 in the high state. However, in the low state, for a simple evaporative ADAF model ($\dot{M} \propto R^{-1}$) (Esin et al., 1997), we find that $dP/dv \propto v^{-2/3}$, which is *not flat*. In order to obtain $dP/dv \propto v^0$, we need to assume a steeper rate of evaporation of the thin disk into the ADAF: $\dot{M} \propto R^{-2}$. Detailed modeling of the power spectrum as disk turbulence at different radii may, therefore, become an important diagnostic of conditions in the optically thin portion of the accretion flow, ADAF and MDAF alike.

Figure 1 shows a schematic picture of GRS 1915+105 in the soft and hard states, the corresponding power spectra, and energy inputs to and outputs from the transition region.

3.2. RELATION TO PRESENTATIONS ON XRBS AT THIS MEETING

Fender et al. (2004) have proposed a phenomenological model for jet production in which the jet speed increases as the inner disk radius decreases. This model explains why strong jet outbursts are seen when the disk transitions to the high/soft state and not when it transitions to the low/hard state: the jet speed *decreases* with time in the latter case, resulting in no formation of a shock.

This model fits well with the MDAF scenario. We identify the low/hard state as one in which the cool accretion disk completely evaporates before the ADAF transitions into an MDAF, *i.e.* for $R > R_1$. In this case, near the central engine, the jet speed is simply the escape speed from the transition radius, or

$$V_{\text{jet}} \sim 2GM/R_1 \quad (5)$$

which gives a non-relativistic jet of $V_{\text{jet}} \sim 0.1 c$. Eventually, as the accretion rate is increased, the cool disk begins to extend *inside* $\sim 100 r_g$, and the ADAF changes from an accretion flow in its own right to simply a corona above a dense cool disk. The ADAF no longer extends inside the truncated cool disk; that region is filled with the MDAF only, extending from the ADAF corona inward. This begins the move toward the high state along the upper horizontal branch in the intensity/hardness plane: the hard ADAF emission begins to be suppressed, the thermal emission from the cool disk gains in strength, the radius R_1 where the transition to MDAF occurs now follows the cool disk truncation radius. The jet velocity from equation

(5) increases as the disk truncation radius decreases. Eventually R_1 reaches all the way to the black hole horizon, and the MDAF is swallowed. This turns off the jet, but not before its velocity reaches close to c as $R_1 \rightarrow r_H$, the horizon radius. It is this fast jet that creates the shock and outburst that we observe.

Malzac et al. (2004) also have interpreted the variability of XTE J1118+480 as coupling between the corona and the jet through a common reservoir where large amounts of accretion power are stored. In the MDAF model we identify the transition region at R_1 as this reservoir. Energy and angular momentum input into this region comes from two sources: the accretion flow from outside and the magnetic coupling to the black hole from inside R_1 . The output power is the jet production that occurs at this radius. It is important to note that the predicted temperature at this transition region is of order a few $\times 10^9$ K, and it lies at $\sim 100 r_g$ in the low state, but can move inward as the accretion rate increases (see above).

3.3. MDAFS AND LOW-LUMINOSITY AGN

Black hole accretion in active galactic nuclei (AGN) is expected to act similarly to that in XRB systems: bright Seyfert and quasar objects are believed to be in a soft state while those AGN without strong optical line emission (low-luminosity AGN [LLAGN], FR I radio galaxies, Sgr A) are believed to be in a low/hard state. While there is some timing data available on these latter objects, a detailed comparison with the MDAF model is not possible at this time as a QPO-producing plateau state has not yet been identified. Our discussion of MDAFs in AGN therefore will be more speculative.

LLAGN do indeed show bandwidth-limited noise, and the cutoff/break at high frequency sometimes is used as an indicator of black hole mass, with $\tau_{\text{br}} \approx 7.7 \text{ d} (M_\bullet / 10^7 M_\odot)$, where τ_{br} is the time scale, in days, where the break occurs in the AGN X-ray power fluctuation spectrum (Papadakis, 2004). The MDAF model provides a physical reason why this *ad hoc* scaling of the break in different systems is a reasonable black hole mass indicator. In the model the frequency of this break will be equal to, or slightly greater than, ν_A (equation 2), so $\tau_{\text{br}} = 1/\nu_A \approx 10 \text{ d} (M_\bullet / 10^7 M_\odot)$.

AGN also display another property similar to that shown by X-ray binaries, and the MDAF model provides the same explanation there as well. Jets produced by quasars and many Seyferts tend to be quite relativistic, even within only a parsec from the black hole core. They therefore may be launched and accelerated rather close to the central black hole. This suggestion is supported by semi-analytic jet acceleration models, which suggest a magnetic foot point only a few gravitational radii from the hole for 3C 345 (Vlahakis and Königl, 2004). However, jets produced by LLAGN and FR Is (and their counterparts, the BL Lacertae objects) are either less relativistic or show no motion at all. A similar model for acceleration of the NGC 6251 jet yields an inner foot-point of $\sim 34 r_g$ for a $6 \times 10^8 M_\odot$ black hole

(Vlahakis and Königl, 2004). Furthermore, M87 shows significant collimation on scales of 60–200 r_g (Biretta et al., 2002), and its jet speed at a distance of 0.16 pc from the core is only 0.1 c . Yet, at kiloparsec distances, M87 shows *superluminal* motions up to 6 c . Jets in AGN systems identified with the low/hard state appear to be launched with smaller velocities and at larger distances from the central black hole.

It appears possible, then, that the jet-production region in LLAGN and FR I objects also may look like that in Figure 1, with the launch point lying many tens of gravitational radii from the black hole. Only through continual, and persistent acceleration by the black hole over large vertical distances (many parsecs to kiloparsecs) do jets in low/hard state AGN achieve the relativistic speeds observed very far downstream of the accretion disk.

4. Conclusions

Interpretation of the photon and power spectra of black hole systems like GRS 1915+105 leads to a new magnetically dominated accretion flow (MDAF) model for the low/hard state with three distinct disk regions:

1. As in previous models, the outer region of the disk is a geometrically thin, optically thick, and cool turbulent disk, driven by the MRI.
2. Likewise, at intermediate radii (~ 100 – $1000 r_g$) there is a *one*-temperature, advection-dominated, turbulent accretion flow (ADAF) disk/corona that is geometrically thick, optically thin, and hot. An evaporation rate into this corona that scales as $\dot{M} \propto R^{-2}$ is more consistent with the power spectrum than other models.
3. The structure inside $\sim 100 r_g$ distinguishes this model from others: at the radius where cooling by relativistic electrons becomes important, the ADAF transitions to an MDAF with $\alpha \gg 1$. The inflow is extremely *inefficient*, non-turbulent and nearly radial along strong magnetic field lines—essentially an inward-facing magnetosphere. The narrow annulus where the flow transitions from ADAF to MDAF is an ideal site for open field lines and the launching an MHD-powered jet.

We identify the bandwidth-limited noise that appears in the low/hard state as the ADAF’s MRI turbulence viewed through the optically thin flow. The MDAF model predicts the observed truncation of that noise at a few Hz and the appearance of a strong QPO at the same place, as well as the very low frequency QPOs at 0.01–0.1 Hz. Finally, the MDAF model is consistent with the phenomenological models of Fender et al. (2004) and Malzac et al. (2004) and provides a physical connection between them and black hole accretion theory. In particular, extension of this model to include an MDAF inside *all* truncated disks naturally predicts the variation in jet speed with inner radius deduced by Fender et al. (2004).

The model suggests a new interpretation of the power spectrum of black hole candidates: like the photon spectrum, each small range in frequency $\Delta\nu$ is contributed by a given annulus ΔR in the accretion disk, with the central frequency corresponding to the Keplerian frequency at that radius. The spectral slopes are due not to the physics of the turbulence itself but rather to variations in disk *structure* with radius. Only the cutoff at a few Hz is indicative of the (high frequency end of the) local power spectrum there.

Acknowledgements

The author is especially grateful to T. Macarone and R. Fender for organizing this conference on black hole accretion on all mass scales. Emphasizing the similarities and scaling of black hole systems contributes greatly to their overall understanding. The author is supported, in part, by a NASA Astrophysics Theory Program grant. This research was performed at the Jet Propulsion Laboratory, California Institute of Technology, under contract to NASA.

References

- Balbus, S.A. and Hawley, J.F.: 1998, *Rev. Mod. Phys.* **70**, 1–53.
 Biretta, J.A., et al.: 1999, *ApJ* **520**, 621–626.
 Biretta, J.A., et al.: 2002, *New Astron. Rev.* **46**, 239–245.
 Blandford, R.D.: 1976, *MNRAS* **176**, 465.
 Esin, A.A., et al.: 1997, *ApJ* **489**, 865.
 Fender, R.P., et al.: 1999, *ApJ* **519**, L165.
 Fender, R.P., et al.: 2004, *MNRAS* **355**, 1105–1118.
 Gammie, C.F.: 1999, *ApJ* **522**, L57–L60.
 Genzel, R., et al.: 2003, *Nature* **425**, 934–937.
 Goldreich, P. and Julian, W.H.: 1969, *ApJ* **157**, 869–880.
 Koide, S., et al.: 2002, *Science* **295**, 1688.
 Lovelace, R.: 1976, *Nature* **262**, 649.
 Malzac, J., et al.: 2004, *MNRAS* **351**, 253.
 Maron, J. and Blackman, E.G.: 2002, *ApJ* **566**, L41–L44.
 Meier, D.L.: 2001, *ApJ* **548**, L9–L12.
 Meier, D.L.: 2004, Proceedings of the X-ray Timing Meeting: *Rossi & Beyond*, in: P. Kaaret, F. Lamb and J. Swank (eds.), 135–142.
 Meier, D.L., Koide, S. and Uchida, Y.: *Science* **291**, 84–92.
 Migliari, S., et al.: 2003, *MNRAS* **342**, L67.
 Misner, C., Thorne, K.S. and Wheeler, J.A.: 1973, *Gravitation*, Freeman.
 Morgan, E.H., et al.: 1997, *ApJ* **482**, 993–1010.
 Narayan, R., Mahadevan, R. and Quataert, E.: 1998, *The Theory of black hole Accretion Disks*, in: M. Abramowicz, G. Bjornsson and J. Pringle (eds.), Cambridge University Press, Cambridge.
 Papadakis, I.E.: 2004, *MNRAS* **348**, 207.
 Ruderman, M.A. and Sutherland, P.G.: 1975, *ApJ* **196**, 51–72.

Shu, F., et al.: 1994, *ApJ* **429**, 781–796.

Shakura, N.I. and Sunyaev, R.A.: 1973, *A&A* **24**, 337–355.

Thorne, K.S., Price, R. and MacDonald, D.A.: 1986, *Black Holes: The Membrane Paradigm*, Yale University Press, New Haven.

Vlahakis, N. and Königl, A.: 2004, *ApJ* **605**, 656–661.

Wheeler, J.C., Meier, D.L. and Wilson, J.: 2002, *ApJ* **568**, 807–819.

BLACK HOLE SYSTEMS SEEN AT HIGH SPECTRAL RESOLUTION: INFLOW AND OUTFLOW

JULIA C. LEE

*Harvard-Smithsonian Center for Astrophysics, 60 Garden Street, MS-6, Cambridge, MA 02138,
USA; E-mail: jclee@cfa.harvard.edu*

(Received 14 December 2004; accepted 1 June 2005)

Abstract. High-resolution *Chandra* and *XMM-Newton* X-ray spectroscopic studies of stellar and supermassive black holes have revealed that these phenomenologically different systems share many common physical characteristics. The observed outflows in the micro-quasar GRS 1915+105, the Seyfert 1 galaxy MCG-6-30-15 and the Seyfert 2 galaxy IRAS 18325-5926 are the focus of this proceeding.

Keywords: galaxies, active, quasars, general, X-ray, black holes, binary, micro-quasars, individual MCG-6-30-15, IRAS 18325-5926, GRS 1915+105

1. Introduction

Despite major advances in our understanding of black hole systems over the past several decades, many questions relating to the structure and dynamics of accretion onto black holes remain unanswered. Taking advantage of the high-resolution spectroscopic capabilities of *Chandra* and *XMM-Newton*, we can improve our understanding through plasma diagnostics of the observed absorption and emission lines. In particular, it has been found that black hole types differing by six to seven orders of magnitude in mass scale, from the stellar to supermassive black holes, display many similar phenomena. Of these, one of the more interesting commonalities are the photoionized outflow seen in many of these systems – this is the primary focus of this proceeding. References will be limited.

2. Common X-ray Spectral Signatures in Stellar and Supermassive Black Holes

The ultimate goal for studying both Galactic ($\sim 10 M_{\odot}$) and extragalactic (10^6 – $10^8 M_{\odot}$) black hole systems is to understand the scaling of the physics over magnitude differences in mass scales, and through this, a deeper comprehension of the generic physics which govern all accretion systems. One way to do so is to assess the similar phenomena governing these systems.



TABLE I
Phenomenologically *different* systems with many *common* characteristics

Classification	GRS 1915+105 micro-quasar	MCG–6-30-15 Seyfert 1	IRAS 18325-5926 Seyfert 2
L_{bol} (erg s ⁻¹) ^a	$\sim 10^{37}\text{--}10^{39}$	$\sim 10^{44}$	$\sim 4 \times 10^{44}$ (IR)
$M_{\text{black hole}}$ (M_{\odot}) ^b	14 [†]	$10^6\text{--}10^8$	$10^6\text{--}10^8$
v_{flow} (km s ⁻¹) ^c	~ 100	$\sim 2000^{\ddagger}$	$\sim 3 \times 10^4$
$M_{\text{accretion}}$ ($\eta \sim 0.1$) ^d	$\leq 10^{-7} M_{\odot} \text{ yr}^{-1}$	$\leq 2 \times 10^{-2}$	$\leq 7 \times 10^{-2}$
M_{flow} ($\Omega/4\pi$) ($M_{\odot} \text{ yr}^{-1}$) ^e	$\sim 2 \times 10^{-7}$	$\sim 7 \times 10^{-1}$	$\sim 2\text{--}9$
Photoionized gas	✓	✓	✓
Neutral material	✓	✓	✓
Winds/outflows	✓	✓	✓
Broad disk emission lines	✓	✓	✓

^aBolometric luminosity.

^bBlack hole mass.

^cVelocity of flow based on observed blueshift of ionized absorption lines.

^dMass accretion rate assuming 10% efficiency.

^eSpherical mass outflow rate modulo covering factor ($\Omega/4\pi$).

[†]Greiner et al. (2001).

[‡]Lee et al. (2002b). Also reported by Sako et al. (2003) and Turner et al. (2003) based on two different *XMM-Newton* RGS pointings, respectively, 120 and 320 ks (see footnote 1).

Here, I concentrate on three *phenomenologically different* systems which share many *common physical characteristics*. For these systems, the relevant comparisons of their properties are listed in Table I.

2.1. OUTFLOWS

Narrow absorption and emission lines are fairly ubiquitous in the astrophysical sources we see at high spectral resolution, and give important information about the state of the plasma, be it X-ray hot or X-ray cold. For the sources of interest in this article, the plasma is photoionized due to its proximity to the black hole. Of particular interest are the blue-shifted absorption features, indicating outflow (i.e. winds or jets), which have been seen in many different forms in *Chandra* and *XMM-Newton* spectra. Key spectroscopic signatures include: (1) Doppler-shifted absorption and/or emission lines which provide information on the kinematics and geometry of the outflow; flows ranging from hundreds of km s⁻¹ (e.g. GRS 1915 + 105: Lee et al., 2002a) to thousands of km s⁻¹ (MCG–6-30-15: Lee et al., 2002b; Sako et al., 2003; Turner et al., 2004) to near relativistic speeds (see “Section 3” below) have been reported; (2) P-Cygni profiles

(red-shifted/rest-frame emission from material out of the line-of-sight, accompanied by blue-shifted absorption lines from the foreground, line-of-sight part of the wind) as seen in both X-ray binaries (e.g. Circinus X-1: Brandt and Schulz, 2000; Schulz and Brandt, 2002) and AGN (e.g. Kaspi et al., 2001, 2002); and (3) more subtle variability effects (e.g. the micro-quasar GRS 1915+105: Lee et al., 2002a). Of these, the most remarkable are those which show relativistic velocities, e.g. the GBHC SS 433 where $v_{\text{jet}} \sim 0.27c$, (Marshall et al., 2002; Lopez et al. 2004), and more recently also seen in a handful of QSOs with known high-velocity UV outflows (Chartas et al., 2002, 2003; Hasinger et al., 2002) and some narrow-line Seyfert galaxies (Pounds et al., 2003a,b; Reeves et al., 2003)¹; the first Seyfert 2 showing such a large outflow is presented (in Table I) and in Lee et al. (in preparation).

From the X-ray measurements of these lines and shifts, a great deal can be learned about the X-ray portion of the flow. For example, based on the line broadening, information about the flow opening angle can be deduced while density diagnostics using observed He-like lines can provide important limits on the mass flow rate. One surprising thing which has emerged from some of these studies is the remarkable amount of material that is being ejected, modulo a covering factor, compared to the mass accretion rate. As can be seen in Table I, our calculations, assuming a spherical wind, imply that the flow rate in these sources is either larger than or comparable to the accretion rate, or that the covering factor is small. This is a topic worthy of further investigation.

3. The Role of High-Resolution X-ray Spectroscopy for Building the Phenomenology Towards Self-Consistent Physical Models of Black Hole Systems

The high-resolution spectral capabilities of the *Chandra* and *XMM-Newton* grating spectrometers will help in answering some of the outstanding questions relating to energetic accretion systems by allowing us to apply atomic physics techniques to the study of astrophysical plasma. A clear understanding of the line diagnostics will allow an accurate assessment of the physics, environment, and geometry governing the regions from nearest to the black hole to those which are the most distant. By studying the smaller GBHCs to compare with the black holes in AGNs, we can work towards finding answers to outstanding questions relating to the ionization structure, geometry and dynamics of the individual systems, and extend these findings to explain the mechanism required for expelling large amounts of mass, as well as the relationship between inflow and outflow. Ultimately, this might help us

¹It should be noted that the high-velocity blueshifts observed in some of these sources (Section 2.1) appear to be coincident with the redshift of the source. As such, the apparent high-velocity flows reported in the literature for the Seyfert galaxies PG 1211+143, PG 0844+349 and MCG-6-30-15 may in actuality be an ionized layer in our own Galaxy instead.

to assess whether black hole winds contribute significantly to enriching the IGM, and possibly the details governing the inter-relation between black hole growth and galaxy formation.

Acknowledgements

JCL thanks and acknowledges support from the *Chandra* fellowship grant PF2–30023 – this is issued by the *Chandra* X-ray Observatory Center, which is operated by SAO for and on behalf of NASA under contract NAS8–39073.

References

- Brandt, W.N. and Schulz, N.S.: 2000, *ApJ* **544**, L123.
- Chartas, G., Brandt, W.N. and Gallagher, S.C.: 2003, *ApJ* **595**, 85.
- Chartas, G., Brandt, W.N., Gallagher, S.C. and Garmire, G.P.: 2002, *ApJ* **579**, 169.
- Greiner, J., Cuby, J.G. and McCaughrean, M.J.: 2001, *Nature* **414**, 522.
- Kaspi, S. et al.: 2001, *ApJ* **554**, 216.
- Kaspi, S. et al.: 2002, *ApJ* **574**, 643.
- Lee, J.C., Canizares, C.R., Fang, T., Morales, R., Fabian, A.C., Marshall, H.L. and Schulz, N.S.: 2002b, *X-ray Spectroscopy of AGN with Chandra and XMM-Newton*, p. 9.
- Lee, J.C., Iwasawa, K. and Canizares, C.R.: 2004, *ApJ*, in preparation.
- Lee, J.C., Reynolds, C.S., Remillard, R., Schulz, N.S., Blackman, E.G. and Fabian, A.C.: 2002a, *ApJ* **567**, 1102.
- Lopez, L.A., Marshall, H.L., Schulz, N.S., Kane, J.F. and Canizares, C.R.: 2004, *ApJ*, submitted for publication.
- Marshall, H.L., Canizares, C.R. and Schulz, N.S.: 2002, *ApJ* **564**, 941.
- Pounds, K.A., King, A.R., Page, K.L. and O'Brien, P.T.: 2003a, *MNRAS* **346**, 1025.
- Pounds, K.A., Reeves, J.N., King, A.R., Page, K.L., O'Brien, P.T. and Turner, M.J.L.: 2003b, *MNRAS* **345**, 705.
- Reeves, J.N., O'Brien, P.T. and Ward, M.J.: 2003, *ApJ* **593**, L65.
- Sako, M. et al.: 2003, *ApJ* **596**, 114.
- Schulz, N.S. and Brandt, W.N.: 2002, *ApJ* **572**, 971.
- Turner, A.K., Fabian, A.C., Lee, J.C. and Vaughan, S.: 2004, *MNRAS* **353**, 319.

BLACK HOLE SPIN IN AGN AND GBHCs

CHRISTOPHER S. REYNOLDS¹, LAURA W. BRENNEMAN¹
and DAVID GAROFALO²

¹*Department of Astronomy, University of Maryland, College Park, MD 20742, U.S.A.;*
E-mail: chris@astro.umd.edu

²*Department of Physics, University of Maryland, College Park, MD 20742, U.S.A.*

(Received 1 October 2004; accepted 1 June 2005)

Abstract. We discuss constraints on black hole spin and spin-related astrophysics as derived from X-ray spectroscopy. After a brief discussion about the robustness with which X-ray spectroscopy can be used to probe strong gravity, we summarize how these techniques can constrain black hole spin. In particular, we highlight *XMM-Newton* studies of the Seyfert galaxy MCG-6-30-15 and the stellar-mass black hole GX 339-4. The broad X-ray iron line profile, together with reasonable and general astrophysical assumptions, allow a non-rotating black hole to be rejected in both of these sources. If we make the stronger assertion of no emission from within the innermost stable circular orbit, the MCG-6-30-15 data constrain the dimensionless spin parameter to be $a > 0.93$. Furthermore, these *XMM-Newton* data are already providing evidence for exotic spin-related astrophysics in the central regions of this object. We conclude with a discussion of the impact that *Constellation-X* will have on the study of strong gravity and black hole spin.

Keywords: accretion disks, black hole physics

1. Introduction

With searches for evidence of the existence of black holes and the dynamical measurements of their masses becoming almost passé, an increasing focus is being placed on detecting the effects of black hole spin. Spin truly is a creature of the relativistic Universe, and the observational investigation of spin puts us one step closer to being able to genuinely test strong-field General Relativity (GR). Even if GR passes all of these tests (which, of course, would be the most “boring” possibility), black hole spin gives us crucial insight into how black holes of all masses are born, and may well be an important ingredient in powering some of the most energetic sources in the Universe.

At the current time, the best evidence for the effects of black hole spin come from X-ray observations, both timing and spectroscopy. X-ray variability studies, particularly investigations of quasi-periodic oscillations (QPOs) have produced tantalizing hints that we might be witnessing the effects of black hole spin (Stella et al., 1999; Strohmayer, 2001). However, the lack of any agreed upon theoretical framework for the high-frequency QPOs prevents us from drawing robust conclusions at this



time. For this reason, the most compelling studies of black hole spin have originated from X-ray spectroscopy.

In this contribution, we describe constraints on black hole spin from X-ray spectroscopy. We will align our discussion around three questions; “Have we seen the effects of strong gravity at all?”, “Have we seen the effects of black hole spin?”, and “Can we probe the exotic astrophysics associated with spinning black holes?” For the impatient reader, the answers to these questions are “Yes!”, “Very probably”, and “We’re maybe just starting to. . .”. We conclude by discussing future prospects for probing black hole spin and testing strong-field GR with both X-rays and gravitational waves.

2. Strong Gravitational Effects in X-ray Spectra

The principal spectroscopic tool used to date to study strong gravity is the characterization of the broad iron- $K\alpha$ fluorescent emission line (see reviews by Fabian et al. (2000) and Reynolds and Nowak (2003)). The essential physics underlying this phenomenon is straightforward. Moderate-to-high luminosity black hole systems accrete via a radiatively-efficient disk. Even in the region close to the black hole, such a disk will (apart from a hot and tenuous X-ray emitting corona) remain optically-thick, geometrically-thin, almost Keplerian, and rather cold ($T < 10^7$ K). X-ray irradiation of the surface layers of the disk by the corona will excite observable fluorescence lines, with iron- $K\alpha$ being most prominent due to the combination of its astrophysical abundance and fluorescent yield. This emission line is then subject to extreme broadening and skewing due to the both the normal and transverse Doppler effect (associated with the orbital velocity of the disk) as well as the gravitational redshift of the black hole (see Figure 1).

So, have we seen these effects in the X-ray spectra of real accreting black holes? Broad emission features that can be modelled as iron emission lines from the central regions of a Keplerian accretion disk are present in the *XMM-Newton* data for over half of the moderate-to-high luminosity Seyfert galaxies, as well as many Galactic Black Hole Candidates (GBHCs) in their intermediate and high state. Given the breadth of these features, it is valid to ask whether continuum curvature and/or unmodelled complex absorption might be mimicking a broad emission line. In some cases, detailed scrutiny of high signal-to-noise *XMM-Newton* data allows one to reject these alternatives, further validating the relativistic line interpretation (e.g. MCG-6-30-15 (Vaughan and Fabian, 2004; Reynolds et al., 2004; also see Fabian et al., 1995), GX 339-4; Miller et al., 2004). In other cases, absorption by large columns of photoionized material appears to be important. In the case of NGC 4151, for example, much of the broad iron line reported by Wang et al. (1999) was probably an artifact of not modelling the complex absorber later identified by Schurch and Warwick (2002) and Schurch et al. (2003). In many other cases, the role that complex absorption has on the presence of a broad iron line remains

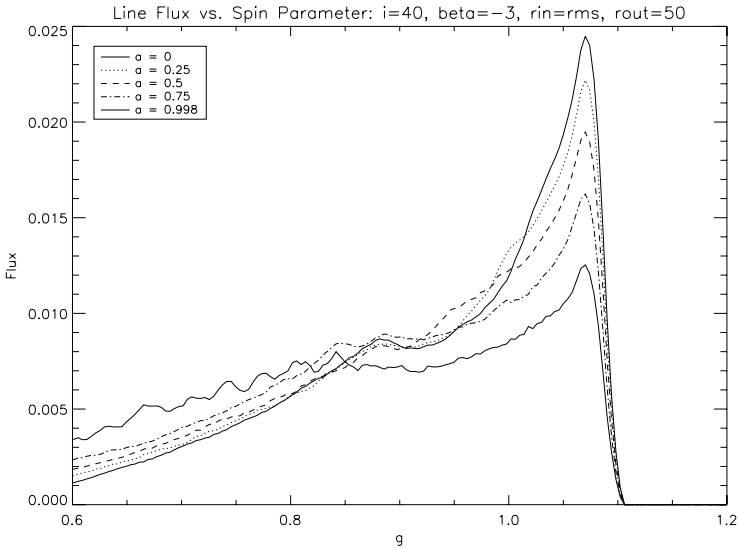


Figure 1. Theoretical lines profiles from a Keplerian accretion disk around a Kerr black hole. We assume an observed inclination angle of $i = 40^\circ$ and a line emissivity that falls off as r^{-3} between the ISCO and $r_{\text{out}} = 50 \text{ GM}/c^2$.

uncertain. It is important to stress, however, that the role of photoionized absorption in masking or mimicking broad iron lines is *knowable*, and will be elucidated by the high-resolution and high count-rate spectra that *Astro-E2* will be obtaining on a regular basis starting in early 2005.

To summarize this section, there are robust examples of broad iron emission lines that are giving us a clean probe of the strong gravity region around both stellar and supermassive black holes. However, while broad iron lines are not rare, the precise fraction of objects in the various classes of accreting black holes that display these features is still uncertain. In addition to obtaining new high-resolution and high count-rate spectra with *Astro-E2*, significant progress is possible in this field via a large and unbiased survey of current *XMM-Newton* data.

3. Constraining Black Hole Spin with X-ray Spectroscopy

Having established that at least some accreting black holes display broad iron lines that cleanly probe the strong gravity region, we now ask whether we can constrain the black hole spin using these features. To sharpen the discussion, we will address whether one can rule out a Schwarzschild metric (i.e., non-spinning black hole) for any given black hole system.

Even with *XMM-Newton*, we cannot probe the iron line on the dynamical timescale of the very centralmost regions of the accretion disk where spin effects

are dominant. We are driven to study line profiles that have been time-averaged over several dynamical timescales – hence, our primary information on black hole spin at the current time will originate from the breadth and redshift of these time-averaged line profiles.

There is a common misconception that rapidly spinning black holes invariably produce broader and more highly redshifted emission lines than slowly spinning black holes. This stems from the fact that the innermost stable circular orbit (ISCO; $6GM/c^2$ for a non-rotating black hole) for a prograde accretion disk pulls in towards the horizon as the spin parameter of the black hole is increased. Hence, the line broadening will increase with black hole spin *if* the line emission is always truncated at the ISCO. But it is important to realize that we can produce arbitrarily redshifted and broadened emission lines from around even a non-rotating black hole *if nature had the freedom to produce line emission from any radius beyond the horizon* (Reynolds and Begelman, 1997). This discouraging fact has led some authors to conclude that current iron line profiles contain essentially no information on the black hole spin (Dovciak et al., 2004).

This would be an overly bleak assessment of our ability to constrain black hole spin. Even the application of some rather weak (i.e., general) astrophysical constraints can impose an inner limit on the radii at which spectral features can be produced. In order to produce any significant iron emission line from the region within the ISCO (which we shall refer to as the plunging region), the disk in this region must be optically thick, not too highly ionized (i.e., a significant fraction of the iron cannot be fully ionized), and illuminated by the hard X-ray continuum. While much work remains to be done on the physical state of matter in the plunging region, it is challenging to construct a model for a non-rotating black hole in which there are appreciable spectral features produced by matter inside of $4\text{--}5 GM/c^2$ (Reynolds and Begelman, 1997). If we require an emitting radius less than this when fitting a non-rotating black hole model to a particular dataset, we can claim to have found good evidence for a spinning black hole.

This is exactly the situation we find when attempting to fit the *XMM-Newton* data for the Seyfert-1 galaxy MCG-6-30-15. The June 2000 observation of this source (reported by Wilms et al. (2000) and Reynolds et al. (2004)) caught it in its enigmatic “Deep Minimum State” first identified with *ASCA* data by Iwasawa et al. (1996) during which the iron line is known to be particularly broadened and redshifted. Fitting the Reynolds and Begelman (1997), Schwarzschild iron line model, which includes emission from within the plunging region, results in essentially all of the emission being placed at $3 GM/c^2$. It is extremely hard to understand how this could be a physical result – the relativistic inflow at this location demands (through mass continuity) that the density be low and, hence, that this material be completely photoionized if it were to experience the irradiation suggested by this fit. Thus, the extreme parameters derived from a fit to a Schwarzschild-based model leads to the conclusion that we are seeing the effects of black hole spin.

Given an observation of a very broad iron line such as that detected in the Seyfert-1 galaxy MCG-6-30-15 or the GBHC GX 339-4 (Miller et al., 2004), we can place constraints on the black hole spin given certain astrophysical assumptions. The systematic exploration of these constraints has only just begun and is still a work in progress. To facilitate this work, we have constructed a new iron line profile code `kerr` (that employs the Kerr metric ray-tracing code of Speith et al., 1995) which treats the black hole spin as a free parameter. This code also takes advantage of modern computing speeds and performs the necessary calculations in real time as the spectrum is being fit with XSPEC. The user may therefore tune the spectral resolution and numerical accuracy of the model to suit the data at hand, a feature that is not available in the tabular models such as `1aor` that have been extensively employed to date.

Preliminary fitting of `kerr` to the highest signal-to-noise data for MCG-6-30-15 (from the June 2001 observation) demonstrates that the black hole must possess a dimensionless spin parameter of $a > 0.93$ (Brenneman and Reynolds, in preparation) *if we impose the condition that no spectral features are produced from within the ISCO*. See Figure 1 for examples of line profiles calculated under this assumption. Current work is focused on obtaining spin constraints once that assumption is relaxed. Note that these fits assume a broken power-law form for the line emissivity as a function of radius. Hence, our limit of $a > 0.93$ is a stronger constraint than $a > 0.94$ deduced by Dabrowski et al. (1997) from *ASCA* data who assumed the line emissivity tracks the radial dissipation profile of a “standard” (Novikov and Thorne, 1974; Page and Thorne, 1974) accretion disk. As will be discussed later, the *XMM-Newton* data are of sufficient quality to actually falsify the Dabrowski et al., assumption.

4. The Exotic Astrophysics of Spinning Black Holes

Rapidly spinning black holes are undoubtedly amongst the most exotic objects in the current-day universe. In this section, we focus on one particular facet of their behaviour – the magnetic interactions between the spinning black hole and surrounding matter including the accretion disk. We argue that *XMM-Newton* data are already hinting at evidence for the magnetic extraction of spin energy from the black hole in MCG-6-30-15.

Analytic (Krolik, 1999; Gammie, 1999) and numerical (Hawley and Krolik, 2001; Reynolds and Armitage, 2002) studies have shown that magnetic forces can couple material within the plunging region to the body of the accretion disk, thereby extracting energy and angular momentum from that region. In an extreme limit, a Penrose process¹ might be realized in which the innermost regions of the

¹We note that Williams (2003) has also argued for the importance of a non-magnetic, particle–particle and particle–photon scattering mediated Penrose process.

accretion flow are placed on negative energy orbits by these magnetic torques (Agol and Krolik, 2000). Together with any Blandford–Znajek process (Blandford and Znajek, 1977) that might result from field lines directly connecting to the (stretched) horizon, these magnetic torques can in principal extract a black hole’s spin energy, depositing it either in the body of the disk or in the form of an outflow of mass and/or Poynting flux. Note that all of this behaviour is in stark contrast to standard black hole disk models (Shakura and Sunyaev, 1973; Novikov and Thorne, 1974; Page and Thorne, 1974) in which material follows conservative orbits once inside the ISCO.

Can we see evidence for any of these processes in the current data? Again, we return to the Deep Minimum State of MCG-6-30-15 which displays one of the broadest and most highly redshifted iron lines known. This immediately tells us that the X-ray reflection features are originating from a region that is extremely centrally concentrated in the accretion disk. For the moment, we assume that the primary continuum X-ray source is located a small distance above the disk surface (the “local corona approximation”) and radiates a fixed fraction of the energy dissipated in the underlying disk. Then, even assuming a near-maximal rotating black hole (with $a = 0.998$), these data cannot be adequately described with a model consisting of a standard Novikov and Thorne (1974) accretion disk – the model simply cannot reproduce the centrally concentrated emission pattern inferred from these data (Figure 2a). One can attempt to rescue the standard disk model by supposing that a larger portion of the total dissipation in the disk is channeled into the X-ray emitting corona as one moves to smaller radii. However, since 30–50% of the bolometric power of MCG-6-30-15 seems to emerge through the X-ray emitting corona, one cannot decouple it entirely from the dissipation distribution. In the most extreme model (which provides an adequate but not the best fit to the data), *all* of the

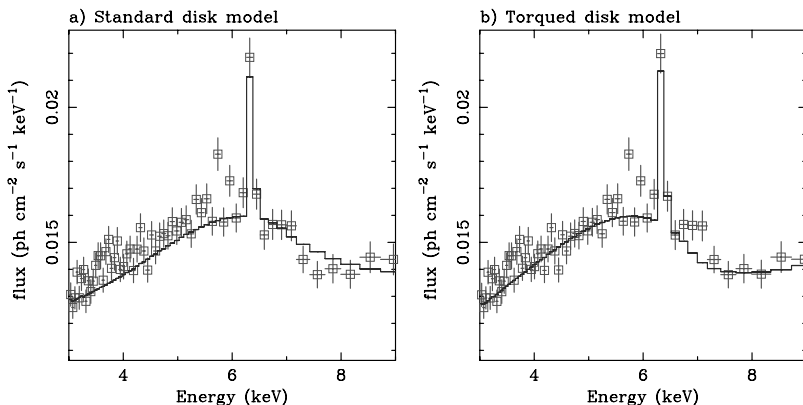


Figure 2. Broad iron line fit assuming that the line emission tracks the underlying disk dissipation of (a) a standard (Novikov and Thorne, 1974) accretion disk and, (b) an Agol and Krolik (2000) torqued accretion disk. Modified from Reynolds et al. (2004).

dissipated energy is channeled into the X-ray emitting corona within the central $5 GM/c^2$, while the X-ray production efficiency is zero beyond that radius.

Our best-fitting model consists of a strongly torqued accretion disk in which the extreme central concentration originates from a magnetic torque by the plunging region or the rotating black hole (Reynolds et al., 2004; Figure 2b) – the work done by the torque is dissipated in the main body of the accretion disk and, with some efficiency, energizes the inner regions of the X-ray emitting corona. If this is really the correct description of the physics at play, the data argue that the accretion disk is in an extreme torque-dominated state, i.e., the disk is predominately shining through the release of black hole spin energy.

MHD simulations suggest that magnetic connections between the plunging region and the body of an accretion disk tend to be rather sporadic. It is then tempting to identify MCG-6-30-15's transition into the Deep Minimum State as the (temporary) onset of a significant inner torque. The fact that the overall luminosity of a disk necessarily increases when an inner torque is applied (due to the dissipation of the extra work done by the inner torque), in contrast to X-ray flux drop observed during the Deep Minimum State, may be a problem for this model. However, the enhanced returning radiation associated with the torque-induced emission will strongly Compton cool the X-ray corona leading to a steepening of the X-ray continuum and (possibly) a large-scale condensation-driven collapse of the corona. Such effects may be responsible for the X-ray flux decrease (Garofalo and Reynolds, 2005).

It is also possible that the local-corona approximation is not valid. If the X-ray emitting source is a significant height above the optically thick part of the accretion disk, the hard X-ray continuum photons will be gravitationally focused into the central regions of the accretion disk (see Andy Fabian's contribution in these proceedings). Aspects of this scenario have been explored by many authors including Martocchia and Matt (1996), Reynolds and Begelman (1997) and Miniutti and Fabian (2004). This suggests an alternative picture in which the Deep Minimum State is produced when the X-ray source is located at mid/high latitudes very close to the black hole. The centrally concentrated X-ray reflection results from the gravitational focusing, and the decrease in the observed continuum X-ray flux is a natural consequence of the fact that the continuum photons are focused *away* from the observer (Reynolds and Begelman, 1997; Miniutti and Fabian, 2004). We note that this scenario does not diminish the need for exotic spin-related astrophysics – the base of a spin-driven magnetic jet is an obvious candidate for this elevated continuum X-ray source.

5. Conclusion and the Future of Black Hole Studies

Current data are already allowing us to probe black hole physics within a few gravitational radii of the event horizon, and may well be giving us the first observational

glimpses of physics within the ergosphere. But this is just the beginning of X-ray astronomy's exploration of strong gravity, not the end of the road. The enormous throughput of *Constellation-X* will allow us to probe detailed time variability of the iron line. Dynamical timescale line variability, an easy goal for *Constellation-X*, will allow us to follow non-axisymmetric structures in the disk as they orbit (Armitage and Reynolds, 2003; also see Iwasawa et al. (2003) for the first hint of such structure in *XMM-Newton* data). This gives us a direct probe of an almost Keplerian orbit close into a black hole. Furthermore, line variability on the light crossing time will allow us to probe relativistic reverberation signatures (Reynolds et al., 1999; Young and Reynolds, 2000), essentially giving us a direct probe of the null geodesics in the spacetime. Together, these variability signatures will allow true tests of strong-field GR.

There is no compelling reason to believe that GR fails on the macroscopic scales probed by either X-ray or gravitational wave studies of astrophysical black holes. In the event that GR is verified, both X-ray and gravitational wave observations will allow unambiguous measurements of black hole spins. Gravitational wave observations with *LISA* of a stellar mass black hole spiraling into a $10^6 M_\odot$ black hole (a so-called Extreme Mass Ratio Inspiral; EMRI) will allow precision measurement of the supermassive black hole's spin as well as tests of the no-hair theorem and the Kerr metric. The event rates of such sources is quite uncertain, however, partially due to the recent evidence for "anti-hierarchical" black hole growth (e.g., Marconi et al., 2004) and its implications for the number density of $10^6 M_\odot$ black holes in the cosmic past. X-ray spectroscopy with *Constellation-X* provides a crucial parallel track of study in which we can obtain measurements of black hole spin across the whole mass range of astrophysical black holes (i.e., stellar, intermediate, and supermassive) using spectral features that are already known to exist. Only then can the demographics and astrophysical relevance of black hole spin truly be gauged.

Acknowledgement

We thank the conference organizers for a stimulating and highly enjoyable meeting. We also thank the National Science Foundation (US) for support under grant AST0205990.

References

- Agol, E. and Krolik, J.H.: 2000, *ApJ* **528**, 161.
 Armitage, P.J. and Reynolds, C.S.: 2003, *MNRAS* **341**, 1041.
 Blandford, R.D. and Znajek, R.L.: 1977, *MNRAS* **179**, 433.
 Dovciak, M., Karas, V. and Yaqoob, T.: 2004, *ApJS* **153**, 205.
 Fabian, A.C., Iwasawa, K., Reynolds, C.S. and Young, A.J.: 2000, *PASP* **112**, 1145.
 Fabian, A.C., et al.: 1995, *MNRAS* **277**, L11.
 Gammie, C.F.: 1999, *ApJ* **522**, L57.

- Garofalo, D. and Reynolds, C.S.: 2005, *ApJ* **624**, 94.
- Hawley, J.F. and Krolik, J.H.: 2001, *ApJ* **548**, 348.
- Iwasawa, K., et al.: 1996, *MNRAS* **282**, 1038.
- Iwasawa, I., Miniutti, G. and Fabian, A.C.: 2004, *MNRAS* **355**, 1073.
- Krolik, J.H.: 1999, *ApJ* **515**, L73.
- Marconi, A., Risaliti, G., Gilli, R., Hunt, L.K., Mailino, R. and Salvati, M.: 2004, *MNRAS* **351**, 169.
- Miller, J.M., et al.: 2004, *ApJL* **606**, L131.
- Miniutti, G. and Fabian, A.C.: 2004, *MNRAS* **349**, 1435.
- Novikov, I.D., Thorne, K.S.: 1974, in: C. DeWitt and D. DeWitt (eds.), *Black Holes*, p. 343.
- Page, D.N. and Thorne, K.S.: 1974, *ApJ* **191**, 499.
- Reynolds, C.S. and Armitage, P.J.: 2002, *ApJ* **561**, L81.
- Reynolds, C.S. and Begelman, M.C.: 1997, *ApJ* **487**, 109.
- Reynolds, C.S. and Nowak, M.A.: 2003, *Phys. Rep.* **377**, 389.
- Reynolds, C.S., Wilms, J., Begelman, M.C., Staubert, R. and Kendziorra, E.: 2004, **349**, 1153.
- Reynolds, C.S., Young, A.J., Fabian, A.C. and Begelman, M.C.: 1999, *ApJ* **514**, 164.
- Schurch, N.J. and Warwick, R.S.: 2002, *MNRAS* **334**, 811.
- Schurch, N.J., Warwick, R.S., Griffiths, R.E. and Sembay, S.: 2003, *MNRAS* **345**, 423.
- Speith, R., Riffert, H. and Ruder, H., *CoPhC*, **88**, 109.
- Stella, L., Vietri, M. and Morsink, S.M.: 1999, *ApJ* **524**, 63.
- Strohmayer, T.E.: 2001, *ApJ* **554**, L169.
- Vaughan, S. and Fabian, A.C.: 2004, **348**, 1415.
- Wang, J.X., Zhou, Y.Y. and Wang, T.G.: 1999, *ApJ* **523**, L129.
- Williams, R.K.: 2003, astro-ph/0306135v1.
- Wilms, J., Reynolds, C.S., Begelman, M.C., Reeves, J., Molendi, S., Staubert, R. and Kendziorra, E.: 2001, *MNRAS* **328**, L27.
- Young, A.J. and Reynolds, C.S.: 2000, *ApJ* **529**, 101.

THE SEYFERT-LINER GALAXY NGC 7213: AN *XMM-NEWTON* OBSERVATION*

R.L.C. STARLING^{1,2}, M.J. PAGE², G. BRANDUARDI-RAYMONT²,
A.A. BREEVELD,² R. SORIA² and K. WU²

¹*Astronomical Institute "Anton Pannekoek", University of Amsterdam, Kruislaan 403, Amsterdam 1098 SJ, The Netherlands; E-mail: starling@science.uva.nl*

²*Mullard Space Science Laboratory, University College London, London, U.K.*

(Received 29 September 2004; accepted 30 November 2004)

Abstract. We examine the *XMM* X-ray spectrum of the low-ionisation nuclear emission-line region (LINER)-AGN NGC 7213, which is best fit with a power law, $K\alpha$ emission lines from Fe I, Fe XXV and Fe XXVI and a soft X-ray collisionally ionised thermal plasma with $kT = 0.18_{-0.01}^{+0.03}$ keV. We find a luminosity of $7 \times 10^{-4} L_{\text{Edd}}$, and a lack of soft X-ray excess emission, suggesting a truncated accretion disc. NGC 7213 has intermediate X-ray spectral properties, between those of the weak AGN found in the LINER M 81 and higher luminosity Seyfert galaxies. This supports the notion of a continuous sequence of X-ray properties from the Galactic Centre through LINER galaxies to Seyferts, likely determined by the amount of material available for accretion in the central regions.

Keywords: X-rays: galaxies, galaxies: active, galaxies: Seyfert, galaxies: individual, NGC 7213

1. Introduction

Low-ionisation nuclear emission-line region (LINER) galaxies are characterised by optical emission-line ratios which indicate a low level of ionisation (Heckman, 1980). The origin of these emission lines is still the subject of debate: the lines are attributed either to shock heating (Baldwin et al., 1981) or to photoionisation by a central AGN (Ferland and Netzer, 1983; Halpern and Steiner, 1983). NGC 7213 is a nearby ($z = 0.006$) S0 galaxy with AGN and LINER characteristics. It is clear that there is an AGN in this source, classified as a Seyfert 1 (Phillips, 1979). Optical emission lines are observed from this galaxy with velocities ranging from 200 to 2000 km s⁻¹ FWHM (Filippenko and Halpern 1984, hereafter FH84). FH84 argue that this emission comes from photoionisation by the AGN of clouds spanning a range of densities and velocities.

Since its discovery as a low luminosity X-ray source (Marshall et al., 1978) NGC 7213 has been observed with several X-ray missions, showing a power law shaped spectrum with an Fe I $K\alpha$ line. Excess emission has been detected at higher

*This work is based on observations obtained with *XMM-Newton*, an ESA science mission with instruments and contributions directly funded by ESA Member States and the USA (NASA).

energies, best explained as weak narrow emission lines from highly ionised iron. The same data have no significant reflection hump, suggesting that the Fe $1\text{K}\alpha$ line originates in Compton-thin material (Bianchi et al., 2003, hereafter B03, *BeppoSAX* PDS+*XMM* pn). The presence of a soft X-ray excess in NGC 7213 was also inferred by those observations and *EXOSAT* results (Turner and Pounds, 1989).

Here we present the full *XMM* observation of NGC 7213 including high-resolution spectra from the RGS instruments. Identifying the physical mechanisms producing the X-ray emission may help to reveal the origin of the optical emission lines where at present neither shock heating nor photoionisation by the AGN can be ruled out. We also discuss the relationship between Seyfert galaxies and LINERs.

2. *XMM* Observations and Spectral Fitting

NGC 7213 was observed on 28/29 May 2001 with *XMM* in the RGS GT Programme. The exposure times are 46 448 s for MOS1, 42 201 s for pn and 46 716 s for each RGS instrument. The source is piled up in MOS2. The MOS1 and pn spectra were combined using the method of Page et al. (2003). The data were processed with *XMM* SAS versions 5.2 and 5.4, and analysed using XSPEC v11.2. The Galactic column used in all fits is $N_{\text{H}} = 2.04 \times 10^{20} \text{ cm}^{-2}$ (Dickey and Lockman, 1990), errors are 90% confidence for one interesting parameter and line energies are rest frame values.

RGS: The RGS spectrum of NGC 7213 is dominated by continuum emission, but emission lines are present, particularly from O VII and O VIII. No significant absorption lines or broad absorption features are observed. The features at 13.08 and 16.43 Å are low signal to noise data points coinciding with chip-gaps in the first order spectra. To model the RGS spectrum we began with a power law, which is rejected at >99.5% confidence. To improve the fit, we added a MEKAL thermal plasma component, and obtain an acceptable fit with a best fit plasma temperature of $kT = 0.18_{-0.01}^{+0.02}$ keV and $\chi^2/\nu = 554/496$. Addition of a second thermal plasma component improves the fit only slightly. The O VII lines are reproduced well by the 0.18 keV thermal plasma component, but there appears to be some emission adjacent to O VIII Ly α in excess of the model prediction, perhaps indicating that the higher temperature component is broadened by Doppler motions. There is no significant blackbody-like soft-excess emission above the power law. The model and data are shown in Figure 1.

The ‘G’ ratio of the intercombination ($x + y$) and forbidden (z) line strengths to the resonance (w) line strength in the He-like triplet of O VII allows us to discriminate collisionally ionised and photoionised emission (Porquet and Dubau, 2003). We obtained the G ratio by fitting the 21–23 Å region with a power law and three emission lines (Figure 2). Collisionally ionised plasmas have $G \approx 1$, consistent with that observed in NGC 7213, while photoionisation-dominated plasmas have $G \geq 4$, which is excluded at >95% confidence. A photoionised plasma that does

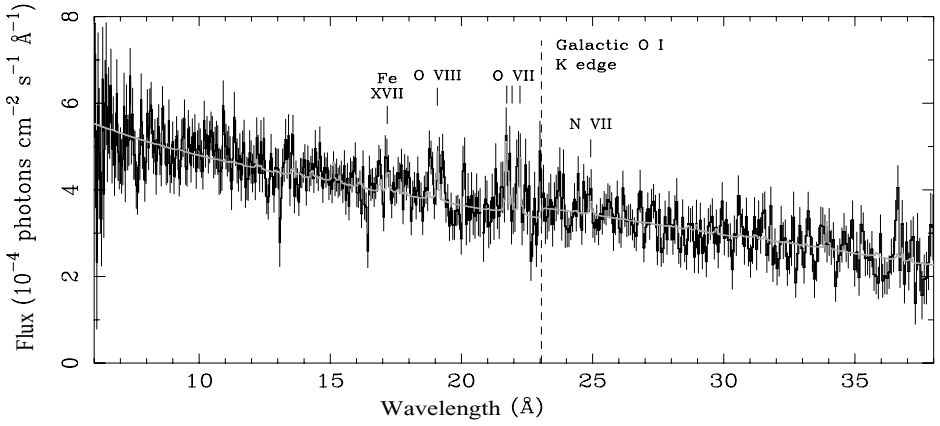


Figure 1. The RGS spectrum of NGC 7213 with the best fitting model overlotted in grey. Prominent emission lines and the O I K edge from the Galactic ISM are labelled.

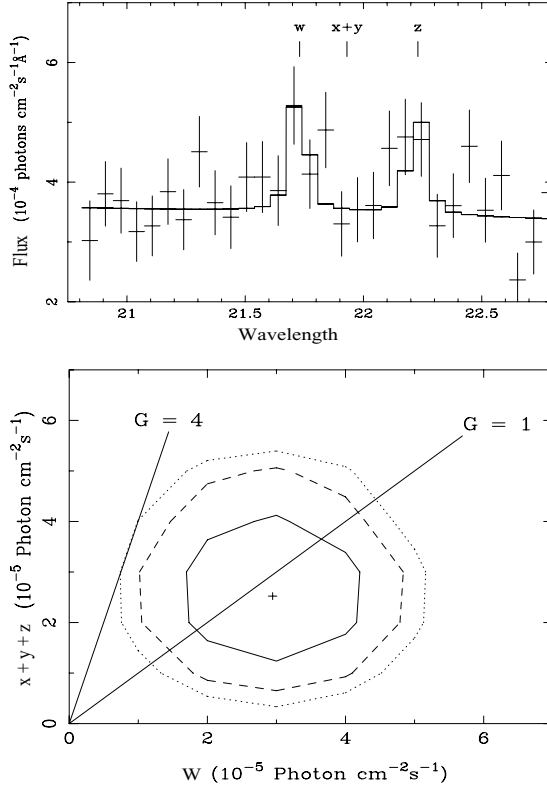


Figure 2. Upper panel: Close up of the He-like O VII triplet with best fitting power law plus 3-Gaussian model. Wavelength in \AA . Lower panel: Confidence contours for the strengths of the forbidden and intercombination lines ($x + y + z$) and the resonance line (w). The solid, dashed and dotted contour lines correspond to 68, 90 and 95% respectively for two interesting parameters. $G = 1$ is expected for a collisionally ionised plasma; a photoionised plasma should lie to the left of the $G = 4$ line.

not lie along the line of sight could have $G < 4$ if the resonance line is enhanced by photoexcitation (Coupé et al., 2004). But the 3d–2p lines of Fe XVII at $\sim 15 \text{ \AA}$ should then also be enhanced relative to the 3s–2p lines at $\sim 17 \text{ \AA}$, as is observed in NGC 1068 (Kinkhabwala et al., 2002). This is not the case in NGC 7213, and so we conclude that the emission lines in the RGS spectrum are predominantly from collisionally ionised gas.

EPIC: A power law is clearly a poor fit to the 2–10 keV EPIC data. The presence of reflection has been ruled out in B03, and these authors conclude that the excess emission is explained with three Fe emission lines. Combination of the EPIC pn and MOS1 data provides better statistics than pn alone. We fit a power law plus three Gaussian lines of fixed narrow width ($\sigma = 1 \text{ eV}$) to the 2–10 keV combined pn–MOS1 spectrum. The best fit ($\chi^2/\nu = 212/169$) has a power law photon index of $\Gamma = 1.73 \pm 0.01$, consistent with that found in the RGS soft X-ray data. The centroid energies of the emission lines in the fit to the combined EPIC data are indeed consistent with iron fluorescence in low ionisation material, Fe XXV and Fe XXVI. We find equivalent widths of Fe I (which will include a small contribution from Fe II to Fe XVII), Fe XXV and Fe XXVI $K\alpha$ emission lines of 82_{-13}^{+10} , 24_{-11}^{+9} and 24_{-13}^{+10} eV, respectively.

3. Discussion

NGC 7213 resembles a typical Seyfert galaxy, in that its 2–10 keV spectrum is dominated by a $\Gamma \sim 1.7$ power law and a 6.4 keV Fe $K\alpha$ emission line. Significant emission from Fe XXV and Fe XXVI is also present, which are not normally observed in the classical luminous Seyfert galaxies (e.g. NGC 5548, Pounds et al., 2003; NGC 7469, Blustin et al., 2003), but appear to dominate the Fe $K\alpha$ emission in the nearby LINER M 81 (Page et al., 2004). The Fe XXV and Fe XXVI lines may be produced by photoionisation of Compton-thin material by the nuclear X-ray source (Bianchi et al., 2004), or may be collisionally ionised like the soft X-ray thermal plasma. The soft X-ray emitting gas in Seyfert galaxies is usually found to be photoionised (eg. IRAS 13349+2438, Sako et al., 2001), but unlike typical Seyferts, the soft X-ray spectrum of NGC 7213 is more consistent with the emission from a collisionally ionised plasma.

Many Seyfert galaxies show compelling evidence for an accretion disc surrounding the black hole in their X-ray spectra. The main indicators are a soft excess, reflection, and broad Fe $K\alpha$ line emission, all of which originate from the inner parts of the accretion disc. None of these indicators are present in the *XMM* spectra of NGC 7213. There is no evidence for an optical/UV bump and consequently the AGN bolometric luminosity does not appear to be dominated by emission from an optically thick, geometrically thin accretion disc. From combining our L_{bol} estimate from the *XMM*+archival data SED with the mass estimate of $M_{\text{BH}} = 10^{8.0} M_{\odot}$ (Nelson and Whittle, 1995), we find that the luminosity of NGC 7213 is low, at

approximately $7 \times 10^{-4} L_{\text{Edd}}$. Therefore, it is likely that if there is an accretion disc in NGC 7213, its inner edge is truncated at a larger radius than is typical in Seyfert galaxies. This could be via an ADAF-type flow (Narayan and Yi, 1995), or the disc may be in a ‘low state’ (Siemiginowska et al., 1996).

The lack of reflection (B03) implies the Fe I $K\alpha$ line arises in Compton-thin material. Thus, the central region of NGC 7213 appears to be deficient in the dense, cool material. That LINERs have gas-poor central regions relative to Seyferts has also been proposed by Ho et al. (2003) on the basis of their optical emission line properties. It appears then that the low luminosities and therefore accretion rates of LINER-AGN are a consequence of a shortage of material in their central regions. In this case, LINERs are just fuel-starved AGN.

If we compare the *XMM* X-ray spectra of NGC 7213 and the nearest LINER galaxy, M 81 (Page et al., 2003, 2004), the broad-band X-ray spectra of these two galaxies look remarkably similar. Whilst the continua are comparable, we find substantial differences in the emission line parameters. The X-ray spectrum of NGC 7213 is much more Seyfert-like than that of M 81, owing to the stronger Fe I $K\alpha$ line and weaker soft X-ray lines. Therefore, NGC 7213 appears to bridge the gap between ‘normal’ Seyfert galaxies and LINER galaxies such as M 81.

It appears that there is likely a continuous distribution of galaxy nuclei between the LINERs and ‘normal’ Seyfert nuclei, over which the X-ray spectral features characteristic of Seyferts such as the neutral Fe $K\alpha$ line, become successively more prominent, while characteristic LINER features such as soft X-ray emission lines diminish in significance. Accretion rate onto the black hole with respect to the Eddington rate is likely to be the overriding factor, with LINER galaxies accreting at much lower rates than Seyfert galaxies (Ho et al., 2003) and containing truncated discs. In fact, if we look at the observational properties of the Galactic Centre we see that it may also fit into this continuous distribution since it contains a low-mass black hole with an extremely low accretion rate: the emission from this region comes predominantly from thermal plasmas with strong soft X-ray emission (Baganoff et al., 2003), and the strongest Fe $K\alpha$ emission is observed at 6.7 keV (Tanaka et al., 2000).

Acknowledgements

RLCS acknowledges support from a PPARC studentship and an EU RTN fellowship.

References

- Baganoff, F.K., et al.: 2003, *ApJ* **591**, 891.
 Baldwin, J.A., Phillips, M.M. and Terlevich, R.: 1981, *PASP* **93**, 5.
 Bianchi, S., Matt, G., Balestra, I. and Perola, G.C.: 2003, *A&A* **407**, L21.
 Bianchi, S., Matt, G., Balestra, I., Guainazzi, M. and Perola, G.C.: 2004, *A&A* **422**, 65.

- Blustin, A.J., et al.: 2003, *A&A* **403**, 481bitem Coupé, S., Godet, O., Dumont, A.-M. and Collin, S.: 2004, *A&A* **414**, 979.
- Dickey, J.M. and Lockman, F.J.: 1990, *ARA&A* **28**, 215.
- Ferland, G.J. and Netzer, H.: 1983, *ApJ* **264**, 105.
- Filippenko, A.V. and Halpern, J.P.: 1984, *ApJ* **285**, 458.
- Halpern, J.P. and Steiner, J.E.: 1983, *ApJ* **269**, L37.
- Heckman, T.M.: 1980, *A&A* **87**, 152.
- Ho, L.C., Filippenko, A.V. and Sargent, W.L.W.: 2003, *ApJ* **583**, 159.
- Kinkhabwala, A., et al.: 2002, *ApJ* **575**, 732.
- Marshall, F.E., et al.: 1978, *BAAS* **10**, 433.
- Narayan, R. and Yi, I.: 1995, *ApJ* **452**, 710.
- Nelson, C.H. and Whittle, M.: 1995, *ApJS* **99**, 67.
- Page, M.J., et al.: 2003, *A&A* **400**, 145.
- Page, M.J., Davis, S.W. and Salvi, N.J.: 2003, *MNRAS* **343**, 1241.
- Page, M.J., Soria, R., Zane, S., Wu, K. and Starling, R.L.C.: 2004, *A&A* **422**, 77.
- Phillips, M.M.: 1979, *ApJ* **227**, L121.
- Porquet, D. and Dubau, J.: 2000, *A&AS* **143**, 495.
- Pounds, K.A., et al.: 2003, *MNRAS* **341**, 953.
- Sako, M., et al.: 2001, *A&A* **365**, L168.
- Siemiginowska, A., Czerny, B. and Kostyunin, V.: 1996, *ApJ* **458**, 491.
- Tanaka, Y., Koyama, K., Maeda, Y. and Sonobe, T.: 2000, *PASJ* **52**, L25.
- Turner, T.J. and Pounds, K.A.: 1989, *MNRAS* **240**, 833.

OBSERVATIONAL EFFECTS OF STRONG GRAVITY

KRIS BECKWITH and CHRIS DONE

Department of Physics, University of Durham, South Road, Durham DH1 3LE, UK;

E-mail: k.r.c.beckwith@durham.ac.uk

(Received 4 January 2004; accepted 1 June 2005)

Abstract. The current paradigm of high energy spectroscopy tells us that light emitted from a wide variety of objects has its origin close to the black hole event horizon. As such, these photons are subject to general relativistic effects such as light-bending, gravitational lensing and redshift, time-dilation, etc. These gravitational effects are well-understood from a theoretical standpoint and therefore, provide a natural mechanism to test the properties of strong gravitational fields. To this end, we have developed a new (semi-analytic) strong gravity code, capable of describing the contribution of photons that perform multiple orbits of the hole. We apply this code to a simple Keplerian accretion disk in order to understand the role played by the angular emissivity, black hole spin and higher order images in forming the line profile.

Keywords: black holes, accretion disks, line profiles, general relativity

1. Introduction

Black holes are the ultimate test of strong gravity, spacetime so warped that not even light can escape. By definition they have no emission (apart from Hawking radiation), yet their immense gravitational potential energy can be tapped by any infalling material. This can power a luminous accretion flow where the emission has its origin close to the black hole event horizon, as is seen in many objects including Active Galactic Nuclei, Galactic black hole binaries, Ultra-Luminous X-ray Sources and Gamma Ray Bursts. Photons emitted in this region are subjected to general relativistic effects such as light-bending, gravitational lensing and redshift, as well as special relativistic effects as the emitting material will be moving rapidly (e.g. Fabian et al., 2000). These are well-understood from a theoretical standpoint, so accreting objects provide a natural laboratory to test the properties of strong gravitational fields.

Calculations of the relativistic corrections to photon properties have been ongoing for nearly three decades, starting with the classic work of Cunningham (1975) who calculated the distortions expected on the spectrum of a geometrically thin, optically thick, Keplerian accretion disc orbiting a Kerr black hole. Interest in these calculations dramatically increased with the realisation that the accretion disc could emit *line* as well as continuum radiation. Iron $K\alpha$ fluorescence resulting from X-ray



irradiation of the accretion disc can give a narrow feature, on which the relativistic distortions are much more easily measured than on the broad accretion disc continuum (Fabian et al., 1989). Since then, several groups have developed numerical codes that are capable of determining these effects both for standard discs (Dovciak et al., 2004) and alternative emission geometries (Bursa et al., 2004).

Observationally, evidence for a relativistically smeared iron line first came from the ASCA observation of the active galactic nuclei (AGN) MCG-6-30-15 (Tanaka et al., 1995). Further observations showed evidence for the line profile being so broad as to require a maximally spinning black hole (Iwasawa et al., 1996). More recent data from XMM are interpreted as showing that the line is even wider than expected from an extreme Kerr disk, requiring direct extraction of the spin energy from the central black hole as well as the immense gravitational potential (Wilms et al., 2001).

Such results are incredibly exciting, but X-ray spectral fitting is not entirely unambiguous. There is a complex reflected continuum as well as the line (Nayakshin et al., 2000; Ballantyne et al., 2001). For an ionised disk (as inferred for MCG-6-30-15) the current models in general use (pexriv in the XSPEC spectral fitting package) are probably highly incomplete (Ross et al., 1999). Complex ionised absorption also affects AGN spectra (e.g. Kaspi et al., 2002) and the illuminating continuum itself can have complex curvature rather than being a simple power law.

However, in MCG-6-30-15 these issues have been examined in detail, and the results on the dramatic line width appear robust (Fabian and Vaughan, 2003 ; Reynolds et al., 2004). Thus, there is a clear requirement that the extreme relativistic effects are well modelled. There are two models which are currently widely available to the observational community, within the XSPEC spectral fitting package, diskline (based on Fabian et al., 1989) and laor (Laor, 1991). The analytic diskline code models the line profile from an accretion disc around a Schwarzschild black hole (so of course cannot be used to describe the effects in a Kerr geometry). Also, it does not include the effects of light-bending (although Fabian et al. (1989) outline a scheme for incorporating this) and hence does not accurately calculate all the relativistic effects for $r < 20r_g$ (where $r_g = GM/c^2$). By contrast, the laor model numerically calculates the line profile including light-bending for an extreme Kerr black hole, but uses a rather small set of tabulated transfer functions which limit its resolution and accuracy (Beckwith and Done, 2004).

In response to these limitations, we have developed a fast, semi-analytic code to calculate relativistic corrections to photons properties in the gravitational field of the Kerr black hole (Beckwith and Done, 2004, 2005). Here, we briefly introduce the method implemented by the code to perform these calculations and apply this technique to a simple Keplerian accretion disk in order to understand the role played by the angular emissivity, black hole spin and higher order images in forming the line profile.

2. Calculating Relativistic Line Profiles

Line emission from a patch of disc with rest energy E_{int} subtends a solid angle $d\Xi = r_o^{-2} d\alpha d\beta$ on the observers sky at an energy E_o . This observer then measures the amount of flux at the energy E_o to be:

$$F_o(E_o) = r_o^{-2} \int \int g^4 \epsilon(r_e, \mu_e) \delta(E_o - g E_{\text{int}}) d\alpha d\beta \quad (1)$$

where $g = E_o/E_{\text{int}}$ is the redshift factor and $d\alpha d\beta$ is the solid angle subtended by each small patch of the disc in the observers frame of reference. The total amount of flux at an energy E_o is then found by summing all $d\alpha d\beta$ that fall within some dE of E_o and the overall line profile is then generated by scanning over all possible E_o .

An additional complication to this calculation is due to the dependence of the observed radiation pattern on the emissivity law $\epsilon(x_i)$ ($i = 1, \dots, n$). Here, we choose the emissivity law to have a two-parameter dependence, (i) the radial coordinate from which the photon is emitted, r_e and (ii) the initial direction of the photon with respect to the z -axis of the local disc frame, μ_e (see Figure 1). We assume that the dependence of the emissivity law is separable, that is, we can write $\epsilon(r_e, \mu_e) = \varepsilon(r_e) f(\mu_e)$. We choose $\varepsilon(r_e) \propto r_e^{-q}$ and take $q = 3$, consistent with gravitational energy release within the disc (Zycki et al., 1999). The choice of the angular dependence is far more complex however, as it depends on the (poorly understood) vertical structure of the accretion disc, in particular, the ionisation state of the material and so the choice of this dependence is not unique.

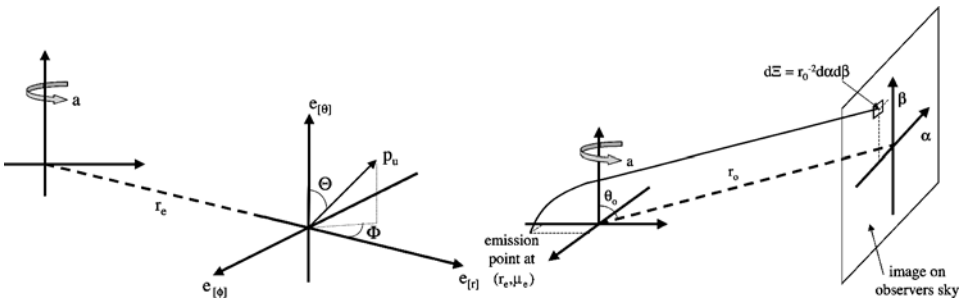


Figure 1. (Left panel) The coordinate system used for the disc. The emission is defined in the rest frame of the disc material. The polar and azimuthal emission angles Θ , Φ are obtained by taking the dot products of the photon four-momentum with the basis vectors of this frame, where $\mu_e = \cos \Theta$. This disc frame can be connected to the frame which co-rotates with the black hole spacetime via a simple boost which depends on the velocity. (Right panel) Diagram showing the link between the observers frame of reference and the global coordinate system defined by the black hole. Photons that are emitted from the disc at some distance r_e from the hole are seen at coordinates α and β on the image of the disc at the observer.

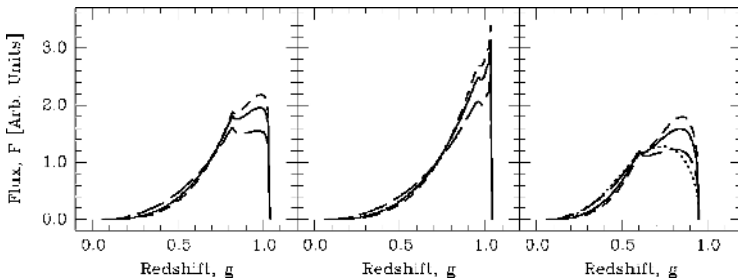


Figure 2. Comparison of the relativistic line profiles generated for a maximal Kerr black hole ($a = 0.998$) viewed at an inclination $\theta_o = 30^\circ$ with the inner edge of the disc located at $r_{\text{ms}} = 1.235r_g$. The line profiles here all implement the standard radial emissivity law of r_e^{-3} and we show the line profiles generated by three different angular emissivities, (i) $f(\mu_e) = 1$ (solid lines); (ii) $f(\mu_e) \propto (1 + 2.06\mu_e)$ (long dashed lines); (iii) $f(\mu_e) \propto \mu_e^{-1}$ (short dashed lines). In the left-hand panel, the outer edge of the disc is located at $20r_g$ and there is a $\sim 35\%$ difference in the height of the blue peak. In the centre panel, the outer edge of the disc is located at $400r_g$, which reduces the difference in the height of the blue peak to $\sim 25\%$. Finally, in the right-hand panel, the outer edge of the disc is located at $6r_g$, (the formal best fit to the MCG-6-30-15 data set), resulting in a difference in the height of the blue peak of $\sim 40\%$. For comparison we also show a limb darkened profile obtained from a very different radial emissivity of $r_e^{-4.5}$ (dotted line), which is very similar in characteristic to the r_e^{-3} optically thin, limb-brightened case (short dashed line).

3. The Role of Angular Emissivity and Black Hole Spin

Different angular emissivity laws can have striking effects on the form of the relativistic line profile, which we illustrate in Figure 2 for a maximal Kerr black hole ($a = 0.998$) viewed at an inclination $\theta_o = 30^\circ$. The line profiles here all implement the standard radial emissivity law of r_e^{-3} and we show the line profiles generated by three different angular emissivities, (i) $f(\mu_e) = 1$ (solid lines), corresponding to an optically thick disk; (ii) $f(\mu_e) \propto (1 + 2.06\mu_e)$ (long dashed lines) corresponding to an optically thick, limb-darkened disk (Laor, 1991); (iii) $f(\mu_e) \propto \mu_e^{-1}$ (short dashed lines) corresponding to an optically thin, limb-brightened disk (the limiting case of ionised material). In the left-hand panel of the figure, the disc extends from the marginally stable orbit, $r_{\text{ms}} = 1.235r_g$ to $r_{\text{out}} = 20r_g$. There is $\sim 35\%$ difference in the height of the blue peak depending of the form of the angular emissivity used.

However, such a limited range of radii is probably not very realistic. The disc should extend out to much greater distances from the black hole, where the relativistic effects (including light-bending) are less extreme. However, realistic emissivities strongly weight the contribution from the innermost regions, so the effective dilution of the relativistic effects by including the outer disc is not overwhelming. The centre panel of Figure 2 shows the line profiles generated using the same angular emissivity laws for a disc extending from 1.235 to $400r_g$, again with $\theta_o = 30^\circ$. There are still significant differences in the line profiles, with $\sim 25\%$ difference in

the height of the blue peak while the red wing slope changes from $F_o(E_o) \propto E_o^{3.5}$ (limb darkened) to $\propto E_o^{2.5}$ (limb brightened).

Despite the expectation of an extended disc, some recent observational studies (e.g. Reynolds et al., 2004) have tentatively suggested that the disc is very small, from ~ 1.235 to $6r_g$. This enhances the importance of light-bending. The right-hand panel of Figure 2 shows the line profiles for a disc extending from 1.235 to $6r_g$. The blue peak height differences are $\sim 40\%$, and the red wing slopes are different. For comparison we also show a limb darkened profile obtained from a very different *radial* emissivity of $r_e^{-4.5}$ (dotted line). This is very similar to the extreme limb brightened profile obtained from the r_e^{-3} radial weighting. We caution that uncertainties in the angular distribution of the line emissivity can change the expected line profile due to light-bending effects even at low/moderate inclinations, and that this can affect the derived radial emissivity.

Currently, the only available models in XSPEC have either zero or maximal spin. A zeroth-order approximation to spacetimes with different spins is to use the maximal Kerr results but with a disc with inner radius given by the minimum stable orbit for the required value of a (e.g. Laor, 1991). We test this for the most extreme case of $a = 0$ modelled by a maximal Kerr spacetime with $r_{\min} = 6r_g$. Figure 3 (left-hand panel) compares this with a true Schwarzschild calculation for a disc extending from 6 to $400r_g$ with $\theta_o = 30^\circ$ for a range of angular emissivities. The differences between the spacetimes (for a given angular emissivity) are at most $\sim 5\%$. This is roughly on the same order as the effect of changing the angular emissivity, which is much reduced here compared to Figure 2 due to the larger

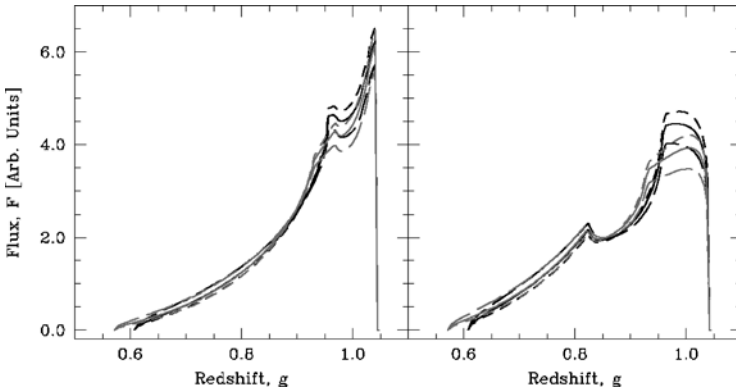


Figure 3. As in Figure 2 for maximal Kerr ($a = 0.998$, black lines) and Schwarzschild ($a = 0$, grey lines) black holes. Here, the disc extends from the minimum stable orbit for the Schwarzschild black hole, $r_{\text{ms}} = 6\text{--}400r_g$ (left-hand panel) and $20r_g$ (right-hand panel). For the extended disc, the differences between the line profiles produced for the same sized disc in different assumed spacetimes is of order $\sim 5\%$ for a given angular emissivity. Reducing the radial extent of the disc enhances these differences to $\sim 15\%$ (left-hand panel).

r_{\min} . Assumptions about both spin and angular emissivity become somewhat more important for smaller outer disc radii. Figure 3 (right-hand panel) shows this for a disc between 6 and $20r_g$.

4. The Contribution of Higher Order Images

The contribution of higher order images to the observed flux is dependent both on the location of the observer and the angular momentum of the hole itself, together with the assumed geometry and emissivity of the accretion flow. For an optically thick accretion disc then any photons which re-intersect the disc after emission will be either absorbed (and then re-emitted) or reflected by the material. Figure 4 shows the contributions of both the direct ($N = 0$) and higher order ($N = 1$ and 2)

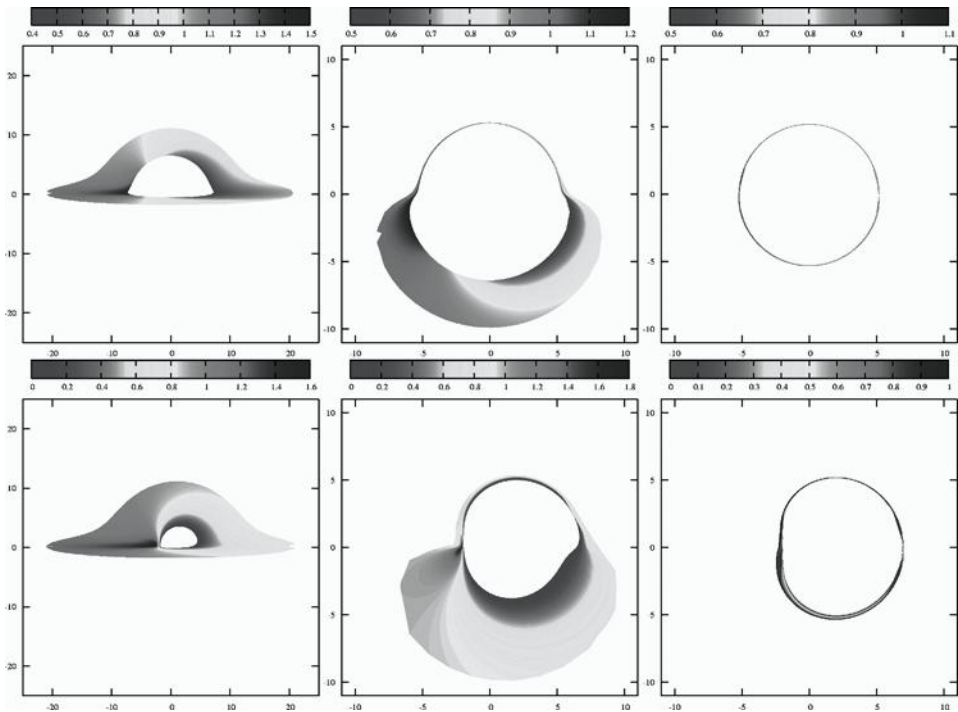


Figure 4. The contribution of orbiting photons (higher order images) to a distant observers image of a geometrically thin, optically thick, Keplerian accretion disc around Schwarzschild (*top row*) and extreme Kerr (*bottom row*) black holes. In both cases the observer is located at radial infinity with $\theta_o = 85^\circ$, the disc extends from the marginally stable orbit ($6r_g$ for Schwarzschild, $1r_g$ for extreme Kerr) to $20r_g$ and the images are coloured by the associated value of the redshift parameter, $g = E_o/E_e$. From left to right, the panels show the contributions from (i) the direct ($N = 0$) image, (ii) the first-order ($N = 1$) image and (iii) the second-order ($N = 2$) image.

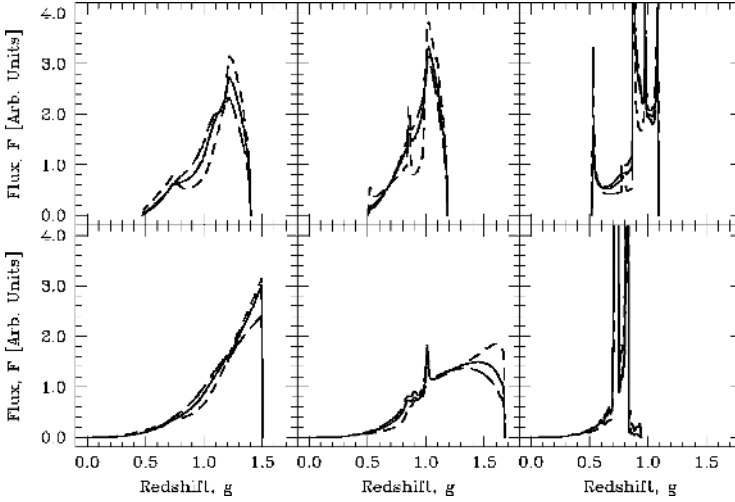


Figure 5. Relativistic line profiles generated from the images shown in Figure 4 using the emissivity laws described in Figure 2. As in Figure 4, lines generated by the Schwarzschild black hole are shown on the top row, extreme Kerr on the bottom and from left to right the panels show the contributions from the $N = 0, \dots, 2$ images. Line profiles generated by the zeroth-order photons have the standard skewed, double peaked structure. Those generated by the first-order photons have a similar structure, whilst those from the second-order photons are far more complex.

images of a geometrically thin disc extending from r_{ms} to $20r_g$, viewed at $\theta_0 = 85^\circ$ for both Schwarzschild and maximal Kerr black holes. The principle effect of black hole spin for the accretion disk dynamics is to move the location of the marginally stable orbit, r_{ms} and hence the location of the inner edge of the accretion disc. In the case of the Schwarzschild hole, the inner edge of the accretion disc is located at $6r_g$, above the radius of the unstable photon orbits ($3r_g$) so higher order image photons which cross the equatorial plane below $6r_g$ are not absorbed by the disc and may be able to freely propagate to the observer. This contrasts with the extreme Kerr hole behaviour, where the accretion disc extends down to $1r_g$, intersecting the allowed radial range of the unstable photon orbits ($1r_g \leq r_c \leq 4r_g$) and hence a large fraction of these orbiting photons return to the disc in the case of a rotating black hole.

To understand how the astrophysical properties of the accretion flow couple to the gravitational field of the black hole, we generate relativistically smeared line profiles, applying the same emissivity laws that were described in the preceding section (Figure 5). The top and bottom rows of the figure again correspond to the Schwarzschild and extreme Kerr cases, respectively, with the image order running from $N = 0$ to 2, left to right.

Turning our attention to the Schwarzschild case, we see that, for the direct image, limb darkening boosts the effects of gravitational lensing, enhancing the flux from the far side of the hole. This is because these photons are strongly bent, i.e. are

emitted from a lower inclination angle than that at which they are observed, so a limb darkening law means that the flux here is higher (Beckwith and Done, 2004). The Doppler shifts are rather small for this material, so this lensing enhances the flux in the middle of the line. Since the line profiles are normalised to unity, this means that the blue wing is less dominant.

The first-order spectra retains the characteristic double peaked and skewed shape, and again the principle effect of the different angular emissivities is to alter the balance between the blue wing and lensed middle of the line. However, there is some new behaviour for the limb brightened emissivity. This has the largest change in emissivity with angle, and this combined with the exquisite sensitivity of lensed paths means that this picks out only a small area on the disc, leading to a discrete feature in the spectrum. The profile also shows enhancement of the extreme red wing of the line, as the photons which orbit generally are emitted from the very innermost radii of the disc.

The discrete features are completely dominant for all emissivities at second-order. These are images of the top of the disc where the photons have orbited the black hole, so the paths are even more sensitive to small changes than first-order. Thus the profiles are significantly more complex in structure, being dominated by lensing. There are blue and red features at the extreme ends of the line profile which are picking out the maximum projected velocity of the innermost radii of the disc. These have the standard blue peak enhancement. However, the two strong features redward of this are a pair of lensed features, from the near and far side of the disc.

For the direct image of the extreme Kerr hole, the line exhibits the characteristic triangular shape previously reported by (Laor, 1991), with the variation in angular emissivity acting to alter the balance between the different regions of the line on a $\sim 5\%$ level. The line associated with the first-order image exhibits a marked difference in comparison to those associated with the Schwarzschild black hole, being both broader and resembling a skewed Gaussian combined with a narrow line (due to caustic formation) at $g \approx 1.0$. Here the principle effect of changes in the angular emissivity is to alter the height of the blue wing, relative to the rest of the line. Again, the line profile associated with the second-order image are completely dominated by discrete features, as in the Schwarzschild case.

5. Conclusion

Recent observational studies have provided evidence for highly broadened fluorescent iron $K\alpha$ lines. While there are a variety of line profiles seen (e.g. Lubinski and Zdziarski, 2001), there are some objects where the line implies that there is material down to the last stable orbit in a maximally spinning Kerr spacetime (most notably MCG-6-30-15: Wilms et al., 2001). However, the strong gravity codes generally used to model these effects are now over a decade old. Increased computer power means that it is now possible to improve on these models. We describe our new code

to calculate these effects, which uses fully adaptive gridding to map the image of the disc at the observer using the analytic solutions of the light travel paths. This is a very general approach, so the code can easily be modified to incorporate different emission geometries.

Relativistically smeared line profiles are generated by convolving the observed area of the disc (at a given energy) with an emissivity law describing energy release in the rest frame of the emitter. This emissivity law is not only dependent on the location of the emitter within the disc, but also the initial direction that a photon is emitted in. Light-bending means that a range of initial photon directions contribute to the observed radiation spectrum at a given inclination. As such, the emissivity law convolves together the effects of strong gravity and the astrophysics of the accretion flow, which in the most extreme case can play a $\sim 40\%$ role in shaping the internal structure of the line profile. By contrast, black hole spin plays at most a $\sim 15\%$ role in shaping the internal structure (keeping the inner edge of the disc fixed).

Our code is capable of calculating both the imaging and spectral contributions of higher order images to the standard picture of relativistically smeared line profiles. As has long been known, the major amplification effects of gravitational lensing are for the first-order paths from the far side of the underneath of the disc viewed at high inclination, i.e. photons initially emitted downwards on the far side of the black hole, which are bent by gravity up above the disc plane. For a disc viewed edge-on, the spectral signature of these first-order photons retains the characteristic skewed, double-peaked shape in the Schwarzschild case, whilst in the extreme Kerr case, the line resembles a skewed Gaussian. By contrast, the spectra of the second-order image is dominated by discrete spectral features in both cases.

References

- Ballantyne, D.R., Ross, R.R. and Fabian, A.C.: *MNRAS* **201**, 327, 10.
 Beckwith, K. and Done, C.: 2004, *MNRAS* **352**, 353.
 Beckwith, K. and Done, C.: 2005, *MNRAS* **359**, 1217.
 Bursa, M., Abramowicz, M.A., Karas, V. and Kluzniak, W.: 2004, astro, astro-ph/0406586.
 Cunningham, C.T., 1975, *ApJ* **202**, 788.
 Dovčiak, M., Karas, V. and Yaqoob, T.: 2004, *ApJS* **153**, 205.
 Fabian, A.C. and Vaughan, S.: 2003, *MNRAS* **340**, L28.
 Fabian, A.C., Rees, M.J., Stella, L. and White, N.E.: 1989, *MNRAS* **238**, 729.
 Fabian, A.C., Iwasawa, K., Reynolds, C.S. and Young, A.J., 2000, *PASP* **112**, 1145.
 Iwasawa, K., Fabian, A.C., Reynolds, C.S., Nandra, K., Otani, C., Inoue, H., Hayashida, K., Brandt, W.N., Dotani, T., Kunieda, H., Matsuoka, M. and Tanaka, Y.: 1996, *MNRAS* **282**, 1038.
 Kaspí, S., Brandt, W.N., George, I.M. et al.: 2002, *ApJ* **574**, 643.
 Laor, A.: 1991, *ApJ* **376**, 90.
 Lubinski, P. and Zdziarski, A.A.: 2001, *MNRAS* **323**, 37.
 Nayakshin, S., Kazanas, D. and Kallman, T.R.: 2000, *ApJ* **537**, 833.
 Reynolds, C.S. and Begelman, M.C.: 1997, *ApJ* **488**, 109.

- Reynolds, C.S., Wilms, J., Begelman, M.C., Staubert, R. and Kendziorra, E.: 2004, *MNRAS* **349**, 1153.
- Ross, R.R., Fabian, A.C. and Young, A.J.: 1999, *MNRAS* **306**, 461.
- Tanaka, Y., Nandra, K., Fabian, A.C., Inoue, H., Otani, C., Dotani, T., Hayashida, K., Iwasawa, K., Kii, T., Kunieda, H., Makino, F. and Matsuoka, M.: 1995, *Nature* **375**, 659.
- Wilms, J., Reynolds, C.S., Begelman, M.C., Reeves, J., Molendi, S., Staubert, R. and Kendziorra, E.: 2001, *MNRAS* **328**, L27.
- Zycki, P.T., Done, C. and Smith, D.A.: 1999, *MNRAS* **305**, 231.

BROAD IRON LINES IN AGN AND X-RAY BINARIES

A.C. FABIAN

Institute of Astronomy, Madingley Road, Cambridge CB3 0HA, UK; E-mail: acf@ast.cam.ac.uk

(Received 25 October 2004; accepted 1 June 2005)

Abstract. Several AGN and black hole X-ray binaries show a clear very broad iron line, which is strong evidence that the black holes are rapidly spinning. Detailed analysis of these objects shows that the emission line is not significantly affected by absorption and that the source variability is principally due to variation in amplitude of a power-law. Underlying this is a much less variable, relativistically-smearred, reflection-dominated, component which carries the imprint of strong gravity at a few gravitational radii. The strong gravitational light bending in these regions then explains the power-law variability as due to changes in height of the primary X-ray source above the disc. The reflection component, in particular its variability and the profile of the iron line, enables us to study the innermost regions around an accreting, spinning, black hole.

Keywords: accretion, accretion disks, black hole physics, x-rays: galaxies

1. Introduction

Radiatively-efficient accreting black holes are expected to be surrounded by a dense disc radiating quasi-blackbody thermal EUV and soft X-ray emission. Hard X-ray emission originates via Comptonization of that soft radiation in a corona above the disc, fed by magnetic fields from the body of the disc. Irradiation of the dense disc material by hard X-rays then gives rise to a characteristic ‘reflection’ spectrum, computed examples of which are shown in Figure 1 (from Ross and Fabian, 2004).

Most of the power is radiated from close to the smallest disc radii which for a non-spinning black hole is $6r_g$, where $r_g = GM/c^2$. For a spinning (Kerr) black hole it reduces as the spin increases (Bardeen et al., 1972) to $1.23r_g$ for what is assume to be maximal spin (Thorne, 1974). Relativistic effects then affect the appearance of the reflection spectrum through Doppler, aberration, gravitational redshift and light bending effects (Fabian et al., 1989; Laor, 1991). The dominant feature in the spectrum seen by a distant observer is an iron line with a broad skewed profile.

Broad iron lines seen in the spectrum of several active galaxies and galactic black hole binaries are reviewed here. The cases for relativistic lines in the Seyfert galaxy MCG-6-30-15 and the X-ray binary GX 339-4 are very strong, indicating that those black holes are rapidly spinning. The puzzling spectral variability of such sources is now beginning to be understood within the context of emission from the strong gravity regime (Miniutti and Fabian, 2004). Some active galactic nuclei (AGN)



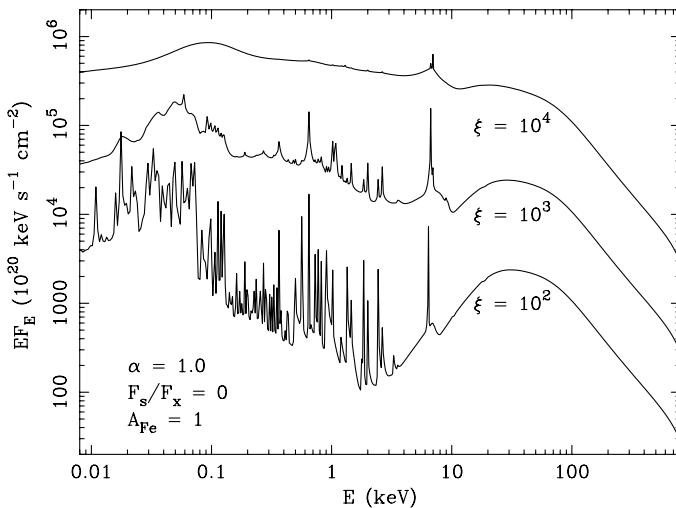


Figure 1. Computed reflection spectrum as a function of $\xi = F/n$, where n is the density of the surface (Ross and Fabian, 2004).

and X-ray black hole binaries show either no line or only a narrow one. This is discussed within the context of state changes and jetted emission observed in the galactic black holes.

2. MCG-6-30-15

The X-ray spectrum of the bright Seyfert 1 galaxy MCG-6-30-15 ($z = 0.00775$) has a broad emission feature stretching from below 4 keV to about 7 keV. The shape of this feature, first clearly resolved with *ASCA* by Tanaka et al. (1995), is skewed and peaks at about 6.4 keV. This profile is consistent with that predicted from iron fluorescence from an accretion disc inclined at 30° extending down to within about six gravitational radii ($6r_g = 6GM/c^2$) of a black hole (Fabian et al., 1989; Laor, 1991). In part of the *ASCA* observation the line extended below 4 keV (Iwasawa et al., 1996) which means that the emission originates at radii much less than $6r_g$, probably due to the black hole spinning. *XMM-Newton* has observed MCG-6-30-15 twice (in 2000, Wilms et al., 2001 and 2001; Fabian et al., 2002a) and in both cases the line extended down to about 3 keV (Figure 2a), implying the spin parameter $a > 0.93$ (Dabrowski et al., 1997; Reynolds et al., 2004). This raises the exciting possibility that the spin energy of the hole is being tapped (Wilms et al., 2001).

The X-ray continuum emission of MCG-6-30-15 is highly variable (see Vaughan et al., 2003, Vaughan and Fabian, 2004 and Reynolds et al., 2004 for recent analyses). If the observed continuum drives the iron fluorescence then the line flux should respond to variations in the incident continuum on time-scales comparable to the

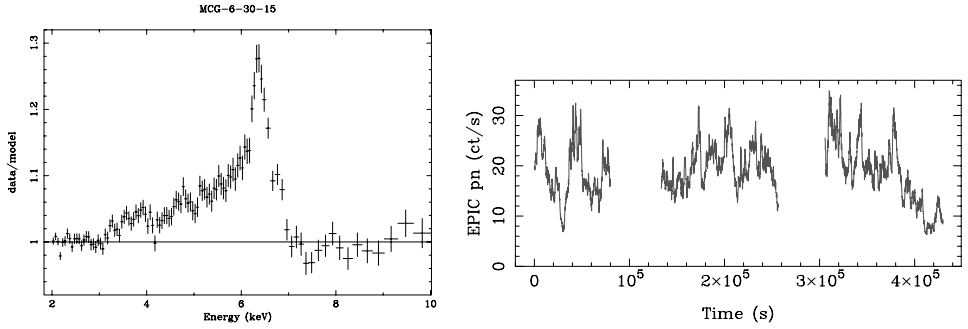


Figure 2. Left panel: The broad iron line in MCG-6-30-15 from 2001 (Fabian et al., 2002). Right panel: The light curve in 2001.

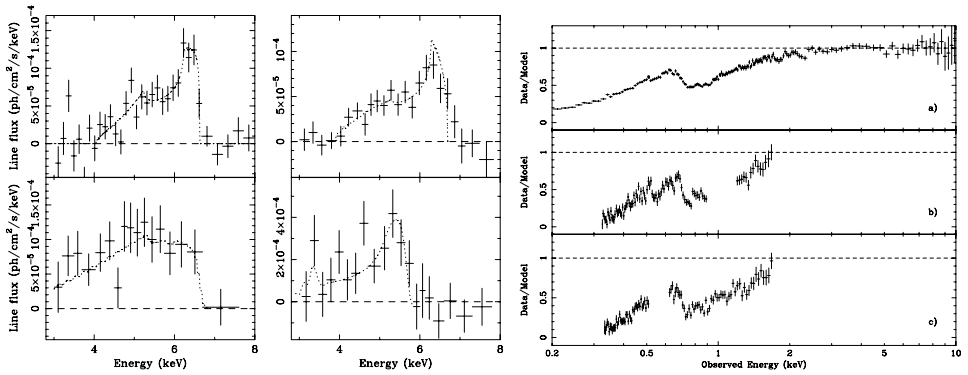


Figure 3. Left panel: Line profile variations in MCG-6-30-15 seen with ASCA in 1994 (left) and 1996 (right). Centre panel: Iron line variability in the last orbit of 2001 (from Iwasawa et al., 2004). Right panel EPIC difference spectrum between the brighter and dimmer parts of the long XMM observation, presented as a ratio to a power-law model fitted over the 3–10 keV band, with similar spectra for RGS1 and 2 below (from Turner et al., 2004).

light-crossing, or hydrodynamical time of the inner accretion disc (Fabian et al., 1989; Stella, 1990; Matt and Perola, 1992; Reynolds et al., 1999). This timescale ($\sim 100 M_6$ s for reflection from within $10r_g$ around a black hole of mass $10^6 M_6 M_\odot$) is short enough that a single, long observation spans many light-crossing times. This has motivated observational efforts to find variations in the line flux (e.g. Iwasawa et al., 1996, 1999; Reynolds, 2000; Vaughan and Edelson, 2001; Shih et al., 2002). These analyses indicated that the iron line in MCG-6-30-15 is indeed variable on time-scales of $\sim 10^4$ s (e.g. Figure 3), but that the general amplitude of the variations was considerably less than expected and not directly correlated with the observed continuum.

The long *XMM-Newton* observation (Fabian et al., 2002) showed that a simple two-component model (Shih et al., 2002) is sufficient to explain the observed

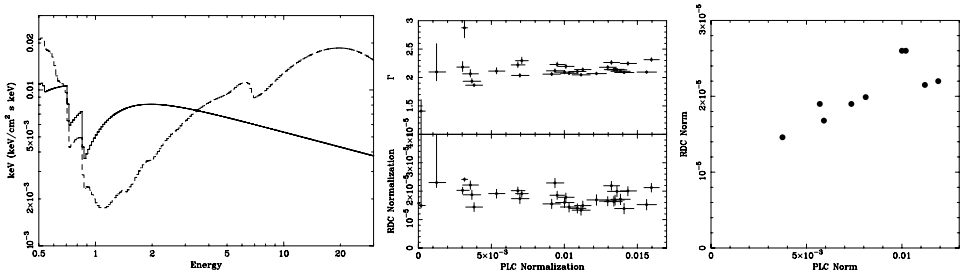


Figure 4. *Left panel:* The two component model in which the PLC (solid line) varies considerably in amplitude while the RDC (dashed line) varies little. *Centre panel (top):* Photon index Γ of the PLC plotted against its normalization, (*bottom*): RDC normalization plotted against PLC normalization for 2001. *Right panel:* RDC vs. PLC normalizations for 2000.

spectral variability (Figure 1; Fabian and Vaughan, 2003; Taylor et al., 2003). The model consists of a highly variable power-law component (PLC) plus a much less variable harder component carrying the iron line (RDC, Figure 2a). It gives an excellent fit to the data, with the harder, line-carrying component dominating lowest flux states of the observation (Fabian and Vaughan, 2003). That the variation is driven by a power-law is evident from the difference spectra made by subtracting the spectra of fainter parts of the lightcurve from those of brighter parts and fitting the resulting ‘difference spectrum’. It is a power-law from 3 to 10 keV with no iron-K features. On the assumption that this power-law continues to lower energies, where attenuation at low energies due to both galactic absorption and the warm absorber in MCG-6-30-15 is seen. This demonstrates that there is no subtle additional absorption influencing the shape of the extensive low-energy “red” wing to the iron line. Small variations in the amplitude of the RDC are seen.

A detailed analysis of the *XMM-Newton* 2001 data by Turner et al. (2003, 2004) shows, from a curve of growth analysis of the absorption lines and difference spectra, that the warm absorber accounts for most of the soft X-ray spectral features and that any distinct relativistically-broadened CNO lines (Branduardi-Raymont et al., 2001; Sako et al., 2003) are weak.

2.1. INTERPRETATION

Explaining the relatively small variability of the RDC, compared with that of the PLC, provides a significant challenge. It appears to be mostly due to reflection but it is not simple reflection of the observed power-law component since that repeatedly varies by factors of two or more on short time-scales; the RDC and PLC appear partially disconnected. Since however, both show the effects of the warm absorber they must originate in a similar location. As the extensive red wing of the iron line in the RDC indicates emission peaking at only a few gravitational radii (GM/c^2) we assume that this is indeed where that component originates. In such extreme

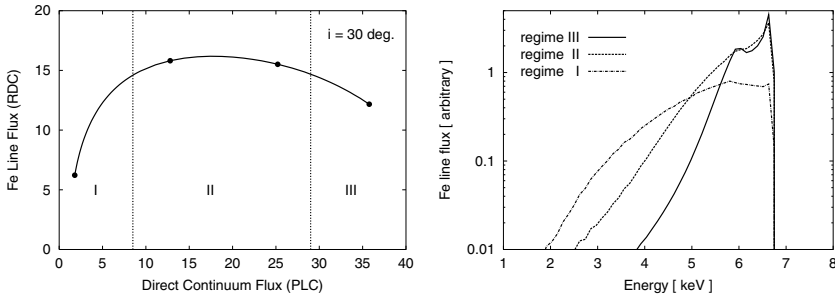


Figure 5. Left panel: Variation in amplitude of the RDC with height (knots at 1, 5, 10, and 20 gravitational radii) of the PLC. Right panel: Line profile changes with PLC height (Miniutti and Fabian, 2004).

gravity the general relativistic bending of light is very large, boosting the strength of reflection (Martocchia et al., 2000, 2002a,b; Dabrowski and Lasenby, 2001) and can account for the behaviour of the components (Fabian and Vaughan, 2003; Miniutti et al., 2003, 2004). How bright the PLC appears depends strongly on its height above the disc. Much of the radiation is bent down to the disc and black hole when the PLC is at a height of a few r_g but less so above $20r_g$ (Figure 5a).

Part of the source variability can thus be explained by an intrinsically constant PLC changing height above the disc. Intrinsic variability of the PLC might also be present. The RDC is expected to change little during PLC variations due to source position but will change with intrinsic variability. Line profile changes with source height is a discriminant (Figure 5b).

Tapping of black holes spin by magnetic fields in the disc is a strong possibility to account for the peaking of the power so close to the hole (Wilms et al., 2001; Reynolds et al., 2004).

3. Galactic Black Hole Binaries and NLS1

Broad iron lines have been found in several galactic black hole binaries (or black hole candidates, BHC). The lines in GX 339-4 (Figure 6a, Miller et al., 2004a,b) and XTE J1650-500 (Figure 6b, Miller et al., 2002a,b,c; Miniutti et al., 2004) are among the best examples (see also Miller et al., 2002a,b,c, 2003; Martocchia et al., 2002a,b). That in GX 339-4 shows a very broad red wing indicating that the black hole is rapidly spinning. Changes in the strength of the iron line as the power-law continuum varied during the outburst of XTE J1650-500 (Rossi et al., 2003) follow the sense of the variation expected from the light-bending model (Figure 5a).

Narrow Line Seyfert 1 galaxies tend to show steep soft X-ray spectra and sometimes broad iron emission features. One extreme such object is 1H 0707-495 which has a marked drop in its spectrum above 7 keV. This is either an absorption edge

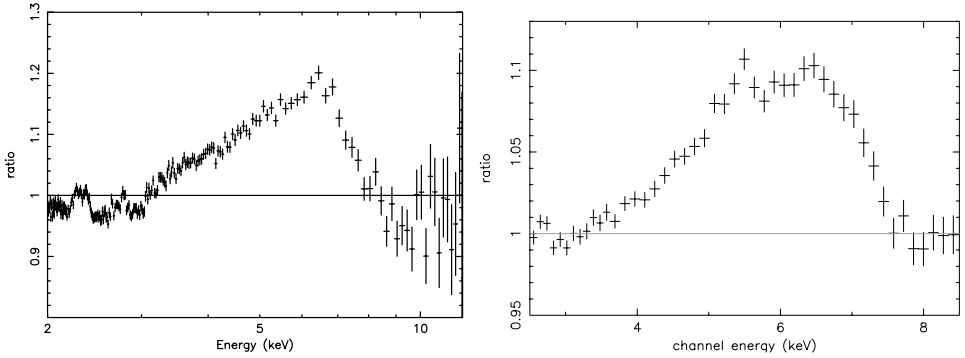


Figure 6. *Left panel:* The line in the BHC GX 339-4 (Miller et al., 2004a,b). *Right panel:* The broad iron line in XTE J1650-500 (Miniutti et al., 2004).

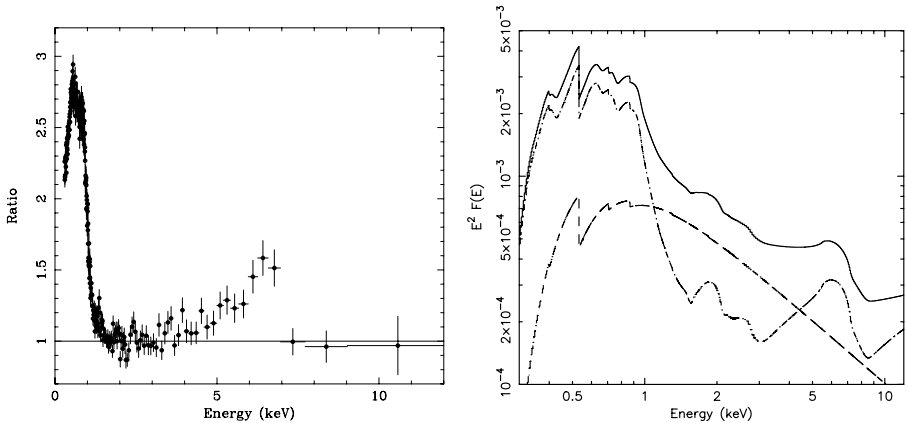


Figure 7. *Left panel:* Ratio of the spectrum of the NLS1 1H0707 to a power-law fitted between 2 and 3 keV and above 7.5 keV. *Right panel:* Spectral decomposition of 1 H0707-495 in terms of a variable power-law (dashed) and a blurred reflection component (dot-dashed) (from Fabian et al., 2004).

showing partial-covering in the source (Boller et al., 2002, 2004) or the blue wing of a massive, very broad, iron line (Figure 7a, Fabian et al., 2002, 2004). A two component, relativistically-blurred reflection plus power-law, model explains all the complex spectrum, including its soft excess and broad line, together with its rapid spectral variability. 1H 0707-495 is therefore an extreme Kerr hole.

4. Broad-Line-Free Sources

Some objects show no evidence for a broad line. Good examples from long *XMM-Newton* exposures are Akn 120, which has no warm absorber (Vaughan et al., 2004), and the broad line radio galaxy 3C 120 (Ballantyne et al., 2004).

Various possibilities for the lack of any line have been proposed by the authors of those papers including: (a) the central part of the disc is missing; (b) the disc surface is fully ionized (i.e. the iron is); (c) the coronal emissivity function is flat, which could be due to (d) the primary X-ray sources being elevated well above the disc at say $100r_g$.

There are also intermediate sources where the data are either poor or there are complex absorption components so that one cannot argue conclusively that there is a relativistic line present. Some narrow line components are expected from outflow, warm absorbers and distant matter in the source. One common approach in complex cases, which is not recommended, is to continue adding absorption and emission components to the spectral model until the reduced χ^2 of the fit is acceptable, and then claim that model as the solution. Very broad lines are difficult to establish conclusively unless there is something such as clear spectral variability indicating that the power-law is free of Fe-K features, as found for MCG-6-30-15, or for GX 339-4 where the complexities of an AGN are not expected.

5. Generalization of the Light-Bending Model

Our interpretation of the spectral behaviour of MCG-6-30-15 and some other sources means that we are observing the effects of very strong gravitational light bending within a few gravitational radii of a rapidly spinning black hole. The short term (10–300ks) behaviour is explained, without large intrinsic luminosity variability, through small variations in the position of the emitting region in a region where spacetime is strongly curved.

This implies that some of the rapid variability is due to changes in the source position. Now BHC in the (intermediate) high/soft state have high frequency breaks at higher frequency, for the same source, than when in the low/hard state (cf. Cyg X-1, Uttley and McHardy, 2004). This additional variability when in the soft state is identified with relativistic light-bending effects on the power-law continuum.

This picture suggests a possible generalization of the light-bending model to unify the AGN and BHC in their different states. Note the work of Fender et al. (2004) which emphasises that jetted emission occurs commonly in the hard state of BHC. The key parameter may be the height of the main coronal activity above the black hole. Assume that much of the power of the inner disc passes into the corona (Merloni and Fabian, 2002) and that the coronal activity is magnetically focussed close to the central axis. Then at low Eddington ratio the coronal height is large (say $100r_g$ or more), the corona is radiatively inefficient and most of the energy passes into an outflow; basically the power flows into a jet. Reflection is then appropriate for Euclidean geometry and a flat disc and there is only modest broadening to the lines. If the X-ray emission from the (relativistic) jet dominates then X-ray reflection is small (see e.g. Beloborodov, 1999). The high frequency break to the power spectrum is low ($\sim 0.001c/r_g$).

When the Eddington fraction rises above say 10%, the height of the activity drops below $\sim 20r_g$, the corona is more radiatively efficient and more high frequency variability occurs due to light bending and the turnover of the power spectrum rises above $0.01c/r_g$. The X-ray spectrum is dominated at low heights by reflection, including reflection-boosted thermal disk emission, and a broad iron line is seen. Any jet is weak.

The objects with the highest spin and highest accretion rate give the most extreme behaviour. Observations suggest that these include NLS1 and some very high state, and intermediate state, BHC. Some broad-line-free sources do not however, fit this model, so more work is required.

6. Summary

A relativistically-broadened iron line is unambiguous in the spectra and behaviour of a few objects. The strength and breadth of reflection features is strong evidence for gravitational light bending and redshifts from a few r_g . They indicate that a dense disc extends close to the black hole, which must therefore, be rapidly spinning ($a/m > 0.8$).

The potential for understanding the accretion flow close to a black hole is enormous. Current observations are at the limit of *XMM-Newton*'s powers, which nevertheless has enabled a breakthrough in understanding the spectral behaviour of MCG-6-30-15 and similar objects. Similarities in the spectral and timing properties of AGN and BHC is enabling further progress to be made. Studies in the near future with ASTRO-E2 followed by XEUS and Constellation-X in the next decade will continue to open up the immediate environment of accreting black holes, within just a few gravitational radii, to detailed study.

Acknowledgements

Thanks to G. Miniutti, S. Vaughan, K. Iwasawa and J. Miller for collaboration and many discussions. The generalization of the light bending modelling was developed with them and A. Merloni. The Royal Society is thanked for support.

References

- Ballantyne, D., Fabian, A.C. and Iwasawa, K.: 2004, *MNRAS* **354**, 839.
- Bardeen, J.M., Press, W.H. and Teukolsky, S.A.: 1972, *ApJ* **178**, 347.
- Beloborodov, A.: 1999, *ApJ* **510**, L123.
- Boller, T., Fabian, A.C., Sunyaev, R.A. et al.: 2002, *MNRAS* **329**, L1.
- Branduardi-Raymont, G., et al.: 2001, *A&A* **365**, L140.

- Dabrowski, Y., Fabian, A.C., Iwasaka, K. et al.: 1997, *MNRAS* **288**, L11.
- Dabrowski, Y. and Lasenby, A.N.: 2001, *MNRAS* **321**, 605.
- Fabian, A.C. and Vaughan, S.: 2003, *MNRAS* **340**, L28.
- Fabian, A.C., Rees, M.J., Stella, L. et al.: 1989, *MNRAS* **238**, 729.
- Fabian, A.C., Vaughan, S.A., Nandra, K. et al.: 2002a, *MNRAS* **335**, L1.
- Fabian, A.C., Ballantyne, D.R., Merloni, A. et al.: 2002b, *MNRAS* **331**, L35.
- Fabian, A.C., Miniutti, G., Gallo, L. et al.: 2004, *MNRAS* **353**, 1071.
- Fender, R., Belloni, T.M. and Gallo E.: 2004, astro-ph/0409360.
- Gallo, L. et al.: 2004, *MNRAS* **353**, 1064.
- Iwasawa, K. et al.: 1996, *MNRAS* **282**, 1038.
- Iwasawa, K. et al.: 1999, *MNRAS* **306**, L19.
- Laor, A.: 1991, *ApJ* **376**, 90.
- Martocchia, A., Matt G. and Karas, V.: 2000, *A&A* **312**, 817.
- Martocchia, A., Matt, G. and Karas, V.: 2002a, *A&A* **383**, L23.
- Martocchia, A., Matt, G. and Karas, V.: 2002b, *A&A* **387**, 215.
- Matt, G. and Perola G.C.: 1992, *MNRAS* **259**, 433.
- Merloni, A. and Fabian, A.C.: 2002, *MNRAS* **332**, 165.
- Miller, J.M. et al.: 2002a, *ApJ* **570**, L69.
- Miller, J.M. et al.: 2002b, *ApJ* **577**, L15.
- Miller, J.M. et al.: 2002c, *ApJ* **578**, 348.
- Miller, J.M. et al.: 2003, *ApJ* **338**, 7.
- Miller, J.M. et al.: 2004a, *ApJ* **601**, 450.
- Miller, J.M. et al.: 2004b, *ApJ* **606**, L131.
- Miniutti, G. and Fabian, A.C.: 2004, *MNRAS* **349**, 1435.
- Miniutti, G., Fabian, A.C. and Miller, J.M.: 2004, *MNRAS* **351**, 466.
- Miniutti, G. et al.: 2003, *MNRAS* **344**, L22.
- Reynolds, C.S. et al.: 2000, *ApJ* **533**, 811.
- Reynolds, C.S.: 2004a, *MNRAS* **349**, 1153.
- Reynolds, C.S.: 2004b, astro-ph/0410116.
- Reynolds, C.S. et al.: 1999, *ApJ* **521**, 99.
- Ross, R.R. and Fabian, A.C.: 2004, *MNRAS*, submitted.
- Rossi, S. et al.: 2003, astro-ph/0309129.
- Sako, M. et al.: 2003, *ApJ* **596**, 114.
- Shih, D.C., Iwasawa, K. and Fabian, A.C.: 2002, *MNRAS* **333**, 687.
- Stella, L.: 1990, *Nature* **344**, 747.
- Tanaka, Y. et al.: 1995, *Nature* **375**, 659.
- Taylor, R., Uttley, P. and McHardy, I.: 2003, *MNRAS* **342**, L31.
- Thorne, K.S.: 1974, *ApJ* **191**, 507.
- Turner, A., Fabian, A. et al.: 2003, *MNRAS* **346**, 833.
- Turner, A., Fabian, A. et al.: 2004, *MNRAS* **353**, 319.
- Vaughan, S. and Edelson, R.: 2001, *ApJ* **548**, 694.
- Vaughan, S. and Fabian, A.: 2004, *MNRAS* **348**, 141.
- Vaughan, S., Fabian, A. and Nandra, K.: 2003, *MNRAS* **339**, 1237.
- Vaughan, S. et al.: 2004, *MNRAS* **351**, 193.
- Uttley, P. and McHardy, I.M.: 2004, astro-ph/0402407.
- Wilms, J. et al.: 2001, *MNRAS* **328**, L27.

THE EVOLUTION OF BLACK HOLE STATES

JEROEN HOMAN¹ and TOMASO BELLONI²

¹*MIT Center for Space Research, 70 Vassar Street, Cambridge, MA 02139, USA*

²*INAF/Osservatorio astronomico di Brera, Via E. Bianchi 46, 23807, Merate (LC), Italy;*

E-mails: jeroen@space.mit.edu, belloni@merate.mi.astro.it

(Received 2 December 2004; accepted 4 January 2005)

Abstract. We discuss the evolution of black hole transients on the basis of a few systems that were intensively observed with the *Rossi X-ray Timing Explorer* (rxte). We focus on the global evolution and the observed state transitions. Rather than giving a numerical recipe for classifying observations, we try to identify times during outbursts at which clear changes occur in the X-ray variability, X-ray spectral, or multi-wavelength properties.

Keywords: accretion, accretion disks, black hole physics, X-rays: stars, X-rays: binaries

1. Introduction

Since the launch of the *Rossi X-ray Timing Explorer* (RXTE) about ~ 20 black hole X-ray transients have been observed with enough coverage to study their global evolution. These observations have provided a wealth of information and have already led to a considerable increase in our understanding of these systems. In a recent review by McClintock and Remillard (2004) a new classification scheme was proposed for the spectral and variability states as observed in black hole transients. McClintock and Remillard (2004) approached the states issue by identifying three ‘stable’ states in black hole transients. In this paper we approach the issue from an other angle, focusing on the observed transitions, the overall evolution during an outburst, and how X-ray changes relate to changes at other wavelengths.

2. State Definitions

Until the late 1990s it was generally assumed that the state of a black hole system was determined by the instantaneous mass accretion rate, \dot{M} . It was believed that as the mass accretion rate increased, a source went through the following states (see e.g. Esin et al., 1997): quiescence \rightarrow low/hard \rightarrow intermediate \rightarrow high/soft \rightarrow very high. Observations with *RXTE* of sources like XTE J1550–564 have shown that such a simple \dot{M} -driven picture, with transitions only being triggered by changes in \dot{M} , is probably not able to explain the observed transition between the states. Homan et al. (2001) suggested that an additional parameter may play a role in those transitions.



They also suggested that the very-high state and the intermediate state(s) are one and the same state and represent transitions between the low/hard and high/soft states at different luminosities. The fact that most of the states were observed over wide and overlapping ranges in luminosity also meant that attributes like ‘low’, ‘high’ and ‘very high’ had lost most of their significance.

McClintock and Remillard (2004) introduced a new classification scheme that is partly based on the old five-state scheme, but no longer uses luminosity as a selection criterion since it appeared that any of the active states may occur at any luminosity. They still recognize a quiescent state, hard state, soft state (renaming the latter the ‘thermal dominant state’), and very-high state (renaming it the steep power-law state), but drop the intermediate state as a bona fide state. The three active states are defined on the basis of the fractional contribution of the disk-flux (or power-law flux) to the 2–20 keV spectrum, spectral power-law index, and the strength of the power spectral continuum. All observations that cannot be classified according to their state definitions, are combined into an intermediate state, in which observations can show properties of any of the three main states.

Some of the state transitions discussed in this paper involve (and are defined on the basis of) sudden changes in the properties of the quasi-periodic oscillations (QPOs) in the ~ 1 –10 Hz range. Currently three types of these low-frequency QPOs are recognized in black hole binaries, called type A, B and C (Wijnands et al., 1999; Remillard et al., 2002). The three types can be distinguished on the basis of strength, coherence, phase lags, energy dependence, harmonic content, and frequency stability on a time scale of days. Type C QPOs are the most common ones; they are observed in the spectrally hard states over a wide range in frequency (~ 0.1 –10 Hz), and are stronger and more coherent than the other two types. Type A and B QPOs have only been observed in a few sources; they are only seen in the very-high/steep power-law state, in a narrow frequency range (~ 4 –8 Hz). Recent observations of H1743–322 (Homan et al., 2005b) suggest that these two types might be more intimately related than was previously believed. Transitions from one type of QPO to another always seem to involve type B (Casella et al., 2004), with transitions between type C and B resulting in a clear change in the shape and strength of noise continuum. The main reason for including QPO type in our discussion of black hole states is that they provide an additional indication for changes in the accretion flow that may not always show up as strong spectral transitions.

3. Global Evolution

Hardness–intensity diagrams (HIDs), in which the X-ray count rate is plotted versus an X-ray color, provide a quick way to study the global evolution of black hole transients during outburst. In Figure 1 we plot the light curves and HIDs of four transients that were observed with *RXTE* between 1999 and 2003. It should be noted that constant count rate levels in these HIDs correspond to substantially

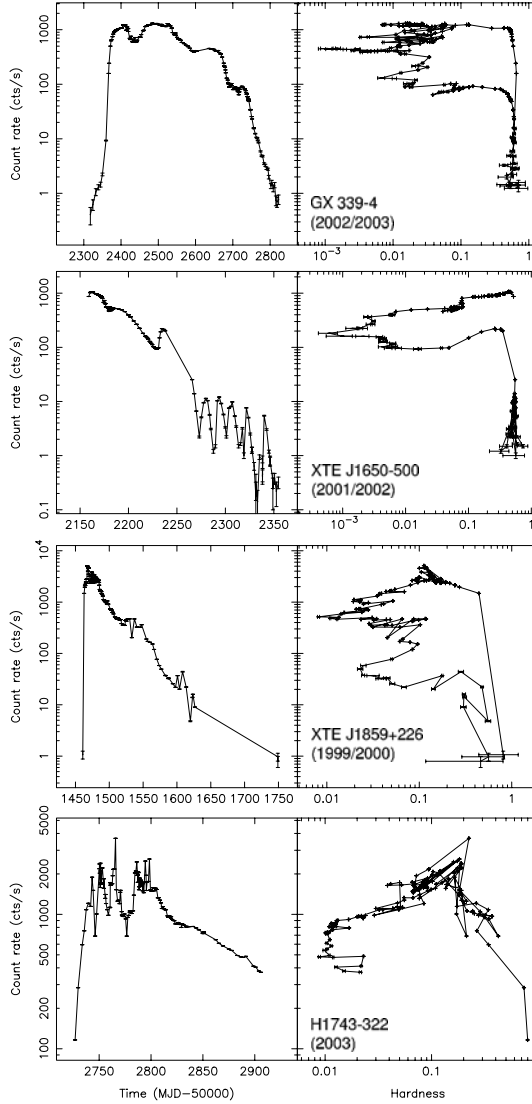


Figure 1. Light curves and hardness–intensity diagrams of four recent transients observed with the *RXTE*/PCA. Count rates are in the ~ 3 –21 keV band and hardness is defined as the ratio of count rates in the ~ 6 –19 and ~ 3 –6 keV bands. For GX 339–4, XTE J1859+226, and H1743–322, the outbursts were observed to start in the upper-right corner, with the sources moving through the diagram in a counter-clockwise direction. For XTE J1650–500 the initial rise was not observed with the PCA, but ASM observations suggest it started in the upper-right corner as well, following a vertical path to the lower-right corner, where the PCA coverage started.

higher luminosities at hardness values close to 1 than at values of 0.001–0.01. The HIDs are similar to each other in that all four sources seem to trace out (part of) a counter-clockwise q-shaped track. Below a certain count rate the spectrum is always very hard (i.e. in the hard state) and above the spectrum is either very hard or very soft, except for two transitional phases (the ‘horizontal’ branches in the HID). This means, as was noted by other authors as well (see e.g. Maccarone and Coppi, 2003), that within a single outburst the hard \rightarrow soft transition occurs at a flux that is about a factor of 10–100 higher than the soft \rightarrow hard transition. Note that in GX 339–4 and XTE J1650–500 the hard \rightarrow soft transition was rather fast, while in XTE J1859+226 and H1743–322 the source lingered for a longer time at intermediate colors.

While the sources shown in Figure 1 show a smooth overall movement through their HID, the fast time variability and multi-wavelength properties allow one to define a few rather sharp boundaries corresponding to state transitions. In the following, we will base our discussion of states mostly on the 2002/2003 outburst of GX 339–4, the results of which will be presented in Belloni et al. (2005b) and Homan et al. (in preparation). Complete references for our discussion can be found in those works.

4. A Detailed Look at the States

4.1. THE HARD STATE—RISE AND DECAY

Since pointed observations of a transient in outburst often start only when the source already has a luminosity that is a factor of more than 10^4 – 10^5 above the quiescent level, not much is known about the early evolution of outbursts. Thanks to a monitoring campaign set up by David Smith and co-workers, the 2002/2003 outburst of GX 339–4 was the first whose evolution could be followed from a flux level that was only a factor of 10 above its 2000 quiescent level (Corbel et al., 2003). In Figure 2 we show the early evolution of GX 339–4. From this figure it is clear that before the first ASM detection the source luminosity had been increasing for at least 40 days, initially slowly and later more rapidly.

Throughout these early stages of the outburst, until it had reached its peak 3–100 keV flux, the source was in the hard state: the strength of the broad-band variability decreased from 45 to 30% rms and the energy spectrum was dominated by a power law component, with the index slowly increasing from 1.3 to 1.4. During the rise the frequencies of the noise components and the occasional QPO increased gradually. An example of a power-density spectrum from this state in GX 339–4 is shown in Figure 3.

Just after reaching its peak flux, increases in the power-law index and noise/QPO frequencies accelerated. Also, a strong increase of the spectrally soft disk component and a substantial decrease in the optical/IR flux (see Figure 4) were observed

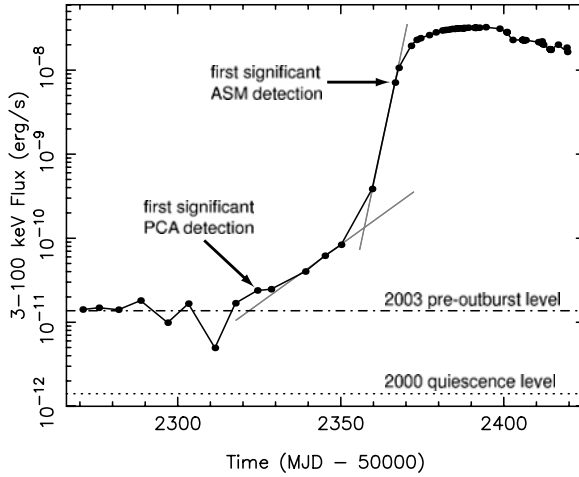


Figure 2. An *RXTE* light curve of the rise of the 2002/2003 outburst of GX 339–4. The times of the first significant PCA and ASM detections are indicated, as are the pre-outburst and quiescence levels. The two gray lines show the presence of two different time scales during the early rise.

at that time, with the latter probably being the result of the jet switching off (or starting to, Homan et al., 2005a). At this point the source entered an intermediate state (see Section 4.2), with the transition from the hard state being visible as an almost 90° turn to the left in the HID. Note that in the definition of McClintock

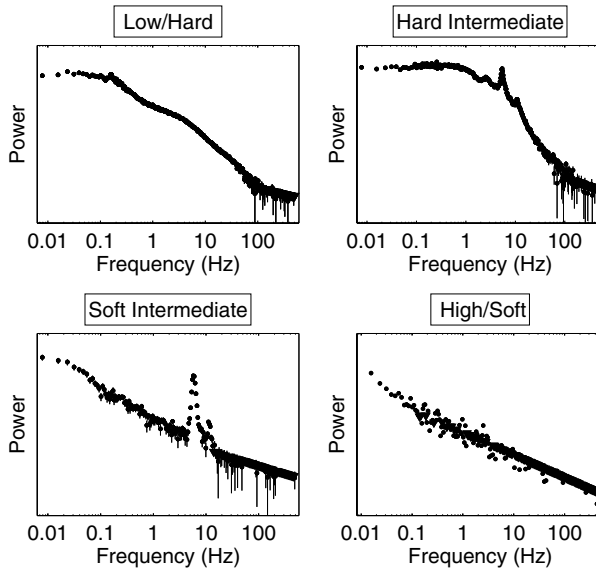


Figure 3. Examples of power-density spectra of GX 339–4 from the four states discussed in the text.

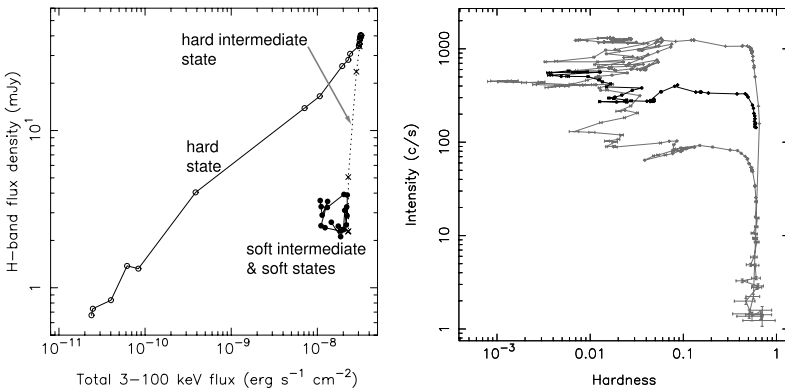


Figure 4. *Left panel:* X-ray/IR correlation for the first part of the 2002/2003 outburst of GX 339–4 (Homan et al., 2005a). The different behavior for the different states is evident. *Right panel:* HID of the two most recent outbursts of GX 339–4: 2002/2003 (gray) and 2004 (black).

and Remillard (2004) sources stay in the hard state until the power-law steepens beyond an index of 2.1. In our view the hard state is limited to only the hardest power-law dominated spectra with indices around 1.3–1.5, as many changes occur (simultaneously) when the power-law becomes steeper.

At the end of the 2002/2003 outburst GX 339–4 returned to the hard state, similar to what is observed in most, if not all, black hole transients. In the HID this can be nicely seen as the lower horizontal branch bending down to start running parallel to, and in fact nearly on top of, the hard state branch that was traced out during the rise. Such ‘saturation’ of the spectral hardness was also observed in XTE J1650–500 (Rossi et al., 2003, see also Figure 1). It is interesting to note that once GX 339–4 reached the hardness at which it originally left the hard state branch, the optical/IR showed a strong increase (see light curves in Bailyn and Ferrara, 2004), indicating that the jet does not become visible in the optical/IR (or switch on) until the hard state branch is reached (as was already suggested by Kalemci et al. (2005) based on observations 4U 1543–47). The spectral hardening towards the hard state is not necessarily a monotonic process, as can be seen in the HID of GX 339–4 and XTE J1859+226.

Observations of hard state branches extending over many orders of magnitude in GX 339–4 and XTE 1650–500 indicate that the hard state accretion flow geometry (which likely gives rise to strong outflows) can exist over a wide range in mass accretion rate.

4.2. THE HARD-STATE \leftrightarrow SOFT-STATE TRANSITIONS

Immediately after leaving and before returning to the hard state, black hole transients are observed in an intermediate state, with spectral power-law indices between

roughly 1.5–2.5. We are not aware of any exception to this. This state is different from the hard state in several aspects. Depending on whether the intermediate state is observed during the hard→soft or soft→hard transition, sources show a clear steepening/flattening of the spectral power law component, a strong increase/decrease in the noise and QPO frequencies, and an increasing/decreasing fractional disk flux, compared to the hard state. All these properties evolve smoothly from and to the hard state. In fact, without the HID and optical/IR information (see Figure 4) it would be difficult to exactly pin-point the transition between these two states. In the case of the hard→soft transition the movement to the left in the HID is due to the combination of increased disk flux and steepening of the power law. In the timing domain, the broad-band variability components seen in the power-density spectrum increase their characteristic frequencies, showing an evolution that clearly links them to the corresponding components in the hard state. A clear type C QPO appears, also with a characteristic frequency increasing with time and decreasing hardness (see Belloni et al., 2005). A typical power-density spectrum from the intermediate state is shown in Figure 3.

It is important to note that the hard→intermediate state transition does not always occur at the same flux level, as can be seen from Figure 4. During the 2004 outburst of GX 339–4 this transition occurred at a flux level that was about a factor of 4 lower than in 2002. The transition in 2004 was preceded by a small hard state outburst, which suggests that the flux level at which the transition occurs depends on the recent accretion history. After passing through the intermediate GX 339–4 continued to brighten in the soft state during its 2004 outburst.

Another important point to note is the fact that the occurrence of the intermediate state does not seem to depend on the time derivative of \dot{M} . In XTE J1650–500 it occurred during the decay, but in GX 339–4 while \dot{M} was apparently still increasing, as witnessed by the second (soft) maximum in the light curve. However, in both cases the transition resulted in a (temporary) drop in the count rate by a factor of ~ 2 .

Taking once more the 2002/2003 outburst of GX 339–4 as a template, we see that when the hardness goes below a well-defined threshold, the timing properties change sharply: a clear type B QPO appears in the power density spectrum (Figure 3, see also Casella et al., 2004 for similar behavior in XTE J1859+226). In most sources the change from type C to type B QPOs seems to take place when the power-law index has a value around 2.5–3.0. In fact, power-laws with such indices are accompanied by a great variety of timing properties: not only type A, B or C QPOs, but also very weak variability like that seen in the soft state.

We will refer to the part of the transition during which the power-law index changes between ~ 1.5 and 2.5 and which shows type C QPOs and strong band-limited noise as the hard intermediate state. The part of the transition where the power-law index is relatively constant around a value of 2.5–3.0 and during which the source occasionally shows type A and B QPOs on top of weaker red noise will be referred to as the soft intermediate state. Note that in GX 339–4 the soft intermediate state also showed observations with weak band limited noise and/or

QPOs that we were not able to classify. It is therefore more a collection of different types of behavior, between which the source could switch on a time scale of a day, rather than a well-defined state.

It is important to note that the change from the hard intermediate to the soft intermediate state was repeated again in the 2004 outburst at the same spectral hardness. During the 2002/2003 outburst a huge radio flare/ejection event was observed around the time of the change from the hard intermediate to the soft intermediate state (Gallo et al., 2004; Fender et al., 2004). Although it is tempting to associate such a flare with this transition, it should be mentioned that similar radio events are also observed in GRS 1915+105 (Belloni et al., 2000), a source for which characteristic type A and B QPOs were not observed to date. However, given the fast time scales of transitions in this system, it is possible that such QPOs appear for intervals shorter than for other sources, which would make them difficult to observe.

It is during the soft intermediate state that most high-frequency QPOs have been detected, indicating that there might be a relation between those and type A/B QPOs; indeed, the frequencies of both features are not observed to vary by a large amount between different observations. It is possible however that the high frequency QPOs in soft intermediate state evolve from broader features in the hard intermediate state, as is suggested by observations of XTE J1650–500 (Homan et al., 2003). Notice that while the soft intermediate state is often observed at high flux between the hard intermediate and the soft states, the same timing properties are not observed at low flux, when the reverse transition takes place. Moreover, in XTE J1550–564 (Homan et al., 2001) type A and B QPOs appeared at several well separated luminosity levels, strongly suggesting they are not strictly related to hard↔soft transitions. In GX 339–4 a strong 1-Hz QPO with some properties similar to those of the type B QPOs is observed at low flux, indicating that it is possible that a similar state exist also at much lower accretion rate, although with different characteristic frequencies (Belloni et al., 2005).

4.3. THE SOFT STATE

During the soft state, which in GX 339–4 took place after the soft intermediate state, the spectral and timing properties are rather well defined, although a single clear transition from the soft intermediate state is hard to identify. The energy spectrum of the soft state is dominated by a strong thermal component, with the presence of a weak steep power-law component, which was not observed to show a high-energy cutoff (see Grove et al., 1998). Variability in the soft state is weak compared to the other states, with typical rms amplitudes of at most a few percent root mean square. Unfortunately, by the time most transients reach the soft state they are usually in the decay phase and observations have become shorter and less frequent, so detailed studies of its variability properties are rare. Nevertheless, a few weak QPOs have been detected in the soft states of GRO J1655–40, XTE J1550–564

and H1743–322. These QPOs all had frequencies that were higher than the other low frequency QPOs detected in those sources and the noise continua could all be fitted with broken power law. Surprisingly, the QPO and break frequencies of these power spectra fall on top of the Wijnands–van der Klis relation (Wijnands and van der Klis 1999) for black holes in the hard and hard intermediate states. This suggests not only that these might be type C QPOs, but more importantly, that variability properties that once were thought to be characteristic of the hard and hard intermediate states are still present in the soft state, although in a much weaker form.

5. Discussion

Although the picture presented here is somewhat simplified, as additional complications have been observed, we can sketch the states by using once more GX 339–4 as a template (see Figure 5 and Fender et al., 2004). As shown above, the hard intermediate and soft intermediate states are kept separate, as both spectral and timing evolution show marked differences.

The hard state and the hard intermediate states have much in common. Spectrally, they are dominated by a hard component for which a high-energy cutoff is observed (Grove et al., 1998). In the timing domain, the components observed in the power-density spectrum in these two states are clearly related, as can be seen from the evolution of their characteristic frequencies (Belloni et al., 2005). Nevertheless, something happens to the accretion flow as the source moves from the low/hard

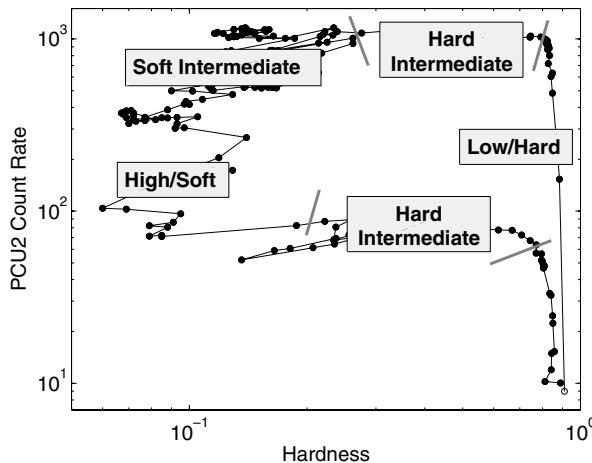


Figure 5. The HID of the 2002/2003 outburst of GX 339–4. Clear transitions are marked by gray segments. The branches corresponding to the four basic states in the q-track are labeled (Belloni et al., 2005).

state to the intermediate state, as can be seen from multi-wavelength studies (Homan et al., 2005a). This is likely to be related to changes in the jet, which could be responsible for part of the observed X-ray flux (Fender et al., 2004) as is also indicated by the fact that radio emission is always observed in these states.

The soft state and soft intermediate state are spectrally somewhat related. The energy spectrum is dominated by the thermal disk component, with a steep hard component with no evidence of a high-energy cutoff. The power density spectrum lacks band-limited components and shows only QPOs superimposed on a power-law component. No radio emission is observed (i.e. only upper limits on the emission from the compact source), indicating that the production of a jet is terminated at the transition to soft intermediate state (Fender et al., 2004) and maybe even before. During these states, the accretion flow is clearly different from the other two. In terms of variability however, the soft state shares some properties with the hard state and hard intermediate state, with the typical variability time scales following the same relation as seen in those states. If the hard-state variability properties are linked to jet production, the presence of related (but much weaker) variability in the soft state could indicate a very weak (i.e. below current detection limits) jet in that state as well.

In addition to these general properties, there is a number of important topics whose detailed discussion is beyond the scope of the present paper. Most notably, the fast transitions observed between different states (never involving the hard state, which is only reserved for the beginning and the end of an outburst) need to be studied in detail, as they probably hold the key for a deeper understanding of the physics of the states and their association to the jet. Also, some sources can have bright outbursts without ever leaving the hard state, indicating that once again the instantaneous mass accretion rate is not what determines the transitions. However, the recent history of the mass accretion rate may play an important role (this can also be seen in Figure 4, as GX 339–4 was observed to leave the hard state at very different flux levels). A secondary accretion flow (Smith et al., 2002; Yu et al., 2004) or changes in the Compton cooling/heating in the accretion disk corona (Meyer-Hofmeister et al., 2005) seem to be promising to explain some of these issues. For example, delays between a fast (i.e. in terms of propagation speed) secondary flow and a slower disk flow could account for the observed hysteresis.

In conclusion, the hysteresis behavior that can be seen from the HIDs in Figure 1, put forward for the first time by Miyamoto et al. (1995), was found with *RXTE* to be a characteristic pattern for black hole transients. Despite many complexities, general features have been shown to relate to the ejection of powerful relativistic jets, which can lead to a deeper understanding of the physical properties of the accretion flow. The picture presented here, scaled to longer time scales, should also be valid for AGNs. In these sources, there is no contribution of the optically thick accretion disk in the X-ray band, but the path shown in Figure 5 is qualitatively similar if the disk contribution is removed. Recently, Cui (2004) presented a very similar diagram for the *RXTE* observations of the highly variable AGN Mkn 421,

showing that indeed the scheme of accretion states could apply to systems over a large scales of masses.

Acknowledgements

JH thanks Jon Miller and Ron Remillard for numerous discussions on the topic of black hole states.

References

- Bailyn, C. and Ferrara, L.: 2004, *Astronom Teleg* **323**, 1.
- Belloni, T., Homan, J., Casella, P., van der Klis, M., Nespoli, E., Lewin, W., Miller, J. and Méndez, M.: 2005, *A&A* **440**, 270.
- Belloni, T., Klein-Wolt, M., Méndez, M., van der Klis, M. and van Paradijs, J.: 2000, *A&A* **355**, 271–290.
- Casella, P., Belloni, T., Homan, J. and Stella, L.: 2004, *A&A* **426**, 587–600.
- Corbel, S., Nowak, M.A., Fender, R.P., Tzioumis, A.K. and Markoff, S.: 2003, *A&A* **400**, 1007–1012.
- Cui, W.: 2004, *ApJ* **605**, 662.
- Esin, A.A., McClintock, J.E. and Narayan, R.: 1997, *ApJ* **489**, 865.
- Fender, R.P., Belloni, T.M. and Gallo, E.: 2004, *MNRAS* **355**, 1105–1118.
- Gallo, E., Corbel, S., Fender, R.P., Maccarone, T.J. and Tzioumis, A.K.: 2004, *MNRAS* **347**, L52–L56.
- Grove, J.E., Johnson, W.N., Kroeger, R.A., McNaron-Brown, K., Skibo, J.G. and Phlips, B.F.: 1998, *ApJ* **500**, 899.
- Homan, J., Buxton, M., Markoff, S., Bailyn, C., Nespoli, E., and Belloni, T.: 2005, *ApJ* **624**, 295.
- Homan, J., Klein-Wolt, M., Rossi, S., Miller, J.M., Wijnands, R., Belloni, T., van der Klis, M. and Lewin, W.H.G.: 2003, *ApJ* **586**, 1262–1267.
- Homan, J., Miller, J.M., Wijnands, R., van der Klis, M., Belloni, T., Steeghs, D. and Lewin, W.H.G.: 2005, *ApJ* **623**, 383.
- Homan, J., Wijnands, R., van der Klis, M., Belloni, T., van Paradijs, J., Klein-Wolt, M., Fender, R. and Méndez, M.: 2001, *ApJ* **132**, 377–402.
- Kalemci, E., Tomsick, J.A., Buxton, M.M., Rothschild, R.E., Pottschmidt, K., Corbel, S., Brocksopp, C. and Kaaret, P.: 2005, *ApJ* **622**, 508.
- Maccarone, T.J. and Coppi, P.S.: 2003, *MNRAS* **338**, 189–196.
- McClintock, J.E. and Remillard, R.A.: 2004, *astro-ph/0306213*.
- Meyer-Hofmeister, E., Liu, B.F. and Meyer, F.: 2005, *A&A* **432**, 181.
- Miyamoto, S., Kitamoto, S., Hayashida, K. and Egoshi, W.: 1995, *ApJ* **442**, L13–L16.
- Remillard, R.A., Sobczak, G.J., Muno, M.P. and McClintock, J.E.: 2002, *ApJ* **564**, 962–973.
- Rossi, R., Homan, J., Miller, J. and Belloni, T.: 2003, *astro-ph/0309129*.
- Smith, D.M., Heindl, W.A. and Swank, J.H.: 2002, *ApJ* **569**, 362–380.
- Wijnands, R., Homan, J. and van der Klis, M.: 1999, *ApJ* **526**, 33.
- Yu, W., van der Klis, M. and Fender, R.: 2004, *ApJ Lett.* **611**, L121–L124.

RAPID X-RAY VARIABILITY OF SEYFERT 1 GALAXIES

S. VAUGHAN¹, A.C. FABIAN² and K. IWASAWA²

¹*X-Ray and Observational Astronomy Group, University of Leicester, Leicester, U.K.;*
E-mail: sav2@star.le.ac.uk

²*Institute of Astronomy, University of Cambridge, Madingley Road, Cambridge, U.K.*

(Received 23 September 2004; accepted 1 June 2005)

Abstract. The rapid and seemingly random fluctuations in X-ray luminosity of Seyfert galaxies provided early support for the standard model in which Seyferts are powered by a supermassive black hole fed from an accretion disc. However, since *EXOSAT* there has been little opportunity to advance our understanding of the most rapid X-ray variability. Observations with *XMM-Newton* have changed this.

We discuss some recent results obtained from *XMM-Newton* observations of Seyfert 1 galaxies. Particular attention will be given to the remarkable similarity found between the timing properties of Seyferts and black hole X-ray binaries, including the power spectrum and the cross spectrum (time delays and coherence), and their implications for the physical processes at work in Seyferts.

Keywords: X-rays, variability, active galaxies

1. Introduction

X-ray variability appears to be ubiquitous in active galactic nuclei (AGN). The rapid and seemingly random fluctuations in the X-ray luminosity of Seyfert galaxies provided early support for the standard black hole/accretion disc model (Rees, 1984) by implying compact emission regions and high luminosity densities (Bar and Mushotzky, 1986).

2. The *EXOSAT* Era

EXOSAT (1983–1986) was the first mission to provide long (~ 3 day), uninterrupted X-ray observations of Seyfert galaxies. From these observations the X-ray power spectra (see van der Klis, 1989) of Seyfert galaxies were measured for the first time (Lawrence et al., 1987; Green et al., 1993; Lawrence and Papadakis, 1993). The *EXOSAT* observations showed that the power spectra of Seyferts above $\sim 10^{-5}$ Hz could be approximated by a power-law: $\mathcal{P}(f) \propto f^{-\alpha}$ where $\mathcal{P}(f)$ is the power at frequency f and α is the power spectrum slope. The measured slopes from the *EXOSAT* observations were typically $\alpha \approx 1.5$. Processes such as these, which have broad-band power spectra with more power at lower frequencies, are called “red



noise” (see Press, 1978). It was noted early on (Lawrence et al., 1987) that this red noise variability of Seyferts is similar to that observed in Galactic Black Hole Candidates (GBHCs; Belloni and Hasinger, 1990; Nowak et al., 1999; McClintock and Remillard, 2004), perhaps suggesting that the same physical processes operate in these sources that differ in black hole mass by factors of $\gtrsim 10^5$.

3. Low Frequency Power Spectra from *RXTE*

The steep slopes found in the *EXOSAT* power spectra required there to be a flattening at even lower frequencies (so that the integrated power remains finite). In recent years long *RXTE* monitoring observations have detected these breaks (e.g. Uttley et al., 2002; Markowitz et al., 2003; see also the article by Ian McHardy in these proceedings). Below the break the slope is typically $\alpha_{lo} \approx 1$ and at frequencies above the break the slope is $\alpha_{hi} \approx 2$. (The *EXOSAT* power spectra spanned intermediate frequencies and often measured an intermediate slope over the break.) The breaks represent “characteristic time scales” in the aperiodic variability of Seyferts and, significantly, appear to scale linearly with the mass of the central black hole: $f_{\text{break}} \propto 1/M_{\text{BH}}$.

4. *XMM-Newton* Results: High Frequency Power Spectra

Until the launch of *XMM-Newton* (Jansen et al., 2001) high frequency timing studies of Seyferts were not able to substantially improve on the *EXOSAT* results. *XMM-Newton*’s success is due to a combination of high throughput, broad energy bandpass and long (~ 2 day) orbit. Figure 1 shows an example of a broad-band (0.2–10 keV) light curve from a single orbit observation.

Several Seyfert 1 galaxies have been studied with long *XMM-Newton* observations and yielded interesting power spectra. These include: NGC 4051 (McHardy et al., 2004), Mrk 766 (Vaughan and Fabian, 2003), MCG – 6-30-15 (Vaughan et al., 2003), NGC 4395 (Vaughan et al., 2004) (and also Ark 564; Vignali et al., 2004). Figure 2 shows the power spectra for three of these. The *XMM-Newton* results clearly reveal similar high frequency breaks in the power spectra (also measured

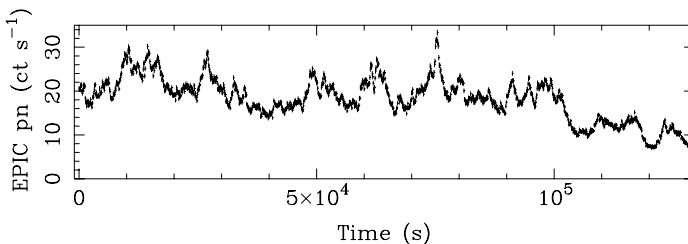


Figure 1. *XMM-Newton* light curve of Mrk 766 binned to 100 sec resolution.

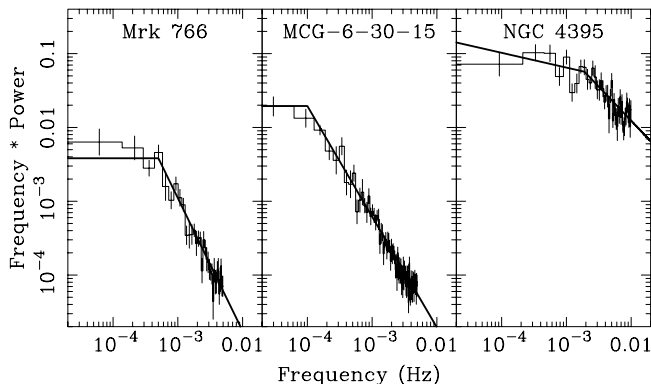


Figure 2. *XMM-Newton* power spectra of three Seyfert 1 galaxies. Shown are the binned data (*histograms*) unfolded using the best-fitting broken power law continuum model (*solid line*). Note that the ordinate is in $f \times P(f)$ units (a slope of $\alpha = 1$ would appear flat). Note that the figure shows *unfolded* data, meaning the data/model residuals multiplied by the best-fitting model. This is necessarily a model-dependent procedure and is not advisable if sharp features are present in the spectrum. However, for these rather broad, smooth spectra unfolding does provide a clear, if slightly crude, impression of the shape of the underlying spectrum free from sampling effects.

by *RXTE* in some cases) but clearly show a substantial object-to-object differences in the normalisation of the power spectrum (which describes the overall variability amplitude).

These *XMM-Newton* observations have also demonstrated the energy dependence of the power spectrum. Above the break frequency the slope α_{hi} tends to be steeper at lower energies. This is clearly observed in MCG-6-30-15 (Vaughan et al., 2003) and NGC 4051 (McHardy et al., 2004) but is not constrained by the other observations. This energy dependence was also measured in NGC 7469 using an intensive *RXTE* monitoring campaign (Nandra and Papadakis, 2001).

5. *XMM-Newton* Results: High Frequency Cross Spectrum

In addition to the energy dependence of the power spectrum, the excellent quality *XMM-Newton* light curves have allowed the cross spectrum to be investigated in several Seyfert 1s for the first time. Prior to *XMM-Newton* only Papadakis et al. (2001) had measured the cross spectrum for a Seyfert (NGC 7469 using *RXTE*).

The cross spectrum compares the variations in one band with those in another as a function of frequency. The amplitude of the cross spectrum gives the coherence (Vaughan and Nowak, 1997) while the argument gives the phase lag (time delay; Nowak et al., 1999). The coherence quantifies any (linear) correlation between the variations in the two bands, irrespective of any time delays. The observations typically show high coherence at the lowest frequencies (i.e. strong correlation) with

a decrease at higher frequencies which implies there are independent variations between the two bands occurring on short time scales (Vaughan et al., 2003; McHardy et al., 2004; Vaughan et al., 2004). At low frequencies, where the coherence is high, the data also exhibit small time delays, with the soft leading the hard variations (Vaughan et al., 2003; McHardy et al., 2004). The magnitude of the time delay decreases with increasing frequency (although the functional form of the relation is poorly constrained).

6. Summary of Results

XMM-Newton has already made significant progress towards improving our understanding of the high frequency variability of Seyfert galaxies. The timing studies have revealed:

- Similar broken power spectra in Seyferts but object-to-object differences in normalisation (variability amplitude) and high frequency slope.
- Energy-dependent high frequency power spectrum slope (steeper at lower energies).
- High coherence at low frequencies, falling off at high frequencies.
- Small ($\Delta T \sim 0.01/f$) soft-to-hard time delays.

7. Comparison with GBHCs

The frequencies of the breaks in the power spectra are broadly consistent with the long-held notion that the characteristic frequencies should scale as $\propto 1/M_{\text{BH}}$ right down to stellar mass black holes. Figure 3 shows the available data for 11 Seyferts. Although the uncertainties are rather large, the data seem consistent with an extrapolation of the $f_{\text{br}} \propto 1/M_{\text{BH}}$ relation from the well-studied GBHC Cygnus X-1 (Belloni and Hasinger, 1990; Cui et al., 1996; Nowak et al., 1999; McClintock and Remillard, 2004). Note that the break frequency measurements come from a combination of *XMM-Newton* and *RXTE* observations. Long *XMM-Newton* observations are sensitive to breaks in the range $\sim 10^{-4}$ – 10^{-2} Hz while the *RXTE* monitoring campaigns are sensitive to breaks at lower frequencies.

The connection between Seyferts and GBHCs is reinforced by the similarity between their cross spectra. It is well known that GBHCs show highly coherent variations at low frequencies with the coherence fading away at the highest frequencies plus frequency dependent time lags similar to those measured in Seyferts (Nowak et al., 1999; McClintock and Remillard, 2004). These all argue for mechanism responsible for producing the X-ray variability in GBHCs.

One may ask what advantage is gained by studying Seyferts in X-rays if GBHCs operate with the same physics but provide much higher quality data? One answer is that Seyferts can in fact provide data that are in some senses better than

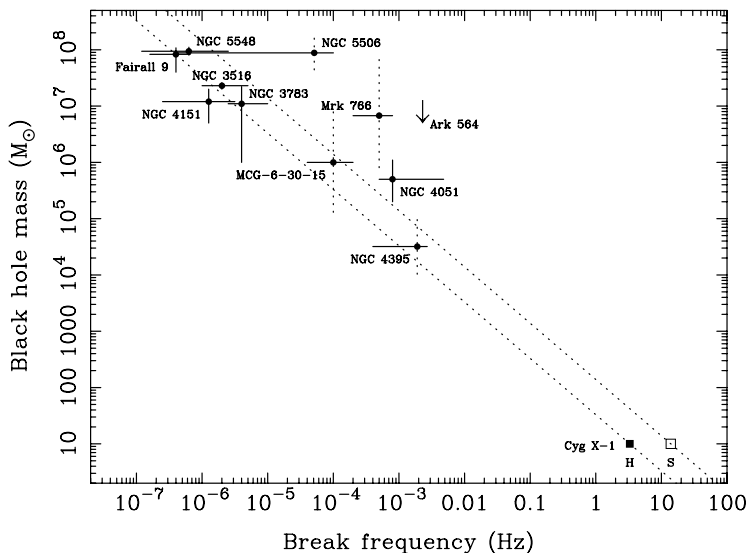


Figure 3. The $M_{\text{BH}} - f_{\text{br}}$ relation for 11 Seyfert galaxies. The masses are from reverberation mapping experiments except for the four objects marked using dotted error bars. Also shown are typical break frequencies for Cyg X-1 in both its low/hard (H) and high/soft (S) states. The dotted lines show example $M_{\text{BH}} \propto 1/f_{\text{br}}$ relations consistent with the Cyg X-1 points.

that from GBHCs for studying the highest frequencies. For example, comparing MCG – 6-30-15 and Cygnus X-1 we see the time scales are longer by $\sim 10^5$ in the Seyfert, but the X-ray flux is smaller by $\sim 10^3$. This means that *per characteristic time scale* the Seyfert provides $\sim 10^2$ more photons! Of course, GBHC enthusiasts can argue that GBHCs reclaim much of their advantage even here because one can always observe many ($\sim 10^5$) more samples of a given time scale in a fixed amount of observing time, even if many less photons are recorded per time scale. Even so the power spectrum of MCG–6-30-15 could be measured up to $\sim 5 \times 10^{-3}$ Hz using the *XMM-Newton* data. This is equivalent to probing ~ 500 Hz in Cygnus X-1, a challenge for even the best *RXTE* observations (Revnivtsev et al., 2000).

8. Implications for the Emission Processes

The X-ray emission mechanism operating in Seyfert galaxies (and GBHCs) is usually thought to be inverse-Compton scattering. In the simplest models harder photons are expected to lag behind the softer photons due to the larger number of scatterings required to produce harder photons; the delay should be of order the light-crossing time of the corona. The direction and magnitude of the observed time lags in Seyfert 1s are consistent with an origin in a Comptonising corona. However, if the lags are frequency dependent (as expected by analogy with Cygnus X-1)

the lags at lower temporal frequencies would become much longer than expected for a compact corona (see discussion in Nowak et al., 1999). In addition, some models of Compton scattering coronae predict the high frequency PSD should be steeper for higher energy photons, due to the high frequency fluctuations being washed out by multiple scatterings (Nowak and Vaughan, 1996), contrary to the observations. Alternatively, the time delay between soft and hard bands could be due to the spectral evolution of individual X-ray events (Poutanen and Fabian, 1999) or propagation of accretion rate variations through an extended emission region (Kotov et al., 2001).

Acknowledgements

Based on observations obtained with *XMM-Newton*, an ESA science mission with instruments and contributions directly funded by ESA Member States and the USA (NASA). SV and KI are supported by the UK PPARC. ACF is supported by the Royal Society.

References

- Barr, P. and Mushotzky, R.F.: 1986, *Nature* **320**, 421.
 Belloni, T. and Hasinger, G.: 1990, *A&A* **227**, L33.
 Cui, W., Zhang, S.N., Focke, W. and Swank, J.H.: *ApJ* **484**, 383.
 Green, A.R., McHardy, I.M. and Lehto, H.J.: 1993, *MNRAS* **265**, 664.
 Jansen, F. et al.: 2001, *A&A* **365**, L1.
 Kotov, O., Churazov, E. and Gilfanov, M.: 2001, *MNRAS* **327**, 799.
 Lawrence, A., Watson, M.G., Pounds, K.A. and Elvis, M.: 1987, *Nature* **325**, 694.
 Lawrence, A. and Papadakis, I.: 1993, *ApJ* **414**, L85.
 Markowitz, A. et al.: 2003, *ApJ* **593**, 96.
 McClintock, J.E. and Remillard, R.A.: 2004, in: W.H.G. Lewin and M. van der Klis (eds.), *Compact Stellar X-ray Sources*, Cambridge University Press, Cambridge, in press (astro-ph/0306213).
 McHardy, I. M.: 1989, in: J. Hunt and B. Battrick (eds.), *Two Topics in X Ray Astronomy*, (ESA SP-296; Noordwijk: ESA), p. 1111.
 McHardy, I.M., Papadakis, I.E., Uttley, P., Page, M. and Mason, K.: 2004, *MNRAS* **348**, 783.
 Nandra, K. and Papadakis, I.E.: 2001, *ApJ* **554**, 710.
 Nowak, M.A. and Vaughan, B.A.: 1996, *MNRAS* **280**, 227.
 Nowak, M.A., Vaughan, B.A., Wilms, J., Dove, J.B., and Begelman, M.C.: 1999, *ApJ* **510**, 874.
 Papadakis, I.E., Nandra, K. and Kazanas, D.: 2001, *ApJ* **554**, L133.
 Poutanen, J. and Fabian, A.C.: 1999, *MNRAS* **306**, L31.
 Press, W.H.: 1978, *Comments on Astrophysics* **7**, 103.
 Rees, M.J.: 1984, *ARA&A* **22**, 471.
 Revnivtsev, M., Gilfanov, M. and Churazov, E.: 2000, *A&A* **363**, 1013.
 Uttley, P. and McHardy I.M.: 2001, *MNRAS* **323**, L26.
 Uttley, P., McHardy, I.M. and Papadakis I.: 2002, *MNRAS* **332**, 231.
 van der Klis M.: 1989, in: H. Ogelman, and E.P.J. van den Heuvel (eds.), *Timing Neutron Stars*, Kluwer, Dordrecht, NATO ASI Series C 262, p. 27.

- Vaughan, B.A. and Nowak, M.A., 1997, *ApJ* **474**, L43.
- Vaughan, S. and Fabian, A.C.: 2003, *MNRAS* **341**, 496.
- Vaughan, S., Fabian, A.C. and Nandra, K.: 2003, *MNRAS* **339**, 1237.
- Vaughan, S., Iwasawa, K., Fabian, A.C. and Hayashida, K.: 2004, *MNRAS* submitted.
- Vignali, C., Brandt, W. N., Boller, Th., Fabian, A.C. and Vaughan, S.: 2004, *MNRAS* **347**, 854.

EPICYCLIC FREQUENCIES DERIVED FROM THE EFFECTIVE POTENTIAL: SIMPLE AND PRACTICAL FORMULAE

M.A. ABRAMOWICZ¹ and W. KLUŻNIAK²

¹*On Leave from Department of Astrophysics, Göteborg University, S-412-96 Göteborg, Sweden, and at Department of Theoretical Physics, Chalmers University, S-412-96 Göteborg, Sweden, Nordita, Copenhagen, Denmark; E-mail: marek@fy.chalmers.se*

²*Institute of Astronomy, Zielona Góra University, Zielona Góra, Poland, and Copernicus Centre, Bartycka 18, PL-00-716 Warszawa, Poland*

(Received 25 November 2004; accepted 1 June 2005)

Abstract. We present and discuss a short and simple derivation of orbital epicyclic frequencies for circular geodesic orbits in stationary and axially symmetric spacetimes. Such spacetimes include as special cases analytically known black hole Kerr and Schwarzschild spacetimes, as well as the analytic Hartle-Thorne spacetime and all numerically constructed spacetimes relevant for rotating neutron stars. Our derivation follows directly from energy and angular momentum conservation and it uses the concept of the effective potential. It has never been published, except for a few special cases, but it has already become a part of the common knowledge in the field.

Keywords: black holes, neutron stars, orbital motion, epicyclic frequencies

1. Introduction

Properties of congruences of nearly circular geodesic orbits in stationary and axially symmetric spacetimes are studied because of their fundamental role in the theory of accretion disks around compact objects with strong gravity. The Keplerian angular frequency Ω_K , the radial epicyclic frequency ω_R and the vertical epicyclic frequency ω_V are the most important characteristics of these orbits. Analytic formulae for the three frequencies in Schwarzschild, Kerr and Hartle-Thorne metrics have been published many times by several authors (see e.g. Wald, 1984; Okazaki et al., 1987; Perez et al., 1997; Nowak and Lehr, 1999; Marković, 2000; Abramowicz et al., 2003) and are well known.

Here, we recall our unpublished (Abramowicz and Kluźniak, 2000) derivation of the epicyclic frequencies in the general case. This fully relativistic derivation is remarkably simple: just four short lines of very transparent, easy to check algebra. It uses only invariantly defined quantities that have obvious physical meaning, and it closely follows the standard Newtonian derivation that is equally short and based on the concept of the effective potential.¹

¹The same simple method was used in the textbook by Wald (1984) in the special case of a static, spherically symmetric metric.



The standard Newtonian derivation of epicyclic frequencies is briefly recalled in Section 2, where we also make a few comments on these properties of the orbital frequencies that are not commonly appreciated. In Section 3, for the completeness of presentation, we review some basic facts concerning relativistic formalism that are directly relevant to the derivation of the orbital frequencies in Einstein's theory. The reader who is interested only in our four-line derivation may skip the next two sections and start reading from Section 4.

2. Nearly Circular Geodesic Motion: Newton's Theory

In Newton's theory, circular geodesic orbits (i.e., Keplerian circular orbits of free particles) occur at locations $r = r_0$, $\theta = \theta_0$, where the effective potential U_{eff} has an extremum with respect to both radial r and polar-angle θ coordinates,²

$$\left(\frac{\partial U_{\text{eff}}}{\partial r}\right) = 0 = \left(\frac{\partial U_{\text{eff}}}{\partial \theta}\right), \quad U_{\text{eff}} \equiv \Phi(r, \theta) + \frac{L^2}{2r^2 \sin^2 \theta}. \quad (1)$$

The derivatives are taken at a constant angular momentum L . The gravitational potential $\Phi(r, \theta)$ is assumed to be stationary – $\partial\Phi/\partial t = 0$; axially symmetric – $\partial\Phi/\partial\phi = 0$; and to have the equatorial symmetry plane at $\theta = \pi/2$. From the last assumption it follows that one can take $\theta_0 = \pi/2$, i.e., that there are circular orbits located in the equatorial plane.

Note, that from the solution $L = L_K(r)$ of Eq. (1) it follows immediately that in the equatorial plane the radial distributions of Keplerian angular momentum L_K and Keplerian angular velocity Ω_K are given by,³

$$L_K = \pm \left(r^3 \frac{\partial \Phi}{\partial r} \right)^{1/2}, \quad \Omega_K = \frac{L_K}{r^2} = \pm \left(r^{-1} \frac{\partial \Phi}{\partial r} \right)^{1/2}. \quad (2)$$

Here, the derivatives are taken at the equatorial plane, $\theta = \pi/2$.

In the linear regime, we can consider separately the case of purely radial, $\delta r = r - r_0$, $\delta\theta = 0$, and purely vertical, $\delta\theta = \theta - \theta_0$, $\delta r = 0$, epicyclic oscillations about circular orbits in the equatorial plane. Take a ‘‘perturbed’’ Keplerian orbit which may be slightly non-circular, or slightly off the equatorial plane, and which has the same angular momentum as the original circular orbit $L = L_0$, but with a slightly larger energy $E = E_0 + \delta E$. Because circular orbits occur at extrema of the effective potential, the Taylor expansion of U_{eff} near a circular orbit starts from

²We use the standard spherical coordinates $[t, r, \theta, \phi]$.

³Obviously, Keplerian orbits are impossible in the region where $(\partial\Phi/\partial r) < 0$.

the second-order term:

$$\delta U_{\text{eff}} = \frac{1}{2} \left(\frac{\partial^2 U_{\text{eff}}}{\partial r^2} \right) \delta r^2, \quad \delta U_{\text{eff}} = \frac{1}{2} \left(\frac{\partial^2 U_{\text{eff}}}{\partial \theta^2} \right) \delta \theta^2. \quad (3)$$

A small change in the orbital energy δE may be therefore expressed as:

$$\delta E = \frac{1}{2} \left(\frac{\partial^2 U_{\text{eff}}}{\partial r^2} \right) \delta r^2 + \frac{1}{2} (\delta \dot{r})^2, \quad \delta E = \frac{1}{2} \left(\frac{\partial^2 U_{\text{eff}}}{\partial \theta^2} \right) \delta \theta^2 + \frac{1}{2} r^2 (\delta \dot{\theta})^2. \quad (4)$$

The energy of the perturbed orbit is obviously a constant of motion, and thus $\delta \dot{E} = 0$, from which it follows that,

$$0 = \delta \dot{r} \left[\left(\frac{\partial^2 U_{\text{eff}}}{\partial r^2} \right) \delta r + \delta \ddot{r} \right], \quad 0 = \delta \dot{\theta} \left[\left(\frac{\partial^2 U_{\text{eff}}}{\partial \theta^2} \right) \delta \theta + r^2 \delta \ddot{\theta} \right]. \quad (5)$$

We are interested in a non-trivial solution $\delta \dot{r} \neq 0 \neq \delta \dot{\theta}$, for which the last two equations take the well-known form of a simple harmonic oscillator,

$$0 = \omega_R^2 \delta r + \delta \ddot{r}, \quad 0 = \omega_V^2 \delta \theta + \delta \ddot{\theta} \quad (6)$$

with the squared eigenfrequencies being the second derivatives of the effective potential with respect to proper geodesic distances in radial R and vertical V directions. The radial and vertical directions are defined in a *coordinate-independent* way that for the particular case of spherical coordinates yields $dR = dr$, $dV = r d\theta$. Thus, one may write,

$$\omega_R^2 \equiv \left(\frac{\partial^2 U_{\text{eff}}}{\partial R^2} \right) = \left(\frac{\partial^2 U_{\text{eff}}}{\partial r^2} \right), \quad \omega_V^2 \equiv \left(\frac{\partial^2 U_{\text{eff}}}{\partial V^2} \right) = \frac{1}{r^2} \left(\frac{\partial^2 U_{\text{eff}}}{\partial \theta^2} \right). \quad (7)$$

From Eq. (7), and Eqs. (1) and (2) it follows that,

$$\omega_R^2 = \Omega_K^2 \left(\frac{d \ln L_K^2}{d \ln r} \right), \quad \omega_V^2 = \Omega_K^2 + \frac{1}{r^2} \left(\frac{\partial^2 \Phi}{\partial \theta^2} \right). \quad (8)$$

Several important deductions could be made from (8). Firstly, it is obvious that $\omega_R = \Omega_K$ everywhere if and only if $L_K^2 \propto r$, and this together with Eq. (2) implies $\Phi \propto 1/r$. Secondly, $\omega_V = \Omega_K$ if (but not only if) the gravitational potential is spherically symmetric. Therefore, one concludes that in the special but important case of the $\Phi = -GM/r$ potential, all three characteristic orbital frequencies are equal and their squares are positive,

$$\omega_R^2 = \omega_V^2 = \Omega_K^2 = \frac{GM}{r^3} > 0. \quad (9)$$

Here M is the mass of the gravity source. The equality of the three frequencies means that the orbits in the $\Phi = -GM/r$ potential are periodic and closed (a fact known already to Kepler, who discovered that they are ellipses). The positive squares imply stability of both radial and vertical oscillations, i.e., the dynamical stability of circular orbits in the $\Phi = -GM/r$ potential.

The third important deduction from (8) is that in the general case, with a potential $\Phi(r, \theta) \neq -GM/r$, the radial epicyclic oscillations around Keplerian circular orbits are stable (i.e., $\omega_R^2 > 0$) if and only if the Keplerian angular momentum, $|L_K(r)|$, is an increasing function of the radius r of these orbits. This statement, of course, is just a special case of the well-known Rayleigh stability criterion.

The last deduction concerns the stability of the vertical epicyclic oscillations. If a non-spherical gravitational potential $\Phi(r, \theta)$ has a *positive* second derivative with respect to θ at the equatorial symmetry plane, the vertical oscillations are stable. Only if the second derivative is negative and sufficiently large may these oscillations be unstable.

Let us illustrate the general discussion given earlier in terms of a specific example. The gravitational potential expansion in terms of spherical harmonics (with $m = 0$ because of the axial symmetry) yields:

$$\Phi(r, \theta) = -\frac{GM}{r} - \frac{GQ P_2(\cos \theta)}{r^3} + \dots, \quad P_2(\cos \theta) \equiv \frac{1}{2}(3 \cos^2 \theta - 1). \quad (10)$$

The higher order terms are $\mathcal{O}(1/r^5)$ because of the equatorial plane symmetry. The quadrupole moment Q is *negative* for an oblate mass distribution, and because rotation typically produces a bulge at the equator, $Q \leq 0$ is the realistic case to consider. Assuming this, and neglecting higher multipoles, we deduce from (10) that:

$$\frac{1}{r^2} \left(\frac{\partial^2 \Phi}{\partial \theta^2} \right) = -\frac{3GQ}{r^5} \geq 0, \quad (11)$$

$$L_K^2 = GMr - \frac{3GQ}{2r} > 0, \quad \left(\frac{d \ln L_K^2}{d \ln r} \right) = \frac{2Mr^2 + 3Q}{2Mr^2 - 3Q} \quad (12)$$

We see from (11) that a negative quadrupole moment never destabilizes vertical oscillations. Equation (12) seems to indicate that a negative quadrupole moment destabilizes radial oscillations at small enough radii:⁴

$$r < r_Q \equiv \sqrt{\frac{3|Q|}{2M}}. \quad (13)$$

⁴If the quadrupole is positive, then for $r < r_Q$ no circular orbits are possible. This provides an example to a situation mentioned in footnote 3.

However, let us write $|Q| = qMR_*^2$, with R_* being the equatorial radius of the star and q being a dimensionless parameter. A body with fixed M and R_* will have the maximal quadrupole if the whole mass is placed in an infinitesimally thin ring of matter located at $r = R_*$, $\theta = \pi/2$. It is trivial to calculate the quadrupole moment in this case:

$$Q \equiv \int_0^M r^2 P_2(\cos \theta) dM \quad (14a)$$

$$= [r^2 P_2(\cos \theta)]_{r=R_*, \theta=\pi/2} \int_0^M dM = -\frac{1}{2} R_*^2 M. \quad (14b)$$

The aforementioned formula proves that the destabilization condition (13) is impossible to fulfill outside the star, because it implies $r < (\sqrt{3}/2)R_* < R_*$.

One concludes that according to Newton's theory, the quadrupole moment cannot destabilize circular orbits (in the equatorial plane) of particles orbiting a body. In the consciousness of many astrophysicists, this conclusion constitutes a "proof" that circular orbits around Newtonian bodies are *always* stable. Thus, the recent finding of Amsterdamski et al. (2002) that near very rapidly rotating Newtonian Maclaurin spheroids there *are* unstable orbits (with $\omega_R^2 < 0$) came as a surprise. Kluźniak et al. (2001) found that radial epicyclic oscillations are destabilized by *octupole* and higher moments in the harmonic expansion of the potentials.

3. Stationary, Axially Symmetric Spacetimes

We assume⁵ that spacetimes considered here are stationary and axially symmetric, which means that they admit two Killing vectors η^i and ξ^i , which obey:

$$\nabla_{(i} \eta_{k)} = 0, \quad \nabla_{(i} \xi_{k)} = 0, \quad \xi^k \nabla_k \eta_i = \eta^k \nabla_k \xi_i. \quad (15)$$

Here ∇_i denotes the covariant derivative, and round brackets denote symmetrization with respect to indices they embrace. All formulae that we use in this contribution are coordinate independent. However, for intuitive illustrations, it is convenient to introduce special coordinates that follow the time and axial symmetries and closely resemble the Newtonian spherical coordinates $[t, r, \phi, \theta]$ used in the previous section. These coordinates are such that:

$$\eta^i = \delta_t^i, \quad \xi^i = \delta_\phi^i, \quad (16)$$

δ_k^i being the Kronecker delta, and the metric takes the form:

$$ds^2 = (\eta\eta) dt^2 + 2(\eta\xi) dt d\phi + (\xi\xi) d\phi^2 + g_{rr} dr^2 + g_{\theta\theta} d\theta^2, \quad (17)$$

⁵We use everywhere the $(+ - - -)$ signature and, occasionally, $c = 1 = G$ units.

with a notation convention $x^i y^k g_{ik} \equiv (xy)$. The metric does not depend on t and ϕ , and we assume that it has an equatorial symmetry “plane,” $\theta = \pi/2$. The geodesic circular motion is characterized by the four-velocity, $u^i = dx^i/ds$ that obeys:

$$u^k \nabla_k u^i = 0, \quad u^i = A(\eta^i + \Omega \xi^i), \quad u^i u^k g_{ik} = 1. \quad (18)$$

Here Ω is the angular velocity, and $A^{-2} = (\eta\eta) + 2\Omega(\eta\xi) + \Omega^2(\xi\xi) > 0$. From (15) and (18) it follows that the energy defined by $\mathcal{E} = (\eta u) = u_t$, and the angular momentum defined by $\mathcal{L} = -(\xi u) = -u_\phi$, are constant of motion, because they obey:

$$u^k \nabla_k \mathcal{E} = 0, \quad u^k \nabla_k \mathcal{L} = 0. \quad (19)$$

Obviously, the specific angular momentum defined by $\ell = \mathcal{L}/\mathcal{E}$, is also a constant of motion. The angular velocity Ω and the specific angular momentum ℓ are related by:

$$\Omega = -\frac{(\eta\eta)\ell + (\eta\xi)}{(\eta\xi)\ell + (\xi\xi)}, \quad \ell = -\frac{(\xi\xi)\Omega + (\eta\xi)}{(\eta\xi)\Omega + (\eta\eta)}. \quad (20)$$

The standard definition of the effective potential is:

$$\mathcal{U}_{\text{eff}} = -\frac{1}{2} \ln(g^{tt} - 2\ell g^{t\phi} + \ell^2 g^{\phi\phi}). \quad (21)$$

This, together with the identity $1 = g^{ik} u_i u_k$ yields:

$$1 = \mathcal{E}^2 e^{-2\mathcal{U}_{\text{eff}}}, \quad \text{or} \quad 0 = \ln \mathcal{E} - \mathcal{U}_{\text{eff}}. \quad (22)$$

The three metric components that appear in the effective potential formula (21) may be invariantly defined in terms of the Killing vectors η^i and ξ^i , and expressed by three scalar functions: $\tilde{\Phi}$ being the gravitational potential, $\tilde{\omega}$ being the angular velocity of frame-dragging, and \tilde{r} being the circumferential axial radius:

$$g^{tt} = e^{-2\tilde{\Phi}} \equiv \frac{(\xi\xi)}{(\eta\eta)(\xi\xi) - (\eta\xi)^2}, \quad (23a)$$

$$g^{t\phi} = e^{-2\tilde{\Phi}} \tilde{\omega} \equiv \frac{-(\eta\xi)}{(\eta\eta)(\xi\xi) - (\eta\xi)^2}, \quad (23b)$$

$$-g^{\phi\phi} = e^{-2\tilde{\Phi}} \frac{1}{\tilde{r}^2} \equiv \frac{-(\eta\eta)}{(\eta\eta)(\xi\xi) - (\eta\xi)^2}. \quad (23c)$$

From these definitions one easily recovers the explicit expressions for the three scalars:

$$\tilde{\omega} = -\frac{(\eta\xi)}{(\xi\xi)}, \quad \tilde{r}^2 = -\frac{(\xi\xi)}{(\eta\eta)} > 0, \quad e^{2\tilde{\Phi}} = (\eta\eta) + \tilde{\omega}(\eta\xi) > 0, \quad (24)$$

which show that their Newtonian limits are, as they should be, $\tilde{\Phi} \rightarrow \Phi$, $\tilde{\omega} \rightarrow 0$, $\tilde{r} \rightarrow r \sin \theta$. From these limits, from (21), (23), (24), and from $\ell \rightarrow L$, $\ell^2/\tilde{r}^2 \ll 1$, one concludes that in the Newtonian limit, the relativistic effective potential goes to the Newtonian effective potential,

$$\mathcal{U}_{\text{eff}} = \tilde{\Phi} - \frac{1}{2} \ln \left(1 - 2\tilde{\omega}\ell - \frac{\ell^2}{\tilde{r}^2} \right) \rightarrow U_{\text{eff}}. \quad (25)$$

Because $\mathcal{E} \rightarrow 1 + E$, and $E \ll 1$, one sees that Eq. (22) has the correct Newtonian limit $\{0 = \ln \mathcal{E} - \mathcal{U}_{\text{eff}}\} \rightarrow \{E = U_{\text{eff}}\}$.

4. The Four Easy Pieces

We now derive simple and practical formulae for both radial and vertical orbital epicyclic frequencies in four lines of easy, fully transparent, algebra. The dot denotes derivative with respect to the proper time s , and x denotes either radial r or polar angle θ coordinate. We use the standard definitions for energy, specific angular momentum and effective potential, $\mathcal{E} = u_t$, $\ell = -u_\phi/u_t$, $\mathcal{U}_{\text{eff}} = -(1/2) \ln(g^{tt} - 2\ell g^{t\phi} + \ell^2 g^{\phi\phi})$. They have been recalled and explained in the previous section. As in the Newtonian derivation described in Section 2, we consider small oscillations with $\delta\ell \equiv 0$, $\delta\mathcal{E} \neq 0$, $\delta\dot{\mathcal{E}} = 0$, that occur either in r or in θ direction, $x(s) - x_0 = \delta x$, $u^x \equiv dx/ds = \delta\dot{x}$. The first r and θ derivatives of the effective potential are zero, which corresponds to an unperturbed circular orbit at the equatorial plane. The Taylor expansion starts from the second term, δx^2 , and also ends there in the lowest order. Our four easy pieces consist of:

$$1 = u_t u_t g^{tt} + 2u_t u_\phi g^{t\phi} + u_\phi u_\phi g^{\phi\phi} + u^x u^x g_{xx}, \quad (26a)$$

$$\mathcal{E}^{-2} = e^{-2\mathcal{U}_{\text{eff}}} + \frac{g_{xx}}{\mathcal{E}^2} (\delta\dot{x})^2, \quad (26b)$$

$$-2\frac{\delta\mathcal{E}}{\mathcal{E}_0^3} = \frac{1}{2} \left(\frac{\partial^2}{\partial x^2} e^{-2\mathcal{U}_{\text{eff}}} \right) (\delta x)^2 + \frac{g_{xx}}{\mathcal{E}_0^2} (\delta\dot{x})^2, \quad (26c)$$

$$-2\frac{\delta\dot{\mathcal{E}}}{\mathcal{E}_0^3} = (\delta\dot{x}) \left[\left(\frac{\partial^2}{\partial x^2} e^{-2\mathcal{U}_{\text{eff}}} \right) \delta x + 2\frac{g_{xx}}{\mathcal{E}_0^2} \delta\ddot{x} \right]. \quad (26d)$$

The last line, with $\delta\dot{\mathcal{E}} = 0$, $\delta\dot{x} \neq 0$, has obviously the form of a simple harmonic oscillator equation, $0 = \omega_x^2 \delta x + \delta\ddot{x}$ and, with the zeroth-order version of Eq. (26b),

this yields the final result:

$$\omega_x^2 = \left(\frac{\partial^2 \mathcal{U}_{\text{eff}}}{\partial X^2} \right), \quad (27)$$

with $dX^2 = -g_{xx}dx^2 > 0$ being the proper length in the x direction.

We see that exactly as in Newton's theory, both radial and vertical epicyclic frequencies (squared) are equal to second derivatives of the invariantly defined effective potential, with respect to the invariantly defined coordinates in radial and vertical directions.

5. Practical Calculations

We gave a simple derivation of general, physically clear, formulae (27) for the two epicyclic oscillation frequencies. In this section, we show that they are also simple to use in practical calculations, in particular when the metric is numerically constructed. Indeed, in order to solve second-order Einstein's field equations and to construct a spacetime numerically (e.g., outside a rotating neutron star), one must calculate the metric, and its first and second derivatives. Thus, one stores during the calculations:

$$g^{tt}, g^{t\phi}, g^{\phi\phi}, g_{rr}, g_{\theta\theta}, \quad (28a)$$

$$g_{[r]}^{tt}, g_{[r]}^{t\phi}, g_{[r]}^{\phi\phi}, g_{[\theta]}^{tt}, g_{[\theta]}^{t\phi}, g_{[\theta]}^{\phi\phi}, \quad (28b)$$

$$g_{[rr]}^{tt}, g_{[rr]}^{t\phi}, g_{[rr]}^{\phi\phi}, g_{[\theta\theta]}^{tt}, g_{[\theta\theta]}^{t\phi}, g_{[\theta\theta]}^{\phi\phi}, \quad (28c)$$

where derivatives of a quantity Y are indicated by indices in square brackets, $\partial Y / \partial x \equiv Y_{[x]}$, $\partial^2 Y / \partial x^2 \equiv Y_{[xx]}$. Let us now restrict to the equatorial symmetry plane, where all $\partial g^{ik} / \partial \theta \equiv g_{[\theta]}^{ik} = 0$. The condition for the circular orbit, $\partial \mathcal{U}_{\text{eff}} / \partial x = 0$ is thus trivially fulfilled for $x = \theta$, and for $x = r$ it gives the equation for the Keplerian angular momentum for circular orbits:

$$g_{[r]}^{tt} - 2\ell g_{[r]}^{t\phi} + \ell^2 g_{[r]}^{\phi\phi} = 0 \quad (29)$$

which has the solution:

$$\ell_K = \frac{g_{[r]}^{t\phi} \pm [(g_{[r]}^{t\phi})^2 - g_{[r]}^{\phi\phi} g_{[r]}^{tt}]^{1/2}}{g_{[r]}^{\phi\phi}}, \quad (30)$$

with the plus sign before the square bracket holding for $\ell_K > 0$ and the minus sign for $\ell_K < 0$.

We use Eq. (20), and the radial derivative of Eq. (26a) for circular orbits, to give two expressions for the orbital Keplerian angular velocity in terms of the first derivatives of the metric:

$$\Omega_K = -\frac{g_{tt}\ell_K + g_{t\phi}}{g_{t\phi}\ell_K + g_{\phi\phi}} = \frac{-(g_{t\phi})_{[r]} \pm [(g_{t\phi})_{[r]}^2 - (g_{\phi\phi})_{[r]}(g_{tt})_{[r]}]^{1/2}}{(g_{\phi\phi})_{[r]}}. \quad (31)$$

Our general result (27), explicitly expressed in terms of the metric and its first and second derivatives, takes the form:

$$\omega_r^2 = +\frac{1}{2g_{rr}} \frac{g_{[rr]}^{tt} - 2\ell_K g_{[rr]}^{t\phi} + \ell_K^2 g_{[rr]}^{\phi\phi}}{g^{tt} - 2\ell_K g^{t\phi} + \ell_K^2 g^{\phi\phi}}, \quad (32a)$$

$$\omega_\theta^2 = +\frac{1}{2g_{\theta\theta}} \frac{g_{[\theta\theta]}^{tt} - 2\ell_K g_{[\theta\theta]}^{t\phi} + \ell_K^2 g_{[\theta\theta]}^{\phi\phi}}{g^{tt} - 2\ell_K g^{t\phi} + \ell_K^2 g^{\phi\phi}}. \quad (32b)$$

These frequencies ω_r , ω_θ are measured with respect to the proper time of a moving observer. After dividing by the squared redshift factor $(u^t)^2 = e^{2U_{\text{eff}}} (g_{tt} + \Omega_K g_{t\phi})^{-2}$, one gets the ‘‘observed’’ frequencies at ‘‘infinity’’, i.e., those measured with respect to the time t of an astronomer at rest very far from the source:

$$\Omega_r^2 = \frac{(g_{tt} + \Omega_K g_{t\phi})^2}{2g_{rr}} [g_{[rr]}^{tt} - 2\ell_K g_{[rr]}^{t\phi} + \ell_K^2 g_{[rr]}^{\phi\phi}], \quad (33a)$$

$$\Omega_\theta^2 = \frac{(g_{tt} + \Omega_K g_{t\phi})^2}{2g_{\theta\theta}} [g_{[\theta\theta]}^{tt} - 2\ell_K g_{[\theta\theta]}^{t\phi} + \ell_K^2 g_{[\theta\theta]}^{\phi\phi}]. \quad (33b)$$

For an application of these formulae to realistic models of rotating neutron stars, see e.g., Kluźniak et al. (2004).

By expanding $(g_{[r]}^{tt} - 2\ell_K g_{[r]}^{t\phi} + \ell_K^2 g_{[r]}^{\phi\phi})_{[r]} = 0$, one finds:

$$\Omega_r^2 = \pm \mathcal{A} \left(\frac{d\ell_K}{dr} \right) [(g_{[r]}^{t\phi})^2 - g_{[r]}^{\phi\phi} g_{[r]}^{tt}]^{1/2}, \quad \mathcal{A} \equiv \frac{(g_{tt} + \Omega_K g_{t\phi})^2}{(-g_{rr})} > 0. \quad (34)$$

Because by construction (30), $\pm \ell_K [(g_{[r]}^{t\phi})^2 - g_{[r]}^{\phi\phi} g_{[r]}^{tt}]^{1/2} > 0$, one concludes that $\Omega_r^2 > 0$ if and only if $d|\ell_K|/dr > 0$.

Thus, the relativistic Rayleigh criterion for circular Keplerian orbits is the same as the Newtonian criterion [cf. Eq. (8)]: for stability, the absolute value of specific angular momentum should be an increasing function of the orbital radius. And, just as in Newtonian theory, the epicyclic frequencies can be derived from the second derivatives of an effective potential [see Eq. (27)].

Acknowledgements

We thank Nordita for generous hospitality and support. The calculations reported here have been done, and the article written, during our several visits to Nordita, that Nordita supported in full. We also thank Dr. Nikolaos Stergioulas for implementing our formulae numerically.

References

- Abramowicz, M.A. and Kluźniak, W.: 2000, unpublished research notes.
- Abramowicz, M.A., Almergren, G.J.E., Kluźniak, W. and Thampan, A.V.: 2003, gr-qc/0312070.
- Amsterdamski, P., Bulik, T., Gondek-Rosińska, D. and Kluźniak, W.: 2002, *A&A* **381**, L21.
- Kluźniak, W., Abramowicz, M.A., Kato, S., Lee, W.H. and Stergioulas, N.: 2004, *ApJ* **603**, L89.
- Kluźniak, W., Bulik, T. and Gondek-Rosińska, D.: 2001, in: B. Battrick (ed.), *Exploring the Gamma-Ray Universe. Proceedings of the Fourth INTEGRAL Workshop*, Alicante, Spain, 4–8 September 2000, A. Gimenez, V. Reglero and C. Winkler (scientific eds.), ESA SP-459, Noordwijk: ESA Publications Division, pp. 301–304.
- Marković, D.: 2000, astro-ph/0009450.
- Nowak, M., Lehr, D.: 1999, in: M.A. Abramowicz, G. Björnsson and J.E. Pringle (eds.), *Theory of Black Hole Accretion Disks*, Cambridge: Cambridge University Press.
- Okazaki, A.T., Kato, S. and Fukue, J.: 1987, *Publ. Astron. Soc. Jpn.* **39**, 457.
- Perez, C.A., Silbergleit, A.S., Wagoner, R.V. and Lehr, D.E.: 1997, *ApJ* **476**, 589.
- Wald, R.W.: 1984, *General Relativity*, Chicago: University of Chicago Press.

X-RAY PERIODICITY IN AGN

KAREN M. LEIGHLY

The University of Oklahoma; E-mail: leighly@nhn.ou.edu

(Received 13 December 2004; accepted 1 June 2005)

Abstract. Significant (marginal) detections of periodic signals have been recently reported in 3 (4) Active Galactic Nuclei. Three of the detections were obtained from long EUVE light curves of moderate-luminosity Seyfert galaxies; the fourth was discovered in Chandra data from the low-luminosity Seyfert 1 galaxy NGC 4395. When compared with Cyg X-1, I find that the period is related to the luminosity as $P \propto L^{2/3}$ rather than the expected one-to-one relationship. This result might be explained if the QPO is associated with the inner edge of the optically thick accretion disk, and the inner-edge radius depends on the source luminosity (or black hole mass). A discussion of uncertainties in the period detection methodology is also discussed.

Keywords: X-ray variability, NGC 4395, Ton S180, RX J0437.1–4711, 1H 0419–577

1. Introduction

Quasiperiodic oscillations are a characteristic feature of solar-mass black hole X-ray variability, especially when the objects are in the very high (or transition) state. Active Galactic Nuclei are similar to stellar-mass black holes in that they are both powered by accretion onto a central black hole. Therefore, it seems plausible, or at least possible, that quasiperiodic oscillations should be observed in active galaxies as well.

The search for periodic signals in AGN light curves has a long and checkered history, however. A number of claims of periodicity have been put forward, only to later be proven faulty. The problems fall into three categories. The first and most common problem involves claims in which the confidence level of the detection is overestimated. An example is the recent claim of a periodic signal with frequency of 2.4×10^{-4} Hz in *XMM-Newton* data from Mrk 766 (Boller et al., 2001). It was later shown by Benlloch et al. (2001) that the simulated light curves used to establish the significance of the detection were not properly randomized. The second problem involves detector artifacts. An example of this problem was the apparent discovery of a decreasing period in *RXTE* data from IRAS 18325–5926 that was eventually demonstrated to be due to detector background (Fabian et al., 1998a,b). A final problem that this author has personal experience with is that of source confusion. *EXOSAT* and *Ginga* data revealed a 12,000 s periodicity in the Seyfert 1 galaxy NGC 6814 (e.g., Leighly et al., 1994). Imaging observations later showed that

the signal was dominated by a cataclysmic variable star only 40 arcminutes away (Madejski et al., 1993).

These misadventures do not, however, preclude the possibility that periodicity or quasiperiodicity could be present in AGN light curves. It may be that we simply are not looking in the right place, or that we don't have the right data. In this contribution, I discuss the significant (marginal) detection of periodicity X-ray data from three (four) Seyfert 1 galaxies.

2. Methodology

A standard Monte-Carlo procedure was used to detect periodicity in the AGN light curves, with small differences between the procedure used in Halpern et al. (2003), which discusses analysis and results of the EUVE light curves, and in Moran et al., 2005, which discusses the Chandra result. First, the slope and normalization of the assumed underlying power-law continuum were determined. In Halpern et al. (2003), 100 long light curves were generated, using the method of Timmer and König (1995), for each point on a grid of trial power-law slopes and normalizations. These long light curves were resampled and rebinned in the same way as the real light curves, appropriate Poisson noise was added, and the periodogram was computed and rebinned. The average and standard deviation periodogram from the situations at each point in the grid was then compared with that of the real data using Chi square. The minimum Chi square was assumed to locate the best-fitting values of the slope and normalization of the continuum. The procedure used for the analysis of the Chandra data from NGC 4395 differed in one respect. Light curves were produced for a range of slopes, but only one normalization. Following Vaughan et al. (2003), the result was scaled to different normalizations, and appropriate Poisson noise computed and added.

Knowing the shape of the power spectrum continuum, 10,000 suitably rebinned and sampled light curves were generated using the method of Timmer and König (1995). The power spectra from these were used to assess the local confidence level of the detection, first by counting the number of incidents in which the power of the simulations exceeded the power of the real data, and second by comparing with a χ^2 distribution (e.g., Leahy et al., 1983). As discussed in Benlloch et al. (2001), one must account for the number of independent frequencies searched to obtain an estimate of the global significance by multiplying the single-trial confidence by that number.

3. Results and Discussion

Halpern et al. (2003) present an atlas of EUVE light curves from Seyfert galaxies. Three objects had exceptionally long light curves: 33 days for Ton S180, 26 days

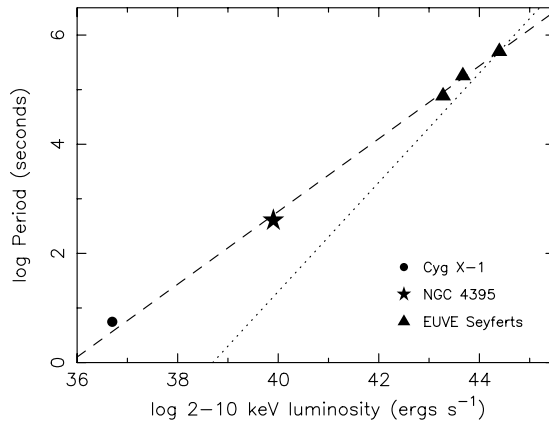


Figure 1. Log of the period as a function of the log of the 2–10 keV luminosity for 4 AGN and Cyg X-1. The dotted and dashed lines have slopes of 1 and 2/3, respectively.

for 1H 0419–577, and 20 days for RX J0437.1–4711. Periodicity analysis as outlined above revealed evidence for a 2.08-day signal in Ton S180 with global confidence level of 98%, a 0.908-day signal in RX J0437.4–4711, and a 5.8-day signal in 1H 0419–577 with a global confidence level of only 64%. Interestingly, the periodic signal in RX J0437.1–4711 appears to be transient; periodicity analysis of the first and second halves of the light curve show no detectable signal, and a signal at 0.89-day with global confidence of 96%, respectively.

Moran et al. (2005) present analysis of the Chandra data from the low-luminosity Seyfert 1 galaxy NGC 4395. A period of 396 s was found in the light curve with estimated global significance of 97.6%. In this case, we again found evidence that the signal is transient; no signal appears in the first half of the observation, but in the second half a strong signal appears with estimated global confidence of 99.95% at a period of 396 s.

It is interesting to note that the presence of a QPO does not appear to depend on Seyfert type. Ton S180 is a narrow-line Seyfert 1 galaxy, 1H 0419–577 is a Seyfert 1.5, and both NGC 4395 and RX J0437.1–4711 are both classified as ordinary Seyfert 1 galaxies.

As noted in Halpern et al. (2003), there is a correspondence between the X-ray luminosity and the period such that more luminous objects have longer periods. This correspondence is expected if the luminosity and characteristic time scales both scale with the black hole mass. Things get interesting when I compare the period and luminosity of NGC 4395 and Cyg X-1 in the hard state, as shown in Figure 1. For Cyg X-1, we use the pre-*RXTE* period of 5.6 s (e.g., Tanaka, 1995), but note that using the *RXTE* values of 0.5–1 s (e.g., Gilfanov et al., 2000) would not change this figure much because it is logarithmic. Remarkably, the linear relationship between the log of the period and luminosity is maintained over the

eight decades of luminosity between Cyg X-1 and 1H 0419–577. However, the slope of the relationship is $2/3$, rather than 1, as would be expected for fixed L/L_{Edd} and emission R/R_{S} . One possibility is that the QPO is associated with the truncation radius of the optically thick, geometrically thin accretion disk, and the dependence on luminosity is a secondary effect, in that the Seyferts are radiating closer to L/L_{Edd} than does Cyg X-1 in the hard state, in which $L/L_{\text{Edd}} = 0.02$. If that were the case, and if $R = 3R_{\text{S}}$ for Ton S180, we infer that $R = 23R_{\text{S}}$ for NGC 4395, and $R = 95R_{\text{S}}$ for Cyg X-1. Interestingly, $R \approx 100R_{\text{G}}$ is approximately the inferred radius of the inner edge of the optically thick accretion disk when Cyg X-1 is in the hard state (e.g., Gilfanov et al., 2000).

4. Caveats and Cautions

What do these results say about the incidence of periodicity in X-ray light curves from AGN? There are thousands of X-ray light curves that have not been tested for periodicity, so one might argue that these are isolated incidents and not representative. However, as discussed in Halpern et al. (2003), if the characteristic period of Seyfert 1 galaxies is 1 day or longer, most of those thousands of light curves will be not suitable for periodicity searches. The EUVE light curves were exceptionally long, and thus the fact that some evidence for periodicity was found in the three longest ones suggests perhaps that periodicity is common in AGN. Then what about NGC 4395? It is notable for being the lowest luminosity Seyfert 1, with a 2–10 keV luminosity of only $8 \times 10^{39} \text{ erg s}^{-1}$ (Moran et al., 2005), much lower than a typical Seyfert 1 galaxy. The fact that we observe the period to scale with the luminosity in the EUVE sample suggests that NGC 4395 should have an exceptionally short period; therefore, since it is unique, luminosity-wise, it makes sense that it is unique, period-wise.

On the other hand, we observe that the periodicity appears to be transient in both NGC 4395 and RX J0437.1–4711 in that in both cases it is detected only in the second halves of the light curves. This suggests that even if periodicity were common in AGN, it may be difficult to observe even in much better data than currently available, simply because too few cycles will be present to detect.

It has been suggested by Vaughan (2005) that the global confidence of the detections claimed in Halpern et al. (2003) and in Moran et al. (2005) have been overestimated for two reasons. The first reason is that we oversample the periodogram; this was done to improve the sensitivity to frequencies other than the usual Fourier frequencies. This is potentially a problem because oversampling the periodogram will produce more higher peaks, and thus comparison of the real data, with spurious high peaks, with the simulated data will result in overly high single-trial probabilities, or false detections. We investigate this problem in Figure 2, for the NGC 4395 data. We find almost the same values for the global significance for the total light curve, possibly because the peak for the oversampled power spectrum

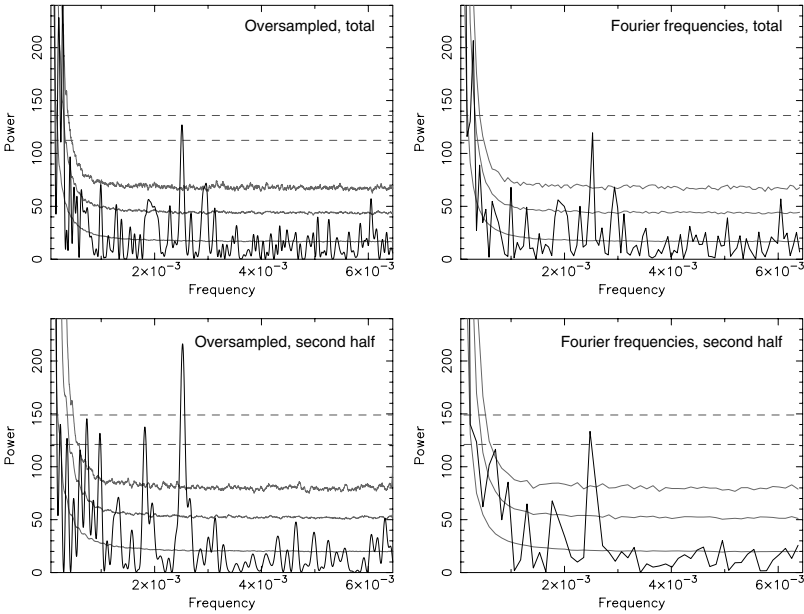


Figure 2. Power spectra for the NGC 4395 Chandra observation (Moran et al., 2005). In each plot, the lower three light-grey lines show the 68, 95 and 99% single-trial significance levels from the simulated data, while the upper two dark-grey dashed lines show the 95 and 99% global significance levels computed assuming Poisson noise continuum.

is only 20% from one of the Fourier frequencies. For the second half of the light curve, where the periodicity appears stronger, the significance of the oversampled peak is much higher than for the Fourier peak. Perhaps this is because that peak lies almost exactly in between Fourier frequencies.

The second criticism raised by Vaughan (2005) is that the standard analysis does not take into account the uncertainty in the shape of the underlying continuum. That is, we assume that once we measure the underlying power-law spectral continuum, it is fixed, whereas in reality there is uncertainty in the slope, normalization, and even the Poisson noise level. This criticism appears to be well founded, and will no doubt lower the global confidence level of the periodicity detections. Quantifying the new global confidence levels is somewhat difficult, though; there is no direct way to do this.

Acknowledgements

KML gratefully acknowledges helpful discussions with Jules Halpern and Andrzej Zdziarski, thanks the organizers for the opportunity to speak on this topic, and acknowledges funding from NASA ADP grant NAG5-13110.

References

- Benlloch, S., Wilms, J., Edelson, R., Yaqoob, T. and Staubert, R.: 2001, Quasi-periodic oscillation in Seyfert galaxies: Significance levels. The case of Markarian 766. *ApJ* **562**, 121.
- Boller, Th., Keil, R., Trümper, J., O'Brien, P.T., Reeves, J. and Page, M.: 2001, Detection of an X-ray periodicity in the narrow-line Seyfert 1 galaxy Mrk 766 with XMM–Newton. *A&A* **365**, L146.
- Fabian, A.C., Lee, J.C., Iwasawa, K., Jahoda, K., Brandt, W.N. and Reynolds, C.S.: 1998b, IRAS 18325–5926. *IAUC* **6871**, 3.
- Fabian, A.C., Lee, J.C., Iwasawa, K., Brandt, W.N. and Reynolds, C.S.: 1998a, IRAS 18325–5926. *IAUC* **6835**, 3.
- Gilfanov, M., Churazov, E. and Revnivtsev, M.: 2000, Frequency-resolved spectroscopy of Cyg X-1: Fast variability of the reflected emission in the soft state. *MNRAS* **316**, 923.
- Halpern, J.P., Leighly, K.M. and Marshall, H.L.: 2003, An extreme ultraviolet explorer atlas of seyfert galaxy light curves: Search for periodicity. *ApJ* **585**, 665.
- Leahy, D.A., Darbro, W., Elsner, R.F., Weisskopf, M.C., Kahn, S., Sutherland, P.G. and Grindlay, J.: 1983, On searches for pulsed emission with application to four globular cluster X-ray sources—NGC 1851, 6441, 6624, and 6712. *ApJ* **266**, 160.
- Leighly, K., Kunieda, H., Tsusaka, Y., Awaki, H. and Tsuruta, S.: 1994, Evidence for X-ray flux and spectral modulation by absorption in NGC 6814. 1: The nature of the most rapid variability. *ApJ* **421**, 69.
- Madejski, G., Done, C., Turner, T.J., Mushotzky, R.F., Serlemitsos, P., Fiore, F., Sikora, M. and Begelman, M.: 1993, Solving the mystery of the periodicity in the Seyfert galaxy NGC 6814. *Nature* **365**, 626.
- Moran, E., Eracleous, C., Leighly, M., Leighly, K.M., Chartas, G., Filippenko, A.V., Ho, L.C. and Blanco, P.R.: 2005, Extreme X-ray behavior and quasi-periodic oscillations in the low-luminosity active nucleus of NGC 4395. *ApJ*, submitted.
- Tanaka, Y.: 1995, Physics of Neutron Stars and Black Holes. In *X-ray Binaries*, Cambridge University Press, Cambridge.
- Timmer, J. and König, M.: 1995, On Generating Power Law Noise. *A&A* **300**, 707.
- Vaughan, S.: 2005, A simple test for periodic signals in red noise. *A&A* **431**, 391.
- Vaughan, S., Fabian, A.C. and Nandra, K.: 2003, X-ray continuum variability of MCG–6-30-15. *MNRAS* **339**, 1237.

RESONANT OSCILLATIONS OF ACCRETION FLOW AND KHZ QPOS*

W. KLUŻNIAK^{1,2} and M.A. ABRAMOWICZ^{3,4}

¹*Copernicus Astronomical Centre, Bartycka 18, PL-00-716 Warszawa, Poland*

²*Institute of Astronomy, Zielona Góra University, Zielona Góra, Poland;*

E-mail: wlodek@camk.edu.pl

³*Department of Astrophysics, Göteborg University, Göteborg, Sweden*

⁴*Department of Theoretical Physics, Chalmers University, S-412-96 Göteborg, Sweden;*

E-mail: marek@fy.chalmers.se

(Received 29 November 2004; accepted 1 June 2005)

Abstract. High-frequency quasi-periodic variations (HF QPOs) in the X-ray light curves of black hole X-ray novae can be understood as oscillations of the accretion disk in a nonlinear 3:2 resonance. An $m = 0$ vertical oscillation near a black hole modulates the X-ray emission through gravitational lensing (light-bending) at the source. Certain oscillations of the accretion disk will also modulate the mass accretion rate, and in neutron-star systems this would lead to nearly periodic variations in brightness of the luminous boundary layer on the stellar surface – the amplitude of the neutron-star HF QPOs would be thus increased relative to the black hole systems.

Keywords: black holes, neutron stars, X-rays, accretion

1. Introduction

A complete theory of the twin high-frequency quasi-periodic variations (HF QPOs) of the X-ray light curve observed in many low-mass X-ray binary (LMXB) systems containing neutron stars or black holes must provide answers to four questions:

1. What is the origin of the observed (\sim kHz) frequencies?
2. What is the physical excitation mechanism?
3. What limits the coherence of the phenomenon?
4. What is the mechanism of X-ray modulation?

One theory of a similar phenomenon in accreting white dwarfs discussed (1) the orbital motion of inhomogeneities in the accretion disk, or “blobs,” (2) their turbulent formation, (3) the destruction of blobs by shear, and (4) the modulation of luminosity by the orbiting blobs; see (Pringle, 1981), for a review. No model of the kHz QPOs in neutron stars and black holes has as yet provided a comparably satisfactory answer to all four questions. Disko-seismology (Wagoner, 1999; Kato,

*The “kHz QPOs” in black holes are in the hecto-Hz range.



2001) came close for black holes, but failed to predict the observed 3:2 ratio of frequencies. For a review of kHz QPOs see van der Klis (2004).

Here, we discuss the nonlinear resonant oscillation model of HF QPOs, where a quantitative answer can already be provided to questions (1) and (4), but only qualitative results are as yet available in addressing questions (2) and (3). A poor understanding of the physics of accretion disks hampers progress.

In a nutshell, we think that one observes the frequencies of two modes of oscillation of accretion disk, that the two modes are in internal resonance in black hole systems, and may be excited by periodic perturbations (at the spin frequency) in neutron-star systems. In this contribution, we focus on the modulation mechanisms.

2. Oscillations of Accretion Disks and Resonance

Much detailed work has been carried out on the theory of disk oscillations in general relativity, and in particular of modes which are trapped in relativistic disks, but not in Newtonian gravity. This was possible after the significance of the presence of a maximum in the radial epicyclic frequency had been appreciated (Okazaki et al., 1987). Several modes have been identified as promising in the context of QPOs, in terms of their (fixed) frequency, coherence, and potential for modulating the light curve (non-axisymmetry, $m \neq 0$). For black holes, the frequency of each mode of a thin disk is a function of the black hole mass and spin. The frequency ratio of two modes is a function of the spin alone. For a review see Wagoner (1999), Nowak and Lehr (1999), or Kato (2001).

When twin HF QPOs were discovered (Strohmayer, 2001), we noticed that their frequencies were in the ratio of 3:2 (Abramowicz and Kluźniak, 2001). Four such systems are now known (McClintock and Remillard, 2003). This ratio is surprising in the context of linear disko-seismology, as it would imply a definite, and identical, spin of the four black holes. However, such a ratio of small integers had been anticipated on the theory that the twin kHz QPOs were a manifestation of a nonlinear resonance (Kluźniak and Abramowicz, 2000, 2001). This gave an impulse to further studies of the resonance model of QPOs. The 3:2 ratio (as opposed to, e.g., 2:1) can be understood as internal resonance between two disk modes of eigenfrequencies close to the vertical and radial epicyclic frequency (Kluźniak and Abramowicz, 2002, 2003, 2004; Abramowicz and Kluźniak, 2004).

3. Neutron-Star kHz QPOs

If the two modes are slightly off-resonance (by a prescribed amount), the ratio of the two frequencies may vary with the QPO frequency, as observed in Sco X-1 (Abramowicz et al., 2003a,b; Rebusco, 2004). This condition may hold in neutron

stars, where the disk may be excited “externally” by the spinning magnetic dipole in its center. When this external disturbance is sufficiently strong, the separation of the two QPOs may be equal to either the spin frequency or half that value (Kluźniak et al., 2004; Lee et al., 2004).

Some aspects of the rich phenomenology of QPOs in general may also be understood in terms of a nonlinear coupling of two high-frequency modes in resonance. For example, a low-frequency modulation of the high-frequency oscillations is quite natural (Horák et al., 2004).

4. Mechanisms of Modulation of the Light Curve

The simplest vertical oscillation mode of a fluid body in orbit, such as a torus of modest radial extent, is a quasi-rigid, axisymmetric, up and down harmonic displacement (up and down with respect to the equatorial plane). One puzzle was how such a volume-preserving, $m = 0$ mode could modulate the luminosity. Two solutions have been found.

One is light bending (Figure 1). The rays of radiation from a disk or torus around a black hole propagate along trajectories which depend on the position of the torus. As the torus moves with respect to the black hole, this gravitational lensing “at the source” leads to variations in the flux detected by a distant observer (Bursa et al., 2004).

The other, relevant to accreting neutron stars, is modulation of the mass accretion rate. It has been suggested that in LMXBs, where no evidence of coherent pulsation was present, the magnetic dipole was sufficiently low for the disk to extend to the marginally stable orbit (ISCO), and for the freely-falling matter within that orbit to heat up the equatorial accretion belt (Kluźniak and Wagoner, 1985; Sunyaev and Shakura, 1986; Kluźniak et al., 1990; Kluźniak and Wilson, 1991).

Because of pressure support, thin accretion disks have their inner edges not exactly at ISCO, but (slightly) closer to the central compact object (Abramowicz et al., 1978). At the inner edge location, one of the equipotential surfaces, called the Roche lobe, self-crosses, forming a potential nozzle, as shown in Figure 2. If the disk overflows its Roche lobe, a dynamical mass loss must occur through the nozzle, rather like in the familiar case of the Roche lobe overflow in close binaries. The mass loss stabilizes the inner part of the disk against local thermal and viscous instabilities (Abramowicz, 1981), as well as against the global Papaloizou and Pringle (1984) dynamical instability (Blaes, 1985).

In this context, Paczyński (1987) pointed out that if the mass accretion rate were slightly modulated close to the nozzle, this would hardly affect the luminosity of the accretion disk itself, but would lead to strong modulation of radiation coming from the accretion belt on the surface of the neutron star. Note that this modulation mechanism can only work if the neutron star radius is smaller than the ISCO

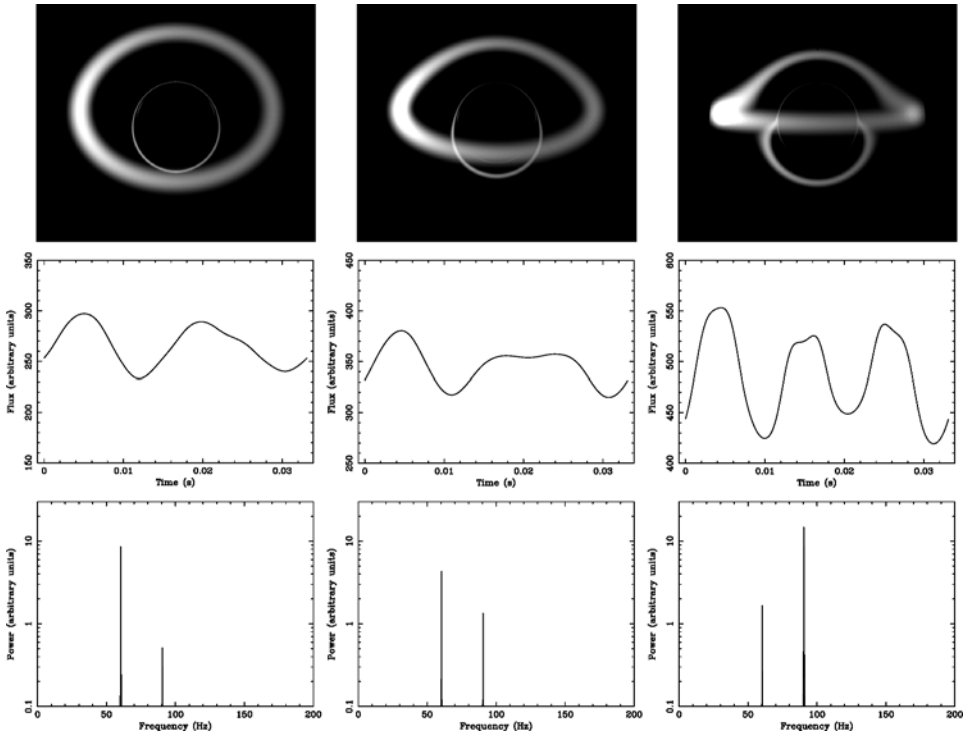


Figure 1. Modulation by light bending (reproduced from Bursa et al., 2004). A snapshot of an oscillating torus, the light curve, and the power spectrum for three different disk inclinations (45° , 65° , 85°).

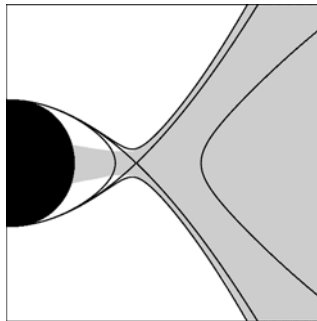


Figure 2. Potential nozzle and the Roche lobe overflow at the inner edge of an accretion disk. Equipotential surfaces are shown by heavy lines, the accretion disks by a shadow. The location where one of the equipotential surfaces crosses itself is always within the innermost circular stable orbit (ISCO). An accreting black hole is shown in the figure, a neutron star would be correspondingly larger.

radius, which means that the mass of the neutron star cannot be too small, and the equation of state of matter at supranuclear densities cannot be too stiff (Kluźniak and Wagoner, 1985).

The accretion rate induced by the mass loss is a very sensitive function of conditions at the nozzle, in particular of the potential difference through the nozzle, ΔW . For a polytropic equation of state, $P = K \rho^{1+1/n}$ it equals (Kozłowski et al., 1978; Abramowicz, 1985),

$$\dot{M} = A(n)K^{-n} \frac{R_{\text{in}}}{\Omega_K(R_{\text{in}})} |\Delta W|^{n+1}, \quad (1)$$

with an analytic expression for $A(n)$ explicitly known in terms of the Euler gamma function, $\Gamma(n)$. This simple analytic formula is in excellent agreement with state-of-the-art, time-dependent, 3-D numerical simulations of accretion flows (Igumenshchev et al., 2004).

Using (1), we find that if the (axisymmetric) nozzle moves up and down (i.e., parallel to the disk axis) the resulting relative variation in the mass accretion rate is given by the simple formula:

$$\Delta \dot{M} / \dot{M} \propto -(\Delta z / H)^2, \quad (2)$$

where Δz is the amplitude of motion, and H is a characteristic inner-disk height. A similar relation also holds, under certain conditions, if it is the disk that undergoes vertical oscillations, while the nozzle itself does not move relative to the equatorial plane. Thus, in a neutron star, an axisymmetric vertical oscillation excited in the inner accretion flow may lead to a large, periodic, luminosity variation.

Acknowledgements

It is a pleasure to acknowledge the generous support and hospitality of Nordita where this contribution has been written. Research supported in part by KBN grant 2P03D01424.

References

- Abramowicz, M.A.: 1981, *Nature* **294**, 235.
 Abramowicz, M.A.: 1985, *Publ. Astron. Soc. Jpn.* **37**, 727.
 Abramowicz, M.A., Bulik, T., Bursa, M. and Kluźniak, E.: 2003a, *Astron. Astrophys. Lett.* **404**, L21.
 Abramowicz, M.A., Jaroszyński, M. and Sikora, M.: 1978, *A&A* **63**, 221.
 Abramowicz, M.A., Karas, V., Kluźniak, W., Lee, W. and Rebusco, P.: 2003b, *Publ. Astron. Soc. Jpn.* **55**, 467.
 Abramowicz, M.A. and Kluźniak, W.: 2001, *Astron. Astrophys. Lett.* **374**, L19.

- Abramowicz, M.A. and Kluźniak, W.: 2004, in: P. Kaaret, F.K. Lamb and J.H. Swank (eds.), *X-ray Timing 2003: Rossi and Beyond*, AIP Conference Proceedings, Vol. 714, American Institute of Physics, Melville, NY, pp. 21–28.
- Blaes, O.M.: 1985, *MNRAS* **216**, 553.
- Bursa, M., Abramowicz, M.A., Karas, V. and Kluźniak, W.: 2004, *Astrophys. J. Lett.* **617**, L45.
- Horák, J., Abramowicz, M.A., Karas, V. and Kluźniak, W.: 2004, *Publ. Astron. Soc. Jpn.* **56**, 819.
- Igumenshchev, I.V., Chen, X. and Abramowicz, M.A.: 2004, *MNRAS* **278**, 236.
- Kato, S.: 2001, *Publ. Astron. Soc. Jpn.* **53**, 1.
- Kluźniak, W. and Abramowicz, M.A.: 2000, *Phys. Rev. Lett.*, submitted for publication, astro-ph/0105057.
- Kluźniak, W. and Abramowicz, M.A.: 2001, *Acta Phys. Polon. B* **B32**, 3605.
- Kluźniak, W. and Abramowicz, M.A.: 2002, *A&A*, submitted for publication, astro-ph/0203314.
- Kluźniak, W., Abramowicz, M.A.: 2003, in: *12th Workshop on General Gravity and Gravitation*, Tokyo University Press, Tokyo, pp. 69–80.
- Kluźniak, W. and Abramowicz, M.A.: 2004, in: P. Kaaret, F.K. Lamb and J.H. Swank (eds.), *X-ray Timing 2003: Rossi and Beyond*, AIP Conference Proceedings, vol. 714, American Institute of Physics, Melville, NY, pp. 379–382.
- Kluźniak, W., Abramowicz, M.A., Kato, S., Lee, W.H. and Stergioulas, N.: 2004, *Astrophys. J. Lett.* **603**, L89.
- Kluźniak, W., Michelson, P. and Wagoner R.V.: 1990 *ApJ* **358**, 538.
- Kluźniak, W. and Wagoner R.V.: 1985, *ApJ* **297**, 548.
- Kluźniak, W. and Wilson, J.W.: 1991, *Astrophys. J. Lett.* **372**, L87.
- Kozłowski, M., Abramowicz, M.A. and Jaroszyński, M.: 1978, *A&A* **63**, 209.
- Lee, W.H., Abramowicz, M.A. and Kluźniak, W.: 2004, *Astrophys. J. Lett.* **603**, L93.
- McClintock J.E. and Remillard R.A.: 2003, astro-ph/0306213.
- Nowak, M. and Lehr, D.: 1999, in: M.A. Abramowicz, G. Björnsson and J.E. Pringle (eds.), *Theory of Black Hole Accretion Disks*, Cambridge University Press, Cambridge.
- Okazaki, A.T., Kato, S. and Fukue, J.: 1987, *Publ. Astron. Soc. Jpn.* **39**, 457.
- Paczyński, B.: 1987, *Nature* **327**, 303.
- Papaloizou, J.C.B. and Pringle, J.E.: 1984, *MNRAS* **208**, 721.
- Pringle, J.E.: 1981, *Ann. Rev. Astron. Astrophys.* **19**, 137.
- Rebusco, P.: 2004, *Publ. Astron. Soc. Jpn.* **56**, 553.
- Syunyaev, R.A. and Shakura, N.I.: 1986 *Sov. Astron. Lett.* **12**, 117.
- Strohmayer, T.E.: 2001, *Astrophys. J. Lett.* **552**, L49.
- van der Klis, M.: 2004, in: W.H.G. Lewin and M. van der Klis (eds.), *Compact Stellar X-ray Sources*, Cambridge University Press, Cambridge, in press, astro-ph/0410551.
- Wagoner, R.W.: 1999, *Phys. Rep.* **311**, 259.

COMPARING BLACK HOLE AND NEUTRON STAR VARIABILITY

M. VAN DER KLIS

Astronomical Institute "Anton Pannekoek", University of Amsterdam, Kruislaan 403, 1098 SJ, Amsterdam, The Netherlands; E-mail michiel@science.uva.nl

(Received 1 February 2005; accepted 1 June 2005)

Abstract. There are remarkable similarities between the rapid X-ray variability of low-magnetic field neutron stars in low mass X-ray binaries, and that of black holes. In particular at frequencies < 100 Hz, their power spectra can be strikingly similar. The highest frequency phenomena (kilohertz QPOs, black hole high-frequency QPOs and neutron star hectohertz QPOs) are the ones that show most differences, perhaps because they originate closest to the compact object. Most variability components vary in frequency in correlation with one another, and the correlations once again are very similar across neutron stars and black holes – some extend even to white dwarfs. Although this does not strictly require that all phenomena whose frequencies are involved are caused by the same physics in all three source types, this does indicate that basic properties of the accretion flow which are the same in all three source types play an important role in generating at least some of the frequencies.

Keywords: X-rays, neutron stars, black holes, rapid variability, QPO

1. Introduction

A neutron star is expected to be only about three times as large as its Schwarzschild radius, so the process of accretion onto low-magnetic field neutron stars and black holes can be expected to show many similarities. Since at least the time of the *Ginga* satellite it has become clear that in low-mass X-ray binaries such similarities between neutron stars and black holes, as diagnosed by similarities in the rapid X-ray variability, are indeed common (e.g., van der Klis, 1994). As the rapid variability originates in the inner regions of the accretion disk, where strong field gravity effects are expected to dominate the dynamics, the constraints put on the nature of the variability by the fact that it occurs in both source types are of particular interest. If a physical phenomenon occurs in both neutron stars *and* black holes then we may conclude that it does not require any property that is unique to either neutron stars *or* black holes. This means that the presence of an event horizon, a solid surface, a non-spin-aligned magnetic field and near-extremal Kerr frame dragging are all excluded as ingredients in the explanation of the phenomenon.

In this talk, I examine these similarities in rapid X-ray variability and their implications for the phenomena involved and consider the possibility of unique variability phenomena, which, by the same reasoning, would be suggestive of models that *do* require such a unique neutron star or black hole property.



2. High-Frequency Phenomena

The highest-frequency variability phenomena seen in low-mass X-ray binaries are the 500–1300 Hz neutron star kilohertz QPOs, the 100–450 Hz black hole high-frequency QPOs and the 100–200 Hz neutron star hectohertz QPOs (Figure 1; see van der Klis, 2000, in press; McClintock and Remillard, in press, for reviews). These high-frequency QPOs are the variability components that seem to differ most between neutron stars and black holes.

The kilohertz quasi-periodic oscillations (kHz QPOs) in neutron stars are the fastest phenomenon seen in X-ray binaries. They were discovered with RXTE in 1996 and occur in a wide variety of low-magnetic-field neutron star systems. The phenomenon has been seen in more than 20 systems and does not occur in black hole candidates – it is sufficiently characteristic to be considered a neutron star signature. Two QPO peaks (the ‘twin peaks’) usually occur in the power spectrum of the X-ray flux variations. They move up and down in frequency together in correlation with source state and often, luminosity. The higher-frequency one of these two peaks is called the ‘upper kHz QPO’, with a frequency ν_u , the lower-frequency one the ‘lower kHz QPO’ with frequency ν_ℓ .

The typically 300-Hz peak separation $\Delta\nu \equiv \nu_u - \nu_\ell$ usually decreases by a few tens of hertz when both peaks move up by hundreds of hertz (Figure 2a). The spin frequency ν_{spin} of the neutron star and $\Delta\nu$ are commensurate (Figure 2b): $\Delta\nu$ is approximately equal to ν_{spin} (in current data, when $\nu_{\text{spin}} < 400$ Hz) or approximately equal to $\nu_{\text{spin}}/2$ (when $\nu_{\text{spin}} \geq 400$ Hz). These commensurabilities strongly suggest some kind of beat frequency interaction where the spin, by beating against one QPO frequency, produces a second QPO, but a simple spin-orbit beat frequency model such as proposed for kHz QPOs by Miller et al. (1998) is incompatible with $\Delta\nu \approx \nu_{\text{spin}}/2$. Models that seek to resolve this make use of resonances of the spin frequency with orbital or relativistic epicyclic frequencies in the accretion disk (see Section 4). Weak sidebands to the lower kHz QPO occur in a number of sources (Jonker et al., 2000, 2005).

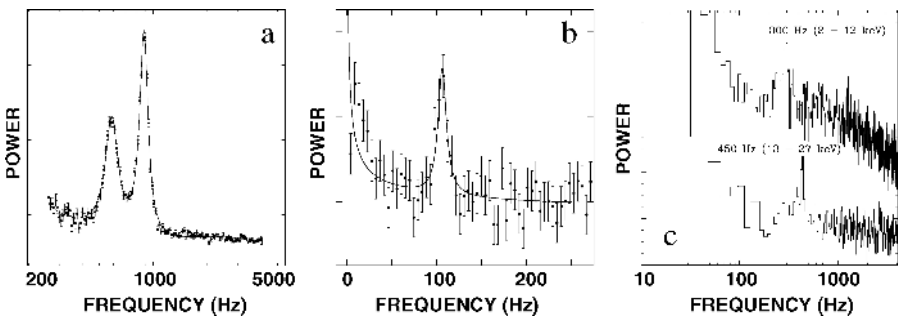


Figure 1. (a) Twin kHz QPOs in Sco X-1 (van der Klis et al., 1997), (b) hectohertz QPO in 4U 0614+09 (van der Klis, in press), (c) HF QPOs in GRO J1655–40 (Strohmayer, 2001).

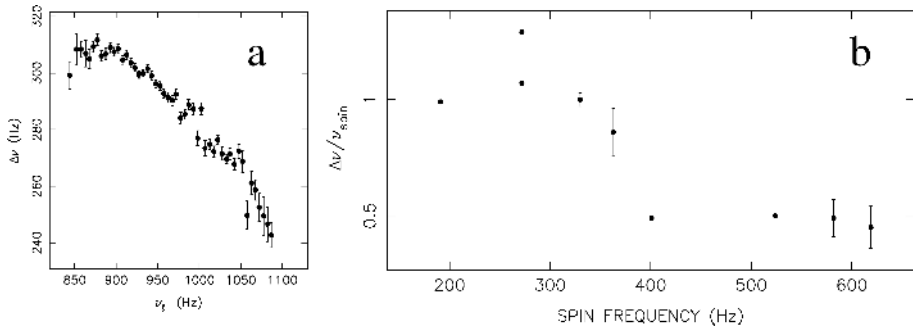


Figure 2. (a) The variation in kHz QPO peak separation as a function of the lower kHz QPO frequency in Sco X-1, after Méndez and van der Klis (1999); (b) $\Delta\nu/\nu_{\text{spin}}$ vs. ν_{spin} , after van der Klis (in press). Vertical bars indicate the range of variation in $\Delta\nu$.

The fastest black hole phenomenon are the high frequency (HF) QPOs. Frequencies range from 100 to 450 Hz (the relation to QPOs in the 27–67 Hz range is not entirely clear). These QPOs are reported to usually occur at fixed values different in each source, possibly related to black hole mass. In a few cases harmonically related (2:3) frequencies have been seen. The phenomenon is weak and transient so that observations are difficult.

The hectohertz (hHz) QPO is a low-magnetic field neutron star phenomenon that usually shows up as a broad bump in the power spectra (but which is sometimes coherent enough to be called a QPO) with a frequency in the 100–200 Hz range. It stands out from all other neutron star components by its approximately constant frequency which is quite similar across sources, perhaps because its frequency derives from compact object properties and the neutron stars in these systems are all similar. The phenomenon is seen simultaneously with kHz QPOs so it clearly is something else than that.

So, the black hole HF QPOs have reportedly constant frequency but high harmonic content, whereas the kHz QPOs have variable frequencies, very weak harmonics (none reported so far) and two peaks with frequencies that are related via the spin frequency. Hectohertz QPOs have constant frequencies like the HF QPOs but, again, no detected harmonics. These differences may indicate different physical mechanisms. It is also possible that some of the basic mechanisms are the same and that the observable differences are due to the different ways these mechanisms work out in the context of neutron star and black hole accretion, respectively. For example, the variable frequency of the kHz QPOs in neutron stars may occur because the phenomenon occurs at a variable (e.g., inner disk) radius set by interaction of the disk flow with either a magnetic field or radiation from the stellar surface; in black holes, in the absence of these influences, the same phenomenon might occur at an approximately constant radius (perhaps, the ISCO); the second kHz QPO may occur only in neutron stars because it is due to the interaction between the disk flow and a magnetic or radiative pattern spinning with the star, which

in view of the no-hair theorem does not occur in black holes; the high harmonic content exclusively seen in black hole QPOs may be due to relativistic effects on the flow (and its emission) that become important only near the ISCO (e.g., extreme Doppler boosting leading to non-sinusoidal light curves caused by orbiting clumps).

Relativistic resonance models have been proposed (Abramowicz and Kluzniak, 2001) for the black hole high-frequency QPOs in which general relativity picks out particular radii in the disk as preferred radii, because only at these radii a pair of general relativistic orbital and epicyclic frequencies have a small integer ratio (e.g., $\nu_r/\nu_\theta = 2:3$), so that a resonant oscillation occurs in the flow at that radius. The periodic forcing of the disk by the neutron star spin by means of magnetic or radiative stresses creates the potential for additional resonances in the flow, and several proposals have been made attempting to explain the neutron star kHz QPO frequency commensurabilities with neutron star spin in terms of such resonances (Wijnands et al., 2003; Kluzniak et al., 2004; Lamb and Miller, 2003).

3. Low-Frequency Phenomena

In the 0.01–100 Hz range a set of usually two to five band-limited noise, peaked-noise and QPO components are observed in both neutron stars and black holes whose frequencies all correlate. This low-frequency complex (cf. van der Klis, in press) is often dominated by strong (tens of % rms), flat-topped band-limited noise with a break in the ~ 0.01 –50 Hz range and a broad hump at frequency ν_h roughly a factor 5 above the break. Both components sometimes feature QPOs located at or around the characteristic frequencies of the broader components. The QPO associated with the hump may show several harmonics and is often called the low-frequency QPO. Both in neutron stars and in black holes differences are sometimes seen between the characteristics (time lags, coherence) of these QPOs that systematically differ between odd and even harmonics. Together, all these components produce power spectra that can be remarkably similar between neutron stars and black holes, particularly in their hard spectral states (which are most common at low luminosity and are known in black holes as the low hard state and in neutron stars as the island state). In these states another band-limited noise component is often present above the frequency of the low-frequency hump and associated QPO. The combination of these three noise components leads to the characteristic power-spectral shapes displayed in Figure 3.

It has been suggested that this third component can be identified with the lower kHz QPO, but at frequencies as low as ~ 10 Hz, and much broader (Psaltis et al., 1999). In neutron stars a fourth band-limited noise component occurs at a higher, > 100 Hz, frequency which connects smoothly with that of the upper kHz QPO and has likewise been suggested to be associated with that high frequency component (van Straaten et al., 2002).

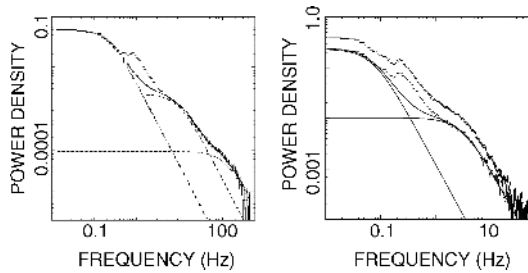


Figure 3. The broad-band power spectra of neutron stars (*left*: 1E 1724–3045) and black holes (*right*: GRO J0422+32) in the low state can be strikingly similar. After Olive et al. (1998).

The <100 Hz variability of black holes and neutron stars in their hard states are very similar and there is little doubt that they are physically related. There also obviously are close relations with, and between, the power spectra of black holes and neutron stars in other states, but the exact nature of these relations is not yet fully established. An important clue is provided by the correlations between the component frequencies (and strengths) which helps to identify components across sources. These are discussed next.

4. Frequency–Frequency Correlations

Similar frequency correlations are seen between phenomena covering a wide range in coherence and frequency in both neutron stars and black holes. Wijnands and van der Klis (1999) noted that in atoll sources (including weak LMXBs) and in black holes, the characteristic frequency of the band-limited noise (ν_{break}) and of the hump or the associated low-frequency QPO (ν_{LF}) often found above this break are correlated over 3 orders of magnitude (WK correlation, Figure 4). Psaltis et al. (1999) were able to select a set of higher-frequency variability components from neutron stars and black holes that seem to follow a common frequency correlation with ν_{LF} that spans nearly three decades in frequency, with the luminous neutron star sources populating the high-frequency range and the weak neutron stars and black holes in the low hard state the low-frequency one, and Cir X-1 filling in the gap in between (Figure 4). This PBK correlation combines features from different sources with very different Q values (in particular, it makes the identification of lower kHz QPO with the third broad component in the low-frequency complex mentioned in the previous section; this is called ν_1 in Figure 4). Further work has produced many further examples of power spectra whose components fit these relations.

The relations of Figure 4 suggest that physically similar phenomena cause the frequencies plotted there. If so, then these phenomena are extremely tunable, in some cases over nearly three orders of magnitude in frequency, and occur in neutron

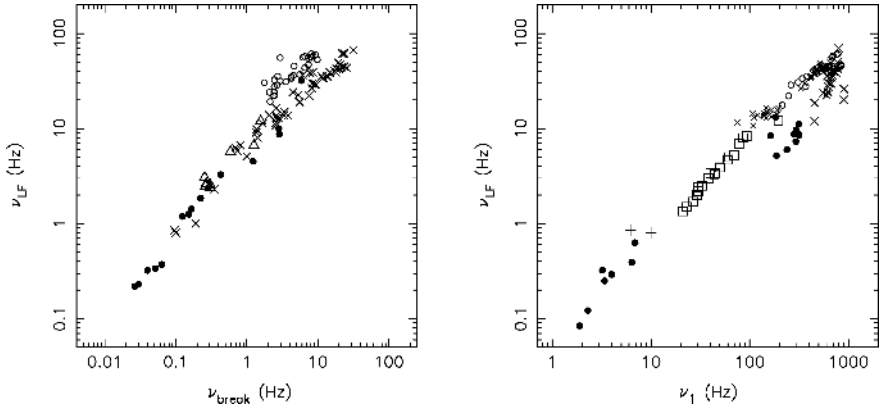


Figure 4. *Left*: WK correlation; *Right*: PBK relation; see text. Filled circles represent black hole candidates, open circles Z sources, crosses atoll sources, triangles the millisecond pulsar SAX J1808.4–3658, pluses faint burst sources and squares Cir X-1.

stars as well as black holes, which probably means they arise in the disk. The so-called relativistic precession models (Stella and Vietri, 1998, 1999) provide one possible way to do this. In these models, the observed frequencies are directly identified with general relativistic orbital and epicyclic frequencies arising at a common radius. It should be noted, however, that to match the observed frequencies for reasonable compact object parameters seems difficult with these models in their initial form. A particularly interesting case is that of the correlation between the upper kHz QPO frequency and the low-frequency QPO in neutron stars. This correlation is often seen to follow a power law with index 2, sometimes remarkably closely, which is exactly as predicted for the relation between the Lense-Thirring precession frequency and the orbital frequency in neutron stars. However, the relation seems to be the same for neutron stars with very different spin frequency, whereas the relativistic precession model predicts them to all have different normalizations (Figure 5). Disk oscillation mechanisms may exist that are able to produce frequencies similar to the free-particle orbital and epicyclic frequencies used in the original relativistic precession models (e.g., Wagoner, 1999; Psaltis and Norman, 2000), perhaps with hydrodynamic corrections and additional frequencies due to coupling between modes.

A further problem to models of this type would seem to be the fact that these correlations may even extend to accreting white dwarfs (in cataclysmic variables), as proposed by Warner and Woudt (2002). If so, then by similar reasoning as above this would seem to exclude large amplitude general relativistic effects as a viable mechanism for the timing phenomena involved in the correlations (even then, orbital motion in the strong-field regime would still be implied in the neutron star and black hole cases). It is important to note, however, that even if the observation that the black holes, neutron stars, and white dwarfs all produce frequencies that follow the

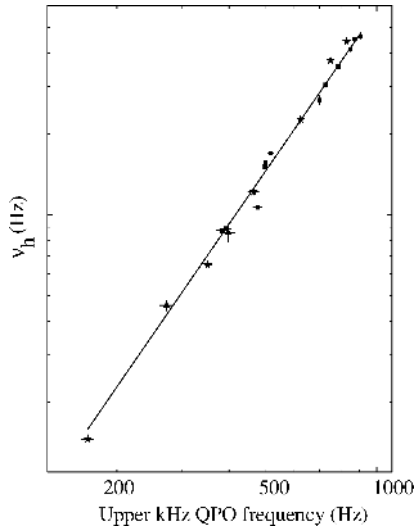


Figure 5. The relation between upper kHz QPO frequency and, ν_h in 3 different atoll sources. Line is power law with index 2.01 (van Straaten et al., 2003).

same correlations means that the same physics underlies the *correlations*, this does not strictly require that all *frequencies* participating in the correlations have similar physical origins in all three types of compact object. An alternative possibility is for example that it is a property of accretion disks to, given one oscillation frequency, produce a second one matching the correlation. A physical phenomenon that occurs in all compact object types (the common frequency – frequency correlation) would then derive from this accretion-disk property, which is not unique to any compact object type, while unique compact object properties (e.g., strong-field gravity effects in neutron stars and black holes) might well be involved in generating the original disk oscillation in the first place. This possibility was alluded to by Abramowicz et al. (2004) using the example of the ‘ninth wave’ phenomenon.

Detailed studies of the properties of these phenomena are needed to be able to confirm or deny that they *can* in fact be attributed to similar physical effects. For neutron stars, van Straaten et al. (2002, 2003, 2005) demonstrated the existence of a number of very similar variability components that follow a universal scheme of correlations for neutron stars distributed over a wide range of luminosities (Figure 6). Accreting millisecond pulsars were shown to follow the same scheme, but some pulsars show a systematic offset by a factor ~ 1.5 in kHz QPO frequencies. A first study of this kind comparing neutron stars and black holes was performed by Klein-Wolt (2004), who demonstrates that the similarity between neutron stars and black holes in the low-hard/extreme-island states can be used as a starting point to identify further correspondence between neutron star and black hole in other states, and that further matches between neutron stars and black holes frequency – frequency correlations can be found based on these correspondences.

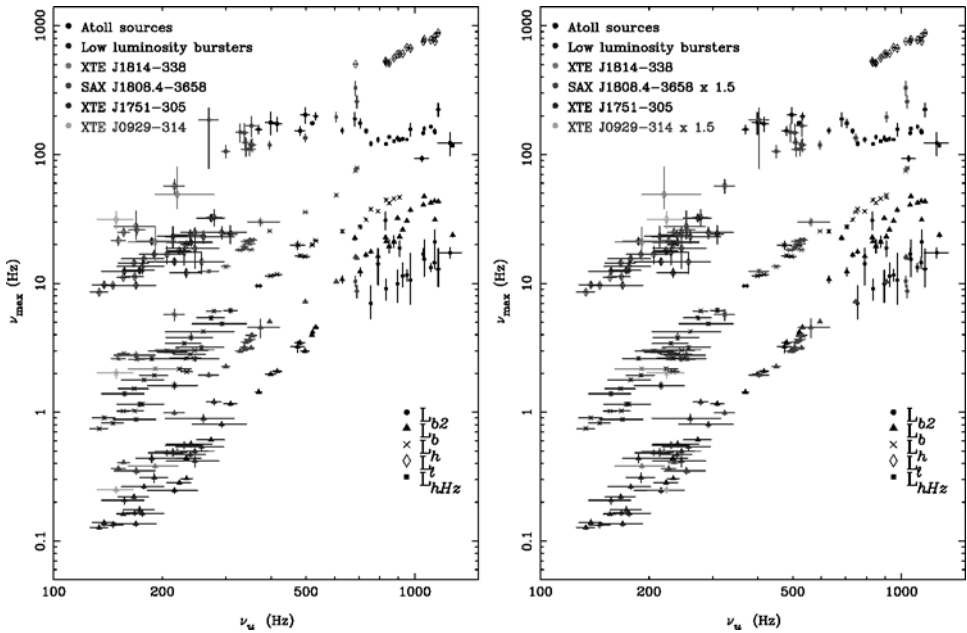


Figure 6. Frequency correlations in a wide variety of low magnetic field neutron stars. *Left*: including all accreting millisecond pulsars as measured. *Right*: same, but millisecond pulsars SAX J1808.4–3658 and XTE J0929–314 shifted up by a factor 1.5 in kHz QPO frequencies only.

References

- Abramowicz, M.A. and Kluźniak, W.: 2001, *A&A* **374**, L19.
 Abramowicz, M.A., Kluźniak, W., Stuchlik, Z. and Torok, G.: 2004, astro-ph/0401464.
 Jonker, P.G., Méndez, M. and van der Klis, M.: 2000, *ApJ* **540**, L29.
 Jonker, P.G., Méndez, M. and van der Klis, M.: 2005, *MNRAS* **360**, 921.
 Klein-Wolt, M.: 2004, PhD thesis, University of Amsterdam.
 Kluźniak, W., Abramowicz, M.A., Kato, S., Lee, W.H. and Stergioulas, N.: 2004, *ApJ Lett.* **603**, L89.
 Lamb, F.K. and Miller, M.C.: 2003, astro-ph/0308179.
 McClintock, J. and Remillard, R.: in press, in Lewin & van der Klis (eds.), *Compact Stellar X-ray Sources*, Cambridge University Press, Cambridge, UK, astro-ph/0306213.
 Méndez, M. and van der Klis, M.: 1999, *ApJ Lett.* **517**, L51.
 Miller, M.C., Lamb, F.K. and Psaltis, D.: 1998, *ApJ* **508**, 791.
 Olive, J.F., Barret, D., Boirin, L., Grindlay, J.E., Swank, J.H. and Smale, A.P.: 1998, *A&A* **333**, 942.
 Psaltis, D., Belloni, T. and van der Klis, M.: 1999, *ApJ* **520**, 262.
 Psaltis, D. and Norman, C.: 2000, astro-ph/0001391.
 Stella, L. and Vietri, M.: 1998, *ApJ* **492**, L59.
 Stella, L. and Vietri, M.: 1999, *Phys. Rev. Lett.* **82**, 17.
 Strohmayer, T.E.: 2001, *ApJ* **552**, L49.
 van der Klis, M.: 1994, *ApJS* **92**, 511.
 van der Klis, M.: 2000, *Ann. Rev. Astr. Ap.* **38**, 717.
 van der Klis, M.: in press, in Lewin and van der Klis (eds.), *Compact Stellar X-ray Sources*, Cambridge University Press, Cambridge, UK, astro-ph/0410551.

- van der Klis, M., Wijnands, R.A.D., Horne, K. and Chen, W.: 1997, *ApJ* **481**, L97.
- van Straaten, S., van der Klis, M., Di Salvo, T. and Belloni, T.: 2002, *ApJ* **568**, 912.
- van Straaten, S., van der Klis, M. and Méndez, M.: 2003, *ApJ* **596**, 1155.
- van Straaten, S., van der Klis, M. and Wijnands, R.: 2005, *ApJ* **619**, 455.
- Wagoner, R.W.: 1999, *Phys. Rep.* **311**, 259.
- Warner, B. and Woudt, P.A.: 2002, *MNRAS* **335**, 84.
- Wijnands, R. and van der Klis, M.: 1999, *ApJ* **514**, 939.
- Wijnands, R., van der Klis, M., Homan, J., Chakrabarty, D., et al.: 2003, *Nature* **424**, 44.

X-RAY AND RADIO MONITORING OF GX 339-4 AND CYG X-1

MICHAEL NOWAK

*Chandra X-Ray Science Center, Massachusetts Institute of Technology, 77 Massachusetts Avenue,
Cambridge, MA, U.S.A.; E-mail: mnowak@space.mit.edu*

(Received 13 October 2004; accepted 1 June 2005)

Abstract. Previous work by Motch et al. [1985, *Space Sci. Rev.* **40**, 219] suggested that in the low/hard state of GX 339-4, the soft X-ray power-law extrapolated backward in energy agrees with the IR flux level. Corbel and Fender [2002, *ApJ* **573**, L35–L39] later showed that the typical hard state radio power-law extrapolated forward in energy meets the backward extrapolated X-ray power-law at an IR spectral break, which was explicitly observed twice in GX 339-4. This has been cited as further evidence that jet synchrotron radiation might make a significant contribution to the observed X-rays in the hard state. We explore this hypothesis with a series of simultaneous radio/X-ray hard state observations of GX 339-4. We fit these spectra with a simple, but remarkably successful, doubly broken power-law model that indeed requires a spectral break in the IR. For most of these observations, the break position as a function of X-ray flux agrees with the jet model predictions. We then examine the radio flux/X-ray flux correlation in Cyg X-1 through the use of 15 GHz radio data, obtained with the Ryle radio telescope, and *Rossi X-ray Timing Explorer* data, from the *All Sky Monitor* and pointed observations. We find evidence of ‘parallel tracks’ in the radio/X-ray correlation which are associated with ‘failed transitions’ to, or the beginning of a transition to, the soft state. We also find that for Cyg X-1 the radio flux is more fundamentally correlated with the hard, rather than the soft, X-ray flux.

Keywords: accretion, accretion disks, black hole physics

1. Introduction

Both Cyg X-1 and GX 339-4 in their spectrally hard, radio-loud states have served as canonical examples of the so-called ‘low state’ (or ‘hard state’) of galactic black hole candidates (Pottschmidt et al., 2003; Nowak et al., 2002). In this state the X-ray spectrum is reasonably well-approximated by a power-law with photon spectral index of $\Gamma \approx 1.7$, with the power-law being exponentially cutoff at high energies (≈ 100 keV). Such spectra have been attributed to Comptonization of soft photons from an accretion disk by a hot corona; however, it recently has been hypothesized that the X-ray spectra of hard state sources might instead be due to synchrotron and synchrotron self-Compton (SSC) radiation from a mildly relativistic jet (Markoff et al., 2001, 2003). Jet models have been prompted in part by multiwavelength (radio, optical, X-ray) observations of hard state systems.



In hard states of GX 339-4, the 3–9 keV X-ray flux (in units of $10^{-10} \text{ erg cm}^{-2} \text{ s}^{-1}$) is related to the 8.6 GHz radio flux (in mJy) by $F_x \approx 0.46 \mathcal{F}_r^{1.42}$ (Corbel et al., 2003). This correlation was seen to hold over several decades in X-ray flux, and also to hold for two hard state epochs that were separated by a prolonged, intervening soft state outburst. It further has been suggested that the $F_x \propto \mathcal{F}_r^{1.4}$ correlation is a universal property of the low/hard state of black hole binaries (Gallo et al., 2003). This specific power-law dependence of the radio flux upon the X-ray flux naturally arises in synchrotron jet models (Falcke and Biermann, 1995; Corbel et al., 2003; Markoff et al., 2003; Heinz and Sunyaev, 2003), where the optically thin synchrotron spectrum, occurring above an IR spectral break, is presumed to continue all the way through the X-ray.

Interestingly, nearly 20 years ago Motch et al. (1985) noted that for a set of simultaneous IR, optical, and X-ray observations of the GX 339-4 hard state, the extrapolation of the X-ray power-law to low energy agreed with the overall flux level of the optical/IR data. Corbel and Fender (2002) reanalyzed these observations (which did not include simultaneous radio data), as well as a set of (not strictly simultaneous) radio/IR/X-ray observations from the 1997 GX 339-4 hard state. They showed that the low energy extrapolation of the X-ray power-laws, and the high energy extrapolation of the radio power-law, coincided with a spectral break in the IR.

2. Observations of GX 339-4

We consider a set of 10 simultaneous radio/X-ray observations of GX 339-4, eight of which come from the 1997 or 1999 hard state (Wilms et al., 1999; Nowak et al., 2002) and two of which come from the 2002 hard state (Homan et al., 2004). All X-ray observations were performed with the *Rossi X-ray Timing Explorer* (*RXTE*). Note that five of these observations are further labeled A–E, as we single these out for special discussion. A and B occurred immediately after the 1999 soft-to-hard state transition (Nowak et al., 2002) and have optically thin radio spectra ($\alpha_r < 0$). C has a very ‘inverted’ radio spectrum (see below). D has only a single radio point, and hence we cannot extrapolate its radio power-law without making further assumptions. E has the brightest X-ray flux in our sample, and is one of the brightest hard X-ray states observed in GX 339-4 to date.

To analyze the X-ray spectra of these observations, *RXTE* response matrices were created using the software tools available in *HEASOFT* 5.3, which we find yield extremely good agreement between the *Proportional Counter Array* (*PCA*) and *High Energy X-ray Timing Explorer* (*HEXTE*) when fitting power-law models to the Crab pulsar plus nebula system. This is true for both the power-law normalization and slope, both of which must be determined very accurately when extrapolating over large energy ranges.

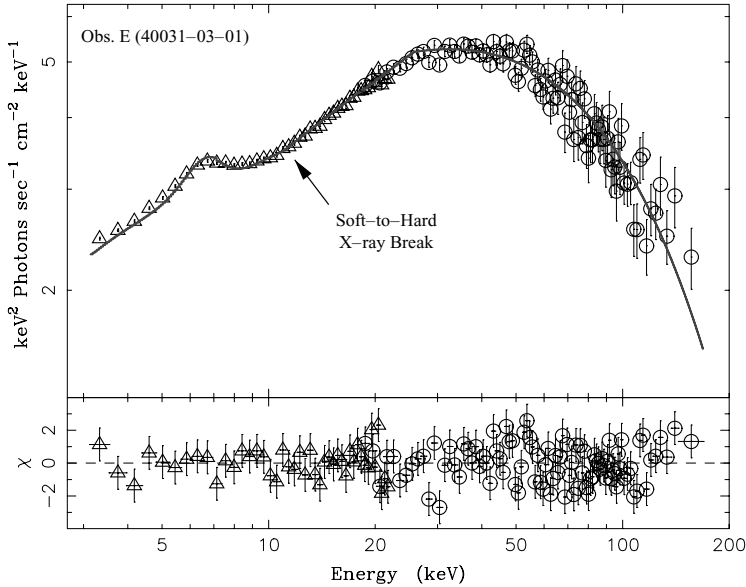


Figure 1. Unfolded spectra of an X-ray spectrum of GX 339-4 fit with an absorbed, exponentially cutoff, broken power-law and a gaussian line. Residuals are from the proper forward folded model fit.

The radio data for observation E were obtained with the *Australia Telescope Compact Array (ATCA)* at 4.8 GHz and 8.6 GHz. The radio data for observation D were also obtained with *ATCA*, but only at 5 GHz. All other radio data can be found in Nowak et al. (2002).

3. A Rant on the Nature of Evil

The observations were analyzed with the Interactive Spectral Interpretation System (ISIS) (Houck and Denicola, 2000). For our purposes, there are several major reasons for our use of ISIS. Data input without a response matrix (i.e., the radio data) are automatically presumed to have an associated diagonal response with 1 cm^2 effective area and 1 s integration time. We convert the radio data from mJy to photon rate in narrow bands around the observation frequencies, and use this as input for the simultaneous radio/X-ray fits.

The other major reason for using ISIS is that it treats ‘unfolded spectra’ (shown in Figure 1) in a model-independent manner. The unfolded spectrum in an energy bin denoted by h is defined by: $F_{\text{unfold}}(h) = ([C(h) - B(h)]/\Delta t)/(\int R(h, E)A(E)dE)$, where $C(h)$ is the total detected counts, $B(h)$ is the background counts, Δt is the integrated observation time, $R(h, E)$ is the unit normalized response matrix describing the probability that a photon of energy E is detected in bin h , and $A(E)$ is the detector effective area at energy E . Contrary to unfolded spectra produced

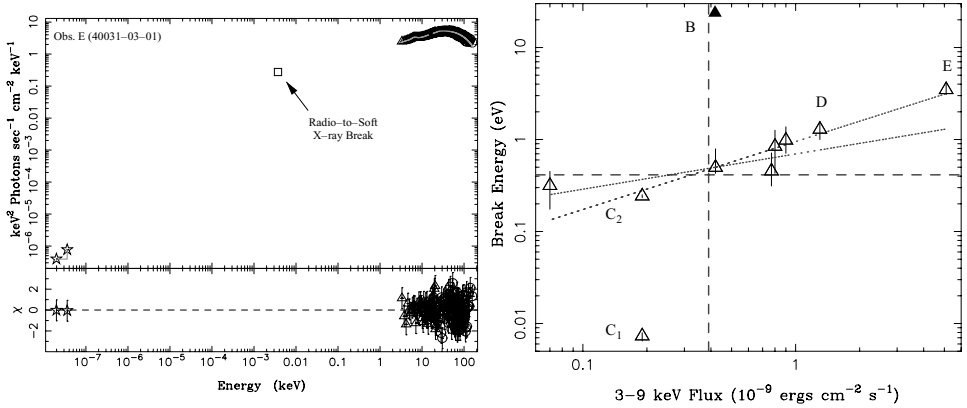


Figure 2. Left: An unfolded, simultaneous radio/X-ray observation of GX 339-4, fit with an absorbed, exponentially cutoff, doubly broken power-law and a gaussian line. Right: Results of broken power-law fits to GX 339-4, showing the location of the break between the radio and soft X-ray power-law as a function of X-ray flux. Dashed lines show the approximate integrated X-ray flux and approximate IR spectral break energy previously observed in GX 339-4 (Corbel and Fender, 2002). Dotted lines are $E_{b-r} \propto F_x^{0.38}$, $E_{b-r} \propto F_x^{0.74}$.

by XSPEC, this definition produces a spectrum that is independent of the fitted model. Any unfolded spectrum should be considered something of a sin; however, ISIS unfolded spectra are only venial sins, whereas XSPEC unfolded spectra should rightly be classified as cardinal sins (*dictum vel factum vel concupitum contra legem aeternam*). In Figure 1, however, the plotted residuals are those obtained from a proper forward-folded fit.

4. Radio-to-X-Ray Break Energy Correlations

We obtain surprisingly good fits for nine of the 10 radio/X-ray spectra using the following simple model (using the ISIS/XSPEC model definitions): absorption (the phabs model, with N_H fixed to 6×10^{21} cm²) and a high energy, exponential cutoff (the hiecut model) multiplying a doubly broken power-law (the bkn2pow model, with the first break being in the far IR to optical regime, and the second break being constrained to the 9–12 keV regime) plus a gaussian line (with energy fixed at 6.4 keV). When considering just the X-ray spectra, a singly broken power-law fits all 10 spectra, with better results than any of the Comptonization models that we have tried.

In Figure 2 we show the fitted radio-to-X-ray break location as a function of 3–9 keV integrated flux. We also show in this figure the approximate integrated 3–9 keV flux and the IR break location for the 1997 observation discussed by Corbel and Fender (2002). For our GX 339-4 observations of comparable 3–9 keV flux, the doubly broken power-law models do indeed produce a break in the IR.

The model fits presented here have predicted radio-to-X-ray breaks ranging all the way from the far IR to the blue end of the optical (and into the X-ray, if one also considers observation B, which has an ‘optically thin’ radio spectrum).

The data point labeled C₁, with a break in the far IR, has an extremely ‘inverted’ radio spectrum ($\alpha_r = 0.58$). This drives the fitted break to low energies, and hence leads to deviations from the overall observed trends shown in Figure 2. Such an inverted spectrum is very unlikely to be intrinsic to the radio jet, and is most likely a signature of free-free absorption at low frequencies (Fender, 2001). If we instead consider only the highest observed radio frequency (8.6 GHz, which is likely less affected by free–free absorption), and fix the radio spectral slope at this point to $\alpha_r = 0.1$, similar to the other observations, we obtain an IR break frequency (labeled C₂) that is consistent with the other inferred breaks.

To assess the correlation of radio-to-X-ray break energy with integrated X-ray flux, we exclude the data points from observation C (likely free–free absorbed), observation B (which has an optically thin radio spectrum), and observation D (which is consistent with the trends if we assume a radio slope of $\alpha_r = 0.1$). A regression fit to the remaining six data points suggests that the radio-to-X-ray break energy, in eV, scales with the 3–9 keV integrated flux as $0.95 F_x^{0.74 \pm 0.05}$.

Using the scale invariance *Ansatz* to describe the jet physics (Heinz and Sunyaev, 2003; Heinz, 2004), we show elsewhere (Nowak et al., 2004) that the predicted scaling between the integrated X-ray synchrotron flux and the radio-to-X-ray break frequency where the jet becomes optically thin to synchrotron self-absorption scales as $\nu_b \propto F_x^{2(p+6)/(p+4)/(p+5)}$, where p is the power-law index of the electron spectrum, and we have used for the X-ray spectral slope $\alpha_x = (1 - p)/2$ from standard synchrotron theory. For the usual range of $-0.65 < \alpha_x < -0.5$ of synchrotron spectra, we obtain $\nu_b \propto F_x^{0.36}$ to $\nu_b \propto F_x^{0.38}$. This prediction is flatter than the observed dependence of extrapolated break frequency upon X-ray flux. However, if one also excludes the highest flux point, then the scaling becomes more consistent with the jet synchrotron prediction, i.e., $\nu_b \propto F_x^{0.38 \pm 0.16}$ (Figure 2).

5. Radio/X-Ray Correlations in Cyg X-1

We now turn to radio/X-ray observations of Cyg X-1 (Pottschmidt et al., 2003; Gallo et al., 2003). The radio data are 15 GHz observations performed at the Ryle Telescope, Cambridge (UK) (Pottschmidt et al., 2003). (These are single-channel observations, so a radio spectral slope cannot be determined.) Most of these observations have occurred simultaneously with pointed *RXTE* observations (Pottschmidt et al., 2003), and nearly all have very good contemporaneous coverage by the *RXTE All Sky Monitor (ASM)*.

In Figure 3 we plot the daily average *ASM* count rate vs. the daily average 15 GHz flux. Ranging from approximately 10–50 cps in the *ASM* there is a clear log-linear

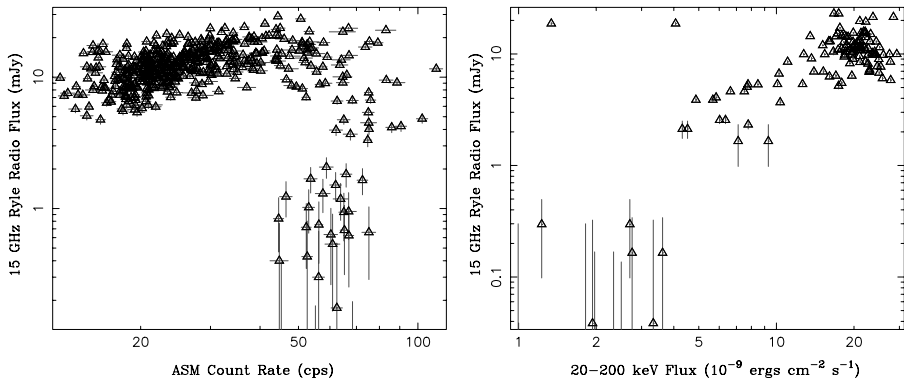


Figure 3. Left: 15 GHz Ryle radio flux (mJy) vs. Cyg X-1 daily mean *ASM* count rate. Right: 20–200 keV flux (units of 10^{-9} ergs $\text{cm}^{-2} \text{s}^{-1}$) vs. the daily average 15 GHz Ryle radio flux (mJy) for pointed observations of Cyg X-1.

correlation between the radio flux and the *ASM* count rate. As for GX 339-4, the radio flux rises more slowly than the *ASM* count rate (\mathcal{F}_R scales approximately as the 0.8 power of the *ASM* count rate). Cyg X-1, however, shows much more scatter in the amplitude of the correlation than does GX 339-4.

As noted elsewhere (Gallo et al., 2003), there is a sharp roll-over for higher *ASM* count rates. However, one can clearly discern on the shoulder of this roll-over (i.e., the upper right corner of Figure 3) four ‘spokes’, consisting of 2–5 data points each. In these spokes, the radio/X-ray correlation appears to hold to high count rates. We have confirmed Nowak et al. (2004) that each of these times are associated with ‘failed transitions’ to the soft state (Pottschmidt et al., 2003), except for the lowest amplitude of these spokes, which occurs immediately preceding a prolonged soft state outburst.

In Figure 3 we also plot the daily average *ASM* count rate vs. the 20–200 keV flux from our pointed *RXTE* observations taken during the same 24 h period (Pottschmidt et al., 2003). We see that hard X-ray/*ASM* correlation traces a similar pattern to the radio/*ASM* correlation. Indeed, when we plot the hard X-ray flux vs. the daily average radio flux we obtain a log-linear relationship, as shown in Figure 3. In Cyg X-1, the radio flux density appears fundamentally to be tied to the hard X-ray emission.

6. Summary

We have considered 10 simultaneous *RXTE*/radio hard state observations of GX 339-4, and over 100 *RXTE*/radio observations of Cyg X-1. We have fit the former spectra with a very simple, but remarkably successful, phenomenological model consisting of a doubly broken power-law with an exponential roll-over plus a gaussian line. For GX 339-4, the break between the radio and soft X-ray power-law

occurs in the IR to optical range, in agreement with prior work (Motch et al., 1985; Corbel and Fender, 2002). In contrast to prior works, we have fit the X-ray data in ‘detector space’ and provided a quantitative assessment of the extrapolated break location.

The scaling of the radio-to-X-ray break location with integrated X-ray flux agrees reasonably well with predictions of jet models wherein a large fraction of the soft X-ray flux is due to synchrotron emission from the jet. At least some fraction of the observed soft X-rays may be attributable to emission from the jet, as opposed to disk or corona. On the other hand, we have evidence in the Cyg X-1 failed state transitions and soft state transition, that the correlation between radio flux and integrated X-ray flux can take on different amplitudes during different hard state episodes. There is also evidence in Cyg X-1 that the radio/X-ray correlation is more fundamental to the hard X-ray band. In jet models, this band, which essentially encompasses the third, highest energy, power-law component in our model fits (and also encompasses the exponential cutoff), is possibly attributable to the synchrotron self-Compton (SSC) emission from the base of the jet (Markoff et al., 2003; Markoff and Nowak, 2004). It is therefore quite reasonable to expect a strong coupling between the radio and hard X-ray flux; however, these models are more complex than simple pure synchrotron models, and are only now beginning to be explored quantitatively (Markoff et al., 2003; Markoff and Nowak, 2004).

The results presented here suggest, at the very least, some obvious observational strategies. Given the break energy correlations, it would be extremely useful to have not only a radio amplitude for each X-ray observation, but also a radio slope. Furthermore, the predicted break for the brightest observation of GX 339-4, E, occurs in the blue end of the optical. Thus, ideally multiwavelength observations would consist of radio, broadband X-ray, and IR through optical coverage. This is an admittedly difficult task, but BHC are demonstrating *via* spectral correlations that all these energy regimes are fundamentally related to activity near the central engine.

Finally, it is important to obtain multiwavelength observations of multiple episodes of each of the spectral states. For example, if there are indeed ‘parallel tracks’ in the radio/X-ray correlations, it would be interesting to determine whether the amplitude of the radio/X-ray correlation is related to the flux at which the outbursting source transits from the low/hard to high/soft state. If such observations can be made with more quantitative detail, we will have vital clues to determining the relative contributions of coronae and jets, and the coupling between these two components, for black hole binary systems.

Acknowledgments

This talk later evolved into the paper cited as Nowak et al. (2004). I would therefore like to thank my coauthors, J. Wilms, S. Heinz, G. Pooley, K. Pottschmidt, and S.

Corbel. It is also a pleasure to acknowledge useful conversations with Sera Markoff and Jeroen Homan. This work has been supported by NASA grants SV3-73016 and GO4-5041X, and NSF grant INT-0233441.

References

- Corbel, S. and Fender, R.P.: 2002, *ApJ* **573**, L35–L39.
- Corbel, S., Nowak, M.A., Fender, R.P., Tzioumis, A.K. and Markoff, S.: 2003, *A&A* **400**, 1007.
- Falcke, H. and Biermann, P.L.: 1995, *A&A* **293**, 665.
- Fender, R.P.: 2001, *MNRAS* **322**, 31.
- Gallo, E., Fender, R.P. and Pooley, G.G.: 2003, *MNRAS* **344**, 60.
- Heinz, S.: 2004, *MNRAS* **355**, 835.
- Heinz, S. and Sunyaev, R.A.: 2003, *MNRAS* **343**, L59–L64.
- Homan, J., Buxton, M., Markoff, S., Bailyn, C., Nespoli, E. and Belloni, T.: 2005, *ApJ* **624**, 295.
- Houck, J.C. and Denicola, L.A.: 2000, ISIS: An interactive spectral interpretation system for high resolution X-ray spectroscopy, in: *ASP Conference Series 216: Astronomical Data Analysis Software and Systems IX*, Vol. 9, p. 591.
- Markoff, S., Falcke, H. and Fender, R.: 2001, *ApJ* **372**, L25–L28.
- Markoff, S. and Nowak, M.: 2004, *ApJ* **609**, 972–976.
- Markoff, S., Nowak, M., Corbel, S., Fender, R. and Falcke, H.: 2003, *A&A* **397**, 645–658.
- Motch, C., Ilovaisky, S.A., Chevalier, C. and Angebault, P.: 1985, *Space Sci. Rev.* **40**, 219.
- Nowak, M.A., Wilms, J. and Dove, J.B.: 2002, *MNRAS* **332**, 856–878.
- Nowak, M.A., Wilms, J., Heinz, S., Pooley, G., Pottschmidt, K. and Corbel, S.: 2005, *ApJ* **626**, 1006.
- Pottschmidt, K., Wilms, J., Nowak, M.A., Pooley, G.G., Gleissner, T., Heindl, W.A., Smith, D.M., Remillard, R. and Staubert, R.: 2003, *A&A* **407**, 1039–1058.
- Wilms, J., Nowak, M.A., Dove, J.B., Fender, R.P. and di Matteo, T.: 1999, *ApJ* **522**, 460–475.

ACCRETION IN STRONG GRAVITY: FROM GALACTIC TO SUPERMASSIVE BLACK HOLES

CHRIS DONE and MAREK GIERLIŃSKI

Department of Physics, University of Durham, UK; E-mail: chris.done@durham.ac.uk

(Received 4 January 2005; accepted 1 June 2005)

Abstract. The galactic black hole binary systems give an observational template showing how the accretion flow changes as a function of increasing mass accretion rate, or L/L_{Edd} . These data can be synthesised with theoretical models of the accretion flow to give a coherent picture of accretion in strong gravity, in which the major hard-soft spectral transition is triggered by a change in the nature and geometry of the inner accretion flow from a hot, optically thin plasma to a cool, optically thick accretion disc. However, a straightforward application of these models to AGN gives clear discrepancies in overall spectral shape. Either the underlying accretion model is wrong, despite its success in describing the Galactic systems and/or there is additional physics which breaks the simple scaling from stellar to supermassive black holes.

Keywords: black holes, accretion flows

1. Introduction

The famous quote by John Wheeler that “Black holes have no hair” refers to their amazing simplicity. Theoretically they can be *completely* described by mass, spin and charge, while in any realistic astrophysical situation this reduces to simply mass and spin. However, black holes are most easily studied if they accrete, where the in-falling material converts some of its immense gravitational potential energy to high energy radiation before disappearing forever below the event horizon. Thus there is another parameter which describes the appearance of the most easily observed black holes, namely their mass accretion rate.

This theoretical simplicity is at first glance wildly at odds with the observed complexity of emission from accreting black holes. This is especially evident in the stellar mass black holes in our galaxy (GBHC), where there is now a huge amount of high signal-to-noise data covering a large range of different mass accretion rates. However, recent progress has shown that these data can all be fit together into a coherent phenomenological framework, and that this can plausibly relate to physically based models of the accretion flow (Done and Gierliński, 2003, hereafter DG03). The general picture emerging from the data is that the major hard-soft transition seen in the GBHC is consistent with being triggered by a change in the nature and geometry of the inner accretion flow from a hot, optically thin, geometrically thick



plasma to a cool, optically thick, geometrically thin disc (Poutanen et al., 1997; Esin et al., 1997).

Here we try to scale up the physical models of accretion, which are so successful in describing the data from the galactic black holes to the accreting supermassive black holes which power active galactic nuclei (AGN) and quasars. The goal is synthesise both theory and observations, to build a physically based model which can explain the data from accretion flows onto all masses of black hole.

2. Galactic Black Hole Binary Systems

The GBHC all have fairly similar mass, but show a wide variety of mass accretion rates due to the disc instability (King and Ritter, 1998). These data give a observational template showing how the accretion flow varies as a function of (predominantly) mass accretion rate, i.e. L/L_{Edd} . The standard disc models predict a very robust quasi-blackbody spectrum, with temperature $kT_{\text{disc}} \sim 1(M/M_{\odot})^{-1/4}(L/L_{\text{Edd}})^{1/4}$ keV, i.e. ~ 1 keV for a $10M_{\odot}$ GBHC accreting at the Eddington limit. Such spectra are seen, but are generally accompanied by a weak (ultrasoft state: US), moderate (high state: HS) or strong (very high state: VHS) X-ray tail to higher energies. Together these form the soft states, which are seen at high L/L_{Edd} . However, at low L/L_{Edd} these objects can also show spectra which look entirely unlike a disk, peaking instead at ~ 100 keV (low/hard states: LS). Figure 1a shows representative spectra from all these GBH states (e.g. the review by Tanaka and Lewin, 1995).

To produce any emission at energies substantially higher than that of the disk *requires* that some fraction of the gravitational energy is dissipated in regions

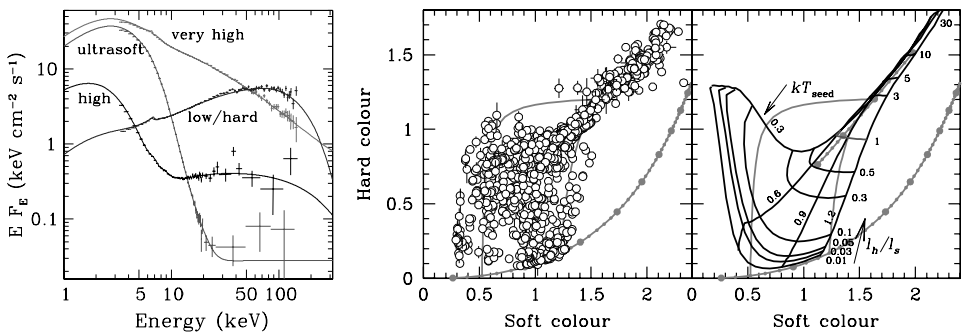


Figure 1. The left panel shows RXTE PCA and HEXTE data from XTE J1550-564 to illustrate the range of spectral shapes seen from the GBH. The middle panel compresses all the spectral information into colours, with soft and hard colours roughly related to the inverse of the mean spectral slope between 3 and 6 keV and 6 and 16 keV, respectively. All the black holes are consistent with the same behaviour. The right panel shows that this behavior can be reproduced using comptonisation models constrained by the sketched geometries shown in Figure 2.

which are optically thin, so that a few electrons gain a large fraction of the energy. These energetic electrons can produce hard X-rays by Compton upscattering lower energy photons, and the shape of this spectrum is determined by the ratio of power in the hot electrons to that in the seed photons illuminating them, $\mathcal{L}_h/\mathcal{L}_s$.

While such comptonization models can explain the broad band spectral shapes, they do not address the underlying problem of the *physical origin* of the hot electrons, or indeed the range $\mathcal{L}_h/\mathcal{L}_s$ required to produce the very different spectra shown in Figure 1a. We can get some insight into these more fundamental issues from recent advances in understanding the physical nature of the accretion disc viscosity as a magnetic dynamo (Balbus and Hawley, 1991). Numerical simulations show that any seed magnetic field can be continuously amplified by the differential rotation of the disc material, and dissipated through reconnection events. Including radiative cooling gives an accretion disc structure which bears some resemblance to the standard accretion disc models, but with some of the magnetic reconnection occurring above the disc as magnetic field loops buoyantly rise to the surface, reconnecting above the bulk of the material in an optically thin environment (e.g. Turner, 2004).

However, these physical viscosity simulations also show that an alternative, *non-disc* solution can exist, where the whole accretion flow is optically thin, so cannot efficiently cool. The accretion flow forms a hot, geometrically thick structure, qualitatively similar to the Advection Dominated Accretion Flows (Narayan and Yi, 1995), but considerably more complex in detail, with convection (e.g. Igumenshchev et al., 2003) and outflows (Blandford and Begelman, 1999) as well as advection (Hawley and Balbus, 2002).

The existence of two very different accretion flow structures gives a very natural explanation for the two very different types of spectra (hard and soft) seen from the GBH. At low L/L_{Edd} the inner optically thick disk is replaced by an optically thin flow. There are few photons from the disk which illuminate the flow, so $\mathcal{L}_h/\mathcal{L}_s \gg 1$ and the comptonised spectra are hard. When the mass accretion rate increases, the flow becomes optically thick, and collapses into an SS disk. The dramatic increase in disk flux drives the hard-soft state transition (Esin et al., 1997). A weak tail on the dominant disk emission can be produced by occasional magnetic field loops buoyantly rising to the surface, reconnecting above the bulk of the material in an optically thin environment (US). Increasing the ratio of power dissipated above the surface to that in the disk increases $\mathcal{L}_h/\mathcal{L}_s$, increasing the importance of the hard X-ray tail. However, the *geometry* of the soft states sets a limit to $\mathcal{L}_h/\mathcal{L}_s$. Flares *above* a disk illuminate the disk surface, where some fraction are absorbed and thermalised. This adds to the intrinsic disk emission, fixing $\mathcal{L}_h/\mathcal{L}_s \lesssim 1$ in the limit where the flares cover most of the disk surface (Haardt and Maraschi, 1993), which always results in a soft comptonised spectrum, forming a power law with energy index $\alpha \gtrsim 1$ (VHS). Figure 2 illustrates the geometries inferred for each state.

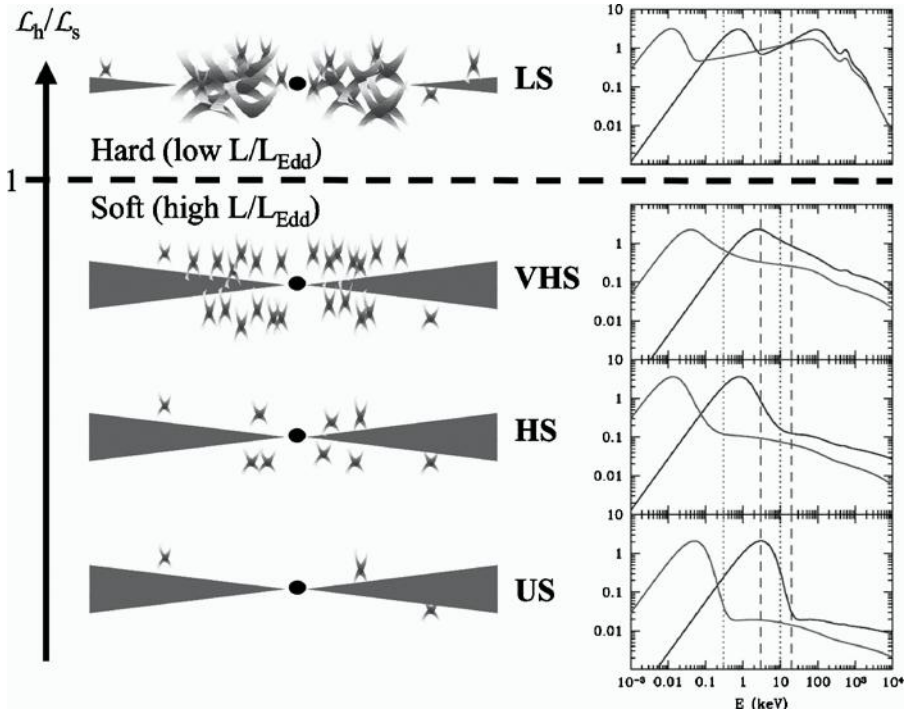


Figure 2. Sketched geometries corresponding to the spectral states, together with the EQPAIR spectra for GBH (higher disc temperature) and AGN (lower disc temperature). The dashed and dotted vertical lines on the spectral panels show the energy ranges for *RXTE* and *XMM-Newton*, respectively.

3. Quantitative Models of the X-ray Spectra of GBH

The picture developed above for the geometry of the accretion flow puts constraints on the expected emission. The energetic electrons in the optically thin regions can produce hard X-rays by Compton-upscattering lower energy photons, and the shape of this spectrum is broadly determined by the ratio of power in the electrons to that in the seed photons illuminating them, L_h/L_s . However, the spectral shape of the comptonised emission also depends to some lesser extent on the details of the electron distribution (its optical depth and whether it is thermal, non-thermal, or has some more complex shape) and seed photons (temperature and spectrum).

Detailed modelling of individual spectra from GBH show that the X-ray emission in the low/hard state it is fairly well modeled by thermal Comptonisation of accretion disc photons by hot, thermal (~ 100 keV) electrons (e.g. Gierliński et al., 1997), although there may be some evidence for non-thermal electrons also being present (McConnell et al., 2002). However, in the soft states the spectral curvature in the tail is clearly best described by a combination of low temperature thermal (~ 10 keV) and non-thermal electrons (Gierliński et al., 1999; Zdziarski et al., 2001;

Frontera et al., 2001; McConnell et al., 2002; Gierliński and Done, 2003; Kubota and Done, 2004). These could be two physically (and perhaps spatially) distinct populations, or a single ‘hybrid’ plasma. The latter idea comes from the fact that even a purely non-thermal acceleration process cannot give rise to a completely power law electron distribution as electron-electron collisions will always give rise to *some* thermalisation at the lowest energies (Coppi, 1999). Alternatively, even assuming that the energy injection to the electrons is purely thermal leads to a non-thermal tail from stochastic scattering (second order Fermi processes) on magnetic field inhomogeneities (Dermer et al., 1996; Liu et al., 2004). Thus it seems very likely that the electron distribution is indeed complex, even if we are dealing with a single acceleration region.

Thus the simplest model for the emission is one where there is a single acceleration process for the magnetic reconnection irrespective of its spatial location (hot inner flow or flares above a disc). We use the sophisticated comptonization code, EQPAIR (Coppi, 1999) to translate this schematic picture into a *quantitative* model. The key advantage of this code is that it does not assume a steady state electron distribution, rather it *calculates* it by balancing heating (injection of power \mathcal{L}_h into thermal and/or non-thermal electrons) and cooling processes (Compton cooling, which depends on \mathcal{L}_s , Coulomb collisions, photon–photon collisions leading to $e^{+/-}$ pair production and annihilation). The resulting spectrum depends primarily on $\mathcal{L}_h/\mathcal{L}_s$, i.e. on the geometry, and on the form of the electron injection. Guided by the results from detailed fits to individual spectra, we choose a constant electron injection spectrum which has optical depth of unity, with the power split equally between non-thermal (power law of $\Gamma_{inj} = 2.5$ up to maximum Lorentz factor of 10^3) and thermal components.

Figure 1c shows a grid of colours resulting from the EQPAIR code for $\mathcal{L}_h/\mathcal{L}_s$ changing from 30 (top right of the diagonal branch) to 0.01 (softest hard colours), assuming seed photons from the disc at 0.3–1.2 keV as expected for the observed range in L/L_{Edd} for a standard disc. Changing only these two *physical* parameters can describe *all* the colour evolution seen from the GBH. These model spectra for each state are shown in the right-hand panel of Figure 2 (darker line, with higher disc temperature), with the dotted lines showing the energy range of the PCA data over which the colours are measured (DG03). These *same* models for the accretion flow (both qualitative and quantitative) can also explain the very different colours seen from the disc accreting neutron star systems. These have similar gravitational fields, so should have similar accretion flows, but with the addition of a boundary layer between the flow and the solid surface (DG03).

4. Application to Supermassive Black Holes

AGN accretion flows should be similar to those in GBH at the same L/L_{Edd} , except that the much larger mass black hole leads to a lower accretion disk temperature

(Shakura and Sunyaev, 1973). However, studying the AGN accretion flows is difficult as the black hole mass is much harder to determine, so giving large uncertainties on L/L_{Edd} . This problem can now be addressed using the recently discovered correlations of central black hole mass with the luminosity/velocity dispersion of the bulge, or the line width of the narrow line region, or reverberation mapping (e.g. Woo and Urry, 2002). The other problem is signal-to-noise, with only the ~ 10 brightest AGN having adequate spectra in RXTE. Again, this is now changing due to the unprecedented sensitivity of the EPIC camera (0.2–10 keV) on ESA's *XMM-Newton* satellite

If the models which describe the GBH spectra really do work then we can use the same code to *predict* what we should see from AGN, assuming that the *only* change in the accretion flow structure is due to the mass of the black hole changing the temperature of the disk. Since $kT_{\text{disk}} \propto M^{-1/4}$ for a given L/L_{Edd} then the GBH temperature range of 0.3–1.2 keV observed in the $10M_{\odot}$ stellar black holes scales to 5–20 eV for a 10^8M_{\odot} AGN. The grey lines in the spectral panels of Figure 2 show the effect of this seed photon temperature change on the EQPAIR Comptonised spectra assuming the *same geometries* as used for the GBH.

The vertical lines on these spectra show the relevant bandpasses of the *RXTE* PCA (GBHC: dashed line) and *XMM-Newton* EPIC instruments (AGN: dotted), respectively. Plainly these models predict that the analogue of the soft states in AGN will have no direct disk emission in the *XMM-Newton* bandpass. The predicted spectra are approximately power laws, and soft excesses should be weak and rare. For all the states, the lower seed photon temperature means that the comptonised spectra extend to lower energies and are slightly softer. Thus the soft state spectra always have comptonised emission with $\alpha > 1$, and even the hard state spectra have $\alpha > 0.8$.

The bright quasar sample are objects selected by their strong blue/UV continuum flux, i.e. have a strong accretion disc component so should correspond to the soft state. This is confirmed by their estimated L/L_{Edd} , with the majority spanning the range between $0.1 < L/L_{\text{Edd}} < 1$. We selected all the publicly available (as of September 2003) X-ray spectra from *XMM-Newton* archive. We fit these 26 objects with a continuum model consisting of two Comptonized components. The hot component produces the power-law spectrum, while the cool one gives freedom to model any soft X-ray excess. Contrary to expectations, *all* the objects *require* a soft excess component. Figure 3a shows the characteristics of the soft excess for each object, plotting temperature against strength of the soft excess, R_{exc} , measured by the ratio of unabsorbed 0.3–2 keV flux in the cool and hot components. The most striking property of the soft excess is its constancy in temperature. It is distributed in a very narrow range of values between 0.1 and 0.2 keV, and does not correlate in any way with the expected disc temperature estimated from black hole mass and L/L_{Edd} . Equally contrary to expectation is the spectral index of the hot comptonisation component. Figure 3b shows this plotted against the estimated L/L_{Edd} for each object. While there is the same general trend as in the GBHC

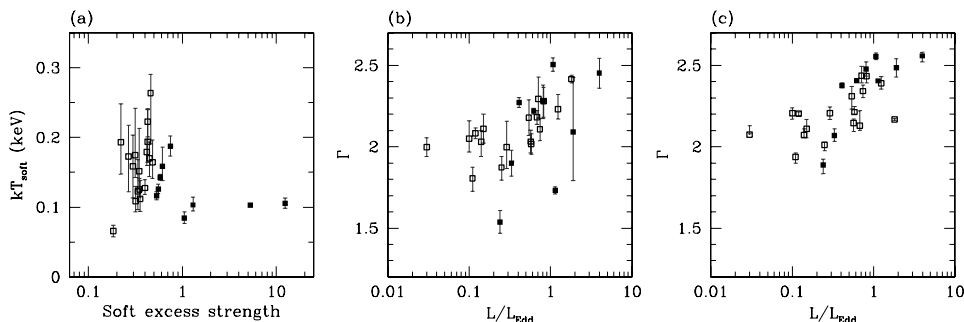


Figure 3.

for high L/L_{Edd} objects to be steeper, there are several AGN which are at high Eddington fractions which have $\alpha = \Gamma - 1 < 1$, and that many of these have strong soft X-ray excesses ($R > 0.5$), denoted by filled symbols (Gierliński and Done, 2004).

PG 1211+143 is the most extreme example of this in our sample. It has $\alpha \sim 0.8$ for the intrinsic (reflection and ionised absorption corrected) continuum, and also has a strong soft X-ray excess. Similar objects are also seen in the literature, with the strongest soft excesses often seen in Narrow Line Seyfert 1's (e.g. 1H 0419-577: Page et al., 2002; 1H 0707-495: Fabian et al., 2002). Plainly there are problems in a simple application of the GBH spectral models to AGN. Either the GBH models are wrong, or there are additional physical processes which break the scaling between AGN and GBH.

5. Additional Complexity in AGN Spectra?

One obvious candidate for additional complexity in the AGN spectra is the generic presence of partially ionised absorption. The environment around an AGN is often gas-rich, and X-ray illumination of distant material such as the molecular torus can form a partially ionised wind (Krolik and Kriss, 2001). However, changes in this absorption on fairly short timescales suggest that at least some component of this is directly associated with the disk (e.g. Pounds et al., 2003). The low disk temperature in AGN means that most of the disk material has substantial opacity from all elements except H and He. There are multiple line transitions from these elements in the UV band, where the disk spectra peak, so these can result in a strong line-driven wind from the disk. By contrast, the higher disk temperature in GBH means the disk has much lower opacity, predicting a much weaker wind (Proga and Kallman, 2002).

The gratings on *XMM-Newton* and *Chandra* have shown the ionised absorption in AGN in unprecedented detail. In general, multiple absorption components are

seen, with different outflow velocities, columns and ionisation states (e.g. Blustin et al., 2002). However, these absorbers are included in the fits to PG 1211+143, and make no substantial difference to the size of soft excess or hardness of the 2–10 keV spectrum. However, these absorption components are identified by their *narrow* atomic features, implying that the dispersion in velocity along the line of sight is rather small. This is *not* what is expected from the disc wind described above. Instead this should be differentially rotating, and outflowing, so has a very complex velocity structure which gives substantial *broadening* (Murray and Chiang, 1997).

We re-fit the data with a model in which there is only one Comptonised component, i.e. no additional soft excess, together with a simple model of the absorption expected from a discwind (an ionised absorber convolved with a Gaussian velocity dispersion). Figure 3c shows the new distribution of spectral indices with L/L_{Edd} . All the AGN now have intrinsically steep spectra ($\alpha > 1$) as expected for the supermassive analogues of the soft state GBHC. The typical velocity dispersions are $\sim 0.1 - 0.3c$, as expected if the wind is launched from close to the last stable orbit of the disc, and the columns required are $\sim 10^{21-23} \text{ cm}^{-2}$ (Gierliński and Done, 2004). Such absorption models can fit the data from individual bright objects as well as a separate soft excess component or ionised reflection (Sobolewska and Done, 2004).

6. Conclusions

All the data from the galactic black hole binaries are consistent with showing the same spectral evolution as a function of increasing L/L_{Edd} . This evolution can be qualitatively modeled by a change in the nature and geometry of the accretion flow, from a hot, geometrically thick plasma to a cool, geometrically thin disc. The implications of this on the emitted spectrum can be quantified using sophisticated comptonisation codes, and these can match the observed data. These models, with the addition of a boundary layer, can also explain the rather different spectral evolution seen from the disc accretion neutron star binary systems.

The comptonisation models can easily be scaled up to *predict* the spectra from AGN and quasars, assuming that the physics of the accretion flow is the same. However, these predictions conflict with the observed spectra of the PG quasar sample. These all have high L/L_{Edd} so should be soft state analogues of the GBHC, but several have rather hard 2–10 keV spectra, and all require an additional soft X-ray component which has no obvious counterpart in the GBHC. Instead we suggest that these spectra *are* as predicted by the models, but that our view of them is distorted by complex, partially ionised absorption from an accretion disc wind. The large velocity shifts in the wind smear the intrinsically narrow absorption features so that the material gives no clearly identifiable signal in high resolution grating data. The difference between the GBHC and AGN is then that the AGN have strong absorption from a discwind, while the GBHC do not. This can easily

be explained by the much lower disc temperature expected in supermassive black holes. Firstly this means that the disc itself retains substantial opacity, so there is much more line driving force for launching the wind, and secondly, heavy elements in the wind are less likely to be completely ionised, so have more effect on the X-ray spectrum. While such models are speculative, the alternative is that we missing some substantial piece of accretion physics in the galactic black hole models.

References

- Balbus, S.A. and Hawley, J.: 1991, *ApJ* **376**, 214.
Blandford, R. and Begelman, M.: 1999, *MNRAS* **303**, 1.
Coppi, P.S.: 1999, in *ASP Conf. Ser.* **161**, 375.
Dermer, C., Miller, J.A. and Li, H.: 1996, *ApJ* **456**, 106.
Done, C. and Gierliński, M.: 2003, *MNRAS* **342**, 1041. (DG03)
Esin, A.A., McClintock, J.E. and Narayan, R.: 1997, *ApJ* **489**, 865.
Fabian, A.C. et al.: 2002, *MNRAS* **331**, 35.
Frontera, F. et al.: 2001, *ApJ* **546**, 1027.
Gierliński, M. and Done, C.: 2003, *MNRAS* **342**, 1083.
Gierliński, M. and Done C.: 2004, *MNRAS* **349**, 7.
Gierliński, M. et al.: 1997, *MNRAS* **288**, 958.
Gierliński, M. et al.: 1999, *MNRAS* **309**, 496.
Haardt, F. and Maraschi, L.: 1993, *ApJ* **413**, 507.
Hawley, J.F. and Balbus, S.A.: 2002, *ApJ* **573**, 738.
Igumenshchev, I.V., Narayan, R. and Abramowicz, M.A.: 2003, *ApJ* **592**, 1042.
King, A.R. and Ritter, H.: 1998, *MNRAS* **293**, L42.
Krolik, J.H. and Kriss, G.A.: 2001, *ApJ* **561**, 684.
Kubota, A. and Done, C.: 2004, *MNRAS* **353**, 980.
Liu, S., Petrosian, V. and Melia F.: 2004, *ApJ* **611**, 101.
McConnell, M. et al.: 2002, *ApJ* **572**, 984.
Murray, N. and Chiang, J.: 1997, *ApJ* **474**, 91.
Narayan, R. and Yi, I.: 1995, *ApJ* **452**, 710.
Page, K. et al.: 2002, *MNRAS* **330**, 1.
Pounds et al.: 2003, *MNRAS* **342**, 1147.
Poutanen, J., Krolik, J.H. and Ryde, F.: 1997, *MNRAS* **292**, 21P.
Proga, D. and Kallman, T.R.: 2002, *ApJ* **565**, 455.
Shakura, N.I. and Sunyaev, R.A.: 1973, *A&A* **24**, 337.
Sobolewska, M. and Done, C.: 2004, in *XDAP 2004*, (astro-ph/0412513).
Tanaka, Y., Lewin, W.H.G.: 1995, in: W.H.G. Lewin, J. van Paradijs and E. van den Heuvel (eds.), *X-Ray Binaries*, Cambridge University Press, Cambridge, p. 126.
Turner, N.: 2004, *ApJL* **605**, L45.
Woo, J. and Urry, C.M.: 2002, *ApJ* **579**, 530.
Zdziarski, A.A. et al.: 2001, *ApJ* **554**, L45.
Zdziarski, A.A., Poutanen, J., Paciesas, W.S. and Wen, L.: 2002, *ApJ* **578**, 357.

LOW-LUMINOSITY ACCRETION IN BLACK HOLE X-RAY BINARIES AND ACTIVE GALACTIC NUCLEI

RAMESH NARAYAN

Harvard-Smithsonian Center for Astrophysics, 60 Garden Street, Cambridge, MA, U.S.A.;
E-mail: narayan@cfa.harvard.edu

(Received 1 November 2004; accepted 1 June 2005)

Abstract. At luminosities below a few percent of Eddington, accreting black holes switch to a hard spectral state which is very different from the soft blackbody-like spectral state that is found at higher luminosities. The hard state is well-described by a two-temperature, optically thin, geometrically thick, advection-dominated accretion flow (ADAF) in which the ions are extremely hot (up to 10^{12} K near the black hole), the electrons are also hot ($\sim 10^{9-10.5}$ K), and thermal Comptonization dominates the X-ray emission. The radiative efficiency of an ADAF decreases rapidly with decreasing mass accretion rate, becoming extremely low when a source reaches quiescence. ADAFs are expected to have strong outflows, which may explain why relativistic jets are often inferred from the radio emission of these sources. It has been suggested that most of the X-ray emission also comes from a jet, but this is less well established.

Keywords: accretion, accretion disks, active galactic nuclei, black hole physics, radiation mechanisms, X-rays: binaries

1. Introduction

The well-known thin accretion disk model has been a staple of accretion theory for more than 30 years (Shakura and Sunyaev, 1973; Novikov and Thorne, 1973). It provides a good description of the soft X-ray spectra of luminous black hole X-ray binaries (XRBs) in the high soft state (see McClintock and Remillard, 2004) and the big blue bump in the optical/UV spectra of bright quasars and active galactic nuclei (AGN; Malkan, 1983; but see Koratkar and Blaes, 1999). However, even from the earliest days (Tananbaum et al., 1972) it was realized that XRBs sometimes switch to a hard spectral state which requires the accreting gas to be hot and optically thin, quite different from the gas in a thin disk which is relatively cool and optically thick.

Observations of a number of XRBs have shown that, at luminosities below a few percent of Eddington, the sources enter the classic low hard state, and at much lower luminosities the quiescent state (McClintock and Remillard, 2004). Both states are characterized by very high temperatures ~ 100 keV or more, optically thin emission, and weak or absent soft X-ray emission. In the case of supermassive black holes, low-luminosity AGN (LLAGN) are noted for the absence of a big blue bump and the presence of substantial hard X-ray and radio emission (Ho, 1999; Quataert et al., 1999; Nagar et al., 2000). This again indicates that a standard thin



accretion disk is either absent or is energetically unimportant, and that a hot flow, similar to those seen in low-luminosity XRBS, is probably present.

In an important paper, Shapiro et al. (1976) introduced the idea of a two-temperature plasma and used it to develop a new hot accretion solution which is distinct from the standard thin disk. However, the solution turned out to be thermally unstable (Pringle, 1976). Fortunately, there is a second hot two-temperature solution called an advection-dominated accretion flow (ADAF; Narayan and Yi, 1994, 1995b; Abramowicz et al., 1995; see Narayan et al., 1988; Kato et al., 1998 for reviews). This solution, which is also referred to as a radiatively inefficient accretion flow (RIAF), was originally discussed in a forgotten paper by Ichimaru (1977; see also Rees et al., 1982). It has been shown to be effectively stable (Kato et al., 1997; Wu, 1997), and it is now recognized to be relevant for understanding low-luminosity accretion flows around black holes.

2. Advection-Dominated Accretion Flow

2.1. BASIC PROPERTIES

The energy equation of gas in a time-steady accretion disk may be written schematically as

$$q_{\text{adv}} \equiv \rho v \frac{T ds}{dR} = q_+ - q_-, \quad (1)$$

where q_{adv} is the rate of advection of energy per unit volume, ρ is the density, v is the radial velocity, T is the temperature, s is the specific entropy, R is the radius, q_+ is the viscous heating rate per unit volume, and q_- is the radiative cooling rate. A thin accretion disk is characterized by the condition $q_+ \sim q_- \gg q_{\text{adv}}$, i.e., viscous heating is balanced by radiative cooling. In contrast, an ADAF satisfies $q_+ \sim q_{\text{adv}} \gg q_-$, i.e., most of the viscous heat remains trapped in the gas (because the gas is radiatively inefficient), and the energy is advected in toward the BH. Technically, since the plasma is two-temperature, it is necessary to write separate energy equations for the ions and the electrons and to model the energy transfer between the two species by Coulomb collisions (Narayan and Yi, 1995b; Nakamura et al., 1997). We do not go into the details here and refer the reader to the review by Narayan et al. (1998).

The ADAF solution has a number of interesting properties:

- (i) The ion temperature varies roughly as $T_i \sim 10^{12} \text{ K}/r$, where $r = R/R_S$ is the radius in Schwarzschild units. The electron temperature, however, saturates at $T_e \sim 10^9 - 10^{10.5} \text{ K}$ for $r \lesssim 10^2 - 10^3$.
- (ii) The large ion temperature implies that the flow is geometrically thick. In fact, an ADAF might be viewed as the viscous rotating analog of spherical Bondi accretion.

- (iii) The gas in an ADAF is optically thin; therefore, the radiation from the hot electrons (which dominate the emission) is primarily by thermal Comptonization. Because Comptonization acts as a natural thermostat, the electron temperature is typically ~ 100 to a few 100 keV and varies by only a factor of a few over a wide range of Eddington-scaled accretion rate $\dot{m} = \dot{M}/\dot{M}_{\text{Edd}}$ (e.g., Esin et al., 1997, 1998; Zdziarski et al., 2003).
- (iv) The ADAF solution exists only for accretion rates \dot{m} below a certain critical rate \dot{m}_{crit} , whose value depends on the viscosity parameter α . For $\alpha \sim 0.1\text{--}0.25$, $\dot{m}_{\text{crit}} \sim 0.01\text{--}0.1$.

2.2. APPLICATION OF THE ADAF SOLUTION TO XRBS AND AGN

Rather miraculously, the properties of the ADAF solution are exactly what are needed to understand XRBS at low luminosities. The radiation in an ADAF is dominated by thermal Comptonization, in agreement with observations of XRBS in the low hard state. The electron temperature is about 100 keV, exactly what is needed to explain X-ray spectra in the low state (e.g., see the ADAF model of GRO J0422+32 shown in Figure 1). Finally, the critical $\dot{m}_{\text{crit}} \sim 0.01\text{--}0.1$ above which the ADAF solution ceases to exist is consistent with the luminosity at which the transition from the low hard state to the high soft state occurs in XRBS.

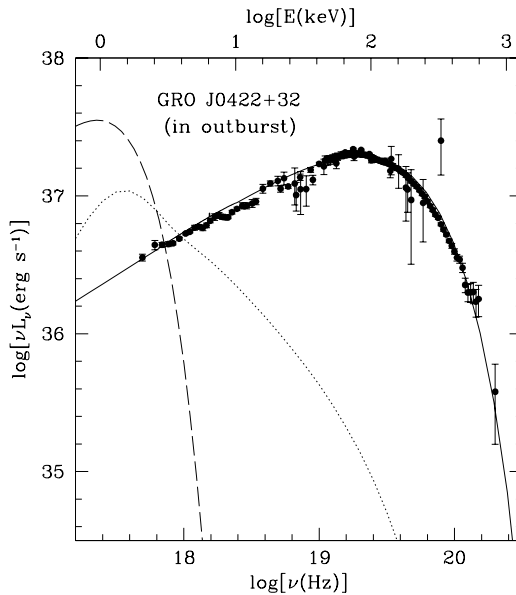


Figure 1. Combined TTM (2–20 keV), HEXE (20–200 keV), and OSSE (50–600 keV) spectrum of GRO J0422+32 in the low hard state. The solid line shows an ADAF fit to the spectrum. (From Esin et al., 1998)

By combining the thin accretion disk model and the ADAF model, Narayan (1996) and Esin et al. (1997) showed that it is possible to understand qualitatively the various spectral states of XRBs. According to their proposal (Figure 2), for $\dot{m} > \dot{m}_{\text{crit}}$, the accretion occurs primarily *via* a thin disk with a corona on top. This corresponds to the high soft state, with the disk providing the bulk of the radiation via a multicolor blackbody component and the corona contributing hard X-rays through Compton scattering (Haardt and Maraschi, 1991). Once \dot{m} falls below \dot{m}_{crit} , a hole opens up at the center of the disk and the hole is filled with a hot ADAF. For $\dot{m} \lesssim \dot{m}_{\text{crit}}$, the hole is relatively small and both the thin disk and the ADAF contribute roughly equally. This corresponds to the intermediate state. With decreasing \dot{m} , the transition radius r_{tr} between the two zones becomes larger and the ADAF dominates the energetics. At very low \dot{m} , i.e., in the quiescent state, r_{tr} is very large (>1000 , e.g., Narayan et al., 1996); in objects such as Sgr A* (Yuan et al., 2003), the outer thin disk may even disappear altogether.

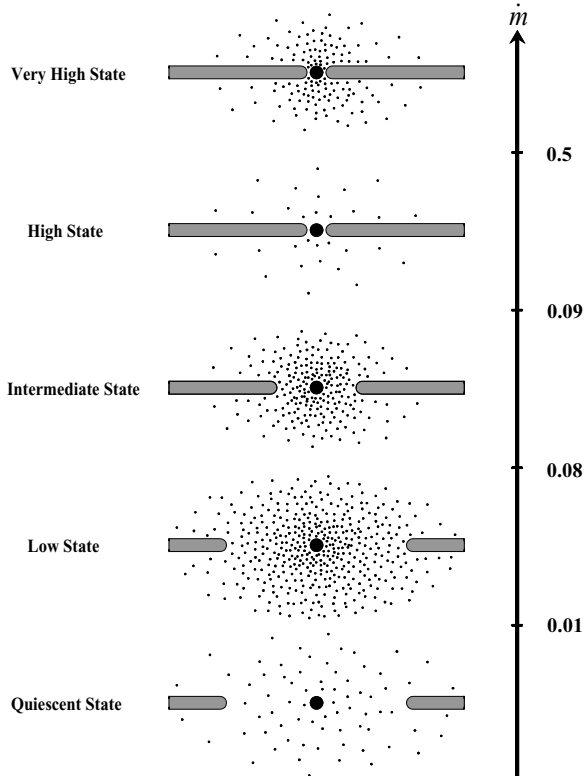


Figure 2. Configuration of the accretion flow around a black hole in different spectral states, shown schematically as a function of the Eddington-scaled mass accretion rate \dot{m} . The ADAF and the corona are indicated by dots and the thin disk by the shaded horizontal bars. (From Esin et al., 1997)

In the intermediate state and at the high end of the low state, the ADAF is only mildly advection-dominated, so the radiative efficiency is fairly large. However, with decreasing \dot{m} , the efficiency drops rapidly. Quiescent systems are, therefore, radiatively very inefficient; Sgr A*, for instance, has a luminosity that is only about 10^{-5} – 10^{-6} of the rate at which rest mass energy accretes from its surroundings (Yuan et al., 2003).

An ADAF has two sources of soft photons for Comptonization, and both are included in models (Narayan et al., 1997): (i) thermal synchrotron photons from the hot electrons in the ADAF (ii) thermal blackbody photons from the outer thin disk. The former dominates at low \dot{m} (quiescent state and lower end of low state) and the latter at higher \dot{m} (upper end of low state and intermediate state).

The above paradigm, which is based on the ADAF model or its variants (ADIOS, Blandford and Begelman, 1999; LHAF, Yuan, 2001; Yuan and Zdziarski, 2004; CDAF, Narayan et al., 2000; Quataert and Gruzinov, 2000), explains qualitatively many observations of XRBs (Esin et al., 1997, 1998, 2001; see Narayan et al., 1998 for other applications). Very recently, Meyer-Hofmeister et al. (2005) have suggested an interesting mechanism involving an interplay between Compton cooling and disk evaporation to explain the hysteresis phenomenon that has been identified in the high-to-low transition of black hole and neutron star X-ray binaries (Miyamoto et al., 1995; Nowak et al., 2002; Maccarone and Coppi, 2003; Zdziarski et al., 2004).

The ADAF model also explains a variety of observations of LLAGN: Sgr A* (Narayan et al., 1995; Yuan et al., 2003), LLAGN in giant ellipticals (Fabian and Rees, 1995; Reynolds et al., 1996; Di Matteo et al., 2003), and LINERs (Lasota et al., 1996; Quataert et al., 1999). In addition, it appears that ADAFs may be present in BL Lac objects (Maraschi and Tavecchio, 2003), FR I sources (Reynolds et al., 1996; Begelman and Celotti, 2004), XBONGs (Yuan and Narayan, 2004), and even some Seyferts (Chiang and Blaes, 2003). Overall, the model has turned out to be quite useful for providing a qualitative understanding of a variety of phenomena in low-luminosity accreting black holes (Quataert, 2001; Narayan, 2002).

2.3. TRANSITION RADIUS

A key element of the model shown in Figure 2 is that the transition radius r_{tr} between the outer thin disk and the inner ADAF varies with \dot{m} . But how exactly does it vary? To calculate this from first principles, one needs a physical theory of what causes the transition between the two kinds of flow. A number of ideas have been discussed in the literature and many efforts have been devoted to estimating $r_{\text{tr}}(\dot{m})$ theoretically (Meyer and Meyer-Hofmeister, 1994; Dullemond and Turolla, 1998; Liu et al., 1999; Rozanska and Czerny, 2000; Spruit and Deufel, 2002), but no model is presently able to provide robust predictions.

An alternative approach is to use the observations themselves to determine $r_{\text{tr}}(\dot{m})$. For a number of sources, by fitting observations one is able to obtain estimates of

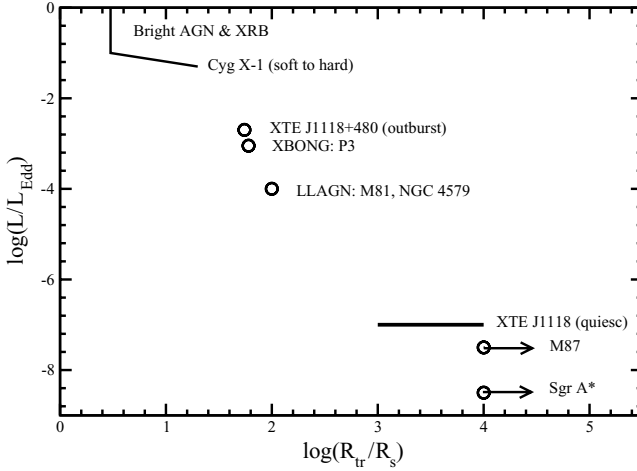


Figure 3. Bolometric luminosity in Eddington units (ordinate) vs. the transition radius in Schwarzschild units (abscissa) for different observed systems. (See Yuan and Narayan, 2004 for details)

the Eddington-scaled luminosity and mass accretion rate, as well as the transition radius. Although there are large uncertainties in some of these quantities, nevertheless the results are interesting when plotted, as discussed in Narayan et al. (1998) and Yuan and Narayan (2004). Figure 3 from the latter paper supports the basic features of the Esin et al. (1997) proposal; specifically, the transition radius r_{tr} seems to increase monotonically with decreasing luminosity, as postulated in the model. Interestingly, both XRBs and LLAGN are included in the plot, and the two classes of sources seem to follow more or less the same trend even though their masses are very different. This confirms that the physics of ADAFs is largely mass-independent (Narayan and Yi, 1995b), once all quantities are scaled suitably in terms of Eddington and Schwarzschild units.

3. Role of Jets

3.1. ADAFs, CONVECTION, OUTFLOWS, AND JETS

One of the interesting properties of ADAFs, highlighted already in the first papers (Narayan and Yi, 1994, 1995a), is that the accreting gas has a positive Bernoulli parameter, i.e., the gas is technically not bound to the BH. One expects, therefore, strong winds and outflows from an ADAF (Narayan and Yi, 1994, 1995a). Another property of ADAFs is that they have unstable entropy gradients and are hence violently unstable to convection (Begelman and Meier, 1982; Narayan and Yi, 1994, 1995a). Both effects have been seen in hydrodynamic and MHD simulations

of ADAFs (Stone et al., 1999; Igumenshchev and Abramowicz, 2000; Narayan et al., 2000; Stone and Pringle, 2001; Hawley and Balbus, 2002; Igumenshchev et al., 2003).

An important consequence of the above effects is that the mass that accretes onto the BH via an ADAF is much less than the mass supplied at the outer edge of the accretion flow. Blandford and Begelman (1999) suggested that the mass accretion rate may scale with radius as $\dot{m} \sim (r/r_{\text{out}})^s$. This scaling has been widely used in ADAF models (e.g., Quataert and Narayan, 1999). One problem is that the value of s cannot be estimated from first principles, though one may be able, in favorable cases, to fit s by comparison to observations. Yuan et al. (2003) estimated $s \sim 0.3$ for the accretion flow in Sgr A*. For this choice of s , the unusually low luminosity of the source is explained partly by the reduced mass accreting on the black hole ($\sim 10^{-2}$ of the mass available at the Bondi radius) and partly by the low radiative efficiency of the accreting gas ($\sim 10^{-3}$).

Once we recognize that ADAFs have powerful outflows, it is natural to think that these flows would have relativistic jets (Meier, 2001). Indeed, such a connection has been established fairly convincingly. XRBs in the low state generally have measurable radio emission, whereas sources in the high state do not. The radio emission has been resolved into a jet in Cyg X-1, and jets are inferred in other sources because of their large brightness temperatures (Fender, 2004). In the case of supermassive BHs again, it is found that LLAGNs are in general radio loud with high brightness temperatures (Nagar et al., 2000; Falcke et al., 2000). Also, BL Lacs, which have been associated with ADAFs (Maraschi and Tavecchio, 2003), are known to have strong jets. Apart from these experimental indications, there is also a strong theoretical argument for jets, viz., an ADAF simply cannot produce the large radio fluxes that are observed. The radio emission has to come from a volume much larger than the ADAF, which suggests that it must originate in a jet.

3.2. DOES THE JET DOMINATE THE HIGH ENERGY EMISSION IN ADAFS?

While the argument for the radio emission originating in a jet is clear, what about the X-ray emission? The ADAF model is quite successful in explaining the X-ray fluxes and spectra of low-luminosity black holes without invoking a jet (e.g., Figure 1). One source of particular interest is XTE J1118+480, for which a nearly complete spectrum has been measured in the low state (McClintock et al., 2001). Esin et al. (2001) proposed a model for this source in which (as in Figure 2) a thin disk is present outside a transition radius $r_{\text{tr}} \sim 50$ and an ADAF is present inside this radius. The model fits the spectral data in the optical, UV, and X-rays quite well.

Soon after this work, Markoff et al. (2001) proposed an alternative model in which they explained the entire spectrum of XTE J1118+480 from radio to X-rays

by means of synchrotron emission from a jet. (They invoked a standard disk for the optical and UV.) As described earlier, a jet is certainly expected in an ADAF system and it is quite natural for the jet to dominate in radio and perhaps infrared. What was surprising was that the Markoff et al. model was able to explain the X-ray emission with the same jet.

The case for a jet became stronger when Corbel et al. (2003) showed that there is a strong correlation between the radio and X-ray emission in the black hole XRB GX 339-4 in the low state and quiescent state. They suggested that a significant fraction of the X-ray emission may originate in a jet. Interestingly, both Markoff et al. and Corbel et al. require a radiatively inefficient ADAF to be present since a radiatively efficient disk would swamp the jet emission in their model. However, the ADAF is postulated to be virtually silent even in the X-ray band, and it is the jet that produces most of the observed radiation.

Heinz and Sunyaev (2003) studied the jet model and worked out a scaling relation between the synchrotron flux at a given frequency, the mass of the black hole, and the mass accretion rate. Their model is applicable to jets anchored in either an ADAF or a standard disk. Merloni et al. (2003) extended this work and showed that accreting black holes follow quite well a “fundamental plane” in the three-dimensional parameter space of radio luminosity, X-ray luminosity, and black hole mass. However, they came down in favor of the ADAF rather than the jet as the source of the X-ray emission in the low hard state. Falcke et al. (2004) argued instead that synchrotron emission from the jet is the source of the X-rays. In a recent paper, Heinz (2004) has presented additional arguments why a synchrotron jet is unlikely to explain the X-ray emission in low hard state binaries.

Apart from the above contradictory arguments, Zdziarski et al. (2003) have presented possible additional difficulties with a jet interpretation of the X-ray emission in the low state. They claim that synchrotron emission cannot produce as sharp a cutoff at high energies as observed (e.g., see the spectrum shown in Figure 1). Also, the predicted spectrum is not as hard as the spectra observed in some low state XRBs. Finally, the fact that the cutoff occurs near 100 or a few 100 keV in several sources (in fact, all sources in which a cutoff has been seen) does not find a natural explanation in the jet model; it requires a degree of fine-tuning of the power-law energy distribution of the radiating electrons. In the ADAF model, on the other hand, thermal Comptonization acts as a thermostat that naturally produces a temperature of the order of 100 keV.

Recently, Yuan et al. (2005) and Malzac et al. (2004) have come up with a jet-ADAF model of J1118+480 in which a jet produces most of the radio and infrared emission, the ADAF produces the X-ray emission, and the outer thin disk produces the optical and UV emission. The model fits the spectral data satisfactorily and also explains the timing and variability data qualitatively. By combining the best features of the ADAF model and the jet model, this work appears to represent an interesting compromise between the two models.

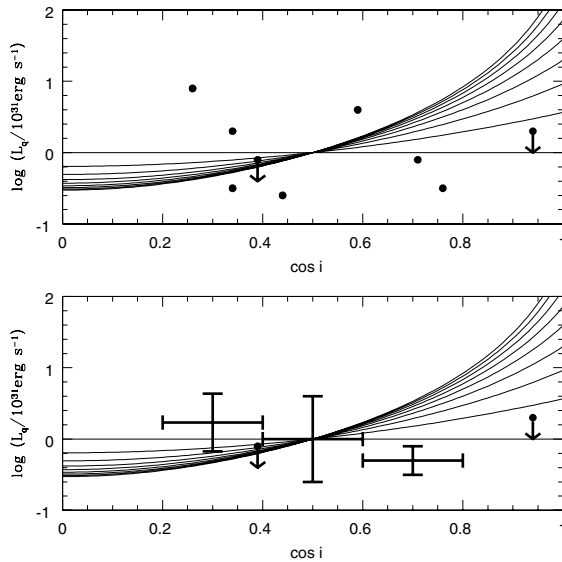


Figure 4. Upper panel: X-ray luminosities of quiescent black hole XRBs in units of 10^{31} erg/s plotted against the cosine of the inclination angle i . The curves indicate the expected variation according to a jet model for different choices of the jet Lorentz factor: $\gamma = 1.0$ (horizontal line), 1.2, 1.4, . . . , 2.6. Lower panel: The same data grouped into bins of width 0.2 in $\cos i$. (From Narayan and McClintock, 2005)

3.3. IS THE X-RAY EMISSION BEAMED?

The most obvious feature of a jet is that it involves outward motion of gas at relativistic speeds. It is therefore natural to expect evidence in the data for relativistic beaming. Observations, however, generally indicate that beaming is not very pronounced. Gallo et al. (2003) and Fender et al. (2004) estimated an upper limit of $\gamma \sim 2$ for the Lorentz factor of the radio-emitting material, while Maccarone (2003) deduced $\gamma \leq 1.4$ for the X-ray-emitting gas in GRO J1655-40.

Figure 4 shows analogous results for the quiescent state of XRBs. Assuming the X-ray emission is from a jet, the different curves show the expected variation of the observed flux as a function of the binary inclination i for different choices of the jet Lorentz factor γ . The calculations assume that the jet is oriented perpendicular to the binary orbit, and the curves have been normalized so as to have the same flux density for $\cos i = 0.5$. Overplotted on the curves are the quiescent X-ray luminosities of a number of black hole XRBs. We see that there is no hint in the data for any increase in the observed luminosity of low-inclination systems ($\cos i \rightarrow 1$). In fact, the most pole-on system in the sample, 4U1543-47, with $i \approx 21^\circ$, has a 95% confidence upper limit on its quiescent luminosity that is below the predicted luminosity for all reasonable values of γ . By visual inspection we conclude that, if the X-ray emission is from a jet, then the Lorentz factor is limited to $\gamma \lesssim 1.2$.

A likely explanation for the data is that the X-ray emission is not primarily from an outflowing jet but from an orbiting ADAF. Note, however, that the argument assumes the jet to be oriented perpendicular to the accretion disk which is not supported by the limited data available (see Narayan and McClintock, 2005).

Jet models generally have radio emission coming from farther out in the jet and X-ray emission from closer to the center. In fact, often the X-rays are postulated to be emitted from the “base of the jet.” In this context, we should note that the base of the jet is probably right inside the ADAF. It then becomes a matter of semantics whether this gas should be called the jet or the ADAF. If the gas were moving rapidly away from the accreting gas and we could see clear evidence for beaming, then we could of course confidently claim that it is a jet. However, as mentioned above, there is no evidence yet for relativistic beaming in either the low state or the quiescent state.

The other distinguishing feature of the jet model is that it invokes synchrotron radiation from nonthermal electrons to explain the X-ray emission. The ADAF model, in contrast, makes use of thermal Comptonization. As mentioned above, the synchrotron model has some difficulty explaining certain aspects of the X-ray spectrum. Nevertheless, the arguments are probably not insurmountable, so the model must be considered viable. If, however, it turns out that the synchrotron idea cannot be made to work for the X-ray emission, and if one needs to invoke something like thermal Comptonization in the jet to explain the data, then the argument for the jet would be significantly weakened. Why refer to it as a jet if the gas is located inside the ADAF, is not moving rapidly, and has all the characteristics of the hot gas in an ADAF? For all practical purposes, such a model would be identical to the jet-ADAF model of Yuan et al. (2005) and Malzac et al. (2004) in which the low-energy radio (and infrared) emission comes from a *bona fide* jet, but the high energy X-ray emission comes from an ADAF. (Malzac et al. also discuss the possibility that the X-rays may come from a patchy corona rather than a standard ADAF.)

One issue still remains to be addressed, viz., the Corbel et al. (2003) correlation between the radio and X-ray emission. This correlation finds a natural explanation in the jet model, but is not so obvious if the X-rays originate in an ADAF. If the jet is part of the general outflow from the ADAF as we have suggested above, then it is conceivable that there would be a correlation between the properties of the jet and those of the ADAF. In this case, even though the radio and the X-rays come from different parts of the system (jet and ADAF, respectively), there might still be a strong correlation between the two. This possibility is discussed in Meier (2001) and needs to be investigated quantitatively.

Acknowledgement

The author thanks Tom Maccarone for comments. This work was supported in part by grants NAG5-10780 from NASA and AST 0307433 from NSF.

References

- Abramowicz, M.A., Chen, X., Kato, S., Lasota, J.-P. and Regev, O.: 1995, *ApJ* **438**, L37.
- Begelman, M.C. and Celotti, A.: 2004, *MNRAS* **352**, L45.
- Begelman, M.C. and Meier, D.L.: 1982, *ApJ* **253**, 873.
- Blandford, R.D. and Begelman, M.C.: 1999, *MNRAS* **303**, L1.
- Chiang, J. and Blaes, O.: 2003, *ApJ* **586**, 97.
- Corbel, S., Nowak, M.A., Fender, R.P., Tzioumis, A.K. and Markoff, S.: 2003, *A&A* **400**, 1007.
- di Matteo, T., Allen, S.W., Fabian, A.C., Wilson, A.S. and Young, A.J.: 2003, *ApJ* **582**, 133.
- Dullemond, C.P. and Turolla, R.: 1998, *ApJ* **503**, 361.
- Esin, A.A., McClintock, J.E., Drake, J.J., Garcia, M.R., Haswell, C.A., Hynes, R.I. and Muno, M.P.: 2001, *ApJ* **555**, 483.
- Esin, A.A., McClintock, J.E. and Narayan, R.: 1997, *ApJ* **489**, 865.
- Esin, A.A., Narayan, R., Cui, W., Grove, J.E. and Zhang, S.-N.: 1998, *ApJ* **505**, 854.
- Fabian, A.C. and Rees, M.J.: 1995, *MNRAS* **277**, L5.
- Falcke, H., K rding, E. and Markoff, S.: 2004, *A&A* **414**, 895.
- Falcke, H., Nagar, N.M., Wilson, A.S. and Ulvestad, J.S.: 2000, *ApJ* **542**, 197.
- Fender, R.P.: 2004, in: W.H.G. Lewin and M. van der Klis (eds.), *Compact Stellar X-ray Sources*, Cambridge University Press, New York, in press (astro-ph/0303339).
- Fender, R.P., Belloni, T.M. and Gallo, E.: 2004, *MNRAS* **355**, 1105.
- Gallo, E., Fender, R.P. and Pooley, G.G.: 2003, *MNRAS* **344**, 60.
- Haardt, F. and Maraschi, L.: 1991, *ApJ* **380**, L51.
- Hawley, J.F. and Balbus, S.A.: 2002, *ApJ* **573**, 738.
- Heinz, S.: 2004, *MNRAS* **355**, 835.
- Heinz, S. and Sunyaev, R.: 2003, *MNRAS* **343**, L59.
- Ho, L.C.: 1999, *ApJ* **516**, 672.
- Ichimaru, S.: 1977, *ApJ* **214**, 840.
- Igumenshchev, I.V. and Abramowicz, M.A.: 2000, *ApJ* **537**, L27.
- Igumenshchev, I.V., Narayan, R. and Abramowicz, M.A.: 2003, *ApJ* **592**, 2042.
- Kato, S., Fukue, J. and Mineshige, S.: 1998, *Black Hole Accretion Disks*, Kyoto University Press, Kyoto, Japan.
- Kato, S., Yamasaki, T., Abramowicz, M.A. and Chen, X.: 1997, *PASJ* **49**, 221.
- Koratkar, A. and Blaes, O.: 1999, *PASP* **111**, 1.
- Lasota, J.P., Abramowicz, M.A., Chen, X., Krolik, J., Narayan, R. and Yi, I.: 1996, *ApJ* **462**, 142.
- Liu, B.F., Yuan, F., Meyer, F., Meyer-Hofmeister, E. and Xie, G. Z.: 1999, *ApJ* **527**, L17.
- Maccarone, T.: 2003, *A&A* **409**, 697.
- Maccarone, T.J. and Coppi, P.S.: 2003, *MNRAS* **338**, 189.
- Malkan, M.A.: 1983, *ApJ* **268**, 582.
- Malzac, J., Merloni, A. and Fabian, A.C.: 2004, *MNRAS* **351**, 253.
- Maraschi, L. and Tavecchio, F.: 2003, *ApJ* **593**, 667.
- Markoff, S., Falcke, H. and Fender, R.P.: 2001, *A&A* **372**, L25.
- McClintock, J.E., Haswell, C.A., Garcia, M.R., Drake, J.J., Marshall, R.I. and Muno, H.L.: 2001, *ApJ* **555**, 477.
- McClintock, J.E. and Remillard, R.A.: 2004, in: W.H.G. Lewin and M. van der Klis (eds.), *Compact Stellar X-ray Sources*, Cambridge University Press, in press (astro-ph/0306213 v4).
- Meier, D.L.: 2001, *ApJ* **548**, L9.
- Merloni, A., Heinz, S. and Di Matteo, T.: 2003, *MNRAS* **345**, 1057.
- Meyer, F. and Meyer-Hofmeister, E.: 1994, *A&A* **361**, 175.
- Meyer-Hofmeister, E., Liu, B.F. and Meyer, F.: 2005, *A&A* **432**, 181.
- Miyamoto, S., Kitamoto, S., Hayashida, K. and Egoshi, W.: 1995, *ApJ* **442**, L13.

- Nagar, N.M., Falcke, H., Wilson, A.S. and Ho, L.C.: 2000, *ApJ* **542**, 186.
- Nakamura, K.E., Kusunose, M., Matsumoto, R. and Kato, S.: 1997, *PASJ* **49**, 503.
- Narayan, R.: 1996, *ApJ* **461**, 136.
- Narayan, R. 2002, in: M. Gilfanov and R. Sunyaev (eds.), *Lighthouses of the Universe*, Springer, Berlin.
- Narayan, R., Barret, D. and McClintock, J.E.: 1997, *ApJ* **482**, 448.
- Narayan, R., Igumenshchev, I.V. and Abramowicz, M.A.: 2000, *ApJ* **539**, 798.
- Narayan, R., Mahadevan, R. and Quataert, E.: 1998, in: M.A. Abramowicz, G. Bjornsson and J.E. Pringle (eds.), *The Theory of Black Hole Accretion Discs*, Cambridge University Press, New York, p. 148.
- Narayan, R. and McClintock, J.E.: 2005, *ApJ* **623**, 1017.
- Narayan, R., McClintock, J.E. and Yi, I.: 1996, *ApJ* **457**, 821.
- Narayan, R. and Yi, I.: 1994, *ApJ* **428**, L13.
- Narayan, R. and Yi, I.: 1995a, *ApJ* **444**, 231.
- Narayan, R. and Yi, I.: 1995b, *ApJ* **452**, 710.
- Narayan, R., Yi, I. and Mahadevan, R.: 1995, *Nature* **374**, 623.
- Novikov, I.D. and Thorne, K.S.: 1973, in: C. DeWitt and B. DeWitt (eds.), *Blackholes*, Gordon and Breach, New York, p. 343.
- Nowak, M.A., Wilms, J. and Dove, J.B.: 2002, *MNRAS* **332**, 856.
- Pringle, J.E.: 1976, *MNRAS* **177**, 65.
- Quataert, E.: 2001, in: B.M. Peterson, R.S. Polidan and R.W. Pogge (eds.), *Probing the Physics of Active Galactic Nuclei by Multiwavelength Monitoring*, Astronomical Society of the Pacific, San Francisco, p. 71.
- Quataert, E., di Matteo, T., Narayan, R. and Ho, L.C.: 1999, *ApJ* **525**, L89.
- Quataert, E. and Gruzinov, A.: 2000, *ApJ* **539**, 809.
- Quataert, E. and Narayan, R.: 1999, *ApJ* **520**, 298.
- Rees, M.J., Begelman, M.C., Blandford, R.D. and Phinney, E.S.: 1982, *Nature* **295**, 17.
- Reynolds, C.S., di Matteo, T., Fabian, A.C., Hwang, U. and Canizares, C.R.: 1996, *MNRAS* **283**, L111.
- Rozanska, A. and Czerny, B.: 2000, *A&A* **360**, 1170.
- Shakura, N.I. and Sunyaev, R.A.: 1973, *A&A* **24**, 337.
- Shapiro, S.L., Lightman, A.P. and Eardley, D.M.: 1976, *ApJ* **204**, 187.
- Spruit, H.C. and Deufel, B.: 2002, *A&A* **387**, 918.
- Stone, J.M. and Pringle, J.E.: 2001, *MNRAS* **322**, 461.
- Stone, J.M., Pringle, J.E. and Begelman, M.C.: 1999, *MNRAS* **310**, 1002.
- Tananbaum, H., Gursky, H., Kellogg, E., Giacconi, R. and Jones, C.: 1972, *ApJ* **177**, L5.
- Wu, X.B.: 1997, *MNRAS* **292**, 113.
- Yuan, F.: 2001, *MNRAS* **324**, 119.
- Yuan, F., Cui, W. and Narayan, R.: 2004, *ApJ* **620**, 905.
- Yuan, F. and Narayan, R.: 2004, *ApJ* **612**, 724.
- Yuan, F., Quataert, E. and Narayan, R.: 2003, *ApJ* **598**, 301.
- Yuan, F. and Zdziarski, A.A.: 2004, *MNRAS* **354**, 953.
- Zdziarski, A.A., Gierlinski, M., Mikolajewska, J., Wardzinski, G., Smith, D.M., Alan, H.B. and Kitamoto, S.: 2004, *MNRAS* **351**, 791.
- Zdziarski, A.A., Lubinski, P., Gilfanov, M. and Revnivtsev, M.: 2003, *MNRAS* **342**, 355.

EXPLORING THE JET/ACCRETION FLOW RELATIONSHIP IN LOW DISK LUMINOSITY SOURCES*

SERA MARKOFF

MIT, Center for Space Research, Cambridge, MA, USA; E-mail: sera@alum.mit.edu

(Received 20 October 2004; accepted 1 June 2005)

Abstract. Astrophysical jets seem to gain strength disproportionate to the power of their associated accretion flow, making low-luminosity sources ideal targets for studies of the role of outflows. Radio/X-ray correlations have supported the case for a strong relationship between the jets and the hard X-ray emitting regions, and here we explore the strongest scenario where the base of the jets subsumes the role of the corona. The properties of coronae, as inferred from spectral models, are very similar to what is empirically required at jet bases assuming conservation laws hold. We present a few preliminary fits to simultaneous radio and X-ray datasets from our GX 339–4 and Cyg X-1 campaigns. The fits are performed in detector space, and include a jet plus thermal disk continuum model, with added Gaussian line and non-relativistic reflection features similar to the approach of other X-ray models. We find that we can fit the entire radio through X-ray spectrum quite well, with any deviation occurring in the line/reflection region. The results suggest that a jet/corona unification can provide a reasonable description of the data. Future work will benefit from a more complex approach to the disk feedback features.

Keywords: X-rays: binaries, black hole physics, radiation mechanisms: non-thermal, accretion, accretion disks, X-rays: general

1. Introduction

Relativistic outflows have been considered part of the big picture for active galactic nuclei (AGN) almost since their discovery, simply because their scales are so large compared to the host galaxy in radio frequencies. The confirmation that jets also exist in smaller accreting compact objects, such as X-ray binaries (XRBs), was not fully established until the late 1970s (SS433; Spencer, 1979). However, XRB jets continued to be treated as distinct components until fairly recently, when correlations between the radio and X-ray luminosities were discovered in the hard state of GX 339–4 (Hannikainen et al., 1998; Corbel et al., 2000, 2003). This correlation is now thought to be fundamental to accreting black holes (Gallo et al., 2003; Merloni et al., 2003; Falcke et al., 2004). The realization that the correlation scales with mass has provided a new method of comparison between AGN and XRBs, and for the exploration of the spectral roles of the individual components.

*NSF Astronomy & Astrophysics Postdoctoral Fellow.



Despite this progress, the details of the inflow/outflow interface are still a matter of significant debate. The nature of the connection is important for models of jet formation, and in general our understanding of the effects of strong gravitational fields on magneto-hydrodynamical plasmas. An important way to approach this problem is to create physical models which consider the system holistically, by both predicting the broadband spectra at the same time as addressing fine features specific to the X-ray band. Since the radio emission in these sources is accepted to come from jets we have a solid anchor for models which probe how jets relate to the X-ray emission.

Low disk luminosity systems are characterized by their sub-Eddington accretion rates and steady compact jets. They are advantageous sources for this study because one can avoid the complications of high accretion rates as seen in, e.g., AGN, especially near the base of the jets where the physics is most in question. Furthermore, because the evidence is increasing that jets dominate the power at low luminosities (e.g., Fender et al., 2003; Malzac et al., 2004) we can better hope to isolate the roles of jets in these sources.

2. Model Background

2.1. JET MODEL DEVELOPMENT

We first explored scaling jet models for Sgr A*, whose quiescent and flared emission can be explained via synchrotron radiation in the radio frequencies, and synchrotron and/or synchrotron self-Compton (SSC) in the X-ray band (Falcke and Markoff, 2000; Markoff et al., 2001b). This model scales with the central mass and accretion power, and thus in principle can be applied to XRBs as well. XTE J1118 + 480 was the ideal test source, with its unprecedented high-quality broadband, quasi-simultaneous data (Hynes et al., 2000; McClintock et al., 2001, and references therein). We had originally set out to model the radio spectrum via synchrotron emission, but it was immediately apparent that the scaling resulted in the optically thick-to-thin break occurring in the infrared/optical bands. More importantly, we found that if a power law distribution of energetic particles exists further out in the jet, it is in fact quite difficult to suppress the optically thin synchrotron radiation from extending out into the X-ray band (Markoff et al., 2001). An accelerated power law distribution of particles is motivated by observations of optically thin emission during radio outbursts in XRBs (e.g., Fender and Kuulkers, 2001) and AGN (e.g., Marscher and Gear, 1985). The jet synchrotron-dominated model presented in Markoff et al. (2001) gives a good description of the broad spectral features of XTE J1118+480, with the ~ 100 keV cutoff following from acceleration saturated by synchrotron cooling. Thermal emission from the inner edge of an accretion disk was included in the calculation both as a weak direct component and as seed photons for inverse Compton scattering, but was not the dominant emission component.

We next considered this model for 13 (quasi)-simultaneous radio/X-ray (and sometimes IR) datasets for GX 339–4 (Corbel et al., 2003). We found again that jet synchrotron could explain the broadband continuum spectra of all the observations, mainly by just varying the power input into the jet (Markoff et al., 2003). We showed in this paper that jet synchrotron emission analytically predicts the slope of the radio/X-ray correlation as a consequence of its scaling with power.

In summary, these simple synchrotron-dominated jet models significantly developed our understanding of the radio/X-ray correlations and scaling. However, they did not attempt to address the fine features in the X-ray spectrum, which are harbingers of interactions with cooler accretion disk material.

2.2. JET/CORONA RELATIONSHIP

Accounting for the hard state X-ray power law spectrum, in combination with the line emission/reflection features attributed to interaction with the accretion disk, led to the development of the corona/disk model (e.g., Haardt and Maraschi, 1991; George and Fabian, 1991). The corona is inferred from X-ray signatures to have several properties, such as quasi-thermal electrons in a reasonably compact geometry. The fraction of reflected hard X-ray emission is often low in the hard state, and this fact is sometimes problematic for corona models (Dove et al., 1997). Various mechanisms have been proposed to decrease the fraction of reflected X-rays, including patchy coronae (Stern et al., 1995), high disk ionization (Ross et al., 1999; Nayakshin, 2000; Ballantyne et al., 2001) and beaming of the coronae away from the disk with mildly relativistic velocities (Beloborodov, 1999; Malzac et al., 2001). This latter approach seems extremely close in principle to the characteristics of the base of a jet.

Unlike coronae jets are observed explicitly: the synchrotron emission tells us that there is a population of accelerated leptons quite far out in the jet. If one believes that there is rough conservation of properties along the jet, then tracing back to the base requires hotter leptons in even denser populations threaded by even stronger magnetic fields. At the same time, magnetohydrodynamical simulations of the inner disk region do not show anything like a stable sphere/disk geometry, but rather a region threaded with fields which naturally leads to outflowing plasma (corona) (e.g., Stone and Pringle, 2001). This beaming will reduce the relevance of the already weak thermal disk photons with respect to locally created photons and lead to an altogether different picture than the static case. We think it is worth exploring the most extreme, and thus easiest to test, case scenario: whether the base of the jets can “subsume” the role of the corona. This is a critical step in the process of disentangling their actual relationship, since if the approach fails, where and how it fails will provide clues as to the nature of the corona as a distinct component. If it does not fail, it may help point the way towards a better understanding of jet formation.

2.3. MODEL BACKGROUND

A more detailed explanation can be found in other papers (Markoff et al., 2001; Markoff et al., 2003; Markoff, Nowak and Wilms, 2005) but the basic model is a freely expanding jet which has a velocity gradient due to acceleration along its axis. Plasma enters the jet at the base, and the radiation is dominated by quasi-thermal leptons which cool radiatively and adiabatically as the jet expands. Further out in the jet the particles encounter an acceleration region where some of them are accelerated into a power law tail. The particles radiate along the entire jet via synchrotron, synchrotron self-Compton (SSC) and external Compton (EC) radiation. The EC only contributes very close to the base of the jet, where it can be comparable to the SSC, both of which contribute to the hard X-rays. Synchrotron emission from $\sim 100 r_g$ dominates in the radio/IR bands, turning over to contribute in the X-ray band.

Our currently favored model is a direct result of our work in (Markoff and Nowak, 2004), where we calculated the reflection from typical jet models based on GX 339–4 spectra. We found this a very useful probe of the geometry of jet emitting regions, which helped define our latest models. If the acceleration region really exists further out in the jet, as we have found for several fits, then the weakly beamed synchrotron radiation cannot result in more than a few percent reflection (assuming perpendicular geometry and a flat disk). SSC near the base of the jets, however, can easily give $\lesssim 20\%$ in the simplest case.

In order to address the fine features of the X-ray spectrum in a statistical manner, we needed to import this model into X-ray data analysis software. Currently it is running in XSPEC and ISIS, and the figures here were made with the latter program. In comparison to models which focus exclusively on the X-ray frequencies, however, we are also importing and fitting the simultaneous radio data with our model. Within the program, we added a single Gaussian line to our continuum model, and allowed it to vary between 6–7 keV. We then convolved the entire spectrum with a non-relativistic reflection model derived from the Greens functions of (Magdziarz and Zdziarski, 1995). Because of the complexities of directly calculating the interaction of jet photons with the accretion disk (see Markoff and Nowak, 2004), we could not self-consistently include these features but include the strength of the reflection hump as a free parameter. This is similar to the general approach chosen by pure Comptonization models (e.g., Coppi, 1992a; Poutanen, 1998). The full calculation of these features requires a Monte Carlo approach, which we will consider elsewhere.

3. Results

Here, we present the best and worst fits so far from three data sets of Cyg X-1 which span its typical range in hard-state spectral characteristics (Figures 1 and 2, respectively). GX 339–4 varies mainly in luminosity rather than spectral shape,

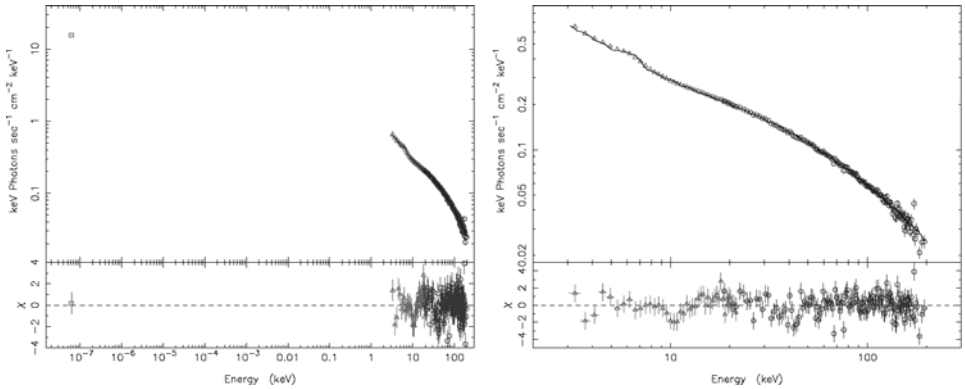


Figure 1. The best fit so far of our three Cyg X-1 simultaneous radio/X-ray observations which span its typical spectral variations in the hard state, $\chi^2 = 208.4/183 = 1.14$. The figures show the unfolded fit plus residuals with an absorbed jet model (including a thermal accretion disk component) plus Gaussian line, convolved with non-relativistic reflection. (a) The entire broadband fit, including the radio data point, (b) close-up on the X-ray bands. X-ray data are from RXTE PCA and HEXTE, radio from the Ryle Telescope.

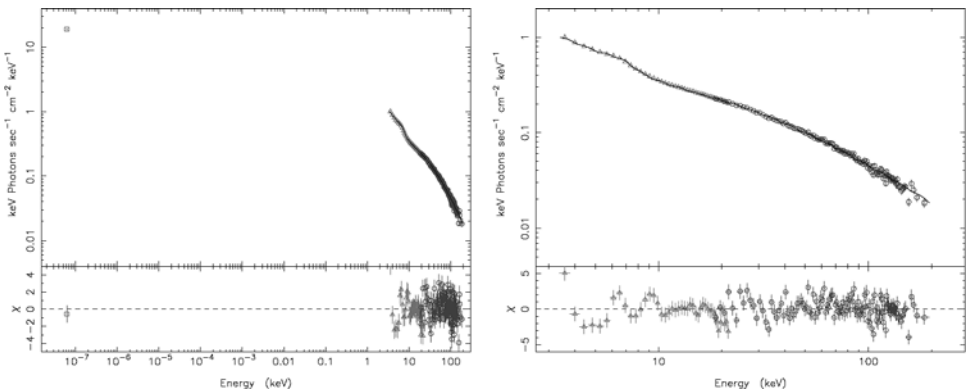


Figure 2. The worst fit so far of our three Cyg X-1 simultaneous radio/X-ray observations which span its typical spectral variations in the hard state, $\chi^2 = 278/162 = 1.72$. Otherwise same format as Figure 1.

and so we present just one typical fit in Figure 3. The data come from the Rossi X-ray Timing Explorer (RXTE), using both the Proportional Counter Array (PCA) and the High Energy X-ray Timing Experiment (HEXTE; Rothschild et al., 1998), extracted with the newest release of the RXTE software, HEASOFT 5.3.1. The radio data come from the ATCA (GX 339–4) and Ryle (Cyg X-1) instruments.

4. Discussion

The fits presented here are comparable to fits of the X-ray data alone made with broken power law models (Nowak, this volume), and thermal Comptonization

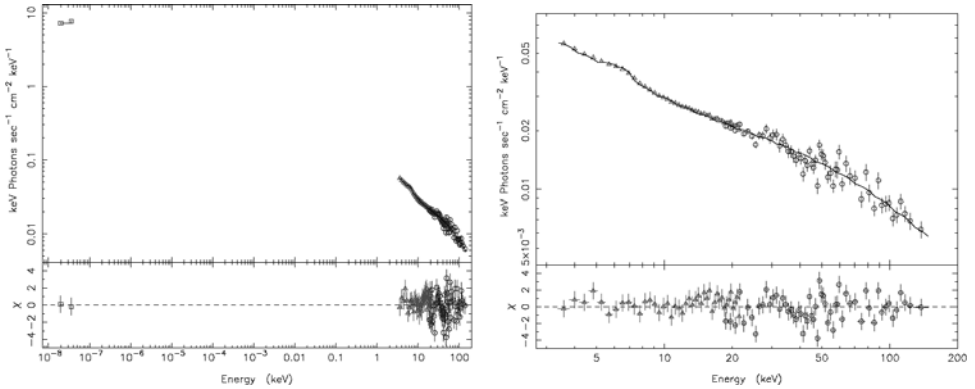


Figure 3. Typical fit from three simultaneous radio/X-ray observations of GX 339–4 which span its luminosity variations in the hard state, $\chi^2 = 138.3/96 = 1.44$. Otherwise same format as Figures 1 and 2.

models (e.g. EQPAIR, Coppi, 1999b). Unfortunately, the multicomponent jet model currently runs significantly slower than single-component corona models, which means we are not able to explore the same amount of parameter space in a reasonable amount of time (yet). However, it is important to realize that since we are including the radio self-consistently, we have a more holistic approach to a system we know is coupled. The main thing to note is that the cutoff region is not where the fit has its limitations, but rather in the line/reflection regime. This is most likely due to the lack of time for finding slightly better parameters, as well as the use of simple, non-relativistic, non-ionized models for the disk component. Secondly, the reflection fractions required for these fits are lower than those inferred for thermal Comptonization models ($\sim 5\text{--}10\%$ compared to $15\text{--}20\%$). This is mainly due to differences in the shape of the continuum for the two types of models, because in the jet model the SSC component already lends its curvature to the hard X-rays, reducing the need for strong reflection. At the same time, these lower reflection fractions are entirely consistent with our estimations of reflection from jet models, and thus demonstrates that the phenomenology of reflection is very dependent on assumptions of the impinging continuum.

So far it seems a model where the jet takes over the role of the corona, or includes it, is statistically feasible. The next step is to consider tighter constraints on the shape of the spectrum at the highest energies near the cutoff, which may break some of the degeneracy. The upcoming mission ASTRO-E2 will hopefully provide useful data for these tests. Similarly, timing studies will be valuable for further constraining the location of the emitting regions.

Acknowledgements

Some parts of this talk evolved into Markoff, Nowak and Wilms (2005), and so thanks go to my collaborators Michael Nowak and Jörn Wilms. I would also like

to thank Heino Falcke, Stéphane Corbel and Rob Fender for their collaboration in the earlier development of this work, as well as Guy Pooley for his persistent monitoring of Cyg X-1. Support for this work was provided by an NSF Astronomy & Astrophysics postdoctoral fellowship under NSF Award AST-0201597, as well as NSF grant INT-0233441.

References

- Ballantyne, D.R., Iwasawa, K. and Fabian, A.C.: 2001, *MNRAS* **323**, 506.
- Beloborodov, A.M.: 1999, *ApJ* **510**, L123.
- Coppi, P.S.: 1992a, *MNRAS* **258**, 657.
- Coppi, P.: 1999b, *PASP Conf. Ser.* **161**, 375.
- Corbel, S., Fender, R.P., Tzioumis, A.K., Nowak, M., McIntyre, V., Durouchoux, P. and Sood, R.: 2000, *A&A* **359**, 251.
- Corbel, S., Nowak, M., Fender, R.P., Tzioumis, A.K. and Markoff, S.: 2003, *A&A* **400**, 1007.
- Dove, J.B., Wilms, J., Maisack, M.G. and Begelman, M.C.: 1997, *ApJ* **487**, 759.
- Falcke, H., Körding, E. and Markoff, S.: 2004, *A&A* **414**, 895.
- Falcke, H. and Markoff, S.: 2000, *A&A* **362**, 113.
- Fender, R.P., Gallo, E. and Jonker, P.G.: 2003, *MNRAS* **343**, L99.
- Fender, R.P. and Kuulkers, E.: 2001, *MNRAS* **324**, 923.
- Gallo, E., Fender, R.P. and Pooley, G.G.: 2003, *MNRAS* **344**, 60.
- George, I.M. and Fabian, A.C.: 1991, *MNRAS* **249**, 352.
- Haardt, F. and Maraschi, L.: 1991, *ApJ* **380**, L51.
- Hannikainen, D.C., Hunstead, R.W., Campbell-Wilson, D. and Sood, R.K.: 1998, *A&A* **337**, 460.
- Hynes, R.I., Mauche, C.W., Haswell, C.A., Shrader, C.R., Cui, W. and Chaty, S.: 2000, *ApJ* **539**, L37.
- Magdziarz, P. and Zdziarski, A.A.: 1995, *MNRAS* **273**, 837.
- Malzac, J., Beloborodov, A.M. and Poutanen, J.: 2001, *MNRAS* **326**, 417.
- Malzac, J., Merloni, A. and Fabian, A.C.: 2004, *MNRAS* **351**, 253.
- Markoff, S., Falcke, H. and Fender, R.: 2001, *A&A* **372**, L25.
- Markoff, S., Falcke, H., Yuan, F. and Biermann, P.L.: 2001b, *A&A* **379**, L13.
- Markoff, S., Nowak, M., Corbel, S., Fender, R. and Falcke, H.: 2003, *A&A* **397**, 645.
- Markoff, S. and Nowak, M.A.: 2004, *ApJ* **609**, 972.
- Markoff, S., Nowak, M.A. and Wilms, J.: 2005, *ApJ*, in press.
- Marscher, A.P. and Gear, W.K.: 1985, *ApJ* **298**, 114.
- McClintock, J.E., Haswell, C.A., Garcia, M.R., Drake, J.J., Hynes, R.I., Marshall, H.L., Muno, M.P., Chaty, S., Garnavich, P.M., Groot, P.J., Lewin, W.H.G., Mauche, C.W., Miller, J.M., Pooley, G.G., Shrader, C.R. and Vrtilik, S.D.: 2001, *ApJ* **555**, 477.
- Merloni, A., Heinz, S. and di Matteo, T.: 2003, *MNRAS* **345**, 1057.
- Nayakshin, S.: 2000, *ApJ* **534**, 718.
- Poutanen, J.: 1998, *Theory of Black Hole Accretion Disks*, Cambridge University Press, Cambridge, 100.
- Ross, R.R., Fabian, A.C. and Young, A.: 1999, *MNRAS* **306**, 462.
- Rothschild, R.E., Blanco, P.R., Gruber, D.E., Heindl, W.A., MacDonald, D.R., Marsden, D.C., Pelling, M.R., Wayne, L.R. and Hink, P.L.: 1998, *ApJ* **496**, 538.
- Spencer, R.E.: 1979, *Nature* **282**, 483.
- Stern, B.E., Poutanen, J., Svensson, R., Sikora, M. and Begelman, M.C.: 1995, *ApJ* L13.
- Stone, J.M. and Pringle, J.E.: 2001, *MNRAS* **322**, 461.

WHAT CAN WE LEARN FROM NEUTRON STAR X-RAY BINARIES' JETS?

SIMONE MIGLIARI¹ and ROB FENDER^{1,2}

¹*University of Amsterdam, Amsterdam, The Netherlands; E-mail: migliari@science.uva.nl*

²*University of Southampton, Southampton, United Kingdom; E-mail: rpf@phys.soton.ac.uk*

(Received 8 April 2005; accepted 1 June 2005)

Abstract. We review our current knowledge of the disk-jet coupling in neutron star X-ray binaries. We compare neutron star and black hole X-ray binaries, by means of radio and X-ray observations, in order to understand the role played in the production of the jet, by characteristics proper of the accreting compact object involved: the existence of a solid surface, the presence of an ergosphere/event horizon, the strength of the magnetic field, the spin of the compact object.

Keywords: binaries, close, stars, jets and outflows, radio continuum

1. Introduction

Multiwavelength studies of X-ray binaries (XRBs), especially in the past decade, have shown that a significant fraction of the dissipated accretion power may be released in the form of radiatively inefficient collimated outflows, or jets. In general, relativistic jets are very common features associated to accretion onto relativistic compact objects on all mass scales, from neutron stars (NSs) and stellar-mass black holes (BHs) in XRB systems to supermassive BHs in active galactic nuclei (AGN), and thought to be at the origin of γ -ray bursts, the most powerful transient phenomena in the universe. The advantage of studying relativistic jets in XRBs is mainly that they vary on much faster (humanly-accessible) timescales, allowing us to observe and follow significant evolutions of the systems, and to investigate the link between the jet production and the different accretion regimes. Most of what we know about jets in XRBs come from studies of black hole candidates. This is mainly because, with the exception of the so-called Z-type NSs, BH XRBs are more radio loud than NSs, and hence easier to detect.

1.1. BLACK HOLE X-RAY BINARIES

A nonlinear correlation has been found, linking the radio to the X-ray luminosities in BH XRB systems over more than three orders of magnitude in X-rays, when the BHs are in the hard state ($L_R \propto L_X^{0.7}$ where L_R and L_X are the radio and X-ray luminosities; Corbel et al., 2003; Gallo et al., 2003). In hard state (i.e., below



a few percent the Eddington luminosity), the radio emission is observed to be optically thick, with a flat or slightly inverted spectrum, and although a jet has been spatially resolved only in two sources so far (Cyg X-1: Stirling et al., 2001; GRS 1915+105: Dhawa et al., 2000), indirect evidence indicates that this is the signature of a continuously replenished steady jet, the so-called ‘compact jet’ (see Fender, 2005 for a review).

In BH XRBs (but maybe also in AGN, see Maccarone et al., 2003) there is evidence for a quenching of radio emission when the source is steadily in the soft state, probably due to a physical suppression of the jet (Fender et al., 1999; Gallo et al., 2003). The rapid X-ray transition from hard to soft states (i.e., very-high state: VHS) is associated with radio flares which show optically thin spectra. These radio flares are signatures of powerful ejection events, spatially resolved as large-scale (of the order of arcsec) extended jets (e.g., Corbel et al., 2001; Gallo et al., 2004). A unified semiquantitative model for the disk-jet coupling in BH XRBs has been presented by Fender et al. (2004).

Extending the correlation found for BH XRBs in hard state also to supermassive BHs, and with the addition of the mass parameter, there is evidence for a ‘fundamental plane of BH activity’ in which a single power-law function can fit all the BH data (XRBs and AGN) for a given X-ray luminosity, radio luminosity and mass of the compact object [$L_R \propto L_X^{0.6} M^{0.8}$ where M is the mass of the compact object (Merloni et al., 2003; Falcke et al., 2004)]. The existence of this relation connecting BH XRBs and AGN points toward the same physical processes as drivers of the disk-jet coupling, regardless of the mass of the BH involved. The radio:X-ray luminosity power-law correlation previously found studying only BH XRBs has, within errors, the same slope found in the correlation of the ‘fundamental plane’ with BH XRBs and AGN. This evidence, further indicates that the study of XRBs can be fundamental for our understanding of the physical properties of disks and jets in compact objects in general, stellar-mass in binary systems, as well as supermassive in the center of far galaxies.

1.2. NEUTRON STAR X-RAY BINARIES

Low-magnetic field NS XRBs have been classified based on their X-ray spectral and timing properties, in two distinct classes whose names derive from the shape they trace in the X-ray color–color diagram (CD): Z-type and atoll-type NSs (see Hasinger and van der Klis, 1989).

Z-type NS XRBs represent a class of six low-mass XRBs (plus Cir X-1 which is considered as a ‘peculiar’ Z source; Shirey et al., 1999) accreting near or at the Eddington rate, and are the most luminous NS XRBs in our Galaxy. The name of this class of sources derives from the typical ‘Z’ track traced by their CD. The three branches which form the Z-shaped CD are called Horizontal (HB), Normal (NB), and Flaring (FB), top-left to bottom-right, and define three distinct spectral states of the systems. Z sources are rapidly variable in X-rays and can trace the whole

CD, transiting in the different states, in hours to days. This variability is thought to be physically related to changes in the mass accretion rate, which should increase along the Z-track from HB to FB (Hasinger and van der Klis, 1989). In the radio band, we also observe large and rapid variability, optically thick and optically thin emission. All the Z-type NS sources have been detected in radio. Looking in detail at the radio behavior of Z sources as a function of X-rays, Penninx et al. (1988) first found in GX 17+2 a qualitative relation between disk and jet properties: the radio emission varies as a function of the position in the X-ray CD, decreasing with increasing (inferred) mass accretion rate from HB (strongest radio emission) to FB (weakest radio emission). A behavior consistent with GX 17+2 has been found also in Cyg X-2 (Hjellming et al., 1990a) and Sco X-1 (Hjellming et al., 1990b). An exception is GX 5-1, which showed a low and steady radio flux when the source was in the HB, then increasing when in the NB (Tan et al., 1991). Extended radio jets have been spatially resolved for two Z sources: Sco X-1 (Fomalont et al., 2001a) and Cir X-1 (Fender et al., 1998). In these two sources there is also evidence, like in BHs, for an association between radio flares and powerful (ultrarelativistic) ejections from the system (Fender et al., 2004; Fomalont et al., 2001b).

Atoll-type NS XRBs share many X-ray spectral and timing properties with BH XRBs and show two distinct (hard and soft) X-ray states, defined by the position in the CD, that can be directly compared to the hard and soft state of BH XRBs: the hardest X-ray state is called 'island' and the softest 'banana'. Although atolls represent the largest class of known X-ray binaries, only a few are detected in the radio band because of their lower radio luminosity (~ 30 times less 'radio loud' than BH and Z-type NS XRBs: Fender and Kuulkers, 2001; Migliari et al., 2003). To date, five atoll sources have been detected in the radio band during simultaneous radio/X-ray observations: 4U 1728-34, 4U 1820-30, Ser X-1, Aql X-1, and MXB 1730-335 (Migliari et al., 2003, 2004; Rupen et al., 2004; Reynolds et al., 1998). In particular, 4U 1728-34, which is to date the only atoll source detected in radio when steady in its hard state, shows a positive correlation between radio and X-ray fluxes, similar to that observed in BHCs (Migliari et al., 2003). Homan et al. (2004) have also investigated the 'peculiar' atoll source GX 13+1 which is persistently at a very high X-ray luminosity of a few tens percent Eddington, showing that its radio behavior is much more similar to Z sources.

Two accreting ms X-ray pulsars, SAX J1808.4-3658 (Gaensler et al., 1999) and IGR J00291+5934 (Pooley, 2004), have shown transient radio emissions in correspondence of a soft X-ray outburst. These radio emissions may be signatures of transient relativistic outflows from the system as observed in BH XRBs and Z sources.

None of the high-magnetic field X-ray pulsars has ever been convincingly detected as a synchrotron radio source (e.g., Fender and Hendry, 2000 and references therein); this has been explained by the fact that high-magnetic field might disrupt the inner regions of the accretion disk around the NS (e.g., White et al., 1995; Bildsen et al., 1997), thought to be strictly coupled to the jet production.

2. The Sample

In Table I we list the names, X-ray states, fluxes, and estimated distances of all the NS XRBs in our sample. See Migliari and Fender (2005) for details on the observations.

2.1. CONVERSION FROM 2–10 KEV LUMINOSITIES TO EDDINGTON UNITS

In order to extrapolate the bolometric flux of the XRBs, and then to convert their X-ray luminosities in Eddington units, we have divided the XRBs in five main groups: BHs in hard state, BHs during X-ray outbursts, atoll sources in hard state, atoll sources in soft state, and Z sources. We assumed that each group has the same fraction of bolometric luminosity in the 2–10 keV band. For each group we used the best-fit model parameters for the PCA-HEXTE energy spectra to create a simulated spectrum with *xspec*. We used PCA and HEXTE response matrices and ancillary files to calculate the flux in the range 3–200 keV, and a Chandra HETGS (MEG) response matrix and ancillary file to extend the range below 3 keV, down to 0.5 keV, especially important for soft X-ray states. The 0.5–200 keV has been taken as a good approximation of the bolometric flux of the sources. The conversion to Eddington units is given dividing the bolometric luminosity by $1.3 \times 10^{38} \times (M/M_{\odot})$ erg/s, where $M = 1.4 M_{\odot}$ for all the NSs, while for the BHs we used the masses listed in Table I of Fender et al. (2004). The bolometric flux will be $F_{2-10} = F_{\text{bol}} \times \xi$ where we used $\xi = 0.2$ for BHs in hard state, $\xi = 0.8$ for BHs during X-ray outbursts, $\xi = 0.4$ for atoll sources in hard state, $\xi = 0.7$ for atoll sources in soft state, and $\xi = 0.8$ for Z sources.

3. Results

3.1. X-RAY/RADIO LUMINOSITIES IN NS XRBs

In Figure 1 we show the radio/X-ray luminosity plane with all the NS XRBs in our sample. Four groups of sources are plotted: Z-sources, atoll sources in hard state, atoll sources steadily in soft state, and sources in soft outbursts (i.e., the rapid burster and the two accreting ms X-ray pulsars). There is an overall positive ranking correlation between radio and X-ray luminosities, at a significance level of >99%. The fit with a power-law Z- and atoll-type NS XRBs gives a slope of $\Gamma \sim 1$.

The Z-sources (triangles) lie on the top-right part of the plot, with higher X-ray and radio luminosities than atolls. We have plotted the mean of the radio and X-ray luminosities: their radio luminosities are the superposition of optically thick emission and optically thin flaring activity, while the X-ray luminosities are the average of the luminosities in their three possible X-ray states. There is only marginal

TABLE I
Name of the source of our sample, X-ray state

Source	X-ray state	F_{2-10} ($\times 10^{-9}$ erg cm $^{-2}$ s $^{-1}$)	$F_{8.5}$ (mJy)	D (kpc)
Atoll-type NSs				
4U 1728-34	LB	1.03 ± 0.05	0.5 ± 0.08	5.3
	IS	2.25 ± 0.15	0.6 ± 0.2	
	LB	1.54 ± 0.10	0.33 ± 0.15	
	IS	1.81 ± 0.11	0.62 ± 0.1	
	IS	2.42 ± 0.16	0.11 ± 0.02	
	IS	0.60 ± 0.07	0.09 ± 0.02	
	IS	0.61 ± 0.06	0.11 ± 0.02	
	IS	0.62 ± 0.06	0.15 ± 0.02	
	IS	0.69 ± 0.12	0.16 ± 0.02	
	IS	0.70 ± 0.05	0.09 ± 0.02	
4U 1820-30	MB	8.7	0.10 ± 0.02	7.1
Ser X-1	MB	4.4	0.08 ± 0.02	11.1
Aql X-1	H-OUTB	0.79	0.210 ± 0.050	5.2
	H-OUTB	1.00	0.214 ± 0.035	
4U 1608-52	IS?	0.93	<0.19	3.3
4U 0614-09	IS	0.78	<0.09	<3
MXB 1730-335	S-OUTB	2.92	0.370 ± 0.030	8.6
	S-OUTB	3.06	0.290 ± 0.030	
	S-OUTB	5.34	0.330 ± 0.050	
Low-magnetic field accreting ms X-ray pulsar				
SAX J1808.4-3658	S-OUTB	0.14	0.8 ± 0.18	2.5
IGR J00291+5934	S-OUTB	0.62	1.1 ± 0.3	$<3?$
Z-type NSs				
Sco X-1	ASM mean	253.80	10 ± 3	2.8
GX 17+2	ASM mean	12.90	1.0 ± 0.3	14
GX 349+2	ASM mean	14.39	0.6 ± 0.3	5
Cyg X-2	ASM mean	10.75	0.6 ± 0.2	13.3
GX 5-1	ASM mean	20.36	1.3 ± 0.3	9.2
GX 340+0	ASM mean	8.54	0.6 ± 0.3	11
GX 13+1	PCA mean	18	1.8 ± 0.3	7
High-magnetic field accreting X-ray pulsars				
X Per	?	0.46	<0.08	1
4U 2206+54	?	0.26	<0.039	3

(Continued on next page)

TABLE I
(Continued)

Note. LB: lower banana; IS: island; MB: middle-banana; H-OUTB: hard outburst; S-OUTB: soft outburst; ASM/PCA mean: the mean over more than one X-ray state. X-ray flux in the range 2–10 keV, radio flux density at 8.5 GHz, distance to the source in kpc. See Migliari et al., 2003, 2004; Jonker and Nelemans, 2004; Heasley et al., 2000; Vacca et al., 1986; Rupen et al., 2004; Migliari and Fender, 2005; Brandt et al., 1992; Rutledge et al., 1998; Moore et al., 2000; Frogel et al., 1995; Gaensler et al., 1999; in 't Zand et al., 2001; Galloway et al., 2005; Pooley, 2004; Fender and Hendry, 2000; Penninx, 1989; Crampton et al., 1976; Bradshaw et al., 1997; Penninx et al., 1988, 1993; Cooke and Ponman, 1991; Christian and Swank, 1997; Hjellming et al., 1990; Cowley et al., 1979; Homan et al., 2004; Delgado-Martí et al., 2001; Blay et al., 2005; Negueruela and Reig, 2001. See Migliari and Fender (2005), for associations of particular references with particular data points.

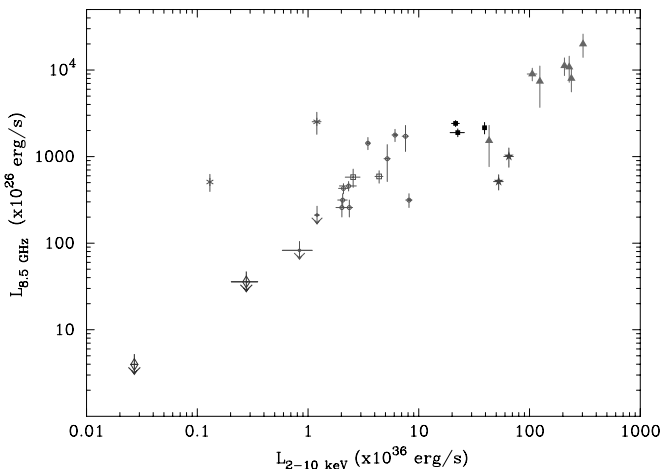


Figure 1. Radio (8.5 GHz) luminosity as a function of X-ray (2–10 keV) luminosity of NS XRBs: atoll sources in hard state (4U 1728-34: open circles; Aql X-1: open stars; 4U 1608-52 and 4U 0614-09: filled circles with radio upper limits), atoll sources steadily in soft state (4U 1820-30 and Ser X-1: filled stars), ‘atoll’ sources in soft X-ray outbursts (MXB 1730-335: filled squares), accreting ms X-ray pulsars in soft X-ray outbursts (SAX J1808.4-3658 and IGR J00291+5934: asterisks), the high-magnetic field XRBs (open diamonds with radio upper limits), and Z sources (filled triangles).

evidence for a positive ranking correlation between radio and X-ray luminosities in the Z sources ($\sim 96\%$ significance level).

Atoll sources in hard X-ray state (4U 1728-34: open circles; Aql X-1: open stars) show a positive correlation between radio and X-ray luminosities on one order of magnitude in X-rays (with the exception of the point with the highest X-ray luminosity: see discussion in Migliari et al., 2003): a rank-correlation test gives a significance of $>99\%$. In order to compare the luminosities correlations in NSs with those in BHs (see also below), we fitted the correlation with a power-law model

(i.e., $L_R \propto L_X^\Gamma$): 4U 1728-34 gives $\Gamma = 1.40 \pm 0.25$, considering also Aql X-1 the fit gives $\Gamma = 1.38 \pm 0.23$. The NS observations, though, span on a range of about one order of magnitude in X-ray luminosity, to be compared with the three orders of magnitude of the BH XRBs. However, we can give constraints to the slope of the power-law on a larger range of luminosities, if we consider also the radio upper limits of 4U 0614+09 at low X-ray luminosities. We obtain a lower limit on the slope of the power-law of $\Gamma > 1.60 \pm 0.27$, clearly indicating that the radio/X-ray luminosity correlation in NSs is steeper than the one in BHs.

Atoll sources steadily in soft state (filled stars) have been detected in radio. This is contrary to what was found in BHs, where there is a quenching of radio emission in the soft state. This finding indicates that NSs may not suppress completely the (compact?) jet in the soft state.

The rapid burster (filled squares) show radio flaring emission associated with soft X-ray outbursts. It has X-ray luminosities consistent with atoll sources in the soft state. There is a significant (99%) positive ranking correlation between radio and X-ray luminosities in atoll sources plus the rapid burster, suggesting that it lies on a sort of natural extension of atolls in hard state (as in persistent and transient BHs; see Fender et al., 2004).

The radio peak of IGR J00291+5934 is consistent with the rapid burster radio peak and with the highest radio emission from 4U 1728-34 (maybe also in a radio flaring emission state; see Migliari et al. 2003). SAX J1808.4-3658 has been detected in radio a few days after the peak of the outburst in 1998, when the X-ray and radio emissions already faded, so that the radio and X-ray luminosities may be considered as lower limits (but see Gaensler et al., 1999).

The high-magnetic field NSs (X Per and 4U 2206+54) have not been detected in the radio band. Their radio upper limits are still consistent with the radio/X-ray luminosity expected extrapolating the correlation for atoll sources to lower X-ray luminosities.

3.2. NEUTRON STARS VS. BLACK HOLES

Is the 'fundamental plane of BH activity' also a fundamental plane for NSs? Put in another way, do the features proper of the compact object in the system play a role in the production of the jet?

Observationally, there is a clear parallel in the disk-jet coupling between the two systems: below a certain X-ray luminosity, in hard state (i.e., $L_X < 0.1 \times L_{\text{Edd}}$), both classes of objects seem to make steady, self-absorbed jets (at least consistent with this picture in the case of NSs), while at higher X-ray luminosities, close to the Eddington limit, bright, optically thin, transient events occur (specifically associated with rapid state changes). In the hard X-ray states, correlations between radio and X-ray emission have been found in both BHs and NSs. This indicates that the link between the power of the jet and the innermost regions of the accretion

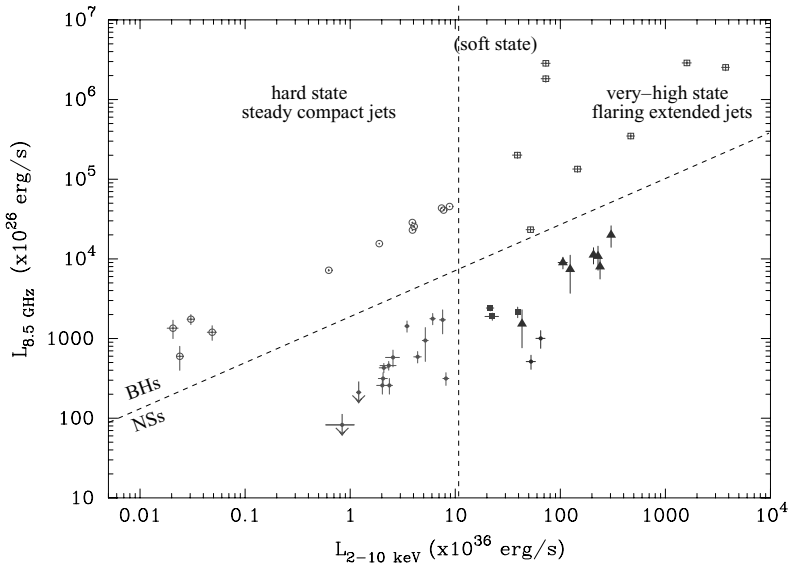


Figure 2. Radio (8.5 GHz) luminosity as a function of X-ray (2–10 keV) luminosity for NS and BH XRBs: GX 339-4 in hard state (open circles), transient BHs (open squares), atoll sources steady in a hard or soft state (filled circles), MXB 1730-335 during a soft outburst (filled squares), and Z sources (filled triangles).

disk does not depend (at least entirely) on the nature of the compact object, but it is related to the fundamental processes of accretion in strong gravity.

Differences between BHs and NSs, however, led to the evidence that, at least partially, characteristics proper of the compact object involved might play a role in the production of the jet: (i) at a given X-ray luminosity (Figure 2), and at a given fraction of Eddington luminosity (i.e., fraction of Eddington accretion rate; Figure 3) the BHs produce more powerful jets than NSs. The difference in radio power is $\gtrsim 30$, which can be reduced to $\gtrsim 7$ if we consider possible mass corrections as derived from the black holes' fundamental plane (e.g., Merloni et al., 2003) or to a factor of $\gtrsim 5$ if we consider the mass correction coming from the conversion of the 2–10 keV luminosities in Eddington units; (ii) the slope of the power-law correlation in the hard state of BHs is 0.7, while for NSs seems to be steeper (possibly ~ 1.4 ; see above); (iii) contrary to BHs, atoll-type NSs have been detected in radio when steadily in soft X-ray states (stars in Figure 1).

4. Discussion

In the following we will briefly discuss some possible implications deriving from the comparison between disk-jet coupling in BHs and NS systems (see Migliari and Fender, 2005, for a broader discussion).

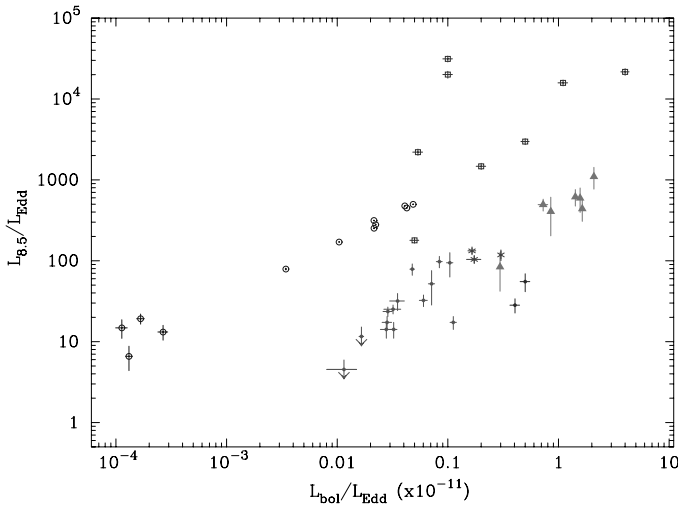


Figure 3. Same as Figure 2, but in Eddington units (see Section 2.1).

4.1. THE ROLE OF THE EVENT HORIZON

Observations of the ultrarelativistic radio jets in the NS XRB Cir X-1 (i.e., with a bulk Lorentz factor > 15 ; Fender et al., 2004) have already shown that the (often accepted) ‘escape velocity’ principle, which states that the jets’ velocity should be about the escape velocity of the compact object involved, is no longer valid. Their observations also indicate that properties unique to BHs are *not necessary* for the production of relativistic jets. However, characteristics proper of the compact object seem to play, at least partially, a role in the jet production.

Do current models have clear predictions on what are the differences we should observe in NSs and BHs disk-jet coupling, depending on some fundamental property of the compact object involved, like the existence of the event horizon? To address this question, we will consider two frameworks: (i) the advection-dominated accretion flow model (ADAF; e.g., Narayan and Yi, 1994, 1995; Narayan et al., 1997), a radiatively inefficient disk model which assumes that a fraction of the accreting matter onto a BH is actually advected through the event horizon. The advection would explain the difference in X-ray luminosity in quiescent BH and NS XRBs; (ii) the existence of jet-dominated states (Fender et al., 2004), which might explain the brightness difference between NS and BH XRB in quiescence, without necessarily requiring the assumption of advection.

We will assume that in hard X-ray states, the radio/X-ray luminosity correlations have power-law slopes of $0.7(\pm 0.2)$ in BHs (Gallo et al., 2003) and $1.4(\pm 0.2)$ in NSs (Migliari et al., 2003; Migliari and Fender, 2005). In hard state the radio emission can be explained as emission from a steady compact jet. All the models of such

compact jets predict that the total jet power L_J and the power irradiated in radio L_R are related as $L_R \propto L_J^{1.4}$ (e.g., Blandford and Konigl, 1979; Falcke and Biermann, 1996; Falcke et al., 2001).

In the ADAF model the X-ray luminosity relates to the mass accretion rate \dot{M} (in Eddington units) in two different ways, depending on the accreting compact object involved: $L_X \propto \dot{M}$ for NSs and $L_X \propto \dot{M}^2$ for BHs. With these scalings, the ADAF can, therefore, naturally explain the observed radio/X-ray luminosity correlations, and the different slopes, if $L_J \propto \dot{M}$. In fact, for NSs from $L_R \propto L_X^{1.4}$ we have: $L_J^{1.4} \propto \dot{M}^{1.4}$ and, within errors, we obtain $L_J \propto \dot{M}$.

In the jet-dominated state framework, the nonlinearity of the radio/X-ray luminosity correlation in BHs leads to the possible existence of a luminosity below which the dominant power output channel is the jet instead of the X-ray emission from the disk. BH XRBs might enter a jet-dominated state already below a luminosity of a few percent the Eddington limit, i.e., for the largest part of the hard state (e.g., Fender et al., 2004; Malzac et al., 2004; Gallo et al., 2005). The transition from a disk-dominated to a jet-dominated state is a transition from a regime where $L_X \propto \dot{M}$ to a regime where $L_X \propto \dot{M}^2$. If also in NS XRBs the slope in the radio/X-ray luminosity correlation would be less than 1.4 (as discussed in Fender et al. (2004) for $\Gamma = 0.7$), since NSs show a radio luminosity which is a factor of 30 less than BHs, the X-ray luminosity limit below which the sources enter the jet-dominated state is lower than for BHs. This would explain the fact that in quiescence (or better, in the X-ray luminosity windows where NSs and BHs in quiescent have been observed), NSs have higher X-ray luminosities than BHs, without the need for advection onto the BH. An X-ray/radio luminosity correlation with a slope of $\Gamma = 1.5$ (in general $\Gamma = 1.4$) in NSs implies that NSs never enter the jet-dominated state (see Figure 4). In this framework, i.e., with no requirement for advection, below a certain luminosity – may be the entire hard state – it holds $L_X \propto \dot{M}$ for NSs and $L_X \propto \dot{M}^2$ for BHs, precisely as in the ADAF model. Therefore, again, the slope differences between the luminosities correlation in NSs and BHs can be explained if $L_J \propto \dot{M}$.

Both frameworks, starting from an opposite assumption on the presence of advection, seem to point to the same relations: $L_X \propto \dot{M}^2$ for BHs, $L_X \propto \dot{M}$ for NSs, and from these, to a relation that link linearly the total power of the jet and the mass accretion rate, $L_J \propto \dot{M}$. A direct strong relation between the jet power and the mass accretion rate is also supported by the correlations found in NSs between radio luminosity and X-ray timing features (Migliari et al., 2003, 2005) possibly directly related to the local mass accretion rate in the inner regions of the disk (see van der Klis, 2005 for a review).

4.2. THE ROLE OF THE MAGNETIC FIELD

It is a general accepted idea that very high-magnetic fields at the surface of the NSs inhibit the production of *steady* jets (while a large amount of energy can be

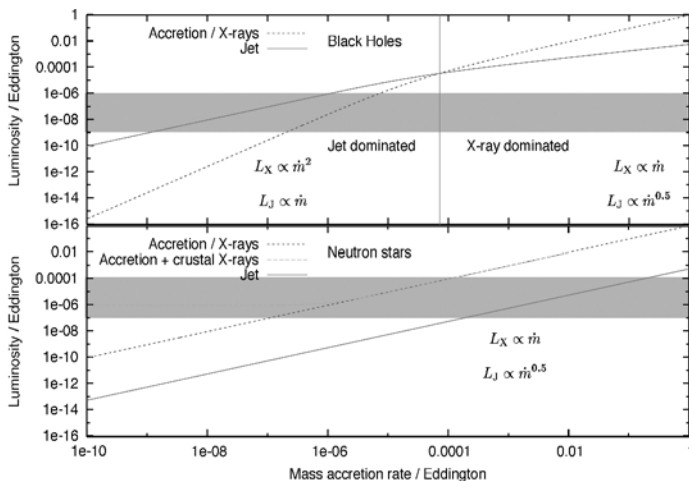


Figure 4. Total (X-ray and jet) luminosity as a function of mass accretion rate in the jet-dominated states framework (Fender et al., 2004) for black holes (top panel) and neutron stars (lower panel). Two regimes exist for black holes: jet-dominated below a certain luminosity (indicated with the vertical solid line) and X-ray dominated above it. In contrast, neutron stars never enter a jet-dominated state.

extracted from magnetic fields to power extremely energetic transient jets: as, e.g., in the case of the magnetar SGR 1806-20). However, besides theoretical arguments, actual observational proofs are missing. The upper limits on previous observations, although significantly lower than radio detections of BH XRBs, are not at all stringent if compared with other NS sources detected in radio, and actually higher than the radio detection levels of atoll sources at the same accretion rate (as traced by the X-ray luminosity). Chakrabarty (2005) suggested that accreting ms X-ray pulsars have a slightly higher magnetic field than other atoll sources. This would suggest that we should see a decreasing radio luminosity (for a given mass accretion rate) from atoll sources to accreting ms X-ray pulsars to high-magnetic field X-ray pulsars. Upcoming radio observations of high-magnetic field and accreting ms X-ray pulsars will give us the opportunity to test these ideas, and in general the role of the magnetic field in the jets production.

References

- Bildsten, L.: 1997, *ApJS* **113**, 367.
 Blandford, R.D. and Konigl, A.: 1979, *ApJ* **232**, 34.
 Blay, P. et al.: 2005, *A&A* **438**, 963.
 Bradshaw, C.F., Fomalont, E.B. and Geldzahler, B.J.: 1997, *ApJ* **484**, L55.
 Brandt, S.: 1992, *A&A* **262**, L15.
 Chakrabarty, D.: 2004, in: F.A. Rasio and I.H. Stairs (eds.), *Binary Radio Pulsars*, ASP Conference Series, in press, astro-ph/0408004.

- Christian, D.J. and Swank, J.H.: 1997, *ApJS* **109**, 177.
- Cooke, P.A. and Ponman, T.J.: 1991, *A&A* **244**, 358.
- Corbel, S.: 2001, *ApJ* **554**, 43.
- Corbel, S.: 2003, *A&A* **400**, 1007.
- Cowley, A.P., Crampton, D. and Hutchings, J.: 1979, *ApJ* **207**, 907.
- Crampton, D.: 1976, *ApJ* **207**, 907.
- Delgado-Martí, H.: 2001, *ApJ* **546**, 455.
- Dhawan, V., Mirabel, I.F. and Rodríguez, L.F.: 2000, *ApJ* **543**, 373.
- Falcke, H. and Biermann, P.L.: 1996, *A&A* **308**, 321.
- Falcke, H., Körding, E. and Markoff, S.: 2004, *A&A* **414**, 895.
- Fender, R.: 2005, in: W.H.G. Lewin and M. van der Klis (eds.), *Compact Stellar X-Ray Sources*, Cambridge University Press, Cambridge (forthcoming).
- Fender, R.P.: 1998, *ApJ* **506**, L121.
- Fender, R.P.: 1999, *MNRAS* **519**, L165.
- Fender, R.P.: 2004, *Nature* **427**, 222.
- Fender, R.P., Belloni, T. and Gallo, E.: 2004, *MNRAS* **355**, 1105.
- Fender, R.P., Gallo, E. and Jonker, P.G.: 2004, *MNRAS* **343**, L99.
- Fender, R.P. and Hendry, M.A.: 2000, *MNRAS* **317**, 1.
- Fender, R.P. and Kuulkers, E.: 2001, *MNRAS* **324**, 923.
- Fomalont, E.B., Geldzahler, B.J. and Bradshaw, C.F.: 2001a, *ApJ* **558**, 283.
- Fomalont, E.B., Geldzahler, B.J. and Bradshaw, C.F.: 2001b, *ApJ* **553**, L27.
- Frogel, J.A., Kuchinski, L.E. and Tiede, G.P.: 1995, *AJ* **109**, 1154.
- Gaensler, B.M., Stappers, B.W. and Getts, T.J.: 1999, *ApJ* **522**, L117.
- Gallo, E.: 2004, *MNRAS* **347**, L52.
- Gallo, E., Fender, R.P. and Pooley, G.G.: 2003, *MNRAS* **344**, 60.
- Gallo, E. et al.: 2005, *Nature* **436**, 819.
- Galloway, D.K.: 2005, *ApJ* **622**, L45.
- Hasinger, G. and van der Klis, M.: 1989, *A&A* **225**, 79.
- Heasley, J.N.: 2000, *AJ* **120**, 879.
- Heinz, S. and Sunyaev, R.A.: 2003, *MNRAS* **343**, L59.
- Hjellming, R.M.: 1990a, *A&A* **235**, 147.
- Hjellming, R.M.: 1990b, *ApJ* **365**, 681.
- Homan, J.: 2004, *A&A* **418**, 255.
- in 't Zand, J.J.M.: 2001, *A&A* **372**, 916.
- Jonker, P.G. and Nelemans, G.: 2004, *MNRAS* **354**, 355.
- Maccarone, T.J., Gallo, E. and Fender, R.P.: 2003, *MNRAS* **345**, L19.
- Malzac, J., Merloni, A. and Fabian, A.C.: 2004, *MNRAS* **351**, 253.
- Markoff, S., Falcke, H. and Fender, R.: 2001, *A&A* **372**, L25.
- Merloni, A., Heinz, S. and Di Matteo, T.: 2003, *MNRAS* **345**, 1057.
- Migliari, S.: 2003, *MNRAS* **342**, L67.
- Migliari, S.: 2004, *MNRAS* **351**, 186.
- Migliari, S. and Fender, R.P.: 2005, *MNRAS*, in press: astro-ph/0510698.
- Migliari, S., Fender, R.P. and van der Klis, M.: 2005, *MNRAS* **363**, 112.
- Moore, C.B.: 2000, *ApJ* **532**, 1181.
- Narayan, R., Garcia, M.R. and McClintock, J.E.: 1997, *ApJ* **478**, L79.
- Narayan, R. and Yi, I.: 1994, *ApJ* **428**, L13.
- Narayan, R. and Yi, I.: 1995, *ApJ* **444**, 231.
- Negueruela, I. and Reig, P.: 2001, *A&A* **371**, 1056.
- Penninx, W.: 1988, *Nature* **336**, 146.
- Penninx, W.: 1993, *A&A* **267**, 92.

- Penninx, W., in: J. Hunt and B. Battrick (eds.), *23rd ESLAB Symposium on Two Topics in X-Ray Astronomy*, Bologna, Italy, ESA SP-296, 185.
- Pooley, G.G.: 2004, *ATEL*, **355**, 1.
- Rupen, M.P., Mioduszewski, A.J. and Dhawan, V.: 2004, *ATEL*, **286**, 1.
- Rutledge, R.: 1998, *IAU Circ.* **6813**, 2.
- Stirling, A.M.: 2001, *MNRAS* **327**, 1273.
- Vacca, W.D., Lewin, W.H.G. and van Paradijs, J.: 1986, *MNRAS* **220**, 339.
- White, N.E., Nagase, F. and Parmar, A.N.: 1995, in: W.H.G. Lewin, E.P.J. van Paradijs van den Heuvel (eds.), *X-Ray Binaries*, Vol. 1, CUP.

A UNIFYING SCHEME FOR LOW-LUMINOSITY XRBs AND AGN

ELMAR KÖRDING^{1,2} and HEINO FALCKE^{3,4}

¹*Max-Planck Institut für Radioastronomie, Auf dem Huegel 69, 53121 Bonn, Germany*

²*School of Physics and Astronomy, University of Southampton, Southampton SO17 1BJ, U.K.;*
E-mail: elmar@koerding.de

³*Radio Observatory, ASTRON, Dwingeloo, P.O. Box 2, 7990 AA Dwingeloo, The Netherlands*

⁴*Department of Astronomy, Radboud Universiteit Nijmegen, Postbus 9010, 6500 GL Nijmegen,*
The Netherlands

(Received 22 October 2004; accepted 1 June 2005)

Abstract. In recent years, significant evidence for the similar nature of active galactic nuclei (AGN) and X-ray binaries (XRBs) has been gathered. We describe a unification scheme for accreting black holes following the idea that weakly accreting systems may be jet dominated. This is tested with the radio/X-ray correlation of XRBs and AGN. The established correlation is further used to diagnose ultra-luminous X-ray sources. For higher accretion rates, we explore high-power jets and the effect of Compton cooling of the jet by the accretion disk.

Keywords: X-rays: binaries, radiation mechanisms: non-thermal, stars: winds, outflows, black hole physics, accretion, accretion disks

1. Introduction

It is generally assumed that active galactic nuclei (AGN) and black hole X-ray binaries (XRBs) have a similar central engine, namely the central black hole, the accretion flow and a relativistic jet (see e.g., Sunyaev and Trümper, 1979; Mirabel and Rodríguez, 1999; Falcke and Biermann, 1996). In recent years, this general idea has been tested with a number of empirical connections (Merloni et al., 2003; Falcke et al., 2004; Abramowicz et al., 2004).

XRBs are often observed in two distinct state: the low/hard (LH) state and the high soft (HS) state (see e.g., McClintock, 2003). When an object is found in its LH state, it usually also shows a jet visible in the radio regime (e.g., Fender, 2001). Its accretion flow is probably radiatively inefficient up to a transition radius where the accretion disk turns into a standard thin disk (Esin et al., 1997). The spectrum in the X-rays is dominated by a hard power law, which is usually explained by Comptonization (cf., McClintock, 2003). However, one can also describe the spectrum with a coupled disk/jet model. Here the X-ray and the radio emission originates mainly from the relativistic jet, while the disk is only visible in the optical to UV, if at all (Markoff et al., 2001).

We follow the idea that XRBs in their LH state may be jet dominated and explore the unification scheme described in Falcke et al. (2004). We discuss the response of



a jet to higher accretion rates and illumination by a radiatively efficient accretion flow as found in HS state objects.

2. Low Power Unification

The two main components of an accreting system (the relativistic jet and the accretion flow with its corona) have anisotropic emission patterns. This is due to obscuration and – for the jet – due to relativistic beaming. The orientation dependence of the jet and the accretion flow of AGN have been utilized in the successful unification schemes of AGN (cf., Antonucci, 1993). In light of the two accretion states of black hole XRBs, the HS and the LH state, one can also classify the different classes of AGN into these two states. This classification can be done by looking for features of the standard disk or an inefficient accretion flow like an advection-dominated accretion flow. One classification in the parameter-space of the accretion rate and the central black hole is shown in Figure 1.

The aforementioned unification scheme can be tested for the non-thermally dominated sources (Falcke et al., 2004). As discussed earlier, the radio and the X-ray emission may originate from synchrotron emission of the relativistic jet in these sources. According to this idea, the radio and X-ray emission of AGN and XRBs are created with the same mechanism and should therefore be correlated. Using scaling laws for jets, where their geometry is scale invariant (e.g., Falcke and

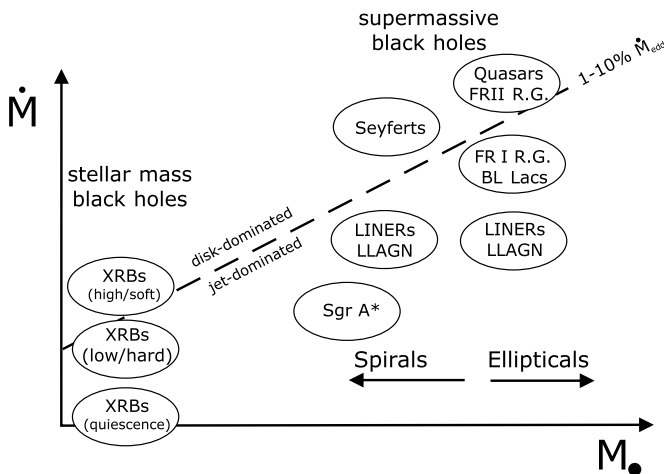


Figure 1. The proposed unification scheme of Falcke et al. (2004) for accreting black holes in the mass and accretion rate plane. The X-axis denotes the black hole mass and the Y-axis the accretion power. For stellar black holes it coincides with the two normal black hole states. For the AGN zoo we include low-luminosity AGN (LLAGN), radio galaxies (RG), low ionization emission region sources (LINER), Seyferts, and quasars.

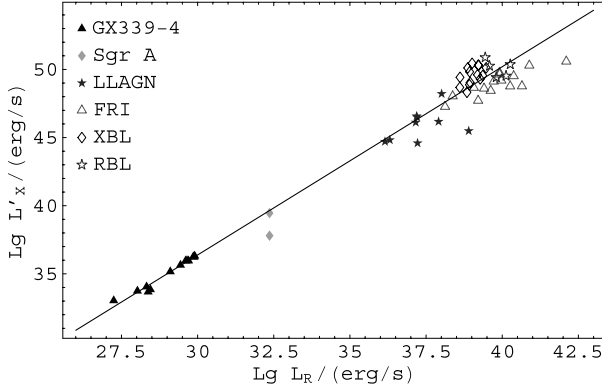


Figure 2. Radio/equivalent X-ray luminosity correlation for a sample of jet-dominated AGN and XRBs. The X-ray flux has been adjusted to correspond to a black hole mass of $6 M_{\odot}$. The term equivalent X-ray flux denotes that this luminosity is extrapolated from the optical fluxes for some AGN sources (FR-I and BI Lac objects). This extrapolation is motivated by the idea that one has to compare synchrotron emission.

Biermann, 1995; Heinz and Sunyaev, 2003; Körding, 2004) one can show that the X-ray luminosity L_X and the radio luminosity $L_R (= F_R \nu_R)$ obey:

$$L_X \propto L_R^{1.38} M^{0.81}. \quad (1)$$

Using mass estimates for AGN, e.g., by the black hole mass/velocity dispersion relation, one can test this scaling law as shown in Figure 2. The correlation of radio and X-rays continues up to the critical accretion rate, where the sources get thermally dominated (Corbel et al., 2000, 2003; Gallo et al., 2003). This can be seen as a hint that the emission in both frequencies, radio and X-rays, originates from the same component of the system.

In case that the X-ray emission originates from synchrotron-self-Compton (SSC) emission of the relativistic jet, the power law of the radio luminosity index in Eq. (1) would be larger (>2) than the measured value (Koerding, 2004). This is due to the fact that the density of the synchrotron seed photons for the Comptonization already scales with roughly the accretion rate squared. Thus, as the density of the Comptonizing electrons also scales with jet power, one gets larger power law indices than for pure synchrotron emission.

3. Radio/X-ray Correlation Used to Diagnose Black Holes

In the previous section, we have established a radio/X-ray correlation for stellar and supermassive black holes. This correlation can be used to study the properties of unknown black holes like those suspected in ultra-luminous X-ray sources (ULXs).

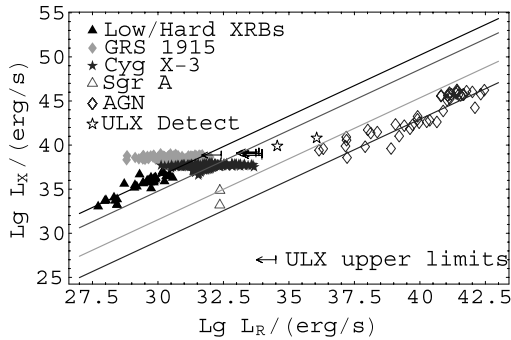


Figure 3. Radio X-ray correlation used to diagnose ULXs. Unlike Figure 2, we do not scale the point for the different black hole masses. The lines denote the scaling of the jet model for 6, 600, 10^6 , and $10^9 M_{\odot}$. Besides the upper limits of Körding et al. (2004) we also include the two published radio detections. The star further to the right side is the ULX in NGC 5408, while the other is the flare in M82 found by Kronberg and Sramek (1985).

These objects are defined as bright ($\geq 10^{39}$ erg/s) off-nucleus X-ray point sources. If those sources emit isotropically and obey the Eddington limit their central black hole needs to be of intermediate masses (100–1000 M_{\odot}). However, these high luminosities can also be explained by anisotropic emission (see e.g., King et al., 2001) or by the microblazar phenomenon (Körding et al., 2002).

Körding et al. (2004) monitored a sample of ULXs with the VLA. Their upper limits and other published radio detections of ULXs are shown in Figure 3. Unlike Figure 2, we do not scale all objects to the mass of an XRB, but give the model scaling for different masses. All upper limits are in agreement with the radio/X-ray correlation, even if all those ULXs indeed have stellar mass black holes. Note, that the correlation is only valid for LH state objects. In HS state objects the radio emission is quenched and they leave the correlation towards lower radio luminosities. Higher radio fluxes can only be obtained by increasing the mass of the central black hole or by the unavoidable scatter. Also shown in the plot are the radio detections of an ULX in NGC 5408 by Kaaret et al. (2003). If this detection is confirmed it would indicate an intermediate mass black hole, as it would be too radio loud even for a ‘radio loud’ stellar source.

4. Towards the High State

Observations of black hole XRBs in the HS state do not show a detectable jet (see e.g., Fender et al., 1999 or McClintock, 2003 and references therein). Thus, the jet is either not launched at all or quenched within a couple of gravitational radii before it is detectable in the radio. Maccarone et al. (2003) suggested that such an effect is also found in AGN, e.g., the ‘radio-quiet’ sources. The very high state of XRBs

shows often a flaring radio jet (see e.g. Fender et al., 2004) and jet in AGN seem to show similar features (Marscher et al., 2002). Thus, it is interesting to discuss the scaling of jets, used to unify the weakly accreting black holes, for higher accretion rates and the effect of the radiatively efficient accretion flow in this state.

Using the idea of scale invariant jets one can establish scaling laws for the total jet emission from all important emission processes. The total synchrotron luminosity scales according to

$$L_{\text{Sync}} \sim \left(\frac{q_j \dot{M}}{\dot{M}_{\text{Edd}}} \right)^2 M, \quad (2)$$

where q_j denotes what percentage of the total accretion power is injected into the magnetic fields in the jet. As these synchrotron photons are the seed photons for SSC emission, the total power emitted through SSC scales with the third power of the accretion rate:

$$L_{\text{SSC}} \sim \left(\frac{q_j \dot{M}}{\dot{M}_{\text{Edd}}} \right)^3 M. \quad (3)$$

On the other hand, external Compton emission is effectively the same as synchrotron if one exchanges the energy density of the magnetic field with the energy density in the external photon field. Thus, the total luminosity scales as:

$$L_{\text{EC}} \sim \left(\frac{q_j \dot{M}}{\dot{M}_{\text{Edd}}} \right)^2 M U_{\text{Ph}}. \quad (4)$$

The scale invariance of the geometry of the jet used here is visible in the linearity of all luminosities on the black hole mass M . The aforementioned formulae can be summarized: a relativistic jet gets increasingly efficient in radiating away the energy contained in relativistic electrons as a function of total jet power. Thus, in powerful jets cooling will play an important role and the approximation used for the derivation of the jet emission will break down. However, observations of powerful jets, e.g., in FR-II radio galaxies, do not show such a cooling dominance. This can only be obtained by leaving equipartition: more internal energy has to be contained in the magnetic fields than in the relativistic particles, e.g., jets have to be launched magnetically.

Besides checking if the jet is cooling dominated one can also calculate, which of the aforementioned processes is dominating the overall emission. As the SSC emissivity scales with \dot{M}^3 while the synchrotron emissivity scales only quadratically, there has to be a accretion rate when SSC dominates over the synchrotron emission. For a typical parameter set this happens at a few percent of the Eddington accretion rate. Thus, the jet of an XRB in the LH state will be synchrotron dominated. Very likely, this change in the jet is not related to the state change of the XRB (LH to HS

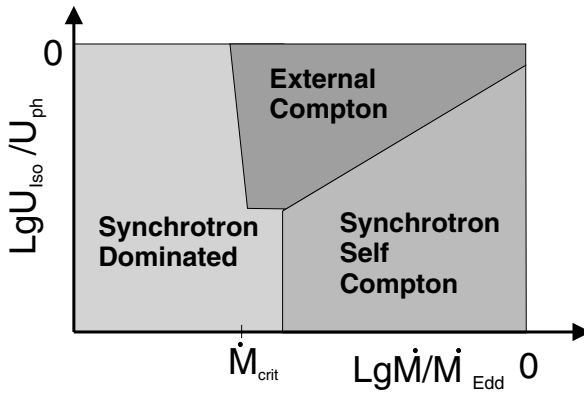


Figure 4. The dominating emission process of a relativistic jet depending on the accretion rate and the fraction of the isotropic radiation field. The accretion disk is thought to be a radiatively inefficient flow for low accretion rates and an efficient standard disk above the critical accretion rate.

state), as the latter is probably due to a different accretion flow configuration (Esin et al., 1997).

External Comptonization from disk photons will not contribute significantly to the total emission as long as the comptonizing photons originate directly from the accretion disk. In this case, they are relativistically deboosted as the jet moves away from the accretion disk. However, if those photons are scattered by surrounding gas and create an isotropic radiation field, they are relativistically boosted. Compared to the former case, this yields an additional factor γ^4 , which allows that this component can dominate the overall emission. The qualitative behavior of the dominating emission process is shown in Figure 4. The upscattered photons would reach very high energies not observed by the current telescopes.

Unlike synchrotron and SSC cooling, external-Compton cooling acts on the whole jet, not only on the relativistic particles. Thus, it could, in principle, quench the whole jet as seen in HS state objects if it is the dominating emission process.

5. Conclusions

The idea of jet domination of weakly accreting systems can be used for a unification scheme of black hole XRBs and AGN. This scheme can be tested with the radio/X-ray correlation for both classes of objects. Even though the correlation has significant scatter it could be used to diagnose the masses of the black holes in ULXs. A radio detection like the one of NGC 5408 is a further hint that the central object might indeed be an intermediate mass black hole.

We have seen that for weakly accreting systems (below a few percent of the Eddington rate) the jet has the possibility to stay in equipartition without losing a

significant fraction of its energy due to radiation. The dominant emission process in this regime is the synchrotron emission also seen in the radio regime. This simple picture breaks down if one increases the accretion rate. Above a critical accretion rate SSC and external Compton emission will play an important role, the jet has to leave equipartition or the energy loss due to radiation has to be taken into account. If there is material around the black hole that scatters the photons from the accretion disk into an isotropic radiation field, external Compton emission could, in principle, quench the whole jet.

References

- Abramowicz, M.A., Kluźniak, W., McClintock, J.E. and Remillard, R.A.: 2004, *ApJ* **609**, L63.
- Antonucci, R.: 1993, *ARA&A* **31**, 473.
- Corbel, S., Fender, R.P., Tzioumis, A.K., Nowak, M., McIntyre, V., Durouchoux, P. and Sood, R.: 2000, *A&A* **359**, 251.
- Corbel, S., Nowak, M.A., Fender, R.P., Tzioumis, A.K. and Markoff, S.: 2003, *A&A* **400**, 1007.
- Esin, A.A., McClintock, J.E. and Narayan, R.: 1997, *ApJ* **489**, 865.
- Falcke, H. and Biermann, P.L.: 1995, *A&A* **293**, 665.
- Falcke, H. and Biermann, P.L.: 1996, *A&A* **308**, 321.
- Falcke, H., Körding, E. and Markoff, S.: 2004, *A&A* **414**, 895.
- Fender, R., Corbel, S., Tzioumis, T., McIntyre, V., Campbell-Wilson, D., Nowak, M., Sood, R., Hunstead, A., Harmon, R., Durouchoux, P. and Heindl, W.: 1999, *ApJ* **519**, L165.
- Fender, R.P.: 2001, *MNRAS* **322**, 31.
- Fender, R.P., Belloni, T.M. and Gallo, E.: 2004, *MNRAS* **355**, 1105.
- Gallo, E., Fender, R.P. and Pooley, G.G.: 2003, *MNRAS* **344**, 60.
- Heinz, S. and Sunyaev, R.A.: 2003, *MNRAS* **343**, L59.
- Kaaret, P., Corbel, S., Prestwich, A.H. and Zezas, A.: 2003, *Science* **299**, 365.
- King, A.R., Davies, M.B., Ward, M.J., Fabbiano, G. and Elvis, M.: 2001, *ApJ* **552**, L109.
- Körding, E.: 2004, PhD Thesis.
- Körding, E., Colbert, E. and Falcke, H.: 2004, manuscript in preparation.
- Körding, E., Falcke, H. and Markoff, S.: 2002, *A&A* **382**, L13.
- Kronberg, P.P. and Sramek, R.A.: 1985, *Science* **227**, 28.
- Maccarone, T.J., Gallo, E. and Fender, R.: 2003, *MNRAS* **345**, L19.
- Markoff, S., Falcke, H. and Fender, R.: 2001, *A&A* **372**, L25.
- Marscher, A.P., Jorstad, S.G., Gómez, J., Aller, M.F., Teräsranta, H., Lister, M.L. and Stirling, A.M.: 2002, *Nature* **417**, 625.
- McClintock, J. and Remillard, R.: 2003. in: W.H.G. Lewin and M. van der Klis (eds.), *Compact Stellar X-ray Sources*, Cambridge University Press, Cambridge.
- Merloni, A., Heinz, S. and di Matteo, T.: 2003, *MNRAS* **345**, 1057.
- Mirabel, I.F. and Rodríguez, L.F.: 1999, *ARA&A* **37**, 409.
- Sunyaev, R.A. and Trümper, J.: 1979, *Nature* **279**, 506.

“LOW-STATE” BLACK HOLE ACCRETION IN NEARBY GALAXIES

LUIS C. HO

*The Observatories of the Carnegie Institution of Washington,
813 Santa Barbara Street, Pasadena, CA 91101, U.S.A.;
E-mail: lho@ociw.edu*

(Received 2 December 2004; accepted 1 June 2005)

Abstract. I summarize the main observational properties of low-luminosity AGNs in nearby galaxies to argue that they are the high-mass analogs of black hole X-ray binaries in the “low/hard” state. The principal characteristics of low-state AGNs can be accommodated with a scenario in which the central engine is comprised of three components: an optically thick, geometrically accretion disk with a truncated inner radius, a radiatively inefficient flow, and a compact jet.

1. AGNs and Black Hole X-ray Binaries

Stellar-mass black holes in X-ray binaries, in response to changes in the mass accretion rate, exhibit distinct spectral “states” (McClintock and Remillard, 2005). Since many aspects of accretion flows are invariant with respect to changes in black hole mass, it is of interest to ask whether there are extragalactic analogs to X-ray binary states in massive black holes in the centers of galaxies. Nuclear black holes outweigh stellar black holes by factors of 10^5 – 10^8 , and so their evolutionary timescales increase in the same proportion. To search for spectral states in massive black holes, one must consider the demographics of accreting nuclear black holes—AGNs—spanning a wide range of luminosity.

In recent years, much attention has been devoted to the study of “narrow-line” Seyfert 1 galaxies, which are widely believed to be the AGN counterparts of X-ray binaries in the “high/soft” state (e.g., Pounds et al., 1995). Indeed, this class of AGNs may be even accreting at super-Eddington rates (Collin and Kawaguchi, 2004).

This contribution focuses on AGNs in the opposite extreme, namely those accreting at highly sub-Eddington rates, which I will argue are close analogs to X-ray binaries in the “low/hard” or “quiescent” states, and which dominate the population of AGNs at $z = 0$.

2. Observational Properties of Low-Luminosity AGNs

Although the physical nature of low-luminosity AGNs (LLAGNs) is still not fully understood, the bulk of the current evidence suggests that a significant fraction of



them are genuinely accretion-powered sources (for a recent review, see Ho, 2004). Here I highlight the most important observational properties of these objects, which, when taken collectively, point to some novel insights on the structure of their central engines.

- *Demography*. LLAGNs are very common. According to the Palomar survey (Ho et al., 1997a), over 40% of nearby galaxies, and an even greater fraction (50–75%) of bulge-dominated (E–Sbc) systems, contain LLAGNs.
- *Low ionization*. The dominant population (two-third) of LLAGNs have low-ionization state spectra (Ho et al., 1997a). They are classified as either low-ionization nuclear emission-line regions (LINERs) or transition objects, which are hypothesized to be related to LINERs (Ho et al., 1993; but see complications discussed in Ho et al., 2003 and Ho, 2004).
- *Low accretion power*. LLAGNs are intrinsically faint, in most cases orders of magnitude less powerful than classical Seyferts and quasars. The optical luminosity function of LLAGNs extends to absolute magnitudes as low as $M_B \approx -6$ (Ho, 2004). Figure 1a, from Ho (2005), shows the distributions of bolometric luminosities for ~ 250 objects from the Palomar survey. Note that nearly all the objects have $L_{\text{bol}} < 10^{44}$ erg s $^{-1}$, and most significantly less. Seyferts are on average 10 times more luminous than LINERs or transition objects.
- *Sub-Eddington*. LLAGNs are highly sub-Eddington systems, as shown in Figure 1b. Essentially, all objects in the Palomar sample have $L_{\text{bol}}/L_{\text{Edd}} < 1$, with the majority falling in the region $L_{\text{bol}}/L_{\text{Edd}} \approx 10^{-5} - 10^{-3}$. Seyferts have systematically higher Eddington ratios than LINERs or transition objects, typically by 1–2 orders of magnitude.
- *Radiatively inefficient*. Direct measurements of accretion rates are not available, but rough estimates can be made of the likely minimum rates supplied *in situ*.

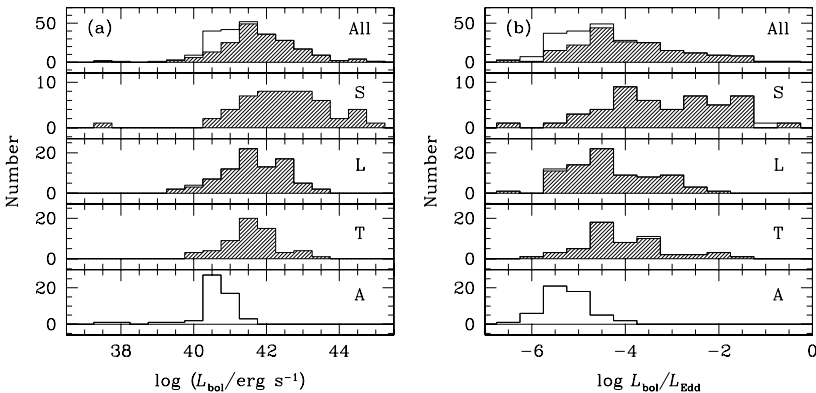


Figure 1. Distribution of (a) nuclear bolometric luminosities and (b) Eddington ratios, $L_{\text{bol}}/L_{\text{Edd}}$. S: Seyferts, L: LINERs, T: transition objects, and A: absorption-line nuclei. Open histograms denote upper limits. From Ho (2005).

Quite apart from any additional fuel furnished by the large-scale disk of the host galaxy or from external sources triggered by tidal interactions, both of which are inconsequential for nearby galaxies (Ho et al., 1997b, 2003), galactic centers contain two reservoirs of fuel that seems inescapable. The first is mass loss from evolved stars, which is readily available from the dense stellar cusps invariably observed in the centers of bulges (e.g., Lauer et al., 1995; Ravindranath et al., 2001). Ho (2005) estimates $\dot{M}_* \gtrsim 10^{-5} - 10^{-3} M_\odot$ per year. The other source of fuel is Bondi accretion of hot gas, which is ubiquitous not only in giant elliptical galaxies, but apparently also in the bulges of disk galaxies (e.g., Shirey et al., 2001; Baganoff et al., 2003). The expected contribution from Bondi accretion turns out to be roughly comparable to \dot{M}_* (Ho, 2005). If this gas were to be all accreted and radiates with a standard efficiency of $\eta = 10\%$, the nuclei should be 1–4 orders of magnitude more luminous than observed. Three possible explanations come to mind: (1) angular momentum transfer is very inefficient, even at these small scales, so that only a tiny fraction of the available fuel makes it to the center; (2) the accretion flow is radiatively inefficient, with η much less than 10%; (3) most of the gas is blown out of the system by winds or outflows, which arise naturally in radiatively (e.g., Blandford and Begelman, 1999). (Note that the third option is not entirely independent from the second.) While it is difficult to rule out the first explanation, it seems plausible that these systems are radiatively inefficient.

- *Unusual SEDs.* With few exceptions, the spectral energy distributions (SEDs) of LLAGNs lack the optical-UV “big blue bump,” a feature usually attributed to thermal emission from an optically thick, geometrically thin accretion disk (Ho, 1999, 2002a; Ho et al., 2000). This is illustrated in Figure 2, which compares the average SED of LLAGNs with the canonical SEDs of radio-loud and radio-quiet quasars (Elvis et al., 1994). Instead of a blue excess, there is a maximum peaking somewhere in the mid-IR. (The exact location of the peak is poorly defined because of the current lack of high-resolution IR data.) One consequence of the deficit of optical-UV omission is that the X-rays become disproportionately important energetically. The standard α_{ox} parameter is typically less than 1, whereas in luminous AGNs $\alpha_{\text{ox}} \approx 1.4$. The X-ray spectra can be well described by a simple power law, with $\Gamma \approx 1.7 - 1.9$, which generally requires only little or modest intrinsic absorption, with no evidence for a soft excess at low energies (e.g., Terashima et al., 2002; Terashima and Wilson, 2003; Ptak et al., 2004).
- *Radio jets.* Another notable feature of the SEDs of LLAGNs is that they tend to be generically radio-loud. This is true of most LINERs (Ho, 1999, 2002b; Ho et al., 2000; Terashima and Wilson, 2003), and, contrary to persistent popular misconception, is so even in most Seyfert nuclei (Ho and Peng, 2001). Detailed modeling of the SEDs (e.g., Quataert et al., 1999; Ulvestad and Ho, 2001; Anderson et al., 2004) shows that neither the radio power nor the detailed radio spectrum agrees with predictions from accretion flow models. Instead, a

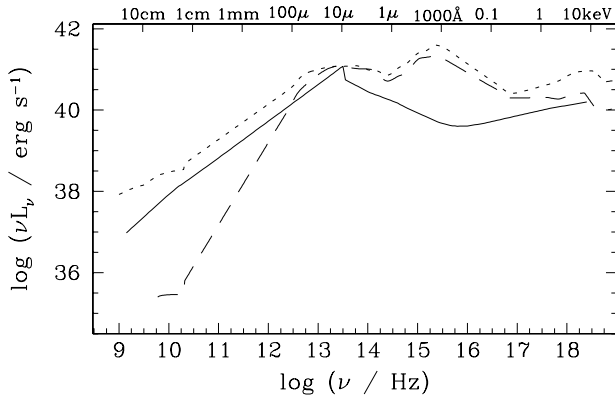


Figure 2. The average SED of low-luminosity AGNs (*solid line*), adapted from Ho (1999). Overplotted for comparison are the average SEDs of powerful radio-loud (*dotted line*) and radio-quiet (*dashed line*) AGNs (Elvis et al., 1994). The curves have been arbitrarily normalized to the luminosity at $10 \mu\text{m}$.

separate, compact jet component is required. This indicates that compact jets develop naturally in LLAGNs.

- *No broad Fe K α line.* The 6.4 keV Fe K α line is detected in some LLAGNs, but it is almost always narrow (Terashima et al., 2002). In well-studied cases (e.g., Ptak et al., 2004), Fe K α emission of any breadth can be ruled out to very high significance. Insofar as the broad iron line is regarded as a signature of a standard optically thick disk, this suggests that such a disk is generically absent or truncated in LLAGNs.
- *Disk-like H α profiles.* Emission lines with broad, double-peaked profiles, taken to be the kinematic signature of a relativistically broadened disk, are found quite often in LLAGNs (Ho et al., 2000, and references therein; Shields et al., 2000; Barth et al., 2001; Eracleous and Halpern, 2001). When fitted with a disk model, one infers that the disk has a relatively large inner radius ($\sim 10^3 R_S$).

3. A Physical Picture of the Central Engine

I propose that the set of characteristics mentioned earlier, common to most LLAGNs studied in detail thus far, suggest that nearby galaxy bulges contain central engines as schematically depicted in Figure 3. Most galaxies with bulges contain active nuclei because most, if not all, bulges contain massive black holes. This is consistent with the picture that has emerged from recent kinematical studies of nearby galaxies (e.g., Richstone, 2004). In the present-day Universe, and especially in the centers of big bulges, the amount of gas available for accretion is quite small, plausibly well below the Eddington rate for the associated black hole mass (Ho, 2005).

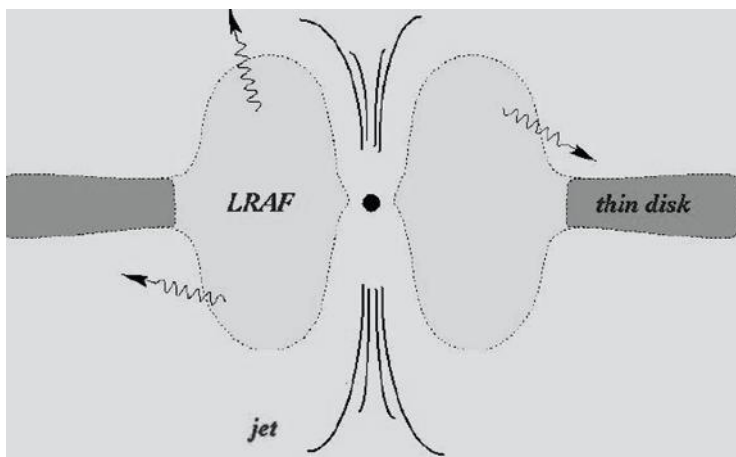


Figure 3. A cartoon depicting the structure of the accretion flow surrounding weakly active massive black holes. An inner low-radiative efficiency accretion flow (LRAF) irradiates an outer, truncated thin disk. An additional compact jet component is needed.

In such a regime, the low-density, tenuous material is optically thin and cannot cool efficiently. Rather than settling into a classical optically thick, geometrically thin disk, the hot accretion flow assumes a quasi-spherical configuration, whose dynamics may be dominated by advection, convection, or outflows (see Quataert, 2001 and Narayan, these proceedings.) For simplicity, I follow Quataert (2001) and simply call these low-radiative efficiency accretion flows (LRAFs). The existence of LRAFs in these systems, or conversely the absence of classical thin disks extending all the way to small radii (few R_S), is suggested by their (1) low luminosities, (2) low Eddington ratios, (3) low inferred radiative efficiencies, (4) lack of a big blue bump, and (5) lack of relativistically broadened Fe $K\alpha$ lines.

Apart from a central LRAF, two additional components generally seem to be required. First, detailed considerations of the broad-band SED show that the baseline LRAF spectrum underpredicts the observed radio power (e.g., Quataert et al., 1999; Ulvestad and Ho, 2001). Most of the radio luminosity, which is substantial because these objects tend to be “radio-loud,” must come from another component, and the most likely candidate is a compact jet. Does the puffed-up structure of an LRAF, or its propensity for outflows, somehow facilitate the generation of relativistic jets? Second, an outer thin disk, truncated at perhaps $\sim 100\text{--}1000 R_S$, seems necessary to explain (1) the existence of the IR excess in the SED (e.g., Quataert et al., 1999) and (2) the prevalence of double-peaked broad emission lines (Chen et al., 1989; Ho et al., 2000). A large truncation radius is also qualitatively consistent with the weakness or absence of broad Fe $K\alpha$ emission.

Lastly, we note that low-ionization spectra may emerge quite naturally in the scenario suggested earlier. In the context of AGN photoionization models, it is well known that LINER-like spectra can be produced largely by lowering the “ionization

parameter" U , typically by a factor of ~ 10 below that in Seyferts (e.g., Halpern and Steiner, 1983; Ferland and Netzer, 1983). The characteristically low luminosities of LINERs (Figure 1a), coupled with their low densities (Ho et al., 2003), naturally lead to low values of U . Two other effects, however, are also important in boosting the low-ionization lines. All else being equal, hardening the ionizing spectrum (by removing the big blue bump) in photoionization calculations creates a deeper partially ionized zone from which low-ionization transitions, especially [O I] $\lambda\lambda 6300, 6363$, are created. Because of the prominence of the radio spectrum, cosmic-ray heating of the line-emitting gas by the radio-emitting plasma may be nonnegligible; one consequence of this process is again to enhance the low-ionization lines (Ferland and Mushotzky, 1984). Both of these effects should be investigated quantitatively.

Acknowledgements

L. C. H. acknowledges financial support from the Carnegie Institution of Washington and from NASA grants.

References

- Anderson, J.M., Ulvestad, J.S. and Ho, L.C.: 2004, *ApJ* **603**, 42.
 Baganoff, F.K. et al.: 2003, *ApJ* **591**, 891.
 Barth, A.J., Ho, L.C., Filippenko, A.V., Rix, H.-W. and Sargent, W.L.W.: 2001, *ApJ* **546**, 205.
 Blandford, R.D. and Begelman, M.C.: 1999, *MNRAS* **303**, L1.
 Chen, K., Halpern, J.P. and Filippenko, A.V.: 1989, *ApJ* **339**, 742.
 Collin, S. and Kawaguchi, T.: 2004, *A&A* **426**, 797.
 Elvis, M. et al.: 1994, *ApJS* **95**, 1.
 Eracleous, M. and Halpern, J.P.: 2001, *ApJ* **554**, 240.
 Ferland, G.J. and Mushotzky, R.F.: 1984, *ApJ* **286**, 42.
 Ferland, G.J. and Netzer, H.: 1983, *ApJ* **264**, 105.
 Halpern, J.P. and Steiner, J.E.: 1983, *ApJ* **269**, L37.
 Ho, L.C.: 1999, *ApJ* **516**, 672.
 Ho, L.C.: 2002a, in: R. Maiolino, A. Marconi, and N. Nagar (eds.), *Issues in Unification of AGNs*, ASP, San Francisco, p. 165.
 Ho, L.C.: 2002b, *ApJ* **564**, 120.
 Ho, L.C.: 2004, in: L.C. Ho (ed.), *Carnegie Observatories Astrophysics Series, Vol. 1: Coevolution of Black Holes and Galaxies*, Cambridge University Press, Cambridge, p. 293.
 Ho, L.C.: 2005, manuscript in preparation.
 Ho, L.C., Filippenko, A.V. and Sargent, W.L.W.: 1993, *ApJ* **417**, 63.
 Ho, L.C., Filippenko, A.V. and Sargent, W.L.W.: 1997a, *ApJ* **487**, 568.
 Ho, L.C., Filippenko, A.V. and Sargent, W.L.W.: 1997b, *ApJ* **487**, 591.
 Ho, L.C., Filippenko, A.V. and Sargent, W.L.W.: 2003, *ApJ* **583**, 159.
 Ho, L.C. and Peng, C.Y.: 2001, *ApJ* **555**, 650.

- Ho, L.C., Rudnick, G., Rix, H.-W., Shields, J.C., McIntosh, D.H., Filippenko, A.V., Sargent, W.L.W. and Eracleous, M.: 2000, *ApJ* **541**, 120.
- Lauer, T.R., et al.: 1995, *AJ* **110**, 2622.
- McClintock, J.E. and Remillard, R.A.: 2005, in: W.H.G. Lewin and M. van der Klis (eds.), *Compact Stellar X-ray Sources*, Cambridge University Press, Cambridge, in press (astro-ph/0306213).
- Pounds, K.A., Done, C. and Osborne, J.P.: 1995, *MNRAS* **277**, L5.
- Ptak, A., Terashima, Y., Ho, L.C. and Quataert, E.: 2004, *ApJ* **606**, 173.
- Quataert, E.: 2001, in: B.M. Peterson, R.S. Polidan, and R.W. Pogge (eds.), *Probing the Physics of Active Galactic Nuclei by Multiwavelength Monitoring*, ASP, San Francisco, p. 71.
- Quataert, E., Di Matteo, T., Narayan, R. and Ho, L.C.: 1999, *ApJ* **525**, L89.
- Ravindranath, S., Ho, L.C., Peng, C.Y., Filippenko, A.V. and Sargent, W.L.W.: 2001, *AJ* **122**, 653.
- Richstone, D.: 2004, in: L.C. Ho (ed.), *Carnegie Observatories Astrophysics Series, Vol. 1: Coevolution of Black Holes and Galaxies*, Cambridge University Press, Cambridge, p. 281.
- Shields, J.C., Rix, H.-W., McIntosh, D.H., Ho, L.C., Rudnick, G., Filippenko, A.V., Sargent, W.L.W. and Sarzi, M.: 2000, *ApJ* **534**, L27.
- Shirey, R. et al.: 2001, *A&A* **365**, L195.
- Terashima, Y., Iyomoto, N., Ho, L.C. and Ptak, A.F.: 2002, *ApJS* **139**, 1.
- Terashima, Y. and Wilson, A.S.: 2003, *ApJ*, in press.
- Ulvestad, J.S. and Ho, L.C.: 2001, *ApJ* **562**, L133.

PRESENT EVIDENCE FOR INTERMEDIATE MASS BLACK HOLES IN ULXs AND FUTURE PROSPECTS

J.M. MILLER

Harvard-Smithsonian CfA, 60 Garden Street, Cambridge, MA, U.S.A.;
E-mail: jmmiller@cfa.harvard.edu

(Received 17 December 2004; accepted 1 June 2005)

Abstract. In a number of the most luminous ULXs (those with $L_X \sim 10^{40}$ erg s $^{-1}$) in nearby galaxies, observations with *XMM-Newton* and *Chandra* are revealing evidence which suggests that these ULXs may harbor intermediate-mass black holes (IMBHs). The detection of accretion disk spectral components with temperatures 5–10 times lower than the temperatures observed in stellar-mass black hole binaries near to their Eddington limit may be particularly compelling evidence for IMBH primaries, since $T \propto M^{-1/4}$ for disks around black holes. In some sources, X-ray timing diagnostics also hint at IMBHs. Evidence for IMBHs in a subset of the most luminous ULXs, a discussion of the robustness of this evidence and alternatives to the IMBH interpretation, and prospects for better determining the nature of these sources in the future, are presented in this work.

1. Introduction to ULXs

Ultraluminous X-ray sources (ULXs) are bright, off-nuclear point sources in nearby normal galaxies, for which the inferred X-ray luminosity exceeds the isotropic Eddington limit for a $10 M_\odot$ black hole ($L \simeq 1.3 \times 10^{39}$ erg s $^{-1}$; Frank et al., 2003). In most ULXs, long-timescale X-ray variability indicates that the ULXs are likely accreting black hole binaries like those known in the Milky Way. The existence of ULXs was first revealed with *Einstein* (Fabbiano, 1989). *Chandra* and *XMM-Newton* have revolutionized the study of these sources by enabling observations which effectively isolate individual sources and which obtain sensitive spectra and lightcurves from the brightest nearby examples. For a recent review of ULXs, see, e.g., Fabbiano and White (2005).

Among the reasons that ULXs are interesting is that they may represent rare phases of accretion in binary systems, rare X-ray states, and/or rare phases of binary evolution; however, the most compelling reason to study ULXs is that their luminosities suggest that they may harbor intermediate mass black holes (IMBHs, $10^{2-5} M_\odot$; for a recent review see Miller and Colbert, 2004). It is well-known that stellar-mass black holes can reach luminosities slightly in excess of their implied isotropic Eddington limit (see, e.g., McClintock and Remillard, 2005), so ULXs at the lower end of the luminosity range (indeed, this is the majority of ULXs) are likely binaries with stellar-mass black hole primaries (or neutron star primaries in rare



cases). However, those ULXs at the upper-end of the luminosity range (arbitrarily, $L_X \geq 10^{40}$ erg s $^{-1}$) may harbor IMBHs. Recent observations with *Chandra* and *XMM-Newton* (in particular) have revealed cool accretion disk components in the spectra of the most luminous ULXs (see Miller et al., 2004a) and other X-ray spectral and timing features which suggest IMBHs. The status of the evidence for IMBHs in ULXs, arguments against IMBHs, and prospects for better understanding the IMBH candidates is discussed below.

2. Evidence for IMBHs in ULXs

Spectra of bright ULXs obtained with *ASCA* were typically described in terms single flux components, and often in terms of hot accretion disk components (Makishima et al., 2000), although weak evidence for two-component spectra consisting of cool accretion disk and hard power-law flux components was also reported (Colbert and Mushotzky, 1999). Recent observations of the most luminous and proximal ULXs with *XMM-Newton* and *Chandra* appear to have resolved this discrepancy: Miller et al. (2003) first reported the detection of a cool accretion disk at the 8σ level of confidence in *XMM-Newton* spectra of NGC 1313 X-1 (see Figure 1). Other significant detections of cool disk components have been reported in *XMM-Newton* and/or *Chandra* spectra of NGC 1313 X-2 (Miller et al., 2003), NGC 5408 X-1 (Kaaret et al., 2003), M81 X-9 (Holmberg IX X-1, Miller et al., 2004a), Antennae

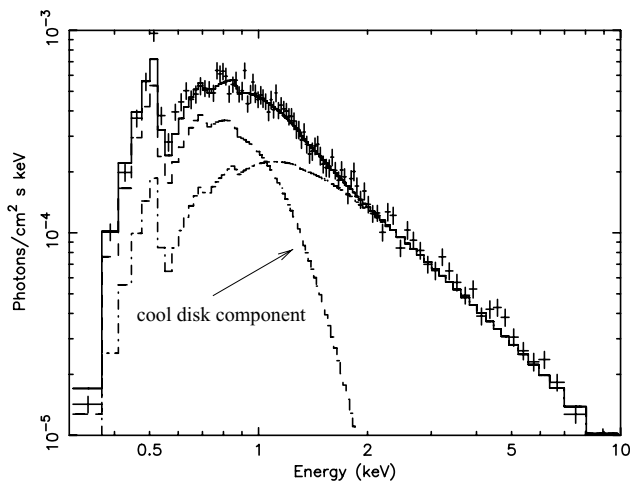


Figure 1. The *XMM-Newton*/EPIC-pn X-ray spectrum of NGC 1313 X-1 is shown above (Miller et al., 2004b). A disk component is shown in blue, and hard power-law emission is shown in red. In this source and a growing number of other ULXs, X-ray spectra require a cool disk component, which may be evidence for an accreting IMBH, e.g., in a binary system.

X-37 (Miller et al., 2004), Holmberg II X-1 (Dewangan et al., 2004), NGC 4559 X-7 (Cropper et al., 2000), and most recently in a ULX in M101 (Kong et al., 2004).

In each of these cases, the luminosity of the ULX is near to or above $L_X \simeq 10^{40}$ erg s $^{-1}$, and the measured disk color temperature is consistent with the $kT \simeq 0.1$ – 0.2 keV range. These ULX disk temperatures are much lower than the $kT \simeq 1$ – 2 keV disk temperatures commonly measured in $\sim 10 M_\odot$ black hole binaries in the Milky Way and LMC when they are observed at luminosities near to their Eddington limit. Indeed, because $T \propto M^{-1/4}$ for standard disks around black holes (Frank et al., 2002), the low disk temperatures measured in these ULXs imply black holes with masses in the $few \times 10^{2-3} M_\odot$ range when scaled to the temperatures seen in stellar-mass black hole binaries. (The normalizations of these disk components can also be scaled and generally imply IMBHs; see Miller et al., 2003.) These ULXs occupy a distinct region of a $L_X - kT$ diagram, which is distinct from the $L \propto T^4$ trend clearly seen in stellar-mass black holes (see Figure 2; see also Miller et al., 2004a). The exceptionally high luminosities inferred in these sources, their low disk temperatures, and their clustering in a $L_X - kT$ diagram makes these sources strong IMBH-candidates.

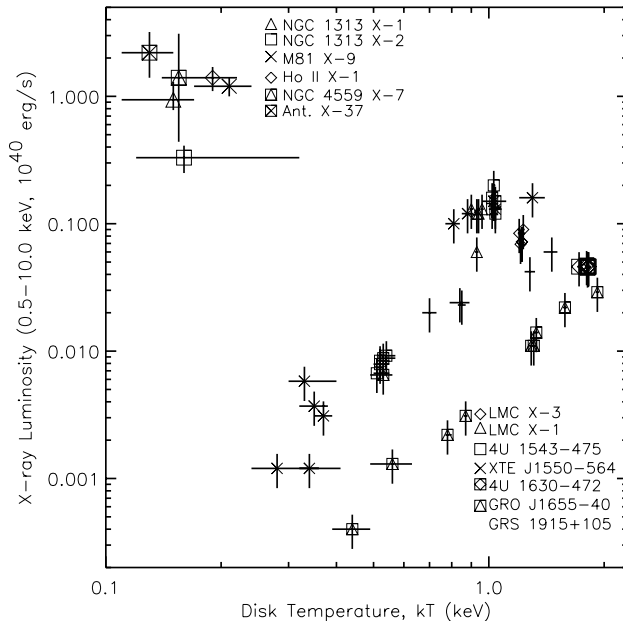


Figure 2. ULXs with cool accretion disks do not lie on the temperature–luminosity trend observed in stellar-mass black holes, and form a rather tight group, suggesting a distinct subclass, which may indeed harbor IMBHs (Miller et al., 2004a).

M82 X-1 may be the single best IMBH-candidate ULX presently known, in part due to its exceptionally high luminosity, which approaches $L_X \simeq 10^{41}$ erg s $^{-1}$. However, the nature of its low energy spectrum is unknown due to contamination from a surrounding thermal plasma. Strohmayer and Mushotzky (2003) have reported the detection of a 54 mHz QPO in the X-ray flux of this ULX, based on observations with *XMM-Newton* and *RXTE*. As QPOs are thought to be disk oscillations, this feature indicates that the X-ray flux is not beamed, and implies the observed luminosity is a true isotropic luminosity, greatly reinforcing an IMBH interpretation when scaling from the Eddington luminosity for a stellar-mass black hole.

A timing diagnostic has been interpreted as tentative evidence for an IMBH in at least one other case: Cropper et al. (2004) have reported a break frequency at 28 mHz in the power density spectrum of NGC 4559 X-7. The break could indicate a mass of $38 M_\odot$ or $1300 M_\odot$, as there are *two* breaks commonly observed in the power spectra of accreting black holes (both in stellar-mass and supermassive black holes; see, e.g., Uttley et al., 2002). It is very difficult to obtain a mass scaling from either a single break or a single QPO, and indeed there is still some ambiguity when two breaks or multiple QPOs are detected since characteristic frequencies drift with flux.

3. On the Robustness of Evidence for IMBHs in ULXs

3.1. DETAILS OF THE SPECTRAL MODELING

Evidence for cool accretion disks in sources with luminosities near to 10^{40} erg s $^{-1}$ is generally quite robust. The requirement for low disk temperature with normalizations also suggesting IMBH primaries does not depend on the choice of disk model (Miller et al., 2004a). Cool disks are required regardless of whether independent flux components or self-consistent Compton up-scattering models are used to fit the X-ray spectra (Miller et al., 2003, 2004). An uncertainty in scaling from disks around stellar-mass black holes to disks around presumed IMBHs exists due to potential differences between the intrinsic disk spectrum and measured spectrum (after transfer through a disk atmosphere). However, it has recently been shown that these effects are remarkably similar in disks around stellar-mass black holes and IMBHs (Fabian et al., 2004). Finally, low metal abundances in absorbing material along the line of sight to these sources does not falsely create a statistical need for a cool disk component in the most sensitive spectra (Miller et al., 2003, 2004).

In the *ASCA* era, the spectra of some of the most luminous ULXs could be described only in terms of a single hot disk component (temperatures approached 2 keV; see Makishima et al., 2000). It is now clear that these sources are generally better described with a combination of a cool disk and hard power-law. Both

Chandra and *XMM-Newton* have much better spatial resolution than *ASCA*, and so fold in far less background (both diffuse and point-source in nature). Moreover, the lower energy bounds of *Chandra* and *XMM-Newton* are lower than the effective lower energy bound of *ASCA*, which gradually increased over the mission lifetime.

Stobbart et al. (2004) recently fit the spectrum of a dipping ULX in NGC 55 ($L_x = 1.6 \times 10^{39} \text{ erg s}^{-1}$) with a model consisting of a hot ($kT = 0.8 \text{ keV}$) disk dominating the high energy spectrum, and a very soft ($\Gamma = 4$) power-law dominating the low energy spectrum. Some parameters were fixed in fits to the spectra of this ULX (this is not a standard practice), so it is not clear that a model consisting of a low temperature disk and hard power-law is inconsistent with the data (though the spectra of dipping sources can be confusing and non-standard). Given the peculiarity of the prior spectral fits, and given that the model is inconsistent with the observed spectra of stellar-mass Galactic black hole binaries and Compton up-scattering models for hard X-ray emission (Stobbart et al. note these facts), re-analysis of the spectra of the ULX in NGC 55 may be in order.

Although this model is likely unphysical, it is interesting to test whether or not it might provide a reasonable alternative (in terms of a goodness-of-fit statistic) to spectra of IMBH-candidate ULXs which are presently well described in terms of cool disks and hard power-law components. Let us take NGC 1313 X-1 as an example. Jointly fitting the *XMM-Newton* PN, MOS1, and MOS2 spectra of NGC 1313 X-1 (see Miller et al., 2003, 2004) with a simple model consisting of multicolor disk black body and power-law components (modified by neutral absorption), the cool disk plus hard power-law model gives a very good fit: $\chi^2/\text{dof} = 885.8/870$ ($kT = 0.18 \text{ keV}$, $\Gamma = 1.8$). Constraining the disk temperature to be $kT \geq 1.0 \text{ keV}$, the resultant fit is significantly worse statistically: $\chi^2/\text{dof} = 965.3/870$ ($kT = 2.6 \text{ keV}$, $\Gamma = 4.3$).

As stated before, M82 X-1 is unlike other IMBH-candidate ULXs in that it is embedded in a region of strong diffuse plasma emission, which makes it very difficult to constrain the nature of its low energy spectrum (see Strohmayer and Mushotzky, 2003). Although other strong IMBH-candidate ULXs are not located within or near to clusters of young stars, it is nevertheless important to understand the extent to which thermal plasmas may contribute to the low-temperature thermal emission. At low temperatures, an O VII or O VIII emission line should be particularly strong, and there is no evidence for such a line in the X-ray spectra of IMBH-candidate ULXs (note that careful fitting of the O K-edge is required to prevent false O VII/VIII line detections; see Miller et al., 2004a). At present, no soft X-ray (i.e., 0.3–3.0 keV) line has been reported in a ULX which is significant at or above the 3σ level. Thus, it presently appears that the low-temperature thermal components detected in some ULXs are due to optically-thick disk components, but improved spectra are required to put strong constraints on possible contributions from an optically-thin thermal plasma.

3.2. RELATIVISTIC BEAMING

Relativistic beaming of source flux has been proposed as a means of explaining luminosities in apparent excess of the isotropic Eddington limit for a $10 M_{\odot}$ black hole (Reynolds et al., 1997; Körding et al., 2002). The very low radio to X-ray flux ratios found in luminous ULXs with cool disks strongly argues against this interpretation, since beaming tends to create flat νF_{ν} spectra (e.g., in blazars; see Fossati et al., 1998 for characteristic blazar spectra; Miller et al., 2003, 2004; Kaaret et al., 2003 for discussions of the relevance to ULXs). Indeed, the ratios found are below the maximum ratios observed in stellar mass black holes which are observed *edge-on* (see Fender and Kuulkers, 2001), rather than along a line of sight coincident with a jet axis. Blackbody components imply a minimum physical size, and here again the cool disks detected argue against relativistic beaming. Finally, it should be noted that in the special case of M82 X-1, the detection of QPO strongly argues that the disk is seen clearly, and therefore argues against relativistic beaming as a viable means of explaining the inferred luminosity (Strohmayer and Mushotzky, 2003).

It is interesting to consider how the broadband properties of IMBH-candidate ULXs with constraining radio limits or detections compare to stellar-mass and supermassive black holes. Merloni et al. (2003) examined the properties of a number of unbeamed black holes, and found a fundamental plane of black hole activity which relates mass, X-ray luminosity, and radio luminosity. Figure 3 shows the fundamental plane, with the addition of the IMBH-candidate ULXs NGC 1313 X-1, M81 X-9, NGC 5408 X-1, and M82 X-1. These black holes lie on the fundamental plane, or only slightly above the plane (but no farther than the scatter in the supermassive black holes population). This again implies that these sources are not beamed, and their position between the stellar-mass black hole population and supermassive black holes again suggests that they may indeed harbor IMBHs.

3.3. DISK ISSUES: FUNNELS, PHOTON BUBBLES, AND SLIM DISKS

It has been suggested that at very high mass accretion rates, a funnel may form at the inner disk and boost luminosities by factors of 10–30 along the funnel axis (King et al., 2001). This model would allow $\sim 10 M_{\odot}$ black holes to apparently violate the isotropic Eddington limit, and could explain the high apparent luminosities seen in some ULXs. The low disk temperatures measured in some IMBH-candidate ULXs already argue against this model, because disk temperatures in the 0.1–0.2 keV range would only signal a high mass accretion rate for IMBHs. Observations of stellar-mass galactic black holes also argue against the formation of such structures: 4U 1543-475 is a Galactic black hole binary viewed at $i = 21^{\circ}$, but it does not exceed its Eddington limit by more than a factor of a few (Miller et al., 2004b; Park et al., 2004). Stronger funneling might be required, but radiation will leak out the

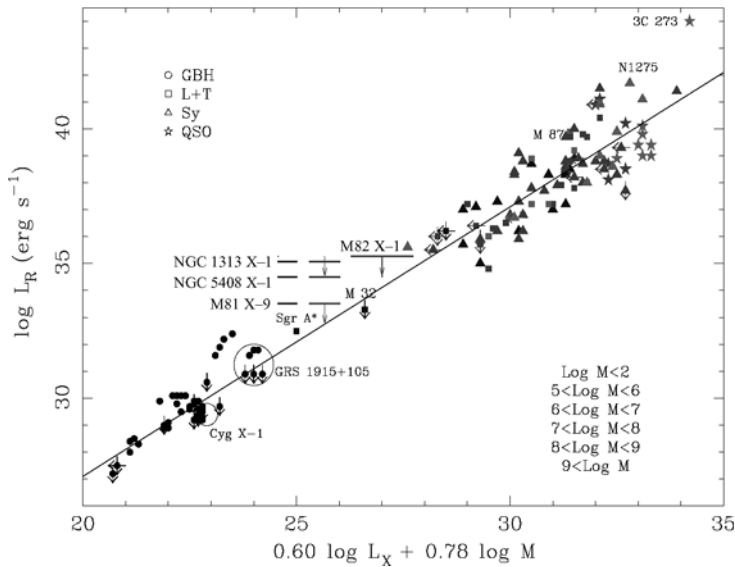


Figure 3. Merloni et al. (2003) found a “fundamental plane” relating black hole mass, X-ray luminosity, and radio luminosity in unbeamed sources. Bright ULXs with cool disks and good limits on radio flux (NGC 1313 X-1: Colbert et al., 1995; M81 X-9: $F \leq 60 \mu\text{Jy}$ at 5 GHz, Jimenez-Garate et al., 2005, in preparation) or radio detections (NGC 5408 X-1: Kaaret et al., 2003), and M82 X-1, fit between stellar-mass and supermassive black holes on the fundamental plane. For M82 X-1, the radio limits and lower mass bound are from Kaaret et al. (2001), and the upper mass bound is from Strohmayer and Mushotzky (2003). For the other sources, solid error bars represent a mass range of $300\text{--}3000 M_{\odot}$, a representative range for disk normalization and temperature scaling, respectively, and the dashed error bars extend down to approximately the mass found from simple Eddington limit scaling. (The fundamental plane makes use of 2–10 keV luminosity values and flux densities at 5 GHz. ULX luminosities reported in Miller et al., 2004a were converted to the 2–10 keV band and flat radio spectra were assumed).

sides of a strong funnel geometry as it becomes ionized and optically-thin, ruining the funnel effect (King and Pounds, 2003). Finally, in the case of Holmberg II X-1, optical spectroscopy of a surrounding nebula reveals that the isotropic luminosity must exceed the Eddington limit for a $10 M_{\odot}$ black hole (Kaaret et al., 2004), and the morphology of optical nebulae around other ULXs does not strongly suggest beaming.

It has also been suggested that radiation pressure-dominated disks might be able to produce super-Eddington fluxes through small-scale photon bubble instabilities (Begelman, 2002). Slim disk solutions (e.g., Watarai et al., 2001) may also allow high fluxes. Where IMBH-candidate ULXs are concerned, the difficulty with both models is that they are expected to hold at very high mass accretion rates – when disks are expected to be hot. The low disk temperatures observed in some IMBH-candidate ULXs means that photon-bubble disk and/or slim disks are not required in these sources.

3.4. PHOTOSPHERES

It has recently been suggested that the basic disk plus corona geometry inferred in black hole systems accreting at high rates may be incorrect, and that a better model may consist of an outflowing photosphere which is optically thick at $r \leq 100 R_{\text{Schw.}}$ and external shocks generating hard X-rays (King and Pounds, 2003). In any case where the flux in the hard spectral component is equal to the flux in the soft component, the photosphere would have to flow at $v = c$ and the photospheric radius would have to equal $1 R_{\text{Schw.}}$ to generate the observed hard X-ray flux, which renders this alternative implausible in most ULXs with cool disks and luminous quasars. Weak X-ray absorption lines in the spectra of some AGN – apparently blue-shifted in the frame of the AGN and cited as evidence in favor of outflowing photospheres – have recently been shown to coincide with the AGN recession velocity in a number of cases, demanding absorption near to the Milky Way (McKernan et al., 2004). Thus, both in the case of AGN and ULXs, the data would seem to argue against this alternative in the majority of cases.

It should be noted that sources like the bright, soft transient in M101 (Kong et al., 2004), as well as “super-soft” sources and “quasi-soft” sources, do not have significant hard components and the photosphere model cannot be excluded in these cases. Apart from the immediate issue of photospheres, the very low flux observed from super-soft and quasi-soft sources makes it nearly impossible to obtain strong spectral and timing constraints, and inferences for IMBHs in these sources require extreme caution as they are necessarily at the level of what the data will allow, rather than what the data strictly require.

3.5. INFERENCES FROM X-RAY LUMINOSITY FUNCTIONS

It is sometimes argued that X-ray luminosity functions demonstrate that all ULXs are stellar-mass X-ray binaries, because the highest luminosity sources appear to extend naturally from the lower-luminosity distribution without a break (see, e.g., Swartz et al., 2004). Several assumptions are implicit in such an argument: first, that IMBHs should have a narrow mass range (a wide range of masses would act to diminish a break); second, that IMBHs should all be accreting at high fractions of their Eddington limit (a range of mass accretion rates like that seen in stellar-mass binaries in the Milky Way and Magellanic Clouds would also act to flatten a break); and third, that a single observation or a few observations can reliably constrain the nature of a source population that is likely to be variable.

The high luminosity end of the X-ray luminosity function of a given galaxy is a regime with very few sources, where strong constraints are not possible. The statistics do not allow one to strongly require or to exclude a break. Consider how different the X-ray luminosity functions of galaxies like M101 (Kong et al., 2004) and NGC 3628 (Strickland et al., 2001) must appear when their transient ULXs (which reach near to or above $L_X \simeq 10^{40} \text{ erg s}^{-1}$) vary by factors of 10 and 1000,

respectively. Again, as this regime is a low-statistics regime, it is unlikely that one source or even two sources could require a break, but it illustrates the danger of drawing conclusions about source populations based on X-ray luminosity functions. In fact, the statistical uncertainty of X-ray luminosity functions is worse than typically presented: errors on luminosity resulting from uncertainties in the absorbing column and differences between spectral models that cannot be distinguished in poor quality spectra are not generally considered.

X-ray luminosity functions do indicate that only a small number of IMBHs are accreting at high fractions of their Eddington limit at any given time in a typical galaxy. This inference is broadly consistent with the behaviors observed from stellar mass and supermassive black holes. Moreover, X-ray luminosity functions may demonstrate that the population of IMBHs which may exist in binaries is likely small relative to the number of black holes and neutron stars in accreting binaries. These inferences are limited, but as such they are fair to the limited statistics at the high luminosity end of X-ray luminosity functions.

4. Future Prospects

It will likely prove to be very difficult to obtain optical/IR radial velocity curves of ULXs to constrain the mass of the primary. Putting even the brightest stellar-mass Galactic binaries at distances of a few Mpc makes them very faint indeed. Further complications arise because most IMBH-candidate ULXs – in contrast to most stellar-mass Galactic black holes – are persistently active; light from the accretion disk will make it difficult to identify and trace features from the companion star. If ULXs are very wide binaries, the long orbital period will make it even harder to obtain radial velocity curves. The optical nebulae found around some IMBH-candidate ULXs (Pakull and Mirioni, 2003) may further complicate spectroscopic studies of the presumed binary system. For the foreseeable future, it is likely that the nature of IMBH-candidate ULXs will be decided based on a preponderance of indirect evidence.

From an X-ray point of view, much longer observations of galaxies harboring IMBH-candidate ULXs are urgently needed. Observations of 300–500 ks (and longer) have been devoted to the study of relativistic effects in accreting sources (e.g., 500 ks to study putative absorption lines from the surface of the neutron star in EXO 0748-676, nearly 400 ks to study the broad Fe $K\alpha$ emission line in MCG-6-30-15, and nearly 300 ks to study the broad Fe $K\alpha$ emission line in GX 339-4). Establishing the presence or absence of IMBHs – a new class of relativistic objects – is a goal as deserving of long observations as the study of phenomena in known classes of relativistic objects.

For ULXs within a few Mpc with $L_X \geq 10^{40}$ erg s⁻¹, an *XMM-Newton* observation of 300–500 ks will achieve the sensitivity required to: (1) detect a broad Fe $K\alpha$ emission line from the accretion disk, which would provide independent evidence

for a standard accretion disk and rule-out relativistic and geometric beaming; (2) detect breaks in the power-density spectrum and/or QPOs, which will enable independent mass estimates based on scaling the characteristic frequencies (indeed, the relation between QPO frequency and break frequency in Galactic black holes and neutron stars found by Wijnands and van der Klis, 1999 may provide an additional pragmatic scaling beyond scalings based only on breaks); and (3) detect any soft X-ray emission lines, enabling the (likely small) flux of any diffuse optically-thin plasma to be separated from an underlying optically-thick disk continuum.

Of course, far better radio and optical constraints are also required. Even though optical/IR radial velocity curves may be difficult to obtain, the value of spectroscopic studies of the nebulae surrounding some ULXs is clear (see Pakull and Mirioni, 2003; Kaaret et al., 2004). Independent luminosity and beaming constraints can impact our view of the nature of IMBH-candidate ULXs. Better radio constraints are needed to rule-out beaming in more sources. Radio detections may not be possible in some cases, but strong limits allow sources to be placed on the “fundamental plane” (for instance), and the position of sources on the “fundamental plane” does reflect their nature (though it does not allow for a precise mass measurement). Mushotzky (2004) and collaborators have undertaken a radio survey of ULXs, and in some cases have found broad contours coincident with the X-ray source positions; the lack of strongly peaked point source emission in most cases may again argue against beaming.

X-rays probe the regions closest to compact objects, and can be expected to have the greatest impact on our understanding of ULXs and IMBH-candidate ULXs in particular. In the long run, planned missions like *Constellation-X* and *XEUS* will revolutionize the study of ULXs. These missions will make it possible to obtain sensitive spectroscopic and timing constraints on ULXs with short observations. Relativistic reverberation mapping in AGN may be a primary goal of missions like *Constellation-X* and *XEUS*, but for a variety of possible designs, these missions will be able to reveal or reject the IMBH hypothesis in a much higher number of ULXs.

5. Summary

The notorious M82 X-1 and at least six ULXs with luminosities near to or above $L_X \simeq 10^{40} \text{ erg s}^{-1}$ and soft components consistent with optically-thick emission from cool ($kT = 0.1\text{--}0.2 \text{ keV}$) accretion disks (Miller et al., 2004b) may be regarded as IMBH-candidates. The properties which have been observed to separate these ULXs from populations of stellar-mass and supermassive black hole appear to be robust. In the cases where they can be strongly tested, alternative explanations for the high inferred luminosities and the nature of the spectra appear to be implausible. This proceedings has attempted to take a critical view of the evidence supporting an IMBH explanation for a subset of very luminous ULXs, but also

a critical view of the counter-arguments. With regard to the counterarguments, it must be noted that at present there is no direct evidence for beaming (whether relativistic or geometric) in any of these IMBH-candidate ULXs, or in any other ULX. Dramatic strides toward resolving the nature of these sources can be made in the near future with optical and radio observations, and principally with very long X-ray observations.

Acknowledgements

Thanks to A. C. Fabian and M. C. Miller for collaboration and discussions. Thanks to A. Merloni for his generous permission to use the fundamental plane figure, and also to M. Jimenez-Garate for his generous communication of the radio limit on M81 X-9. Thanks to P. Martinez. Final thanks to the National Science Foundation for support through their Astronomy and Astrophysics Postdoctoral Fellowship.

References

- Begelman, M.: 2002, *ApJ* **538**, L97.
- Colbert, E.J.M. and Mushotzky, R.F.: 1999, *ApJ* **519**, 89.
- Cropper, M.C., Soria, R., Mushotzky, R., Wu, K., Markwardt, C. and Pakull, M.: 2004, *MNRAS* **349**, 39.
- Dahlem, M. and Stevens, I.R.: 2001, *ApJ* **560**, 707.
- Dewangan, G., Miyaji, T., Griffiths, R.E. and Lehmann, I.: 2004, *ApJ* **608**, L57.
- Fabbiano, G.: 1989, *ARA&A* **27**, 87.
- Fabbiano, G. and White, N.E.: 2005, in: M. van der Klis and W.H.G. Lewin (eds.), *Compact Stellar X-Ray Sources*, Cambridge University Press, New York, in press, astro-ph/0307077.
- Fabian, A.C., Ross, R.R. and Miller, J.M.: 2004, *MNRAS* **335**, 359.
- Fender, R.P. and Kuulkers, E.: 2001, *MNRAS* **324**, 923.
- Fossati, G., Maraschi, L., Celotti, A., Comastri, A. and Ghisellini, G.: 1998, *MNRAS* **299**, 413.
- Frank, J., King, A.R. and Raine, D.: 2002, in: *Accretion Power in Astrophysics*, Cambridge University Press, Cambridge.
- Kaaret, P.: 2001, *MNRAS* **321**, L29.
- Kaaret, P., Corbel, S., Prestwich, A.H. and Zezas, A.: 2003, *Science* **299**, 365.
- Kaaret, P., Ward, M.J. and Zezas, A.: 2004, *MNRAS* **351**, 83.
- King, A.R., Davies, M.B., Ward, M.J., Fabbiano, G. and Elvis, M.: 2001, *ApJ* **552**, L109.
- King, A.R. and Pounds, K.: 2003, *MNRAS* **345**, 657.
- Kong, A.K.H., DiStefano, R. and Yuan, F.: 2004, *ApJ* **617**, L49.
- Körding, E., Falcke, H. and Markoff, S.: 2002, *A & A* **382**, L13.
- Makishima, K.: 2000, *ApJ* **535**, 632.
- McClintock, J.E. and Remillard, R.A.: 2005, in: M. van der Klis and W.H.G. Lewin (eds.), *Compact Stellar X-Ray Sources*, Cambridge University Press, New York, in press, astro-ph/0306213.
- McKernan, B., Yaqoob, T. and Reynolds, C.S.: 2004, *ApJ*, submitted, astro-ph/0408506.
- Miller, J.M., Fabbiano, G., Miller, M.C. and Fabian, A.C.: 2003, *ApJ* **585**, L37.
- Miller, J.M., Fabian, A.C. and Miller, M.C.: 2004a, *ApJ* **614**, L117.
- Miller, J.M., Fabian, A.C. and Miller, M.C.: 2004b, *ApJ* **607**, 931.

- Miller, J.M., Zezas, A., Fabbiano, G. and Schweizer, F.: 2004, *ApJ* **609**, 782.
- Miller, M.C. and Colbert, E.J.M.: 2004, *IJMPD*, **1**.
- Mushotzky, R.: 2004, in: *The Proceedings of Kyoto, 2003*, in press, astro-ph/0411040.
- Pakull, M. and Mirioni, L.: 2003, in: *New Visions of the X-Ray Universe in the XMM-Newton and Chandra ERA* (ESA SP-488; Noordwijk: ESA), astro-ph/0202488.
- Park S.Q.: 2004, *ApJ* **610**, 378.
- Reynolds, C.S., Loan, A.J., Fabian, A.C., Makishima, K., Brandt, W.N. and Mizuno, T.: 1997, *MNRAS* **286**, 349.
- Stobart, A.-M., Roberts, T.P. and Warwick, R.S.: 2004, *MNRAS* **351**, 1063.
- Strickland, D., Colbert, E.J.M., Heckman, T.M., Weaver, K.A., Swartz, D.A., Ghosh, K.K., Tennant, A.F. and Wu, K.: 2004, *ApJS* **154**, 519.
- Uttley, P., McHardy, I.M. and Papadakis, I.E.: 2002, *MNRAS* **332**, 231.
- Watarai, K., Mizuno, T. and Mineshige, S.: 2001, *ApJ* **549**, L77.

FINDING FAINT INTERMEDIATE-MASS BLACK HOLES IN THE RADIO BAND

T.J. MACCARONE¹, R.P. FENDER² and A.K. TZIOUMIS³

¹*University of Amsterdam, Amsterdam, The Netherlands*

²*School of Physics and Astronomy, University of Southampton, Southampton,
Hampshire S017 1BJ, UK*

³*Australian National Telescope Facility, CSIRO, P.O. Box 76, Epping, NSW 1710, Australia;
E-mail: tjm@phys.soton.ac.uk*

(Received 28 October 2004; accepted 1 June 2005)

Abstract. We discuss the prospects for detecting faint intermediate-mass black holes, such as those predicted to exist in the cores of globular clusters and dwarf spheroidal galaxies. We briefly summarize the difficulties of stellar dynamical searches, then show that recently discovered relations between black hole mass, X-ray luminosity and radio luminosity imply that in most cases, these black holes should be more easily detected in the radio than in the X-rays. Finally, we show upper limits from some radio observations of globular clusters, and discuss the possibility that the radio source in the core of the Ursa Minor dwarf spheroidal galaxy might be a $\sim 10,000\text{--}100,000 M_{\odot}$ black hole.

Keywords: accretion, accretion disks, black hole physics, globular clusters: general, globular clusters: individual: Omega cen, radio continuum: general

1. Introduction

Black holes are generally found to exist in two classes – the stellar mass (i.e. about $10 M_{\odot}$) black holes which are usually found as a result of their being in X-ray binaries, and the galactic mass (i.e. $10^6\text{--}10^9 M_{\odot}$) black holes found in the cores of massive galaxies. Some recent evidence has begun to develop for black holes with masses just below $10^6 M_{\odot}$ (e.g. Filippenko and Ho, 2003; Greene and Ho, 2004), and some of the ultraluminous X-ray sources show evidence for spectral (e.g. Jon Miller's contribution in this volume) and variability (Strohmayer and Mushotzky, 2003) characteristics that would indicate black holes of $100\text{--}1000 M_{\odot}$.

Whether globular clusters and dwarf spheroidal galaxies have black holes in their centers is an especially controversial topic. Some authors have argued that globular clusters should build up black holes of roughly 0.1% of their total mass through mergers of stellar mass black holes (Miller and Hamilton 2002); this fraction of the total mass is roughly the same as the fraction of galactic bulges' masses locked up in their central black holes (Magorrian et al., 1998), and there have been some claims of observational evidence for these intermediate-mass black holes (see e.g. Gebhardt et al., 2002; Gerssen et al., 2002). On the other hand, it has been argued that



the central increases in mass-to-light ratio in globular clusters can be equally well explained by concentrations of white dwarfs (e.g. Baumgardt et al., 2003; Gerssen et al., 2003; Pasquali et al., 2004), and that black holes should be dynamically ejected from globular clusters (Portegies Zwart and McMillan, 2000). It has been suggested (Drukier and Bailyn, 2003) that searches for individual high velocity stars could be the most effective way to search for dynamical evidence of black holes in globular clusters, but that there might not be enough stars to sample the gravitational potentials of globular clusters well enough to make use of this method.

In dwarf spheroidal galaxies, the determination of whether there are intermediate-mass black holes is at least as wide open. As the escape velocities of dwarf spheroidal galaxies are typically smaller than those of globular clusters, it is more likely that the gravitational radiation recoil effect should work to eject black holes participating in unequal mass mergers from these systems (e.g. Favata et al., 2004). On the other hand, it has been suggested on theoretical grounds that because the dwarf galaxies are likely to be the first galaxies formed, they should have the densest peaks in their early-universe densities, and hence might have formed very high mass black holes during their Population III phases – black holes with 5–40% of their stellar mass (Ricotti and Ostriker, 2004). Observational constraints on the central mass concentrations of dwarf spheroidal galaxies are generally quite poor.

In both the dwarf spheroidal galaxy and globular cluster cases, it seems reasonable to search for new means of finding these black holes. Almost 30 years ago, it was suggested that the X-ray emission from globular clusters might be intermediate-mass black holes accreting from the interstellar medium (Bahcall and Ostriker, 1975). The detection of Type I X-ray bursts from the bright globular cluster sources has since ruled out this possibility, but much deeper observations from the Chandra Observatory have placed tight constraints on the X-ray emission that could be coming from such sources (Grindlay et al., 2001; Ho et al., 2003). In a few globular clusters (M 15 and 47 Tuc), variations in the pulsar dispersion measures provide measurements of the density of the interstellar medium (Freire et al., 2001), and combining these gas-density measurements with the X-ray upper limits in these globular clusters still fails to prove that black holes of about 1/1000 of the total mass of the cluster are not present, if one makes reasonable assumptions about the fraction of the Bondi–Hoyle rate that is typically accreted in low luminosity systems (see e.g. Bower et al., 2003; Perna et al., 2003) and on the radiative efficiency of this accreted material (see e.g. Narayan and Yi, 1994; Fender et al., 2003). In light of the new fundamental plane relations for black hole activity (Merloni et al., 2003; Falcke et al., 2004), which show that the radio luminosity, L_R and the X-ray luminosity L_X of a black hole with mass M_{BH} are related such that $L_X \propto L_R^{0.6} M_{BH}^{0.8}$, it has been shown that the most efficient way to search for evidence of accretion from low luminosity, high mass black holes such as those predicted to exist in globular clusters and dwarf spheroidal galaxies is by searching for radio emission (Maccarone, 2004). For example, a single 12-h observation of M 15 with the VLA would place a better constraint on the existence of a $1000 M_\odot$

black hole than would the entire mission lifetime of the Chandra Observatory. The prospects for improving the sensitivity limits in the radio in the near future are excellent; the VLA expansion project will improve its sensitivity by a factor of about 10, making μJy level observations possible in quite short exposure times; the High Sensitivity Array is already allowing μJy level VLBI scale interferometry, and the Square Kilometer Array project provides some hope that these (and better) sensitivity levels will be reachable from the Southern Hemisphere within the next 20 years.

In this contribution, we will outline the basic method by which we attempt to predict the radio fluxes from intermediate-mass black holes in globular clusters, and then we will describe some progress that has been made towards this goal.

2. Methodology

In Maccarone (2004), a methodology for going from a globular cluster's mass and distance to its expected radio flux was laid out. In this paper, we will briefly summarize the assumptions of that work, but we refer the reader to Maccarone (2004) and to the other cited references for a full justification of each assumption. Specifically, we assume:

- A black hole mass of 0.1% of the globular cluster's stellar mass (Miller and Hamilton, 2002)
- A gas density of 0.15 H cm^{-3} , approximately the value estimated from pulsar dispersion measures in M 15 and 47 Tuc, and expected from stellar mass loss (Freire et al., 2001).
- Accretion at 0.1–1% of the Bondi rate, with the sub-Bondi rate due to disk winds and/or convection as constrained by observations of low luminosity AGN in the Galactic Center and in elliptical galaxies and the lack of observations of isolated neutron stars accreting from the interstellar medium (e.g. Bower et al., 2003; Perna et al., 2003).
- A radiative efficiency in the X-rays of

$$\eta = (0.1) \times \left(1 + \frac{A^2}{2L_{\text{tot}}} - A \sqrt{\frac{A^2}{4L_{\text{tot}}^2} + \frac{1}{L_{\text{tot}}}} \right), \quad (1)$$

with A a constant to be fitted from observations (and being larger when the jet's kinetic power is a larger fraction of the total accretion power), and L_{tot} the radiative plus kinetic luminosity of the system in Eddington units, as used by Fender et al. (2003) to explain the $L_X - L_R$ correlation observed by Gallo et al. (2003), with the idea being that enough kinetic power is pumped into a jet to make the accretion flow radiatively inefficient (see also, e.g. Malzac et al., 2004). Whether the radiative inefficiency is due to mass and energy loss into a jet or also partially due to advection into the black hole (e.g. Ichimaru, 1977; Narayan

and Yi, 1994) is not clearly established by these relations, and does not affect the results presented here. We have set $A = 6 \times 10^{-3}$ for these calculations, which is based on a conservative estimate of the jet power. This relation is used to convert a calculated accretion rate (from the assumed fraction of the Bondi – Hoyle rate) into a calculated X-ray luminosity.

- The fundamental plane relationship among X-ray luminosity, radio luminosity and black hole mass of Merloni et al. (2003), parameterized for convenient applications to Galactic globular clusters:

$$F_{5\text{GHz}} = 10 \left(\frac{L_X}{3 \times 10^{31} \text{ ergs/s}} \right)^{0.6} \left(\frac{M_{\text{BH}}}{100 M_{\odot}} \right)^{0.78} \left(\frac{d}{10 \text{ kpc}} \right)^{-2} \mu\text{Jy}. \quad (2)$$

This relation is used to convert the calculated X-ray luminosity from the previous step into a radio flux. We note that the relation found by Falcke et al. (2004), which considered only flat spectrum, low luminosity radio sources like those we expect to see in the centers of dwarf galaxies or globular clusters, is consistent with this relation within the uncertainties. Following these assumptions, several globular clusters should have central radio sources brighter than a few μJy , but only Omega Cen should have a radio source brighter than $40 \mu\text{Jy}$, and even Omega Cen should be that bright only if the accretion rate is closer to 1% of the Bondi–Hoyle rate than it is to 0.1% of the Bondi–Hoyle rate. Nonetheless, the predicted X-ray fluxes for the globular clusters are generally well below detectability levels, even with very long observations by the Chandra Observatory.

3. Applications to Globular Clusters

We have applied this method to two globular clusters so far, and in both cases have found no evidence for an accreting central black hole. Omega Cen was observed by us with the Australian Telescope Compact Array (ATCA) simultaneously at 4.8 and 8.6 GHz for 12 h on 8 May 2004, with no detection made at either frequency. The non-detection yielded a 3σ upper limit on the flux of just under $100 \mu\text{Jy}$, under the assumption that the radio spectrum of the source should be flat. Maccarone (2004) predicted that the flux level should be at least $150 \mu\text{Jy}$ under the most conservative set of parameter values used in that paper. This would seem to imply that there cannot be a black hole with 0.1% of the cluster’s mass in Omega Cen, but given the scatter in the fundamental plane relation, and the fact that the gas density in Omega Cen has been assumed to be similar to those in M 15 and 47 Tuc, rather than measured, this upper limit should not be interpreted as such strong evidence against an intermediate-mass black hole. The upper limit does, however, provide strong evidence against the combination of 0.1% of the cluster mass being in an intermediate black hole, with an accretion rate of $\sim 1\%$ or more of the Bondi rate.

We have also considered previous radio observations of M 15 which were made with the Very Large Array (VLA) for the purposes of finding radio pulsars (Johnston

et al., 1991). These data were taken at 1.4 GHz, and reached a noise level of $43 \mu\text{Jy}$, with no unidentified sources found within the core of the globular cluster. The upper limits are thus rather similar to those found for Omega Cen, in terms of flux level. The constraints on whether there exists a black hole with 1/1000 of the cluster mass, though, are much weaker, because the cluster is smaller and further away than Omega Cen. A useful constraint can be made on whether there exists a black hole substantially more massive than this. In the context of the assumptions listed above, the 3σ upper limit for the radio flux corresponds to the flux level expected from a $700 M_{\odot}$ black hole accreting 0.1% of its Bondi rate – therefore, the upper limit on the radio flux measured in this cluster’s core can be taken as evidence against the claimed $2500 M_{\odot}$ black hole in M 15 (Gerssen et al., 2002), although it should be noted that the uncertainty on this mass measurement was rather large, and the measurement was not inconsistent with a black hole of $700 M_{\odot}$. Proposed High Sensitivity Array observations could reduce the noise level in the radio data by a factor of about 10, which could, in turn allow for either a detection of the black hole or a truly constraining upper limit on its possible mass.

4. Applications to Dwarf Spheroidal Galaxies

We have also searched the NRAO VLA Sky Survey (NVSS) catalog around the centers of the Milky Way’s Northern Hemisphere dwarf spheroidal galaxies. This catalog has some sources as faint as 1 mJy, but is complete only at the level of about 3–4 mJy, and it covers the entire sky north of a declination of -40 degrees at a frequency of 1.4 GHz (Condon et al., 1998). One source was found within the 3σ error circle of the center of a dwarf spheroidal galaxy – a 7.1-mJy source about $20''$ from the reported center of the Ursa Minor dwarf spheroidal galaxy. The Ursa Minor galaxy is one of the nearest ($d = 66$ kpc), most diffuse (the $20'$ offset is roughly the 1σ error in the centroid position of the galaxy), and most massive ($M = 2.3 \times 10^7 M_{\odot}$) of the Milky Way’s dwarf spheroidal satellites (see Mateo, 1998 for a review of the properties of dwarf spheroidal galaxies including measurements of parameter values). The density of NVSS sources on the sky is such that there is about a 5% chance of finding a source within the 3σ error box of the center of the Ursa Minor dwarf spheroidal galaxy. The other dwarf galaxies are further away and more centrally concentrated, so their centroid positions are more well established and the chance of a spurious coincidence between a radio source and their core positions would be quite small. On the other hand, because they are further away and less massive, their expected radio fluxes would be smaller than that of the Ursa Minor’s core, if one assumes there should be a linear correlation between galaxy mass and black hole mass. The measurements of gas contents of dwarf spheroidal galaxies are mostly upper limits (although see Bouchard et al., 2003 for one detection), so it is not as straightforward to convert a radio flux into a black hole mass as it would be in a globular cluster. If we assume that the gas

density is 1/30 to 1/100 as high in dwarf spheroidal galaxies as in globular clusters (because the dwarf spheroidals are more diffuse), then we find a black hole mass of about $1-2 \times 10^5 M_{\odot}$ would be required to produce the observed radio flux. The expected X-ray luminosity from such an object would be \sim a few $\times 10^{34}$ ergs/sec, below the detection limits of past X-ray observations (e.g. Markert and Donahue, 1985; Zang and Meurs, 2001), but easily detectable by Chandra or XMM. Because the error circle of the NVSS source is about $4''$ in radius, it is not possible to identify a unique optical counterpart and determine whether this radio source is more likely to be in the Ursa Minor galaxy or a background AGN. Follow-ups in radio and X-ray have been proposed, both to obtain a better positional accuracy for the radio source, and to determine its X-ray to radio flux ratio.

5. Prospects for Future Improvements

One key area for future improvements of this work is to get deeper radio observations of the globular clusters and dwarf spheroidal galaxies most likely to show radio sources associated with intermediate-mass black holes. This work is already in progress, with an application in submission for High Sensitivity Array time to observe M 15. Unfortunately, most of the best globular cluster candidates are in the Southern Hemisphere, and with the ATCA data showing only upper limits for Omega Cen, the prospects of detecting a black hole in any other globular cluster by using ATCA seem remote.

The other key area that needs more work is in improving our measurements of the gas densities in these systems, especially in the dwarf spheroidal galaxies. The methodology for doing so is not as clear. Searches for absorption lines in the spectra of background AGN seem to be one of the most promising routes (Tinney et al., 1997), and such AGN should be detected as part of any program searching for X-ray emission from a central black hole as well.

Acknowledgements

It is a pleasure to thank the following for useful discussions which contributed to this work: Dave Meier, Heino Falcke, Eva Grebel, Russell Edwards, Andrea Merloni, Cole Miller, Simon Portegies Zwart, Fred Rasio, Ben Stappers and Kathy Vivas.

References

- Bahcall, J.N. and Ostriker, J.P.: 1975, *Nature* **256**, 23.
 Baumgardt, H., Hut, P., Makino, J., McMillan, S. and Portegies, S.: 2003, *Astrophys. J. Lett.* **582**, L21.

- Bouchard, A., Carignan, C. and Mashchenko, S.: 2003, *AJ* **126**, 1295.
- Bower, G.C., Wright, M.C.H., Falcke, H. and Backer, D.C.: 2003, *ApJ* **588**, 331.
- Condon, J.J., Cotton, W.D., Greisen, E.W., Yin, Q.F., Perley, R.A., Taylor, G.B. and Broderick, J.J.: 2003, *AJ* **126**, 1295.
- Drukier, G.A. and Bailyn, C.D.: 2003, *Astrophys. J. Lett.* **597**, L125.
- Falcke, H., Körding, E. and Markoff, S.: 2004, *A&A* **414**, 895.
- Fender, R.P., Gallo, E. and Jonker, P.G.: 2003, *MNRAS* **343**, L99.
- Fillipenko, A.V. and Ho, L.C.: 2003, *Astrophys. J. Lett.* **588**, 113.
- Freire, P.C., Kramer, M., Lyne, A.G., Camilo, F., Manchester, R.N. and D'Amico, N.: 2001, *Astrophys. J. Lett.* **557**, L105.
- Gallo, E., Fender, R.P. and Pooley, G.G.: 2003, *MNRAS* **344**, 60.
- Gebhardt, K., Rich, R.M. and Ho, L.C.: 2002, *Astrophys. J. Lett.* **578**, L41.
- Gerssen, J., van der Marel, R.P., Gebhardt, K., Guhathakurta, P., Peterson, R.C. and Pryor, C.: 2002, *AJ* **124**, 3270.
- Gerssen, J., van der Marel, R.P., Gebhardt, K., Guhathakurta, P., Peterson, R.C. and Pryor, C.: 2003, *AJ* **125**, 376.
- Greene, J.E. and Ho, L.C.: 2004, *ApJ* **610**, 722.
- Grindlay, J.E., Heinke, C., Edmonds, P.D. and Murray, S.S.: 2001, *Science* **5525**, 2290.
- Ho, L.C., Terashima, Y. and Okajima, T.: 2003, *Astrophys. J. Lett.* **587**, L35.
- Ichimaru, S.: 1977, *ApJ* **214**, 840.
- Johnston, H.M., Kulkarni, S.R. and Goss, M.W.: 1991, *Astrophys. J. Lett.* **382**, L89.
- Maccarone, T.J.: 2004, *MNRAS* **351**, 1049.
- Magorrian, J., Tremaine, S., Richstone, D. et al.: 1998, *AJ* **115**, 2285.
- Malzac, J., Merloni, A. and Fabian, A.C.: 2004, *MNRAS* **351**, 253.
- Markert, T.H. and Donahue, M.E.: 1985, *ApJ* **297**, 564.
- Mateo, M.: 1998, *Annu. Rev. Astron. Astrophys.* **36**, 435.
- Miller, M.C. and Hamilton, D.P.: 2002, *MNRAS* **330**, 232.
- Narayan, R. and Yi, I.: 1994, *Astrophys. J. Lett.* **428**, L13.
- Pasquali, A., De Marchi, G., Pulone, L. and Brigas, M.S.: 2004, *A&A* **428**, 469.
- Perna, R., Narayan, R., Rybicki, G., Stella, L. and Treves, A.: 2003, *ApJ* **594**, 936.
- Portegies Zwart, S.F. and McMillan, S.L.W.: 2000, *Astrophys. J. Lett.* **528**, L17.
- Ricotti, M. and Ostriker, J.P.: 2004, *MNRAS* **352**, 547.
- Strohmayer, T.E. and Mushotzky, R.F.: 2003, *Astrophys. J. Lett.* **586**, L61.
- Tinney, C.G., Da Costa, G.S. and Zinnecker, H.: 1997, *MNRAS* **285**, 111.
- Zang, Z. and Meurs, E.J.A.: 2001, *ApJ* **556**, 24.

FORMATION AND EVOLUTION OF INTERMEDIATE MASS BLACK HOLE X-RAY BINARIES

SIMON F. PORTEGIES ZWART^{1,2}, JASINTA DEWI³ and TOM MACCARONE¹

¹*Astronomical Institute 'Anton Pannekoek', University of Amsterdam, Kruislaan 403, The Netherlands*

²*Institute for Computer Science, University of Amsterdam, Kruislaan 403, The Netherlands; E-mail: spz@science.uva.nl*

³*Department of Astrophysics, University of Oxford, Keble Road, Oxford OX1 3RH, UK*

(Received 30 September 2004; accepted 1 June 2005)

Abstract. The evolution of young ($\lesssim 10$ Myr) star clusters with a density exceeding about 10^5 star pc⁻³ are strongly affected by physical stellar collisions during their early lifetime. In such environments the same star may participate in several tens to hundreds of collisions ultimately leading to the collapse of the star to a black hole of intermediate mass. At later time, the black hole may acquire a companion star by tidal capture or by dynamical – three-body – capture. When the captured star evolves it starts to fill its Roche-lobe and transfers mass to its accompanying black hole. This then leads to a bright phase of X-ray emission, which lasts for the remaining main-sequence lifetime of the donor. If the star captured by the intermediate mass black hole is relatively low mass ($\lesssim 2 M_{\odot}$) the binary will also be visible as a bright source in gravitational waves. Based on empirical models we argue that, for as long as the donor remains on the main sequence, the source will be ultraluminous $L_x \gtrsim 10^{40}$ erg s⁻¹ for about a week every few month. When the donor star is more massive $\gtrsim 15 M_{\odot}$ or evolved off the main sequence the bright time is longer, but the total accretion phase lasts much shorter.

Keywords: black holes, compact objects, simulation, star clusters, X-ray binaries

1. Introduction

There are six star clusters younger than 10 Myr with a density exceeding about 10^5 stars pc⁻³ in the Milky Way Galaxy (hereafter named YDC from Young Dense Clusters), they are: Arches (Figer et al., 2002), IRS13 (Maillard et al., 2004) and IRS16 (Portegies Zwart et al., 2003; Eckart et al., 2004), NGC3603 (Brandl et al., 1999), Quintuplet (Figer et al., 1999) and Westerlund 1 (Vrba et al., 2000).

The young age of these clusters guarantees that stars of all masses are still present, offering critical insights into the stellar initial mass function and cluster structural properties at formation. The term “dense” means that dynamical evolution and physical collisional processes can operate fast enough to compete with and even overwhelm stellar evolutionary timescales; dense stellar systems are places where wholly new stellar evolution channels can occur, allowing the formation of



stellar species completely inaccessible by standard stellar and binary evolutionary pathways.

There are no examples of the older ($\gtrsim 10$ Myr) siblings of these clusters in the Milky Way Galaxy. For the Arches and Quintuplet this may not be so surprising, as they dissolve in the tidal field of the Galaxy in at most a few tens of million years (Kim et al., 2000; Portegies Zwart et al., 2002), and even if they survive longer they will become hard to detect against the dense background stellar population (Portegies Zwart et al., 2001a,b). For the two rather isolated clusters, NGC 3603 and Westerlund 1, it is rather curious that there are no examples of their 10–100 Myr descendants in the Milky Way.

The other characteristic of YDCs is the high density. The few clusters near the Galactic center must have a high density, as otherwise they would be disrupted easily by the strong tidal field. The clusters further out, however, do not have this constraint and it is interesting to note that clearly these clusters were born without much knowledge of the local potential of the Galaxy, i.e., they behave as isolated clusters.

In this paper, we discuss the formation and evolution of X-ray binaries consisting of an intermediate mass black hole and a Roche-lobe filling companion star. This study was initiated by the detailed observations of the star cluster MGG11 (McCraday et al., 2003) at about 200 pc from the nucleus of the starburst galaxy M82 at a distance of about 3.6 Mpc.

The star cluster MGG11 has an age of about 7–12 Myr (McCraday et al., 2003), a line-of-sight velocity dispersion of $\sigma_r = 11.4 \pm 0.8 \text{ km s}^{-1}$ and a projected half-light radii, $r = 1.2 \text{ pc}$. The cluster mass then totals $\sim 3.5 \times 10^5 M_\odot$. The cluster mass function seems to be deficient of stars below about $1 M_\odot$, but follow a Salpeter slope for the higher masses.

One of the most fascinating characteristics of MGG11, however, is arguably the tentative presence of an ultraluminous X-ray source (ULX) in the cluster center (Matsumoto et al., 2001; Kaaret et al., 2001).

2. Early Core Collapse and the Growth of an Intermediate Mass Black Hole

Portegies Zwart (2004) recently performed a large number of detailed N -body simulations of up to 585 000 stars for this cluster and for its neighbor MGG9. Their main conclusion are that clusters like MGG11 can produce an intermediate mass black hole of several hundred M_\odot by stellar coagulation.

Driven by the massive stars, the cluster experiences an early core collapse (Portegies Zwart et al., 2004; Gürkan, 2004), which leads to subsequent collisions between massive stars. The result of this is the growth of one of the initially most massive stars through repeated collisions, to a total mass of about 1000–3000 M_\odot . In the end, the massive star may collapse to an intermediate mass black hole (Portegies Zwart et al., 2004). (Several alternative theoretical models exist for producing black

holes of $\sim 10^2\text{--}10^4 M_\odot$; Portegies Zwart and McMillian 2002; Miller and Hamilton 2002; Madau and Rees 2001).

Hopman et al. (2004) proposed that an intermediate mass black hole can capture a companion star in a tight orbit. Further tidal interaction between the black hole and the captured star then circularize the orbit. They further assume that the captured star is on the main sequence, but the same argument can be made for evolved stars. By the time the orbit has been fully circularized the captured star under-fills its Roche-lobe only slightly. During its remaining main-sequence lifetime the star grows in size by about a factor of two and gravitational wave radiation reduces the orbital separation. Ultimately, the star fills its Roche-lobe and starts to transfer mass to the intermediate mass black hole.

3. The Evolution of the Intermediate Mass Black Hole Binary

After tidal capture we evolve the binaries through various stages using the binary evolution code of Eggleton (Pols et al., 1995 and references therein), assuming a population I chemical composition ($Y = 0.98$, $Z = 0.02$), mixing-length parameter of $\alpha = 2.0$ and with convective overshooting constant $\delta_{\text{ov}} = 0.12$ (Pols et al., 1998). We adopted black hole masses of $100\text{--}2000 M_\odot$ and the mass of the donor was either 2 , 5 , 10 , or $15 M_\odot$ with initial orbital periods P such that the donor fills its Roche-lobe at birth.

Results on such evolution are published by Portegies Zwart et al. (2004). They calculated the orbital evolution of the binary systems, as they are affected by the emission of gravitational waves (Landau and Lifshitz, 1958), Roche-lobe overflow and by mass loss via a wind (Portegies Zwart et al., 2004). During mass transfer the black hole was assumed to accrete matter up to the Eddington limit (see, e.g., King, 2000). The remaining mass is lost from the system with the specific angular momentum of the black hole.

Binaries which start Roche-lobe contact at the ZAMS undergo case A mass transfer. This prolongs their main-sequence lifetime considerably. The most peculiar evolution in our sample is arguably that of the $2 M_\odot$ donor. After transferring about $1 M_\odot$ the star starts to develop a convective envelope and magnetic braking sets in. This mechanism ceases when the whole star becomes convective with a homogeneous composition of $X = 0.66$. Some time later, the central temperature drops below the hydrogen burning limit and thermonuclear fusion stops: this happens at about $t = 630$ Myr. At that point, the system remains detached for about 8 Myr before it undergoes another phase of mass transfer until about 1.2 Gyr, after which the donor turns in a $m_{\text{don}} \simeq 0.01 M_\odot$ brown dwarf. Under the influence of gravitational-wave radiation, the donor spirals in toward the black hole until they merge some 74 Myr later.

The $10 M_\odot$ donor experiencing case A mass transfer ends as a helium star. This star experiences helium shell burning, lasting for about 40 000 years, during which

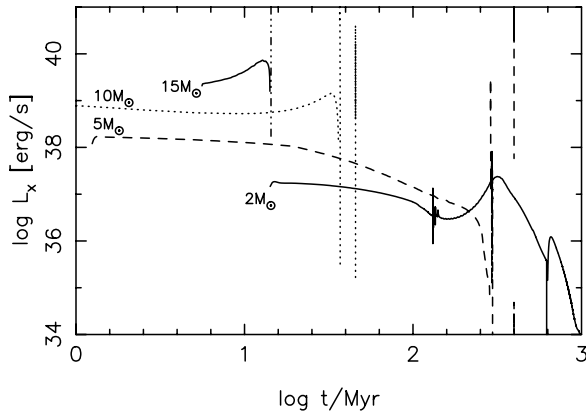


Figure 1. The X-ray luminosity as a function of time for four initial donor masses which are born in a semi-detached binary with a $1000 M_{\odot}$ black hole. The initial orbital periods are 0.5, 0.6, 0.8, and 1.2 days for the 2, 5, 10 and $10 M_{\odot}$ donors, respectively. Only the 10 and $15 M_{\odot}$ donors exceed a luminosity of $10^{40} \text{ erg s}^{-1}$ for more than a few million years, while the donor is on the main sequence. On the giant branch even the $5 M_{\odot}$ donor exceeds $10^{40} \text{ erg s}^{-1}$. The $2 M_{\odot}$ donor never reaches a luminosity exceeding $10^{38} \text{ erg s}^{-1}$. Note, however, that these are secular luminosities, derived from the mean accretion rate over time intervals of 50 000 years.

mass transfer starts again at a rate of $\dot{m} = 3 \times 10^{-6} M_{\odot}$ per year, for black holes of 100–2000 M_{\odot} . These phases of mass transfer are shown by the second spikes in Figure 1 for 5 and $10 M_{\odot}$ donors. Though seemingly unresolved, some of these spikes last for several million years and are well resolved in our simulations.

For the more massive stars, case A mass transfer is followed by mass transfer when the star ascends the giant branch during hydrogen shell burning (case AB), lasting for 8.3 Myr (for $m_{\text{don}} = 5 M_{\odot}$), 0.26 Myr (for $10 M_{\odot}$) and 0.05 Myr (for $m_{\text{don}} = 15 M_{\odot}$). The mass transfer rate increases dramatically in this phase to $\dot{m} = 5.2 \times 10^{-7}$, 3.7×10^{-5} and $2.3 \times 10^{-4} M_{\odot}$ per year for the $m_{\text{don}} = 5$, 10, and $15 M_{\odot}$ donor, respectively; as shown by the first spike in the secular evolution of the X-rays luminosity in Figure 1. These mass transfer rates result in secular X-ray luminosities in excess of $10^{41} \text{ erg s}^{-1}$.

Binaries initialized with a larger orbital period experience mass transfer when the donor is evolved to a giant (case B) or supergiant (case C). The case B systems remain detached for only 0.29 Myr ($5 M_{\odot}$) to 0.05 Myr ($10 M_{\odot}$) at mass transfer rate of $\dot{m} = 2.4 \times 10^{-5}$ ($5 M_{\odot}$) to $7 \times 10^{-4} M_{\odot}$ per year ($10 M_{\odot}$).

3.1. THE GENERATION OF X-RAYS

In this section, we apply and discuss an empirical observational model based on our understanding of low-mass X-ray binaries in the Galaxy, but then applied to the earlier discussed binary systems. We note that in the interests of keeping this

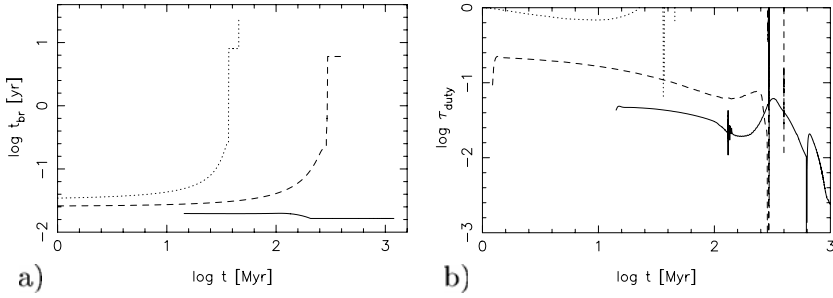


Figure 2. (a) Time spend (on average) per duty cycle as a $L_x > 10^{40} \text{ erg s}^{-1}$ X-ray source for a binary with a $1000 M_{\odot}$ black hole and a $m_{\text{don}} = 10 M_{\odot}$ (dotted line), $5 M_{\odot}$ (dashes), and $2 M_{\odot}$ (solid) donor which starts Roche-lobe overflow at birth. (b) Duty cycle (for $L_x > 10^{40} \text{ erg s}^{-1}$) for the three binaries with starts RLOF at birth with a 2, 5, and $10 M_{\odot}$ donor (the same line styles are adopted). A duty cycle $\tau_{\text{duty}} > 1$ indicates that the source is persistent.

paper brief, we have stated some results without justification; we refer the interested reader to the appendix of (Portegies Zwart et al., 2004) for further details.

The binary evolution simulations provide us with the donor mass (m_{don}), accretor mass, orbital period (P) and a secular mass accretion rate (\dot{m}), all as a function of time. With these we can calculate the secular X-ray luminosity, as we present in Figure 1, and with the empirical model we compute the recurrence time and duty cycle (Portegies Zwart et al., 2004).

The difference between secular accretion rates and instantaneous accretion rates is very important, considering the rather high accretion rates, which, within the adopted model, results in long quite times lasting a few months, between relatively short bright episodes (see Figure 2).

We require that in order to recognize the source as a ULX it has to be brighter than L_{br} , for which we adopt $L_{\text{br}} = 10^{40} \text{ erg s}^{-1}$. This is done in the following way: First we calculate the total energy (in erg s^{-1}) with $\log E = 45 + \log(P/10 \text{ h})$, which is based on a fit to the empirical data. We note that this equation appeared in our previous paper (Portegies Zwart et al., 2004) without the plus sign, but that the equation presented here is correct. The recurrence time is subsequently a function of the total energy E and the rate of mass transfer via, $t_r = E/(0.1\dot{m}c^2)$. The bright time is then calculated by integrating the luminosity curve.

The bright time starts with a peak luminosity of $L_{\text{peak}} = 2L_{\text{Edd}} \times (P/10 \text{ h})$, which we assume to decay exponentially until it drops below L_{br} . The bright time results then in $t_{\text{br}} = t_d - \log(L_{\text{br}}/2L_{\text{Edd}})$, where we adopt the factor two in the denominator. Here the decay time is derived from empirical data, which suggests also that the light curves for Galactic black hole X-ray transients in the Milky Way can be approximated by are exponentially decay with decay time scale

$$t_d = 6 \text{ days} \times \min \left(1, \frac{P_{\text{orb}}}{10 \text{ h}} \right). \quad (1)$$

Here P_{orb} is the orbital period of the binary system. The duty cycle is subsequently determined as $\tau_{\text{duty}} = t_{\text{br}}/t_{\text{r}}$.

In Figure 2, we present the duty cycle τ_{duty} and the bright time T_{br} for a selection of binaries with $m_{\text{don}} = 2, 5, \text{ and } 10 M_{\odot}$ donors which start to transfer mass at the zero-age main sequence (ZAMS) to a $1000 M_{\odot}$ black hole. Binaries which start at wider orbits and the simulations for $\gtrsim 15 M_{\odot}$ donors which starts RLOF at the ZAMS are persistent X-ray source with luminosities well above L_{br} . The binaries with a relatively wide initial orbit, however, remain bright for only a short while, which therefore requires a high birthrate for a reasonable probability of observed any of these systems (Portegies Zwart et al., 2004).

4. Summary

Young and dense star clusters are promising engines for producing intermediate mass black holes via stellar coagulation. Upon formation the black hole is still deeply embedded in the potential well of the cluster. The frequent close encounters between cluster members and the intermediate mass black hole can then lead to the capture of a main-sequence star in a tight orbit around the black hole. In due time, this star will start to fill its Roche-lobe, resulting to a phase of mass transfer. We combine the results of detailed binary evolution calculations with an empirical model for the generation of X-rays in such a binary.

Our main conclusions are that a massive $\gtrsim 15 M_{\odot}$ main-sequence star which fills its Roche-lobe to an intermediate mass black hole provides a promising explanation for the bright X-ray source observed in the young and dense star cluster MGG11. Such high-mass donors in relatively short period binaries provide steady sources with ultraluminosity X-ray emission.

An interesting possibility is provided by a $\sim 2 M_{\odot}$ donor which starts to transfer mass to an intermediate mass black hole at birth. Such a binary is likely to be visible as a bright transient X-ray source and simultaneously as gravitational wave source in the *LISA* band to a distance of several 100 kpc.

Acknowledgments

I am grateful to Holger Baumgardt, Clovis Hopman, Piet Hut, Jun Makino and Steve McMillan for numerous discussions, and in particular to Jun for the excessive use of his GRAPE-6, on which these simulations are performed. Additional simulations are performed at the GRAPE-6 systems at Drexel University and the MoDeStA computer at the University of Amsterdam. This work was supported by NASA ATP, the Royal Netherlands Academy of Sciences (KNAW), the Dutch organization of Science (NWO), and by the Netherlands Research School for Astronomy (NOVA).

References

- Aarseth, S.J.: 1999, *PASP* **111**, 1333.
- Aarseth, S.A.: 2003, *Gravitational N-Body Simulations*, Cambridge University Press, Cambridge.
- Brandl, B., et al.: 1999, *A&A* **352**, L69.
- Eckart, A., Moutaka, J., Viehmann, T., Straubmeier, C. and Mouawad, N.: 2004, *ApJ* **602**, 760.
- Figer, D.F., et al.: 2002, *ApJ* **581**, 258.
- Figer, D.F., McLean, I.S. and Morris, M.: 1999, *ApJ* **514**, 202.
- Gürkan, M.A., Freitag, M. and Rasio, F.A.: 2004, *ApJ* **604**, 632.
- Hopman, C., Portegies Zwart, S.F. and Alexander, T.: 2004, *ApJL* **604**, L101.
- Kaaret, P., et al.: 2001, *MNRAS* **321**, L29.
- Kim, S.S., Figer, D.F., Lee, H.M. and Morris, M.: 2000, *ApJ* **545**, 301.
- King, A.R.: 2000, *MNRAS* **312**, L39.
- Landau, L.D., Lifshitz, M.: 1958, *The Classical Theory of Fields*, Pergamon Press, Oxford, London, New York, Paris.
- McCrary, N., Gilbert, A.M. and Graham, J.R.: 2003, *ApJ* **596**, 240.
- Maillard, J.P., Paumard, T., Stolovy, S.R. and Rigaut, F.: 2004, *A&A* **423**, 155.
- Matsumoto H., et al.: 2001, *ApJL* **547**, L25.
- McMillan, S.L.W. and Portegies Zwart, S.F.: 2003, *ApJ* **596**, 314.
- Portegies Zwart, S.F., Baumgardt, H., Hut, P., Makino, J. and McMillan, S.L.W.: 2004, *Nature* **428**, 724.
- Portegies Zwart, S.F., Dewi, J. and Maccarone, T.: 2004, *MNRAS* **357**, 1104.
- Portegies Zwart, S.F., Makino, J., McMillan, S.L.W. and Hut, P.: 2001a, *ApJL* **546**, L101.
- Portegies Zwart, S.F., Makino, J., McMillan, S.L.W. and Hut, P.: 2002, *ApJ* **565**, 265.
- Portegies Zwart, S.F., McMillan, S.L.W. and Gerhard, O.: 2003, *ApJ* **593**, 352.
- Portegies Zwart, S.F., McMillan, S.L.W., Hut, P., Makino, J.: 2001b, *MNRAS* **321**, 199.
- Pols, O.R., Schroder, K., Hurley, J.R., Tout, C.A., Eggleton, P.P.: 1998, *MNRAS* **298**, 525.
- Pols, O.R., Tout, C.A., Eggleton, P.P. and Han, Z.: 1995, *MNRAS* **274**, 964.
- Soberman, G.E., Phinney, E.S. and van den Heuvel, E.P.J.: 1997, *A&A* **327**, 620.
- Vrba, F.J., et al.: 2000, *ApJL* **533**, L17.

TeV GAMMA RAYS FROM THE GALACTIC CENTER DIRECT AND INDIRECT LINKS TO THE MASSIVE BLACK HOLE IN Sgr A*

FELIX AHARONIAN¹ and ANDRII NERONOV²

¹Max-Planck-Institut für Kernphysik, Saupfercheckweg, Heidelberg, Germany;
E-mail: felix.aharonian@mpi-hd.mpg.de

²Ecole Polytechnique Federale de Lausanne, BSP, Lausanne, Switzerland

(Received 4 November 2004; accepted 1 June 2005)

Abstract. The recent detection of TeV gamma-radiation from the direction of the Galactic Center within several arc-minutes around Sgr A* is the first model-independent evidence of existence of high-energy particle accelerator(s) in the central 10 pc region of our Galaxy. This is an extraordinary site that harbours many remarkable objects with the compact radio source Sgr A* – a hypothetical super-massive black hole (SMBH) – in the dynamical center of the Galaxy. Here we explore the possible *direct* and *indirect* links of the reported TeV emission to the SMBH. We show that at least three γ -ray production scenarios that take place close to the event horizon of the SMBH can explain the reported TeV fluxes. An alternative (or additional) channel of TeV radiation is related to the run-away protons accelerated in Sgr A*. Quasi-continuous injection of relativistic protons into the surrounding dense gas environment initiates detectable high-energy gamma-ray emission. The absolute flux and the energy spectrum of this radiation component strongly depend on the history of particle injection and the character of diffusion of protons during the last 10^5 yr. For a reasonable combination of a few model parameters, one can explain the detected gamma-ray flux solely by this diffuse component.

Keywords: galactic center, black holes, gamma rays, X-rays

1. Introduction

The recent detection of TeV gamma-ray emission from the direction of the Galactic Center by three independent groups, CANGAROO (Tsuchiya et al., 2004), Whipple (Kosack et al., 2004) and HESS (Aharonian et al., 2004), is a remarkable result which will have a strong impact on our understanding of high-energy processes in the central region of the Galaxy. The localisation of the TeV signal by HESS within a few angular minutes indicates that the gamma-ray source(s) is (are) located in the central ≤ 10 pc region. Among the possible sites of production of TeV gamma-rays are Sgr A*, the young supernova remnant Sgr A East, the Dark Matter Halo, and finally the whole diffuse 10 pc region. It is possible that some of these potential gamma-ray production sites comparably contribute to the observed TeV flux. Moreover, the same source could be responsible for two different components of radiation: (i) the *direct* gamma-ray component produced *inside* the particle accelerator, and (ii) the *indirect* component produced by runaway protons which are



accelerated in the same source, but later injected into the surrounding dense gas environment.

Below we discuss these two components of TeV radiation in the context of acceleration of particles in the proximity of the SMBH and their radiation both inside and outside of Sgr A*.

2. Production of High-Energy Gamma-Rays in Sgr A*

The temporal and spectral features of Sgr A* are unusual and, as a whole, different from other well-studied compact Galactic and extragalactic sources containing black holes. This concerns, first of all, the extraordinary low luminosity of Sgr A*. In addition the other important astrophysical implications, the low luminosity of Sgr A* has a dramatic effect on the visibility of the source in gamma-rays (Aharonian and Neronov, 2005).

2.1. TRANSPARENCY OF SGR A* FOR HIGH-ENERGY GAMMA-RAYS

Because of internal photon–photon pair production, the high-energy gamma-ray emission of these objects (both of stellar mass and super-massive BHs) is generally suppressed, and consequently the unique information on possible particle acceleration processes near the event horizon of the BH is essentially lost. But this is not the case of the super-massive BH located at the dynamical center of our Galaxy (Sgr A*), which thanks to its extraordinary low bolometric luminosity ($\leq 10^{-8} L_{\text{Edd}}$) is transparent for very high-energy gamma-rays. It is seen from Figure 1 that indeed up to 10 TeV the source is transparent for gamma-rays even if one assumes that gamma-rays are produced within $2R_g$. Note that the decrease of the $\gamma\gamma \rightarrow e^+e^-$ cross-section well above the pair production threshold makes the source again transparent at $E \sim 10^{18}$ eV.

High-energy gamma-rays from compact regions close to the event horizon of the SMBH can be produced in various ways due to acceleration of protons and/or electrons and their interactions with ambient magnetic and radiation fields, as well as with the thermal plasma.

2.2. SYNCHROTRON AND CURVATURE RADIATION OF PROTONS

Synchrotron and curvature radiation of protons are important processes in the so-called extreme accelerators (Aharonian et al., 2002) where particles are accelerated at the maximum possible rate, $\dot{E} = eB$. However, even for an “ideal” combination of parameters allowing the most favourable acceleration/cooling regime, the characteristic energy of synchrotron radiation is limited by $\epsilon_{\text{max}} = (9/4)\alpha_f^{-1}m_p c^2 \simeq 0.3$ TeV (Aharonian, 2000). This implies that the proton-synchrotron radiation cannot

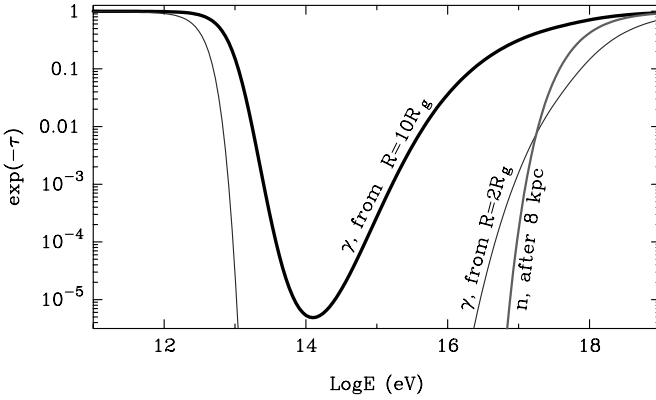


Figure 1. Attenuation of gamma-rays in Sgr A* due to internal photon–photon pair production dominated by interactions of high-energy gamma-rays with radiation of the compact infrared source. Two solid curves marked “ γ ” are calculated assuming that the infrared emission of Sgr A* is produced within $10R_g$ and $2R_g$ around the central black hole of mass $3 \times 10^6 M_\odot$. The curve marked “ n ” shows attenuation of the neutron flux $\exp(-d/\Lambda)$, where $\Lambda \approx 10(E/10^{18} \text{ eV}) \text{ kpc}$ is the decay mean free path of a neutron of energy E , and $d = 8 \text{ kpc}$ is the distance to the Galactic Center.

explain the flux observed from the direction of GC up to several TeV, unless the radiation takes place in a source moving towards the observer with bulk motion Lorentz factor $\Gamma \geq 10$. Another possibility could be if the *proton-acceleration* and *synchrotron gamma-ray production* regions are *separated*, e.g. when protons are accelerated in a regular B-field while moving along field lines, and later are injected into a region of chaotic magnetic field.

In this scenario we should expect γ -rays also from the regular B-field region – due to the proton curvature radiation. The contribution of the latter in the high-energy radiation of SMBHs could be quite significant (Levinson, 2000). The curvature radiation of protons can extend to $\epsilon_{\max} = 3E_p^3/2m^3R \simeq 0.2(B/10^4)^{3/4} \text{ TeV}$ (hereafter all estimates correspond to the black-hole mass $3 \times 10^6 M_\odot$). Formally, this equation allows extension of the spectrum to 10 TeV, provided that the magnetic field exceeds $B \simeq 10^6 \text{ G}$. However, such a strong field would make the source opaque for TeV gamma rays (Aharonian and Neronov, 2005).

2.2.1. Photo–Meson Interactions

The protons accelerated in the region close to the event horizon of SMBH to energies $E \sim 10^{18} \text{ eV}$, start to interact with soft photons of the compact infrared source located at $\sim 10R_g$. Despite the low luminosity of the source, the density of infrared photons appears sufficiently high for reasonably effective photo–meson interactions. Indeed, the mean free path of protons through the photon field is estimated $\Lambda_{p\gamma} \sim (\sigma_{p\gamma} f n_{\text{ph}})^{-1} \simeq 10^{15} (R_{\text{IR}}/10^{13} \text{ cm})^2 \text{ cm}$. This means that approximately $R/\Lambda_{p\gamma} (\sim 0.01)$ of the energy of protons is converted into secondary particles (neutrinos, photons, and electrons).

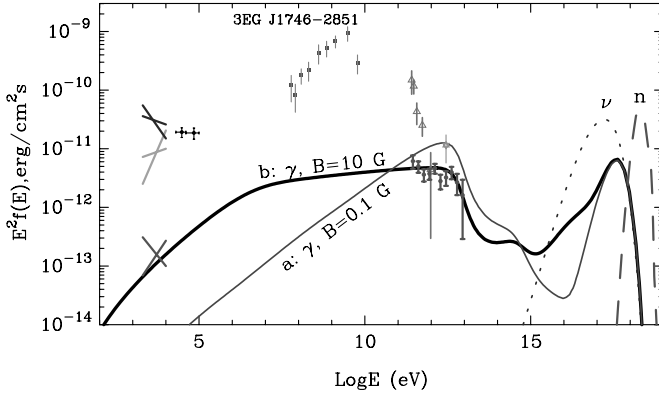


Figure 2. Broad-band Spectral Energy Distribution (SED) of gamma-rays (*solid lines*), neutrons (*dash line*) and neutrinos (*dots*) from Sgr A* due to interactions of ultra high-energy protons with ambient photon and magnetic fields. Protons accelerated to energies 10^{18} eV in the regular magnetic field close to the gravitational radius $R \sim R_g$, propagate through the infrared emission region of size $R = 10R_g$. The calculations correspond to two assumptions for the strength of the magnetic field in the region of the infrared emission: $B = 0.1$ G (a) and $B = 10$ G (b). The experimental points in X-ray and gamma-ray bands are from the compilation of Aharonian and Neronov (2005).

While neutrinos and neutrons, as well as gamma-rays of energies below 10^{12} eV escape freely the emission region, gamma-rays above 10^{12} as well as secondary electrons from π^\pm -decays effectively interact with the ambient photon and magnetic fields, and thus initiate IC and/or (depending on the strength of the B-field) synchrotron cascades. The cascade development stops when the typical energy of γ rays is dragged to 1 TeV. Gamma-rays produced in this way can explain the observed TeV flux, if the acceleration power of 10^{18} eV protons is about 10^{37} erg/s. The energy spectra of gamma-rays produced in this scenario are shown in Figure 2.

2.2.2. Proton-Proton Scenario

Acceleration of protons to extremely high energies, $E \sim 10^{18}$ eV, is a key condition for effective photo-meson interactions. This model requires existence of strong magnetic field, $B \geq 10^4$ G, in the compact region limited by a few gravitational radii. If the field close to the black hole is weaker, the interactions of protons with the ambient thermal gas become the main source of production of gamma-rays and electrons of “hadronic” origin.

Protons can also be accelerated to TeV energies in the accretion disk, e.g. through strong shocks developed in the accretion flow. The efficiency of gamma-ray production in this case is determined by the ratio of accretion time $R/v_r \sim 10^3 - 10^4$ s (depending on the accretion regime) to the p-p cooling time, $t_{pp} \simeq 1.5 \times 10^7 (n/10^8 \text{ cm}^{-3})^{-1}$ s. For any reasonable assumption concerning the density of the ambient thermal plasma and the accretion regime, the acceleration power of

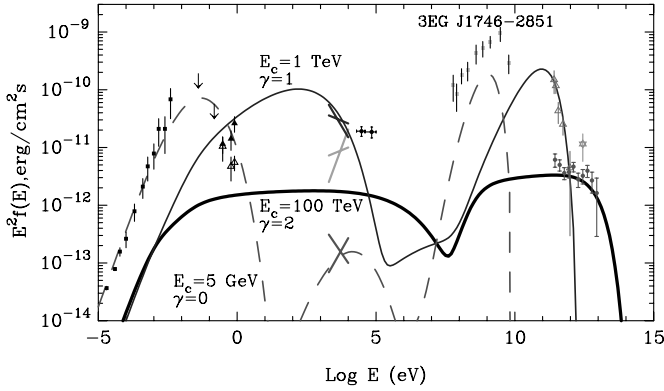


Figure 3. SED of the broad-band electromagnetic radiation initiated by p-p interactions in the accretion disk (from Aharonian and Neronov 2005). It is assumed that the accelerated protons with spectrum $E^{-\Gamma} \exp(-E/E_c)$ are injected into the thermal plasma of density 10^8 cm^{-3} , and together with the accretion flow cross the region of the size $R \approx 10R_g$ cm and fall under the black hole horizon after 10^4 s. The following parameters have been assumed: (1) *heavy solid curve*: $\Gamma = 2$, high-energy exponential cut-off at $E_c = 100 \text{ TeV}$, total acceleration rate $L_p = 5 \times 10^{38} \text{ erg/s}$; (2) *thin solid curve*: $\Gamma = 1$, $E_c = 1 \text{ TeV}$, $L_p = 10^{40} \text{ erg/s}$; (3) *dashed curve*: narrow ($\Gamma = 0$, $E_c = 5 \text{ GeV}$) distribution of protons, $L_p = 10^{40} \text{ erg/s}$. For all three cases the magnetic field is assumed to be $B = 10 \text{ G}$.

high-energy protons should exceed $L_p \approx 10^{39} \text{ erg/s}$ in order to provide detectable fluxes of TeV gamma-rays (see Figure 3).

2.3. CURVATURE RADIATION-INVERSE COMPTON (CRIC) MODEL

The models of gamma-ray emission associated with accelerated protons provide rather modest efficiencies of conversion of the energy of accelerated protons to gamma-rays. The radiative energy loss rate of electrons is much higher, and therefore the models associated with accelerated electrons provide more economic ways to produce high-energy gamma-rays. Obviously, these electrons should be accelerated to at least $E_{\text{max}} \sim 10 \text{ TeV}$. This immediately constrains the strength of the chaotic component of the magnetic field; even under an extreme assumption that the acceleration proceeds at the maximum possible rate, $(dE/dt)_{\text{acc}} \simeq eB$, one gets $B \leq 10(E_{\text{max}}/10 \text{ TeV})^{-2} \text{ G}$.

The requirement of particle acceleration at the maximum rate imposes strong restrictions on the geometry of magnetic field and possible acceleration mechanisms. In this regard, acceleration in ordered electric and magnetic fields, e.g. by the rotation-induced electric field, provides maximum energy gain. Moreover, in the ordered field the energy dissipation of electrons is reduced to the curvature radiation losses; this allows acceleration of electrons up to $E_{e,\text{max}} \simeq 10^{14}(B/10\text{G})^{1/4} \text{ eV}$.

The curvature radiation peaks at $\epsilon_{\text{curv}} \simeq 2 \times 10^8 (E_e/10^{14} \text{ eV})^3 \text{ eV}$. The Compton scattering of same electrons leads to the second peak at much higher energies,

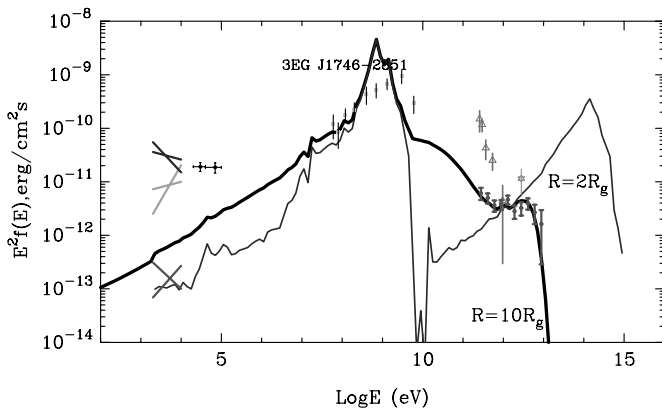


Figure 4. Broad-band SED of radiation produced by electrons within the *CRIC* model (from Aharonian and Neronov 2005). *Thin solid curve*: gamma-ray production spectrum formed as superposition of the Curvature and inverse Compton emission components which accompany electron acceleration by the rotation-induced electric field within $R = 2R_g$; *heavy solid curve* – the spectrum of gamma-rays modified after the passage through the infrared source of size $R = 10R_g$. The strength of the regular magnetic field in the electron acceleration region is assumed $B = 10$ G. The strength of the random magnetic field in the region of infrared emission is assumed $B = 30$ G.

$E_\gamma \sim E_e \sim 10^{14}$ eV (because the scattering proceeds in the Klein–Nishina limit). However, because of interactions with infrared photons, gamma-rays of energy exceeding 10 TeV can not freely escape the source. Synchrotron radiation and Compton scattering of the secondary (pair-produced) electrons lead to re-distribution of the initial gamma-ray spectrum.

We call this scenario of production of *Curvature Radiation* and *IC* photons by electrons accelerated in regular magnetic/electric fields as *CRIC* model. Quantitative calculations of high-energy radiation within framework of this model require a “self-consistent” approach which should take into account the radiation reaction force. An example of such self-consistent computation is shown in Figure 4.

3. Diffuse Gamma Radiation of Runaway Protons

A significant fraction of protons accelerated near the black hole may escape the source and enter the surrounding dense gas environment. The interactions of these runaway protons with the interstellar medium lead to production of gamma-rays the luminosity of which could exceed the gamma-ray luminosity of the central engine.

The flux of this radiation component depends not only on the density of the ambient gas and the injection rate of protons, but also on the speed of their propagation in the interstellar medium. The TeV radiation detected by HESS is localised within several angular minutes. This implies that, for the distance to the Galactic

Center $d \simeq 8$ kpc, the linear size of production region of gamma-rays can be as large as 10 pc. The density of the diffuse interstellar gas in this region is very high, $n \simeq 10^3 \text{ cm}^{-3}$. The lifetime of protons in this dense environment against nuclear p - p interactions is $t_{pp} \approx 5 \times 10^4$ yr. Thus, in the case of absolute confinement of protons, the gamma-ray luminosity after $\sim 10^5$ years of continuous injection of protons achieves its maximum (saturated) level, $L_\gamma = \eta \dot{W}_p$, with an efficiency $\eta \simeq 1/3$ (the fraction of energy released in neutral π -mesons). However, the confinement time in the 10 pc region is rather limited; even in the Bohm diffusion regime the escape time of protons from this region is $t_{esc} \sim R^2/r_g c \simeq 3 \times 10^5 (E/100 \text{ TeV})^{-1} (B/100 \mu\text{G})$ yr. Thus, for any realistic diffusion coefficient $D(E)$, TeV protons leave the region before they loose their energy in p - p interactions. This not only reduces the gamma ray production efficiency but also, in the case of energy-dependent diffusion, modifies the energy distribution of protons established within the 10 pc region.

The impact of the energy-dependent diffusion on the resulting radiation spectra is demonstrated in Figure 5. It is assumed that during 10^5 years protons are injected (quasi)continuously into the interstellar medium of density $n = 10^3 \text{ cm}^{-3}$. The initial spectrum of protons is assumed in the form of power-law with an exponential cutoff, $Q(E) = Q_0 E^{-\alpha} \exp(-E/E_0)$. The cutoff energy is fixed at $E_0 = 10^{15}$ eV, which is an obvious condition for effective production of gamma-rays to at least 10 TeV. The choice of the power-law index depends on the assumed diffusion coefficient, if one intends to explain the energy spectrum of gamma-rays detected by HESS, $J(E) = (2.5 \pm 0.21) \times 10^{-12} E^{-\Gamma} \text{ ph/cm}^2 \text{ s TeV}$ with $\Gamma = 2.21 \pm 0.09$ (Aharonian et al. 2004).

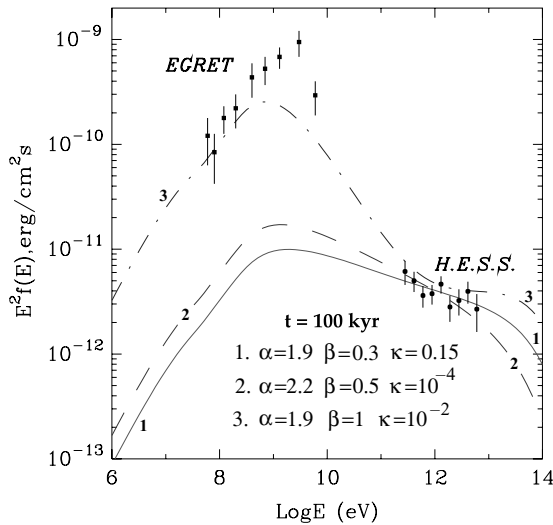


Figure 5. Energy spectra of diffuse gamma rays expected from the central 10 pc region of the Galactic Center within different assumptions concerning the diffusion coefficient and the proton injection spectrum (see the text).

The diffusion coefficient is assumed in the following form: $D(E) = 10^{28}(E/1 \text{ GeV})^\beta \kappa \text{ cm}^2/\text{s}$. The values of $\kappa \sim 1$ and $\beta \sim 0.5$ correspond to the CR diffusion in the galactic disk. Of course, in the central region of the Galaxy one may expect significant deviation from the character of particle diffusion in “ordinary” parts of the galactic disk. In the case of effective confinement of protons, e.g. with $\kappa = 10^{-4}$ and $\beta = 0.5$, the escape time of multi-TeV protons is comparable with the characteristic time of p-p interactions. This prevents strong modification of the initial proton spectrum. Therefore, the injection spectrum of protons with power-law index $\alpha = 2.2$ fits quite well the observed TeV spectrum (curve 2 of Figure 5). Because of the effective confinement, the required injection rate of protons is rather modest, $\dot{W}_p = 7 \times 10^{36} \text{ erg/s}$.

In the case of faster diffusion, the spectral index of injection is determined as $\alpha \simeq \Gamma - \beta$. For example, for $\kappa = 0.15$ and $\beta = 0.3$ (a diffusion regime which corresponds to the Kolmogorov type turbulence), the γ -ray observations are well explained assuming the following parameters $\alpha = 1.9$ and $\dot{W}_p = 7.5 \times 10^{37} \text{ erg/s}$ (curve 1 in Figure 5).

Finally, one should note that the injection spectrum remains unchanged with very fast escape. For example, for $\kappa = 10^{-2}$ and $\beta = 1$ (an energy-dependence close to the one expected in the Bohm diffusion, but with much larger diffusion coefficient), the particles propagate in the diffusion regime until energies of several TeV. At higher energies they escape the source almost rectilinearly on timescales $R/c \sim 30$ years. This implies that while at low energies the protons inside the 10 pc region suffer significant spectral deformation, $\alpha' \rightarrow \alpha + \beta$, at very high energies the shape of the initial spectrum is essentially recovered. Such an interesting modulation of the proton spectrum is reflected in the resulting gamma-ray spectrum (curve 3 in Figure 5). In this case, the requirement to the injection power of protons is higher than in the previous cases, $\dot{W}_p = 10^{39} \text{ erg/s}$.

The π^0 -decay radiation of protons is always accompanied by synchrotron radiation of secondary electrons – the products of charged π -mesons. In the case of extension of the proton spectrum to 10^{15} eV , and for the magnetic field exceeding $100 \mu\text{G}$, the spectral energy distribution (SED) of synchrotron radiation of secondary electrons peaks in the X-ray domain. This seems an attractive mechanism for explanation of the diffuse X-ray emission of the Galactic Center, given the serious problems of interpretation of this radiation within the “standard” (thermal and nonthermal) models (Muno et al., 2004). However, for a relatively flat SED of TeV gamma-rays (like the one observed by HESS) the energy flux of X-rays is always less, by a factor of 3 to 10, than the energy flux of γ -rays. Therefore for the spectra shown in Figure 5 only a small fraction (10 pc or so) of the observed X-ray flux can be contributed by secondary electrons.

Formally, the flux of the secondary-electron-synchrotron component can be significantly increased, without getting in conflict with the TeV data, if one assumes very hard spectrum of protons, e.g. with power-law spectral index $\alpha \leq 1.5$. Such a spectrum cannot explain the TeV data. However, assuming that the spectrum of

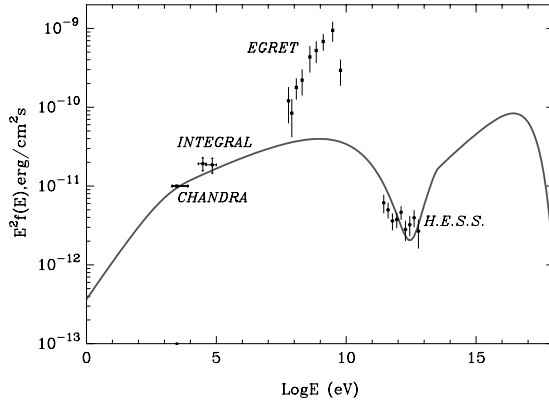


Figure 6. The broad-band spectrum of radiation initiated by interactions of ultrahigh-energy protons in the central 10 pc region. The injection spectrum is assumed in the form of power-law with $\alpha = 1.5$ and low and high-energy cutoffs at $E_1 = 2 \times 10^{14}$ eV and $E_1 = 1.5 \times 10^{18}$ eV. The proton injection rate is assumed $\dot{D} = 1.5 \times 10^{38}$ erg/s to match the reported X-ray (Chandra-Muno et al. 2004, INTEGRAL-Belanger et al. 2004) and TeV fluxes (Aharonian et al., 2004). The diffusion coefficient is characterised by $\beta = 0.3$ and $\kappa = 10^{-3}$. The number density of the gas and magnetic field in the central 10 pc region are assumed $n = 10^3$ cm $^{-3}$ and $B = 1$ mG, respectively. The effect of spectral modulation due interactions with the 2.7 K CMBR is not shown. Note that for the distance to the GC the absorption becomes noticeable ($\sim e^{-1} \approx 1/3$) only at energies around 10^{15} eV.

protons extends to $E_0 \sim 10^{18}$ eV, a new TeV gamma-ray component, due to the synchrotron radiation of the secondary ultrahigh-energy electrons, could dominate over the π^0 -decay component. The possibility of producing high fluxes of X-rays and gamma rays through the synchrotron radiation of secondary electrons is demonstrated in Figure 6. Note that although the parent protons interact with the ambient gas throughout the central 10 pc region of the Galactic Center (thus the radiation can be dubbed as diffuse), the observer would detect a point-source like TeV signal centered on Sgr A*. The reason is that the ultrahigh-energy protons injected into the surrounding medium propagate radially (like photons) without significant deflection in the interstellar magnetic field. Since the characteristic energy of parent protons, which are responsible for the secondary synchrotron X-rays, is smaller by a factor of $(\text{TeV}/\text{keV})^{1/2} \sim 10^4 - 10^5$, the angular size of X-rays should be larger. This scenario predicts a tendency of decrease of the angular size of the X-ray signal with increase of the photon energy. This hypothesis can be inspected also by detection of direct gamma-rays from photomeson interactions up to $\sim 10^{17}$ eV. Above several TeV this radiation component dominates over the secondary synchrotron radiation.

4. Summary

The origin of TeV radiation detected from the direction of the Galactic Center is not yet established. The 3-arcmin upper limit on the source size, assuming Gaussian

distribution of the source brightness (Aharonian et al. 2004), implies that several objects, in particular the Dark Matter Halo, the young SNR Sgr A East, the central compact source Sgr A*, as well as the entire central diffuse region filled by dense molecular clouds and cosmic rays, are likely candidates for TeV emission within the central 10 pc region. In fact, each of these sources may contribute significantly into the observed gamma-ray flux. In this paper we present the results of our study of several gamma-ray production scenarios with both direct and indirect links to the massive black hole in the Galactic Center, Sgr A*.

The results shown in Figures 2–4 demonstrate that at least three gamma-radiation scenarios, which take place in vicinity of the massive black hole, can explain the TeV observations without apparent conflicts with observations of Sgr A* at lower frequencies. The hadronic models based on photo–meson or p–p interactions cannot provide efficiency higher than 0.1%, therefore they require an acceleration rate of protons of about 10^{39} erg/s or larger. Although this is larger than the total electromagnetic luminosity of Sgr A*, it is still acceptable for a black hole of mass $3 \times 10^6 M_{\odot}$. On the other hand, the electronic model *CRIC*, based on the curvature and synchrotron radiation channels, allows an economic way of conversion of energy of electrons to gamma-rays.

The p–p hadronic model predicts X-ray fluxes comparable with X-ray observations in high state, but an order of magnitude higher than in the quiescent state. The photomeson and *CRIC* models predict an order of magnitude lower X-ray fluxes. On the other hand, the photomeson model predicts detectable fluxes of ultrahigh-energy gamma-rays and neutrons. The *CRIC* model predicts high gamma-ray fluxes at MeV/GeV energies which should be easily detected by GLAST.

The gamma-radiation in all three models is generally expected to be variable on timescales as short as 1 h. Therefore the detection of a variable component of radiation on such short timescales would be a strong argument in favour of gamma-ray production near the massive black hole. On the other, although the lack of variations of the TeV flux could be naturally interpreted as gamma-ray production in extended regions, it cannot be used as a decisive argument against the black-hole origin of TeV emission.

In addition to the gamma-rays emitted in compact regions in the vicinity of the massive black hole, one should expect also a diffuse (extended) component of radiation associated with interactions of the runaway protons with the surrounding dense interstellar gas. The relative contribution of this component to the total TeV flux, as well as the spectral and angular characteristics of π^0 -decay gamma-rays significantly depend on the rate of injection of protons by Sgr A* into the interstellar medium, as well as on the regime of (energy-dependent) diffusion of protons in the dense central region. For certain combinations of principal model parameters the diffuse gamma-rays from p–p interactions can satisfactorily explain both the absolute flux and energy spectrum of TeV radiation reported by HESS. Although this component can be extended well beyond the Galactic Center region, because of enhanced gas density in the central 10 pc region one should expect a bright gamma-ray

core within several arcminutes around Sgr A*. In the case of extension of the spectrum of protons to $E \simeq 10^{18}$ eV, one may expect another diffuse component related to the synchrotron radiation of ultrahigh-energy secondary electrons (from π^\pm -decays). Since the gyroradius of parent protons is comparable or exceeds 10 pc, the observer would detect this TeV component as a point-like source.

References

- Aharonian, F. and Neronov, A.: 2005, *ApJ* **20** January issue (astro-ph/0408303).
Aharonian, F. et al.: 2004, (H.E.S.S. collaboration), *A&A* **415**, L13.
Aharonian, F. et al.: 2002, *Phys. Rev.* **D66**, 023005.
Aharonian, F.: 2000, *New Astr. Rev.* **5**, 377.
Belanger, G. et al.: 2004, *ApJ* **601**, L163.
Kosack, K. et al.: 2004, *ApJ Lett.* **608**, L97.
Levinson, A.: 2000, *Phys. Rev. Lett.* **85**, 912.
Muno, M.P. et al.: 2004, *ApJ* **613**, 326.
Tsuchiya, K. et al.: 2004, *ApJ Lett.* **606**, L115.

AGNS AND MICROQUASARS AS HIGH-ENERGY γ -RAY SOURCES

JOSEP M. PAREDES

*Departament d'Astronomia i Meteorologia, Universitat de Barcelona, Av. Diagonal 647,
08028 Barcelona, Spain; E-mail: jmparedes@ub.edu*

(Received 23 September 2004; accepted 1 June 2005)

Abstract. The extragalactic analogs of the microquasars, the quasars, are strong γ -ray emitters at GeV energies. It is expected that microquasars are also γ -ray sources, because of the analogy with quasars and because theoretical models predict the high-energy emission. There are two microquasars that appear as the possible counterparts for two unidentified high-energy γ -ray sources.

Keywords: X-rays: binaries, stars: individual: LS 5039, LS I +61 303, gamma-rays: observations

1. Introduction

The microquasar phenomenon has grown in prominence recently, as it has been found that most X-ray binaries show radio emission, associated with jets-collimated beams of relativistic plasma. The ejection takes place in a bipolar way perpendicular to the accretion disk associated with the compact star, a black hole or a neutron star. The word microquasar itself was chosen by the analogy of these astronomical objects with quasars and other active galactic nuclei (AGNs) at cosmological distances (Mirabel and Rodríguez, 1999). The analogy quasar–microquasar goes beyond a simple morphological resemblance. Today, there is growing evidence to think that the physics involved in both types of objects is the same, or at least very similar. The key difference would be the distinct order of magnitude of the most significant parameters, especially the mass of the compact object.

2. AGNs as γ -Ray Sources

AGNs are extragalactic sources whose spectra extend from radio waves to γ -rays. Thanks to the Compton Gamma Ray Observatory (CGRO) it is now well established that AGNs are strong γ -ray emitters. The Energetic Gamma Ray Experiment (EGRET) on board the CGRO produced the third EGRET catalogue (Hartman et al., 1999) that contains 271 sources detected at energies >100 MeV. Most of them (about 168 sources) remain unidentified and 72 of these unidentified sources



are at absolute Galactic latitudes lower than 10° . The identified sources are mainly AGNs (Thomson et al., 1995), and more AGNs are expected to be found among the still unidentified sources with high Galactic latitude. All of these detected AGNs are blazars; no radio-quiet AGNs has been identified so far in the EGRET data. In fact, this is not surprising because blazars are able to generate high-energy particles that can produce γ -rays via inverse Compton (IC) scattering, as well as present relativistic beaming, which is important to avoid photon–photon collision and amplify the flux.

More than two dozen jets have been detected at X-rays in AGNs, with most of them being radio galaxies (both FRI and FRII). Although synchrotron self Compton (SSC) models cannot generally explain the level of X-ray emission, those models based on the IC scattering of seed photons of the nucleus and the CMB radiation by the relativistic electrons in the jet not only can better explain such X-ray levels but also can produce efficiently high-energy γ -ray emission (Tavecchio et al., 2000; Celotti et al., 2001).

3. X-ray Binaries and Microquasars

The most recent catalogue of High Mass X-ray Binaries (HMXBs) contains 131 sources (Liu et al., 2000), while the catalogue of Low Mass X-ray Binaries (LMXBs) amounts to 149 objects (Liu et al., 2001). Considering both catalogues together, there are a total of 43 radio emitting sources. Some of these sources, those which we define as microquasars, show direct evidence for a relativistic radio jet (Ribó, 2002, 2004), while many others show radio emission which is also almost certainly associated with a jet (Fender, 2005).

At the time of writing, a total of 15 microquasar systems have been identified. The observational data of these microquasars at energies from soft to very high-energy γ -rays, are quoted in Table I.

The top part of the table is reserved for HMXBs, while the bottom part contains those of low mass. In the second column of Table I we list their flux (count/s) and error or upper limit in the energy range of 40–100 keV obtained with the IBIS γ -ray imager on board INTEGRAL, covering the first year of data (Bird et al., 2004).

The Burst and Transient Source Experiment (BATSE), aboard the CGRO, monitored the high-energy sky using the Earth occultation technique (EOT). A compilation of BATSE EOT observations has been published recently (Harmon et al., 2004). From this catalogue we have selected the data on microquasars in the energy range 160–430 keV in mCrab units and is listed in the third column.

Among the sources detected by the instrument COMPTEL (Schönfelder et al., 2000), also aboard the CGRO, there is the microquasar Cygnus X-1, as well as two sources, GRO J1823–12 and GRO J0241+6119, possibly associated with two other microquasars. See fourth column in Table I.

TABLE I
High-energy emission from microquasars

Name	INTEGRAL ^a 40–100 keV (count/s)	BATSE ^b 160–430 keV (mCrab)	COMPTEL ^c 1–30 MeV (GRO)	EGRET ^d > 100 MeV (3EG)	Others ^e
High Mass X-ray					
Binaries (HMXB)					
LS I +61 303	–	5.1 ± 2.1	J0241+6119?	J0241+6103?	
V4641 Sgr	–	–	–	–	
LS 5039	–	3.7 ± 1.8	J1823–12?	J1824–1514?	
SS 433	<1.02	0.0 ± 2.8	–	–	
Cygnus X-1	66.4 ± 0.1	924.5 ± 2.5	Yes	–	S
Cygnus X-3	5.7 ± 0.1	15.5 ± 2.1	–	–	O, T?
Low Mass X-ray					
Binaries (LMXB)					
Circinus X-1	–	0.3 ± 2.6	–	–	
XTE J1550–564	0.6 ± 0.07	-2.3 ± 2.5	–	–	
Scorpius X-1	2.3 ± 0.1	9.9 ± 2.2	–	–	
GRO J1655–40	–	23.4 ± 3.9	–	–	O
GX 339–4	0.55 ± 0.03	580 ± 3.5	–	–	S
1E	4.32 ± 0.03	61.2 ± 3.7	–	–	S
1740.7–2942					
XTE J1748–288	–	–	–	–	S
GRS 1758–258	3.92 ± 0.03	38.0 ± 3.0	–	–	S
GRS 1915+105	8.63 ± 0.13	33.5 ± 2.7	–	–	S, T?

^aThe first IBIS/ISGRI soft gamma-ray galactic plane survey catalog (Bird et al., 2004).

^bBATSE Earth occultation catalog, Deep sample results (Harmon et al., 2004).

^cThe first COMPTEL source catalogue (Schönfelder et al., 2000).

^dThe third EGRET catalog of high-energy γ -ray sources (Hartman et al., 1999).

^eS: SIGMA instrument onboard GRANAT satellite; O: OSSE; T: TeV source.

4. Microquasars Associated with EGRET Sources

According to the quasar–microquasar analogy (Mirabel and Rodríguez, 1999), one could also expect the jets in microquasars to be GeV emitters. Several models aimed to predict the high-energy γ -ray emission from microquasars have been developed during the last years. A general description of such models can be found in Romero (2005). Up to now, there are two HMXB microquasars, LS 5039 and LS I +61 303, that are associated with two EGRET sources.

4.1. LS 5039/3EG J1824–1514

The discovery of the microquasar LS 5039, and its possible association with a high-energy γ -ray source ($E > 100$ MeV), provides observational evidence that

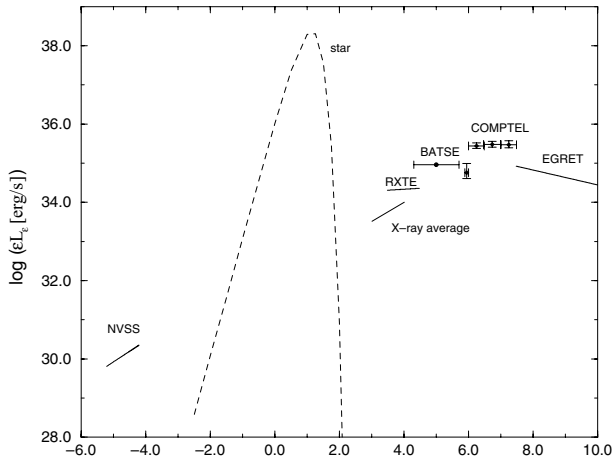


Figure 1. Observed spectral energy distribution of LS 5039.

microquasars could also be sources of high-energy γ -rays (Paredes et al., 2000). It is important to point out that this was the first time that an association between a microquasar and a high-energy γ -ray source was reported. This finding opened up the possibility that other unidentified EGRET sources could also be microquasars. LS 5039 is the only X-ray source from the bright ROSAT catalogue whose position is consistent with the high-energy γ -ray source 3EG J1824–1514. LS 5039 is also the only object simultaneously detected in X-rays and radio which displays bipolar radio jets at sub-arcsecond scales. New observations conducted with the EVN and MERLIN confirm the presence of an asymmetric two-sided jet reaching up to ~ 1000 AU on the longest jet arm (Paredes et al., 2002; Ribó, 2002).

Recently, Collmar (2003) has reported the detection of an unidentified γ -ray source, GRO J1823–12, at galactic coordinates ($l = 17.5^\circ$, $b = -0.5^\circ$) by the COMPTEL experiment. This source is among the strongest COMPTEL sources. The source region, detected at a high significance level, contains several possible counterparts, LS 5039 being one of them. It is also worth noting that BATSE has detected this source at soft γ -rays (see Table I). Taking into account these observational evidences, from radio to high-energy γ -rays, LS 5039 appears to be a very likely counterpart of the EGRET source 3EG J1824–1514. Figure 1 shows the observed spectral energy distribution of LS 5039.

4.2. LS I +61 303/3EG J0241+6103

After the discovery of relativistic jets in LS I +61 303, this source has been classified as a new microquasar (Massi et al., 2001, 2004). This object has also been proposed to be associated with the γ -ray source 2CG 135+01 (=3EG J0241+6103) (Gregory and Taylor, 1978; Kniffen et al., 1997). Although the broadband 1 keV–100 MeV

spectrum of LS I +61 303 remains uncertain, because OSSE and COMPTEL observations were likely dominated by the quasar QSO 0241+622 emission, the EGRET angular resolution is high enough to exclude this quasar as the source of the high-energy γ -ray emission (Harrison et al., 2000). BATSE marginally detected the source, the quasar also being excluded as the origin of this emission (see Table I).

Recently, Massi (2004) has carried out a timing analysis of pointed EGRET observations (Tavani et al., 1998) suggesting a period of 27.4 ± 7.2 days, in agreement with the orbital period of this binary system, of 26.496 days. This result, if confirmed, would clearly support the association of LS I +61 303 with 3EG J0241+6103.

This microquasar also seems to be a fast precessing system. MERLIN images obtained in two consecutive days show a change in the direction of the jets of about 50° that has been interpreted as a fast precession of the system (Massi et al., 2004). If this is confirmed, it could solve the puzzling VLBI structures observed so far, as well as the short term variability of the associated γ -ray source 3EG J0241+6103.

Up to now, the only existing radial velocity curve of LS I +61 303 was that obtained by Hutchings and Crampton (1981). Recently, after a spectroscopic campaign, an improved estimation of the orbital parameters has been obtained (Casares et al., 2005). Here, we will just mention the new high eccentricity ($e = 0.72 \pm 0.15$) and the periastron orbital phase at ~ 0.2 . These values are a key information for any interpretation of the data obtained at any wavelength.

Hall et al. (2003) gave upper limits on the emission associated to LS I +61 303/3EG J0241+6103 at very high-energy γ -rays from observations performed by the Cherenkov telescope Whipple. Several models have been proposed to explore the high-energy emission of this source (e.g. Taylor et al., 1996; Punsly, 1999; Harrison et al., 2000; Leahy, 2004). The most recent theoretical work has been presented by Bosch-Ramon and Paredes (2004), who explore with a detailed numerical model if this system can both produce the emission and present the variability detected by EGRET (> 100 MeV). Figure 2 shows the observed spectral energy distribution of the microquasar LS I +61 303.

Bosch-Ramon et al. (2005) developed a detailed numerical model that includes both external and SSC scattering. The computed spectral energy distribution of a EGRET source high-mass microquasar is presented in Figure 3. Looking at Figures 1 and 2, and comparing them with Figure 3, it is seen how the IC jet scenario reproduces fairly well the data, giving further support to the proposal of microquasars as γ -ray sources.

5. VHE γ -ray Sources

The very high-energy sky map contains a reduced number of sources. The number of confirmed and probable catalogued sources presently amounts to 14 (6 AGN,

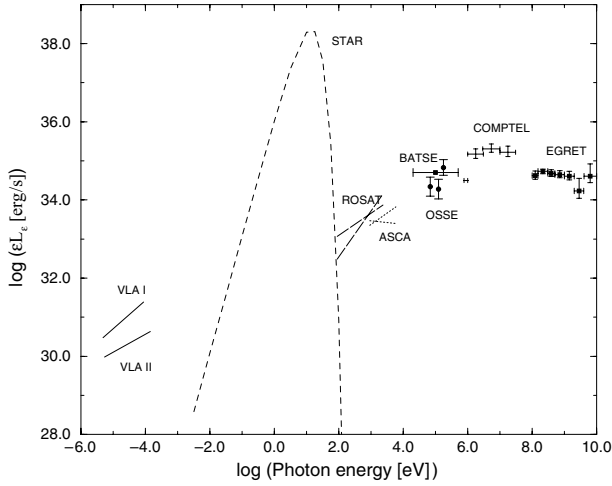


Figure 2. Observed spectral energy distribution of LS I +61 303.

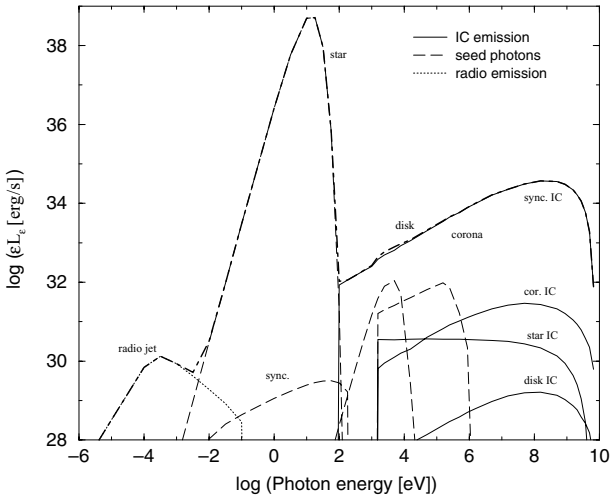


Figure 3. Spectral energy distribution model of a high-mass microquasar (Bosch-Ramon et al., 2005).

3 pulsar wind nebulae, 3 supernova remnants, 1 starburst galaxy, and 1 unknown) (Ong, 2004). Some microquasars have been observed in the energy range of TeV γ -rays with the imaging atmospheric Cherenkov telescopes, but none of them has been detected with high confidence yet. Historically, Cygnus X-3 was widely observed with the first generation of TeV instruments. Some groups claimed that they had detected Cygnus X-3 (Chadwick et al., 1985), whereas other groups failed to detect it (O'Flaherty et al., 1992). As the claimed detections have not been confirmed, and the instrumentation at this epoch was limited, these results have not been

considered as positive detections by the astronomical community. The HEGRA experiment detected a flux of the order of 0.25 Crab from GRS 1915+105 during the period May–July 1996 when the source was in an active state (Aharonian and Heinzlmann, 1998). This source has also been observed with Whipple, obtaining a 3.1σ significance (Rovero et al., 2002). More recently, an upper limit of 0.35 Crab above 400 GeV has been quoted for GRS 1915+105 (Horan and Weekes, 2003). LS I +61 303 was observed too, but was not detected in the TeV energy range (see Section 4).

Acknowledgements

I acknowledge partial support by DGI of the Ministerio de Ciencia y Tecnología (Spain) under grant AYA2001-3092, as well as partial support by the European Regional Development Fund (ERDF/FEDER).

References

- Aharonian, F.A. and Heinzlmann, G.: 1998, *Nucl. Phys. B.* **60B**, 193.
Bird, A.J., Barlow, E.J., Bassani, L., et al.: 2004, *ApJ* **607**, L33.
Bosch-Ramon, V. and Paredes, J.M.: 2004, *A&A* **425**, 1069.
Bosch-Ramon, V., Romero, G.E. and Paredes, J.M.: 2005, *A&A* **429**, 267.
Casares, J., Ribas, I., Paredes, J., Martí, J. and Allende Prieto, C.: 2005, *MNRAS* **360**, 1105.
Chadwick, P.M., Dipper, N.A., Dowthwaite, J.C., et al.: 1985, *Nature* **318**, 642.
Celotti, A., Ghisellini, G., Chiaberge, M., et al.: 2001, *MNRAS* **321**, L1.
Fender, R.P.: 2005, in Lewin, W.H.G. and van der Klis, M. (eds.), *Compact Stellar X-Ray Sources*, Cambridge, Univ. Press, Cambridge.
Collmar, W.: 2003, Proc. 4th Agile Science Workshop, Frascati (Rome) on 11–13 June 2003.
Gregory, P.C. and Taylor, A.R.: 1978, *Nature* **272**, 704.
Hall, T.A., Bond, I.H., Bradbury, S.M., et al.: 2003, *ApJ* **583**, 853.
Harmon, B.A., Wilson, C.A., Fishman, G.J., et al.: 2004, *ApJS* **154**, 585.
Harrison, F.A., Ray, P.S., Leahy, D.A., et al.: 2000, *ApJ* **528**, 454.
Hartman, R.C., Bertsch, D.L., Bloom, S.D., et al.: 1999, *ApJS* **123**, 79.
Horan, D. and Weekes, T.: 2003, private communication.
Hutchings, J.B. and Crampton, D.: 1981, *PASP* **93**, 486.
Kniffen, D.A., Alberts, W.C.K., Bertsch, D.L., et al.: 1997, *ApJ* **486**, 126.
Leahy, D.A.: 2004, *A&A* **413**, 1019.
Liu, Q.Z., van Paradijs, J. and van den Heuvel, E.P.J.: 2000, *A&AS* **147**, 25.
Liu, Q.Z., van Paradijs, J. and van den Heuvel, E.P.J.: 2001, *A&A* **368**, 1021.
Massi, M., Ribó, M., Paredes, J.M., et al.: 2001, *A&A* **376**, 217.
Massi, M., Ribó, M., Paredes, J.M., et al.: 2004, *A&A* **414**, L1.
Massi, M.: 2004, *A&A* **422**, 267.
Mirabel, I.F., and Rodríguez, L.F.: 1999, *ARA&A* **37**, 409.
O’Flaherty, K.S., Cawley, M.F., Fegan, D.J., et al.: 1992, *ApJ* **396**, 674.
Ong, R.A.: 2004, astro-ph/0304336.
Paredes, J.M., Martí, J., Ribó, M. and Massi, M.: 2000, *Science* **288**, 2340.

- Paredes, J.M., Ribó, M., Ros, E., et al.: 2002, *A&A* **393**, L99.
- Punsly, B.: 1999, *ApJ* **519**, 336.
- Ribó, M.: 2002, PhD Thesis, Universitat de Barcelona.
- Ribó, M.: 2004, in: J. D. Romney and M. J. Reid (eds.), *ASP Conference Series: Future Directions in High Resolution Astronomy: A Celebration of the 10th Anniversary of the VLBA*, [astro-ph/0402134].
- Romero, G.E.: 2005, *ChJAA* **5**, 110.
- Rovero, A.C., Fegan, S., Weekes, T.C.: 2002, *BAAA* **45**, 66.
- Schönfelder, V., Bennett, K., Blom, J.J., et al.: 2000, *A&AS* **143**, 145.
- Tavani et al.: 1998, *ApJ* **497**, L89.
- Tavecchio, F. et al.: 2000, *ApJ* **544**, L23.
- Taylor, A.R., Young, G., Peracaula, M., et al.: 1996, *A&A* **305**, 817.

LARGE SCALE JETS IN MICROQUASARS

STÉPHANE CORBEL

Université Paris 7 Denis Diderot and Service d'Astrophysique, CEA Saclay, F-91191 Gif sur Yvette, France; E-mail: corbel@discovery.saclay.cea.fr

(Received 27 October 2004; accepted 1 June 2005)

Abstract. Relativistic jets are now believed to be a fairly ubiquitous property of accreting compact objects, and are intimately coupled with the accretion history. Associated with rapid changes in the accretion states of the binary systems, ejections of relativistic plasma can be observed at radio frequencies on timescale of weeks before becoming undetectable. However, recent observations point to long-term effects of these ejections on the interstellar medium with the formation of large-scale relativistic jets around binary systems. In this paper, we review the observations of these large-scale structures in microquasars, highlighting their contributions at high energies.

Keywords: black hole physics, radio continuum, stars, ISM, jets and outflows

1. Introduction: Relativistic Ejections from X-ray Binaries

During periods of outburst activity in black hole (BH) binaries, strong radio flares are sometimes observed around the transition from the hard state to the soft state (more precisely from the intermediate state to the steep power law state; Corbel et al., 2004). This is usually interpreted as synchrotron emission from relativistic electrons ejected from the system with large bulk velocities. In a few cases, such jets have been directly resolved into one-sided (or two-sided) components moving away from the stationary core with apparent velocities greater than the speed of light. After ejection, the moving plasma condensations are observed in the radio band for a few weeks until their emission fades below detection level due to adiabatic expansion. GRS 1915+105 (Mirabel and Rodríguez, 1994) and GRO J1655–40 (Tingay et al., 1995; Hjellming and Rupen, 1995) are the first two so-called superluminal sources.

Since 1994, the number of BHs displaying apparent superluminal motion has greatly increased. For example XTE J1550–564 (Hannikainen et al., 2001), XTE J1748–288 (Rupen et al., 1998), V4641 Sgr (Hjellming et al., 2000; Orosz et al., 2001) and GX 339-4 (Gallo et al., 2004; Hynes et al., 2004) exhibited such behaviours and it is reasonable to think that all BHs (and also some neutron stars) are likely to exhibit highly relativistic jets at some point in their lifetimes. In fact, in recent years, almost all active BHs have been associated with radio emission.

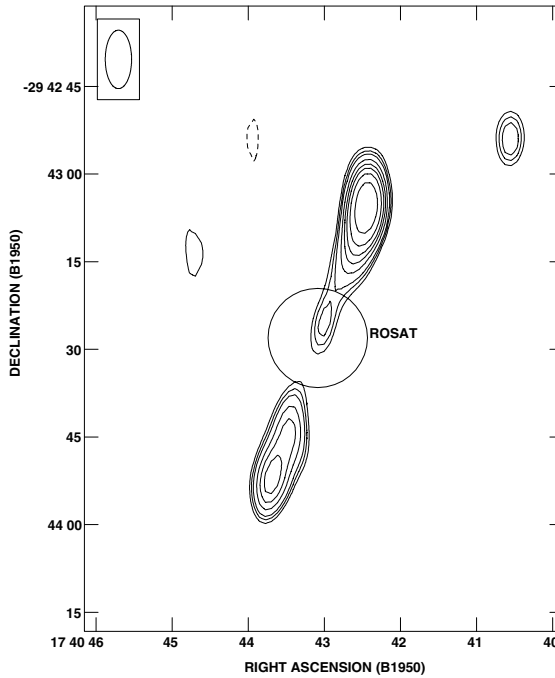


Figure 1. Large-scale radio jets (at 4.8 GHz) from 1E1740.7-2942 (Mirabel et al., 1992).

2. The Historical Large Scale Radio Lobes: 1E 1740.7–2942 and GRS 1758–258

Historically, the “morphological bridge” (and hence the name microquasar) between the Galactic stellar mass black holes and the supermassive black hole at the center of Active Galactic Nuclei has been brought to light in 1992 with the discovery of large-scale radio jets in two Galactic systems. Indeed, the BHs 1E 1740.7–2942 (Figure 1 from Mirabel et al., 1992) and GRS 1758–258 (Martí et al., 2002) in the Galactic Bulge are located at the center of two large (about 3 light years) scale radio lobes, probably indicating the long-term action of past relativistic ejections on the surroundings ISM.

3. Large Scale Decelerating X-ray Jets In XTE J1550–564

Recently, X-ray observations (Figure 2) by Chandra have led to the discovery of extended (up to 30'') X-ray jet emission from the microquasar XTE J1550–564. In observations made between June 2000 and January 2003, two sources moving away from the XTE J1550–564 black hole are detected. The most likely scenario (Corbel et al., 2002) is that the eastern jet is the approaching jet and the western jet

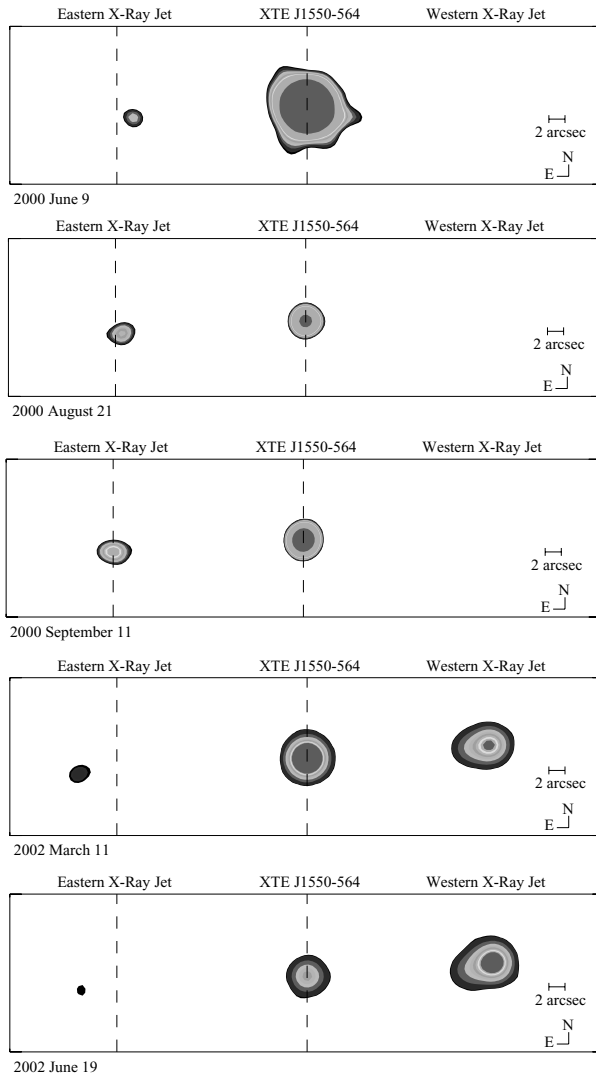


Figure 2. Five *Chandra* 0.3–8 keV images showing the evolution of the eastern and western X-ray jets from XTE J1550–564, between June 2000 and June 2002. The observations are ordered chronologically from top to bottom, and each image is labeled with the observation date. The dashed lines mark the positions of XTE J1550–564 and the eastern X-ray jet on September 11, 2000. Adapted from Corbel et al., 2002; Kaaret et al., 2003; Tomsick et al., 2003.

the receding jet, and that the jet material was ejected from the black hole during a major radio flare in September, 1998 (Hannikainen et al., 2001). Both the radio and X-ray emission of the western jet appeared extended towards XTE J1550–564, and the morphologies associated with each wavelength matched well. The broadband spectra of the jets are consistent with synchrotron emission from high-energy (up

to 10 TeV) particles accelerated in shocks formed by the interaction of the jets with the ISM (Corbel et al., 2002) (i.e. similar to the stationary non-thermal emission from the large-scale lobes in SS 433 (Seward et al., 1980).

The full set of X-ray and radio observations also provided the first direct evidence for gradual deceleration of relativistic material in a jet. More details on the X-ray jets of XTE J1550–564 can be found in Corbel et al. (2002), Tomsick et al. (2003) and Kaaret et al. (2003). These results indicate that emission due to relativistic plasma ejected in September, 1998 has been detected for at least 5 years (Corbel et al., in press) as direct beamed X-ray emission, and demonstrate that Galactic BHs are able to accelerate particles up to very high energies.

4. A Large Scale Fossil X-ray Jet in 4U 1755–33

Very recently, Angelini and White (2003) reported the *XMM-Newton* detection of large-scale ($7'$) persistent X-ray jets (Figure 3) centered on the position of 4U 1755–33, a black hole candidate. Chandra observations (Park et al., 2004) confirm that the jet-like feature observed by *XMM-Newton* is truly diffuse and is not associated with knots like emission. 4U 1755–33 had been a bright, persistent source for at least 20 years, until it became X-ray, quiet in 1995. If the jet had a velocity close to c , then it would have taken about 13 years to expand to its currently observed length of ≈ 4 pc (for a distance of 4 kpc). The jet/ISM interaction in 4U 1755–33 might be similar to that seen in XTE J1550–564, provided the jets were being ejected quasi-continuously over its 20 years of X-ray activity.

The scale of the moving X-ray and radio lobes (0.5–0.8 pc) in XTE J1550–564 is intermediate in size between the moving “superluminal” ejections very close

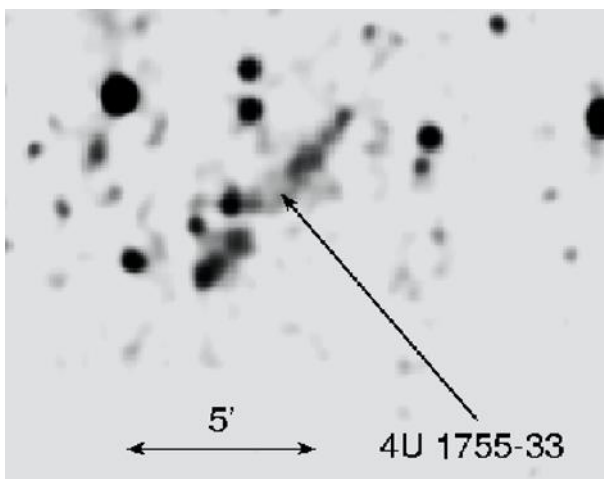


Figure 3. *XMM-Newton* image of 4U 1755–33 (Angelini and White, 2003). The arrow indicates the position of 4U 1755–33. Figure adapted by Kaaret et al. (2003b).

(<0.1 pc) to the compact object (like in, e.g. GRS 1915+105) and the stationary lobes (1–4 pc) such as in 1E 1740.7–2942 or in 4U 1755–33. This suggests a morphological evolution: The large-scale stationary lobes would be the results of the long-term action of past relativistic ejections on the local ISM.

5. Further Large Scales Jets in Microquasars

5.1. GX 339–4

GX 339–4 is one of the best-studied black hole binaries, and has been the key source for unravelling the association of X-ray states and the formation of jets in accreting black holes (Fender et al., 1999; Corbel et al., 2000, 2003; Gallo et al., 2004). Following more than 2 years in quiescence, the source re-brightened in early 2002 to its brightest level in a decade. In May 2002, while brightening in X-rays, GX 339–4 produced an intense and rapid radio flare, further observations with ATCA have tracked the formation of a well-collimated one-sided jet extending to about 12", implying an apparent velocity greater than $0.9c$ given the 4 kpc distance estimate favoured at the time of those observations (Gallo et al., 2004), but more recent work has placed a lower limit on the distance to GX 339-4 of 6 kpc, making this jet superluminal (Hynes et al., 2004). This jet is consistent with shocks waves formed within the jet itself (as several radio flares were observed) and/or by the action of an underlying highly relativistic outflow on the ISM. The luminosity of the jets decreased much more rapidly than in the case of XTE J1550–564, by being undetectable at radio frequencies in less than a year (Gallo et al., 2004). No X-ray emission has been reported from its large-scale jets.

5.2. H 1743–322

In March 2003, INTEGRAL detected new activity from IGR J17464–3213 that was later found to correspond to the X-ray transient H 1743–322, originally discovered with Ariel 5 in August, 1977. After its reactivation in 2003, a radio counterpart was found with the VLA and a bright radio flare (likely associated with a massive ejection event) was observed on April 8, 2003 (Rupen et al., 2003). Similarly to XTE J1550–564, this ejection event was observed later to interact with the ISM with the formation of large-scale lobes at radio and X-ray frequencies (see Figure 4). For further details, see Corbel et al. (2005).

5.3. OTHER BLACK HOLE SYSTEMS

5.3.1. *GRS 1915+105*

GRS 1915+105 is the first Galactic black hole system displaying relativistic jets with apparent superluminal motion on arcsecond scales (Mirabel and Rodríguez,

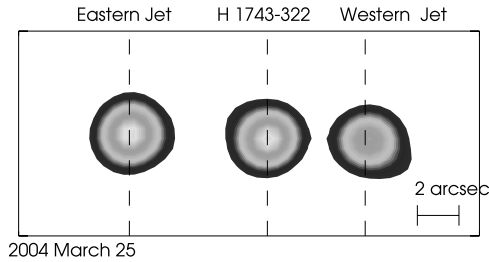


Figure 4. *Chandra* 0.3–8 keV image of H 1743–322 in 2004 (Corbel et al., 2004). The black hole (at the center) as well as the two jets are detected.

1994). A tentative association with two apparently symmetric IRAS sources (located $17'$ from the jet's core) has been proposed by Chaty et al. (2001). Kaiser et al. (2004) also suggest that these two IRAS sources may represent the impact site of the jets of GRS 1915+105 with the ISM.

5.3.2. *XTE J1748–288*

After ballistic ejections in XTE J1748–288 during its 1998 outburst, the jet was observed to stop (and brighten) over the course of a few weeks, presumably following a collision with environmental material (Kotani et al., 2000).

5.3.3. *Cir X–1 and Sco X–1*

Some neutron star systems are also associated with highly relativistic outflows: Sco X-1 (Fomalont et al., 2001) and Cir X–1 (Fender et al., 2004). In those cases, the knots moving with mildly relativistic bulk velocity (from 0.01 to $0.5c$) are energized by an unseen beam of particles that could be ultra-relativistic with bulk Lorentz factor >10 for Cir X–1 (Fender et al., 2004) and >3 for Sco X-1 (Fomalont et al., 2001). In these cases, the observed synchrotron emission could be powered locally during the interaction of the unseen beam with the interstellar medium (ISM) or by moving shocks within the flow itself.

5.3.4. *XTE J1650–500*

Corbel et al. (2004) reported the detection in 2002 of radio emission from XTE J1650–500 in a thermal dominant state. This is contrary to what would have been expected in this state, which has always been associated with quenched radio emission (e.g. Fender et al., 1999; Corbel et al., 2000). It is possible that the observed radio emission is the result of the interaction of material previously ejected from the system with the ISM. If this is the case, then these interactions would have occurred very close to the BH and therefore, cannot be considered a large-scale jet as in, e.g. XTE J1550–564.

Acknowledgements

I would like to acknowledge Rob Fender, Phil Kaaret, John Tomsick, Tasso Tzioumis and Jerry Orosz for stimulating discussions and for their help in the various campaigns of multi-wavelength observations. I would also like to thank the conference organizers for this very interesting meeting.

References

- Angelini, L. and White, N.E.: 2003, *ApJ* **586**, L71.
- Chaty, S. et al.: 2001, *A&A* **366**, 1035.
- Corbel, S., Fender, R.P., Tzioumis, A.K., Nowak, M., McIntyre, V., Durouchoux, P. and Sood, R.: 2000, *A&A* **359** 251.
- Corbel, S., Fender, R.P., Tzioumis, A.K., Tomsick, J.A., Orosz, J.A., Miller, J.M., Wijnands, R. and Kaaret, P.: 2002, *Science* **298**, 1963.
- Corbel, S., Nowak, M.A., Fender, R.P., Tzioumis, A.K. and Markoff, S.: 2003, *A&A* **400**, 1007.
- Corbel, S., Fender, R.P., Tomsick, J.A., Tzioumis, A.K. and Tingay, S.: 2004, *ApJ* **617**, 1272.
- Corbel, S., Kaaret, P.K., Fender, R.P., Tzioumis, A.K., Tomsick, J.A. and Orosz, J.A.: 2005, *ApJ* **632**, 504.
- Fender, R., Wu, K., Johnston, H., Tzioumis, T., Jonker, P., Spencer, R., and van der Klis, M.: 2004, *Nature* **427**, 222.
- Fender, R. et al.: 1999, *ApJ* **519**, L165.
- Fomalont, E.B., Geldzahler, B.J. and Bradshaw, C.F.: 2001, *ApJ* **558**, 283.
- Gallo, E., Corbel, S., Fender, R.P., Maccarone, T.J. and Tzioumis, A.K.: 2004, *MNRAS* **347**, L52.
- Hannikainen, D., Campbell-Wilson, D., Hunstead, R., McIntyre, V., Lovell, J., Reynolds, J., Tzioumis, T. and Wu, K.: 2001, *Ap&SSS* **276**, 45.
- Hjellming, R.M. and Rupen, M.P.: 1995, *Nature* **375**, 464.
- Hjellming, R.M. et al.: 2000, *ApJ* **544**, 977.
- Hynes, R.I. et al.: 2004, *ApJ* **609**, 317.
- Kaaret, P., Corbel, S., Tomsick, J.A., Fender, R., Miller, J.M., Orosz, J.A., Tzioumis, T. and Wijnands, R.: 2003, *ApJ* **582**, 945.
- Kaaret, P. et al.: 2003, *Proc. The Restless High-Energy Universe*, astro-ph/0409155.
- Kaiser, C.R., Gunn, K.F., Brocksopp, C. and Sokoloski, J.L.: 2004, *ApJ*, **612**, 332.
- Kotani, T., Kawai, N., Nagase, F., Namiki, M., Sakano, M., Takeshima, T., Ueda, Y., Yamaoka, K. and Hjellming, R.M.: 2000, *ApJ* **543**, L133.
- Martí, J., Mirabel, I.F., Rodríguez, L.F. and Smith, I.A.: 2002, *A&A* **386**, 571.
- Mirabel, I.F. and Rodríguez, L.F.: 1994, *Nature* **371**, 46.
- Mirabel, I.F., Rodríguez, L.F., Cordier, B., Paul, J. and Lebrun, F.: 1992, *Nature* **358**, 215.
- Park, S.Q., Miller, J.M., McClintock, J.E. and Murray, S.S.: 2004, *ApJ*, submitted for publication.
- Rupen, M.P., Hjellming, R.M. and Mioduszewski, A.J.: 1998, *IAU Circ.*, 6938.
- Rupen, M.P., Mioduszewski, A.J. and Dhawan, V.: 2003, *ATel*, 142.
- Seward, F., Grindlay, J., Seaquist, E. and Gilmore, W.: 1980, *Nature* **287**, 806.
- Tingay, S.J. et al.: 1995, *Nature* **374**, 141.
- Tomsick, J.A., Corbel, S., Fender, R.P., Miller, J.M., Orosz, J.A., Tzioumis, T., Wijnands, R. and Kaaret, P.: 2003, *ApJ* **582**, 933.

IS GRS 1915+105 A MICROQUASAR?

CHRISTIAN R. KAISER¹, J.L. SOKOLOSKI², KATHERINE F. GUNN¹
and CATHERINE BROCKSOFF³

¹*School of Physics & Astronomy, University of Southampton, Southampton, SO17 1BJ, U.K.;*
E-mail: c.r.kaiser@soton.ac.uk

²*Harvard-Smithsonian Center for Astrophysics, Cambridge, MA 02138, U.S.A.;* ³*Mullard Space
Science Laboratory, University College London, Dorking, Surrey, RH5 6NT, U.K.*

(Received 27 September 2004; accepted 1 June 2005)

Abstract. The large mechanical luminosity of the jets of GRS 1915+105 should give rise to luminous emission regions, similar to those observed in radio galaxies, where the jets interact with the gas surrounding the source. However, no radio synchrotron emission of the expected morphology has been found. Here we present the results of a study suggesting that radio bremsstrahlung from the compressed and heated ISM in front of the jets should be detectable, while the synchrotron lobes may be too faint. We identify these jet impact sites with two well-known IRAS regions. This identification suggests a distance of GRS 1915+105 of 6.5 ± 1.6 kpc, significantly closer than the usually assumed distance of 11–12 kpc. We discuss the implications of this reduced distance estimate. The non-detection of the synchrotron radio lobes implies a significant fraction of non-radiating particles, possibly protons, in the jets. The apparent motion of small-scale jet components is not superluminal, so if superluminal motion is required for an object to be termed a microquasar, GRS 1915+105 actually does not qualify. The mass of the black hole in the system is increased to $21 \pm 9 M_{\odot}$, while the mechanical luminosity of the jets is reduced to 14% of the Eddington luminosity.

1. A Primer in Large-Scale Radio Structures Caused by Jets

Jets can efficiently carry an enormous amount of energy from the central engine to sites far removed from their acceleration regions. The dissipation of the jet's energy can give rise to spectacular large-scale structures, often observed in the radio. It is these structures we are trying to identify for the powerful jets of the microquasar GRS 1915+105.

Jets are usually thought to be ballistic after their initial acceleration. Ballistic jets are not luminous as they do not dissipate much of their bulk kinetic energy. However, unless the gas surrounding the jet flow has a very steep negative density gradient, the jet will eventually have to collimate by developing a reconfinement shock (Falle, 1991). After passing through this shock, the jet is in pressure equilibrium with its surroundings and can become susceptible to turbulent disruption. If the jet flow becomes fully turbulent, its energy is dissipated slowly over a large volume and therefore the resulting radiation is often not very luminous. For radio galaxies, such a turbulent jet flow would result in a radio structure of type FR I



(Fanaroff and Riley, 1974). If the jet stays laminar, it will end in a strong shock where it impacts on the surrounding gas. This shock or working surface is identified as the very luminous radio hot-spots of radio galaxies with an FR II-type morphology. After passing through the hot-spot, the jet material inflates more diffuse, but still luminous radio lobes (Scheuer, 1974). The radio emission of the hot-spots and the lobes is synchrotron radiation from relativistic electrons accelerated by the shock at the end of the jet (Hargrave and Ryle, 1974). Laminar jets deliver virtually all their energy to the working surface where the energy is dissipated in a small volume; therefore, they can give rise to much more luminous large-scale radio structures than their turbulent counterparts. It is not surprising that the original morphological distinction between FR Is and FR IIs is also reflected in a sharp division in radio luminosity between the two classes. This distinction demonstrates that the detection of the large-scale radio structure of any jet source will be much simplified if the jets of this source stay laminar throughout their length.

The expansion of the jets and their lobes drives a bow shock into their gaseous environment. The shock-compressed and heated gas will also emit radiation. The frequency and spectrum of this radiation depends crucially on the conditions in the gas. For the hot ($\gtrsim 10^7$ K) and therefore fully ionised IGM surrounding the large-scale structures of radio galaxies, the shocked gas will emit thermal bremsstrahlung at X-ray frequencies (e.g. Smith et al., 2002). The colder ISM surrounding microquasar jets may only be partially ionised by the passage of the bow shock, and features like recombination lines and emission from heated dust could arise. The partially ionised ISM can still produce thermal bremsstrahlung, but due to the lower temperatures this radiation will be emitted at radio wavelengths rather than in X-rays. Laminar jets typically dissipate about half of their total bulk kinetic energy in the shock-compressed gas surrounding their lobes (Kaiser and Alexander, 1997) and so this material may contribute substantially to the overall emission from the large-scale structure caused by the jets.

In summary, we may expect to detect the following components of the large-scale structure caused by laminar microquasar jets:

- Compact radio synchrotron emission regions at the shocks at the end of the jets.
- Extended, diffuse radio synchrotron emission lobes.
- Extended radio bremsstrahlung, recombination lines and heated dust emission surrounding the lobes.

The synchrotron radio lobes of microquasar jets have been detected in several sources (SS433, Dubner et al., 1998; 1E1740.7-2942, Mirabel et al., 1993; Cir X-1, Stewart et al., 1993). However, in the case of GRS 1915+105, searches have been unsuccessful (Rodríguez and Mirabel, 1998). In the following we will show that some signs of the interaction of the jets of GRS 1915+105 with the ISM have been observed already, but they do not include the radio synchrotron lobes.

2. What Can We Expect in the Case of GRS 1915+105?

As we pointed out in the previous section, our chances for detecting the large-scale jet structure of GRS 1915+105 are greatly enhanced if its jets stay laminar after coming into pressure equilibrium with their surroundings. Following a simple momentum conservation argument (Cantó and Raga, 1991), we show in Kaiser et al. (2004b) that the jets should stay laminar over a length of at least a few to several parsec even if they are in direct contact with a very dense ($n \sim 3000 \text{ cm}^{-3}$) ISM. For an average ISM density of $n \sim 1 \text{ cm}^{-3}$, this estimate increases by a factor of roughly 50. Also, it is likely that the lobes inflated by the jets extend all the way back to the acceleration region (Heinz, 2002), thereby creating a protective environment and greatly extending the range over which the jet flows can remain laminar.

In Kaiser et al. (2004b) we demonstrate that the impact site of one of these laminar jets should generate a bremsstrahlung flux of

$$F_{1\text{GHz}} \sim 5 \left(\frac{Q}{10^{37} \text{ erg s}^{-1}} \right) \left(\frac{T}{10^4 \text{ K}} \right)^{-2} \left(\frac{x}{0.01} \right) \left(\frac{D}{\text{kpc}} \right)^{-2} \text{ Jy}, \quad (1)$$

where Q is the total energy transport rate of the jet, x the ionisation fraction of the shocked ISM, and D the distance of GRS 1915+105. Note that this flux does not depend on the density of the ISM nor on the volume occupied by the emitting gas. The jet impact sites should therefore be easily detectable in the radio at GHz frequencies. Furthermore, given the likely temperature of the compressed ISM of $T \sim 10^4 \text{ K}$, we expect to detect recombination lines from hydrogen. If the ISM in front of the jet is multi-phase, then we expect to detect emission lines from various molecules as well as dust emission.

Estimating the radio synchrotron flux of the lobes is more complicated as this depends crucially on the physical size of the lobes and the gas density in their environment. We defer a discussion of this emission to the next section.

3. Identification of the Jet Impact Sites

Given the expected properties of the jet impact sites, they can only be identified with IRAS 19124+1106 and IRAS 19132+1035 (see Figure 1 and Kaiser et al. (2004a)). Their flat radio spectra (Rodríguez and Mirabel, 1998) and their luminosities are consistent with radio bremsstrahlung. The detected radio recombination lines and molecular emission lines (Chaty et al., 2001) support the identification. The observed IR fluxes are consistent with emission from heated dust (Kaiser et al., 2004a).

These emission properties are also consistent with an interpretation of the IRAS objects as star-forming H II regions. However, a chance alignment of two such H II

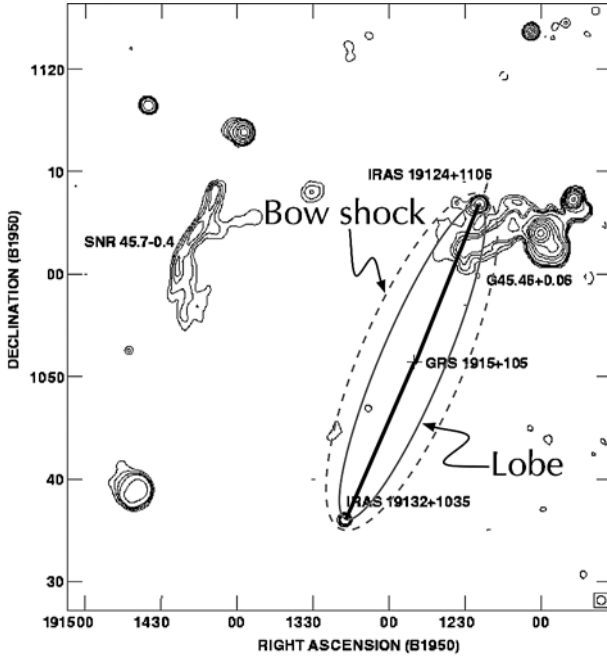


Figure 1. Radio map of the surroundings of GRS 1915+105 taken with the VLA at 20 cm with the postulated large-scale jet structure superimposed. The thick, solid lines show the two jets.

regions along the jets of a microquasar is small (Kaiser et al., 2004b). Furthermore, the elongated, non-thermal emission feature connected to IRAS 19132+1035 noted by Rodríguez and Mirabel (1998) points back to the position of GRS 1915+105 and may be a transient hot-spot at the end of the southern jet. We believe that these results lend strong support to our interpretation.

In Kaiser et al. (2004a) we present upper limits for the surface brightness of potential radio lobes employing the usual minimum energy arguments (e.g. Longair, 1994). We find that these limits lie below the current detection limits of radio maps of the vicinity of GRS 1915+105 (Rodríguez and Mirabel, 1998). However, in that paper we neglected the fact that most of the ISM compressed by the bow shock in front of the jets will not be collisionally ionised at the temperature of $T \sim 1.2 \times 10^4$ K, inferred from the width of observed emission lines. Taking into account the appropriate ionisation fraction of about 2% implies a density of the unshocked ISM in the vicinity of the jets of $n \sim 3000 \text{ cm}^{-3}$. This new estimate also changes our upper limit for the surface brightness of the lobes due to radio synchrotron to

$$S_{1\text{GHz}} \sim 100 \left(\frac{D}{\text{kpc}} \right)^{1/8} (k+1)^{-7/4} \text{ mJy beam}^{-1}, \quad (2)$$

where D is the distance of GRS 1915+105 and k the ratio of energy in non-radiating particles to the sum of the energy stored in the relativistic electrons and the energy in the magnetic field. For ideal minimum energy conditions we require $k = 0$. We assume a beam size of $4''$, appropriate for the observations of Rodríguez and Mirabel (1998).

Clearly, the synchrotron radio lobes of GRS 1915+105 should be detected in current radio maps which have a limit of $0.2 \text{ mJy beam}^{-1}$, unless $k > 34$, which is not unreasonable (e.g. Bell, 1978). Therefore, given the estimate of $S_{1 \text{ GHz}}$ above, the non-detection of synchrotron lobes implies a jet composition other than a pure pair plasma.

4. Implications of Our Identification

If the two IRAS sources are indeed the impact sites of the jets of GRS 1915+105, then this microquasar must be located at the same distance of $6.5 \pm 1.6 \text{ kpc}$ (Kaiser et al., 2004a) as opposed to the traditionally assumed distance of 11–12 kpc. This revised distance is consistent with all previous distance estimates (Fender et al., 1999; Dhawan et al., 2000a,b; Chapius and Corbel, 2004) except one (Greiner et al., 2001) and has some profound implications for the inferred properties of this system.

The jets of GRS 1915+105 travel with a bulk velocity of $0.66 \pm 0.15 c$ at an angle of $52.6 \pm 7.2^\circ$ to our line of sight. The apparent velocity of the jet ejecta on the sky is $0.66 \pm 0.18 c$, which is clearly not superluminal. The luminosity of any unbeamed emission will be reduced by a factor ~ 3 compared to the usually assumed distance. The lower limit on the power of the jets during the formation of the moving ejecta observed on small angular scales is reduced by more than 2 orders of magnitude to $2 \times 10^{37} \text{ erg s}^{-1}$. The total, time-averaged mechanical luminosity of the jets derived from the dynamical model of the jet expansion is $Q \sim 4 \times 10^{38} \text{ erg s}^{-1}$. Note that this estimate is a factor 50 larger than our original estimate (Kaiser et al., 2004a) because of the revised density estimate for the ISM in the vicinity of GRS 1915+105 from taking into account the partial ionisation of the hydrogen gas (Kaiser et al., 2004b). Finally, the mass of the black hole in the system is increased to $21 \pm 9 M_\odot$, resulting in a total mechanical jet luminosity of 14% of the Eddington luminosity.

The question of whether or not GRS 1915+105 is a microquasar hinges mainly on whether the definition of the term ‘microquasar’ includes the requirement for superluminal jets. If it does, then the first object with apparently superluminal jets in the Galaxy is not a microquasar, and it is therefore somewhat different from other microquasars that clearly show highly relativistic jet flows (e.g. Cir X-1; Fender et al., 2004). It is also interesting to note that GRS 1915+105 appears to be a binary system with a far less energetic jet, but a more massive black hole than previously appreciated.

References

- Bell, A.R.: 1978, *MNRAS* **182**, 443.
- Cantó, J. and Raga, A.C.: 1991, *ApJ* **372**, 646.
- Chapius, C. and Corbel, S.: 2004, *A&A* **414**, 659.
- Chaty, S., Rodríguez, L.F., Mirabel, I.F., Geballe, T.R., Fuchs, Y., Claret, A., Cesarsky, C.J. and Cesarsky, D.: 2001, *A&A* **366**, 1035.
- Dhawan, V., Goss, W.M. and Rodríguez, L.F.: 2000a, *ApJ* **540**, 863.
- Dhawan, V., Mirabel, I.F. and Rodríguez, L.F.: 2000b, *ApJ* **543**, 373.
- Dubner, G.M., Holdaway, M., Goss, W.M. and Mirabel, I.F.: 1998, *AJ* **116**, 1842.
- Falle, S.A.E.G.: 1991, *MNRAS* **250**, 581.
- Fanaroff, B.L. and Riley, J.M.: 1974, *MNRAS* **167**, 31.
- Fender, R., Wu, K., Johnston, H., Tzioumis, T., Jonker, P., Spencer, R. and van der Klis, M.: 2004, *Nature* **427**, 222.
- Fender, R.P., Garrington, S.T., McKay, D.J., Muxlow, T.W.B., Pooley, G.G., Spencer, R.E., Stirling, A.M. and Waltman, E.B.: 1999, *MNRAS* **304**, 865.
- Greiner, J., Cuby, J.G. and McCaughrean, J.: 2001, *Nature* **414**, 522.
- Hargrave, P.J. and Ryle, M.: 1974, *MNRAS* **166**, 305.
- Heinz, S.: 2002, *A&A* **388**, L40.
- Kaiser, C.R. and Alexander, P.: 1997, *MNRAS* **286**, 215.
- Kaiser, C.R., Gunn, K.F., Brocksopp, C. and Sokoloski, J.L.: 2004a, *ApJ* **612**, 332.
- Kaiser, C.R., Gunn, K.F., Sokoloski, J.L. and Brocksopp, C.: 2004b, *ApJ Lett.*, submitted for publication.
- Longair, M.S.: 1994, *High energy Astrophysics*, Cambridge University Press, Cambridge.
- Mirabel, I.F., Rodríguez, L.F., Cordier, B., Paul, J. and Lebrun, F.: 1993, *A&A Suppl.* **97**, 193.
- Rodríguez, L.F. and Mirabel, I.F.: 1998, *A&A* **340**, L47.
- Scheuer, P.A.G.: 1974, *MNRAS* **166**, 513.
- Smith, D.A., Wilson, A.S., Arnaud, K.A., Terashima, Y. and Young, A.J.: 2002, *ApJ* **565**, 195.
- Stewart, R.T., Caswell, J.L., Haynes, R.F. and Nelson, G.J.: 1993, *MNRAS* **261**, 593.